Metal-organic frameworks for the structure determination of non-crystalline compounds via the crystalline sponge method

Faiza Habib

Supervisors: Prof. Claire Carmalt and Prof. Derek Tocher

University College London

2022

DECLARATION

I, Faiza Habib confirm that the work presented in this thesis is my own. Where information has been derived from other sources, I confirm that this has been indicated in the thesis.

Faiza Habib

ABSTRACT

In this thesis, the most commonly studied crystalline sponge [{$(ZnI_2)_3$(tris(4-pyridyl)-1,3,5-triazine)$_2$·x($CHCl_3$)}$_n$] (**1**) was used to produce three novel complexes. The structure of three terpenes namely farnesol, geraniol and β-damascone were determined in the pores of sponge **1**. Despite being the most successful crystalline sponge **1,** has a few limitations such as exhibiting a hydrophobic pore environment, small pore size and instability in the presence of polar solvents and nucleophiles. Literature MOFs were searched for alternative crystalline sponges to overcome these limitations. The MOF {[Co_2(L)(H_2O)$_3$]·(solvent)$_x$}$_n$ L = bis-(3,5-dicarboxy-pheny1)terephthalamide (**3**) was investigated as an alternative crystalline sponge and studies resulted in two novel complexes with 3-phenylpropanol and 2-phenylethanol. In sponge **3** guest binding occurred via hydrogen bonding and the hydrophilic pore environment was suitable to accommodate polar solvents. Another literature MOF {[Cd_7(BTA)$_4$(H_2O)(DMF)]·(solvent)$_x$}$_n$ BTA = 4,4'4''-[1,3,5-benzenetriyltris(carbonylimino)]-trisbenzoic acid (**4**) was also investigated as an alternative crystalline sponge. Due to different synthetic procedures being used, a new structure of the MOF **4** was developed and that was used in subsequent studies. Sponge **4** outperformed sponge **1** in terms of stability and was stable in the presence of polar aprotic, polar protic solvents and Lewis bases. Inclusion complexes with the solvents, acetonitrile, acetone, and isopropanol demonstrated a hydrophilic pore environment where these guest molecules were fixed via hydrogen bonding. In contrast, pyridine was accommodated in sponge **4** via the coordinative alignment method (CAL). This observation led to the generation of five novel inclusion complexes with 4-aminopyridine, 3,5-lutidine, 3-bromopyridine, 4-acetylpyridine and 4,4'-bipyridine, which were accommodated in **4** via CAL. Another investigation was made to compare the closely similar structures of sponge **4** and pyridine derived sponge **4'**. *N*,*N*-dimethylaniline and propiophenone were accommodated in the pores of both the sponges and the differences in the host-guest interactions were studied. In the inclusion complexes of **4** and **4'** with *N*,*N*-dimethylaniline hydrogen bonding was not observed as the dominant host-guest interaction.

IMPACT STATEMENT

The crystalline sponge method (CSM) is an exciting technology which allows precise molecular determination of non-crystalline compounds such as oils, liquids, powders, and volatiles without the need to crystallise them independently. First developed in 2013,[1] the CSM involves using a porous framework material such as a metal-organic framework (MOF), into which target compounds in a solution can be soaked, allowing molecular structure determination of non-crystalline compounds via single crystal X-ray diffraction (SCXRD). Since this technique was introduced, the method has developed rapidly, and proved useful in a number of research fields. The CSM was used in synthetic organic chemistry for the structure determination of metabolites,[2–4] reaction intermediates[5–7] and short-lived species.[8,9] These compounds are difficult to isolate and produced in minute quantities. Therefore, structure elucidation of such compounds without isolation and crystallisation is the holy grail in organic chemistry. The CSM technique was utilised in understanding reaction mechanisms such as Pd-catalysed aryl bromination.[10] One of the major advantages of the CSM is that it can be applied to compounds present in nanogram-microgram quantities. Hence, the CSM is especially appealing for identifying mass-limited natural products and has been utilised in the absolute structure determination of several natural products.[11–15]

The CSM is currently in use by several industries and pharmaceutical companies are using CSM in drug development. Knowing the three-dimensional structure of the active pharmaceutical ingredients is essential because a slight alteration in the structure can transform it from an effective medicine to a dangerous poison. Hopefully, structure elucidation of any dangerous metabolites can be achieved by using CSM, before the drug is tested on patients. *Merck KGaA* has a Crystalline sponge innovation project in collaboration with *Rigaku Corporation*.[16] According to their scientists, by using this technology pharmaceutical companies could improve risk management associated with pharmaceutical development and achieve a reduction in the costs of developing new drugs.

Other than drug development the CSM is finding its use in companies that produce flavours and fragrances. Usually, the aromatic oils present in plants and fruits which contribute to the unique flavour and smell are too volatile to be crystallised, therefore CSM can be applied to answer the question in this area. The structure of the pungent-smelling component of Japanese wasabi was

determined by CSM.[17] Agricultural industries are also interested in investigating the structures of pesticides, fungicides, and herbicides and their metabolic products. *Syngenta group* uses the CSM technology to determine the structures of fungicide metalaxyl-M and herbicide S-metolachlor.[18]

This thesis contributed to the expansion of the CSM technology. The molecular structure of terpenes is determined. A versatile hydrophilic crystalline sponge is developed and provided the information on the host-guest interactions responsible to bind guest molecules in place. This new sponge has the potential to be used for the structure determination of pharmaceutical ingredients.

The CSM is developing rapidly with new applications. This technology has the potential to impact several research areas and maybe even revolutionise entire industries. In 30 years, this technology may be a commodity with broad enough applicability to enable completely new applications that cannot be foreseen today.

ACKNOWLEDGMENTS

Firstly, I would like to express my deepest gratitude to my supervisors at UCL, Prof. Claire Carmalt and Prof. Derek Tocher. Their active involvement in the project and guidance through the challenging times helped me in emerging as an independent researcher. A particular thanks to Prof. Carmalt for her understanding and constant support during the COVID-19 pandemic which kept me going and helped to focus on my goal. I had a difficult time after having a baby amidst PhD and it was extremely helpful that Prof. Carmalt herself being a woman and mother understood my position. So, cheers to womanhood and lived perspective!

Also, I would like to thank the Carmalt/Parkin conglomerate with whom I had the pleasure of sharing an office and lab. Special thanks to Dr Caroline Knapp for helping me with structure refinements and ordering liquid nitrogen for the single crystal diffractometer all the time.

I would be amiss to not mention my master's supervisor Prof. Masahiro Yamashita. Yamashita Sensei is a kind and caring supervisor, and he has continued to support and encourage me even after graduating from his group. He continued to offer his support during the worldwide lockdown. Special thanks to Dr Hiroaki Iguchi for introducing me to the field of MOF chemistry.

And of course, money! So, a huge thanks to both UCL for the Overseas Research Scholarship which took care of the humongous international tuition fee and the Schlumberger Foundation's Faculty for The Future Fellowship for generous PhD stipend and conference support.

Most importantly, I would like to thank my family, especially my dear husband, Mudasir, for his constant support and motivation. Thank you for believing in me and my abilities more than I did. Also, I am grateful to my mother and mother-in-law who came all the way from India to London to look after my little son, Daaim, so that I can devote more time to my PhD. Lastly, thank you Daaim for coming into our world and filling it with bursts of happiness with a topping of sleepless nights.

PUBLICATIONS

1. Faiza Habib, Derek A. Tocher and Claire J. Carmalt., **Applications of the crystalline sponge method and developments of alternative crystalline sponges**, *Materials Today: Proceedings*, 2022, **56**, 3766-3773

2. Faiza Habib, Derek A. Tocher, and Claire J. Carmalt., **Structure determination of terpenes by the crystalline sponge method** *Microporous & Mesoporous Materials.* 2020, **308**, 110548

Table of Contents

LIST OF FIGURES

LIST OF TABLES

LIST OF ACRONYMS

µL	microlitres
2PE	2-Phenylethanol
3PP	3-Phenylpropanol
a,*b*,*c*	Unit cell axis
α,*β*,*γ*	Unit cell angles
ADP	Atomic Displacement Parameters
BDTA	bis-(3,5-dicarboxy-phenyl)terephthalamide
BTA	4,4',4''-(1,3,5-benzenetriyltris(carbonylimino)]-trisbenzoic acid
CD	Cyclodextrins
CMOMs	Chiral Metal-Organic Frameworks
CSM	Crystalline Sponge Method
DMF	Dimethylformamide
DMSO	Dimethylsulfoxide
GC	Gas Chromatography
h	hours
HPLC	High Performance Liquid Chromatography
IR	Infrared Spectroscopy
mL	mililitres
MOFs	Metal-Organic Frameworks
nm	nanometers
NMR	Nuclear Magnetic Resonance
POMs	Porous Organic Materials
R_1	R-factor
SCXRD	Single Crystal X-Ray Diffraction
TPT	tris(4-pyridyl)-1,3,5-triazine
wR_2	Weighted R-factor

INTRODUCTION AND LITERATURE REVIEW 1

1.1 INTRODUCTION

Structural determination is an essential component of the characterisation of new compounds, and single-crystal X-ray diffraction (SCXRD) is recognised as the most reliable technique. Other analytical techniques, such as nuclear magnetic resonance (NMR), mass spectrometry (MS), and infrared spectroscopy (IR) give essential information such as molecular formulae, bond connectivity, and functional groups. However, only SCXRD provides direct structural information at the atomic level, such as the unit cell parameters, bond length, bond angle, ordering information, and stereochemistry. Unfortunately, as the name implies, the limitation of this method is that it requires a crystal for analysis. Therefore, powder, amorphous solid, liquid, volatile matter, or oily state are not suitable for this type of analysis. A technique that would allow these states to be fully characterised is therefore highly desirable. Thus, "crystalline sponge", a technology allowing precise molecular determination of any non-crystalline compound in low quantity would be a holy grail of chemistry. The crystalline sponge method (CSM) involves using a porous framework material such as metal-organic frameworks (MOFs), into which compounds in a solution can be soaked, allowing molecular structure determination of non-crystalline compounds along with the framework via SCXRD. This technique was first introduced by Fujita and coworkers.[1] in 2013 and since then has grown rapidly and proved helpful in the structure elucidation of powders, liquids, and other volatile compounds.

This technique would be useful in biomedical research for investigating the adopted conformation of molecules. The knowledge of the conformation of molecules with an affinity to proteins plays a vital role in the determination of protein structures.[16] Similarly, in drug development knowing the three-dimensional architecture of the compound is essential since a slight alteration in the structure can transform it from an effective medicine to a dangerous poison. In addition, structure elucidation of drug metabolites during the drug development process enables the identification of

any dangerous metabolites which may cause an adverse effect before the drug is tested on patients.[16]

The crystalline sponge method (CSM) functions on the principle of hosting the guest molecules within the cavity of crystalline supramolecules. This approach of entrapping guest molecules in a confined cavity is not novel and has been previously used in the field of supramolecular chemistry such as host-guest chemistry of discrete cages in solution and self-assembled cages and capsules.[19–21] These areas of study provide background to the crystalline sponge method and are discussed in the next section briefly.

1.1.1 A brief introduction to supramolecular chemistry

Supramolecular chemistry is an interdisciplinary field of science involving the chemical, physical, and biological properties of molecular assemblies having a greater complexity than the individual molecules themselves.[22] Jean-Marie Lehn[23] defined supramolecular chemistry as "*chemistry beyond the molecule, bearing on the organised entities of higher complexity that result from the association of two or more chemical species held together by intermolecular forces*". In contrast to traditional chemistry, which focuses on the covalent bond, supramolecular chemistry examines the weaker and reversible non-covalent interactions between molecules. For example, hydrogen bonding, dipole-dipole and ion-dipole interactions and hydrophobic interactions, such as van der Waals, π-π interactions, and dispersion interactions.[24] The most spectacular example of supramolecular chemistry was found in nature as the DNA structure, which has complicated packing, replication mechanisms. Detailed mechanistic studies of supramolecular assemblies are important not only for understanding the self-assembly processes but also for designing assemblies for specific applications. For synthetic chemistry, self-assembly represents a powerful synthetic methodology in the creation of large, discrete, ordered structures from relatively simple components. These macromolecular systems have been applied to various chemistry problems such as selective substrate binding, trapping reactive intermediates or protecting unstable species, and influencing reaction chemistry within-host cavities.[25] One of the major interests in supramolecular chemistry is to design well-defined structures with dynamic and stimulus-responsive properties. Dynamic and adaptive supramolecular materials that self-assemble from multiple components have a wide range of applications in materials and medicines.[26] For example, cyclodextrins (CD) formed from *D*-glucose units have a hydrophobic cavity and a hydrophilic

outer surface allowing them to accommodate small hydrophobic drugs or moieties inside the cavity hence forming an inclusion complex. These inclusion complexes enhance the physicochemical characteristics of the drugs such as drug solubility and stability. The use of CD can improve drug permeation and bioavailability without changing the intrinsic properties of the drug molecule. CDs are widely used in pharmaceuticals, drug delivery systems, cosmetics, and the food and chemical industries.[27]

1.1.2 Introduction to host-guest chemistry

Host–guest chemistry has been at the forefront of supramolecular chemistry since it can bind molecular components together to form supramolecular assemblies. Typically, host-guest complexes consist of a macrocyclic molecule that functions as a 'host' by encapsulating suitable 'guest' molecules within their cavity. Guest molecules that satisfy the required steric and charge characteristics can be bound or trapped by the host system. In 1944,[28] porous hosts capable of capturing guest molecules in their cavity were termed *clathrates*. The word *clathrate* is derived from the Latin *clathratus* (*clatratus*), meaning 'with bars'. Clathrate compounds are polymeric and completely envelop the guest molecule, but in modern usage clathrates also include host-guest complexes and inclusion compounds. According to IUPAC, *clathrates are inclusion compounds in which the guest molecule is in a cage formed by the host molecule or by a lattice of host molecules.* Tetraarylporphyrin sponges are the most versatile range of clathrates and are extensively studied for various applications.[29] Porphyrin-based host lattices are capable of accommodating an extremely wide range of guest species. In these materials, sheets of tightly packed porphyrin molecules stack to form arrays of parallel channels. Figure 1.1 illustrates a few examples of tetraphenylporphyrin-based clathrates with monosubstituted six-membered rings.[30] The driving force for guest incorporation is the fact that the large, rigid, highly symmetric host molecules cannot pack efficiently in three dimensions. Therefore, the introduction of guest molecules into the crystalline lattice provides the degrees of freedom necessary to achieve more efficient packing. Similarly, compounds known as molecular containers are macromolecule hosts that have interior cavities large enough to accommodate guest molecules.[20] These macromolecules include carcerands, cavitands, cyclodextrins, hemicarcerands and cucurbiturils. Some of these hosts have portals in their shells that allow the guest to pass through in either direction between the inner and bulk phases. In contrast, there are hosts, which have closed-surface spheres whose

guest molecules are permanently incarcerated during synthesis for example the so-called molecular flasks.

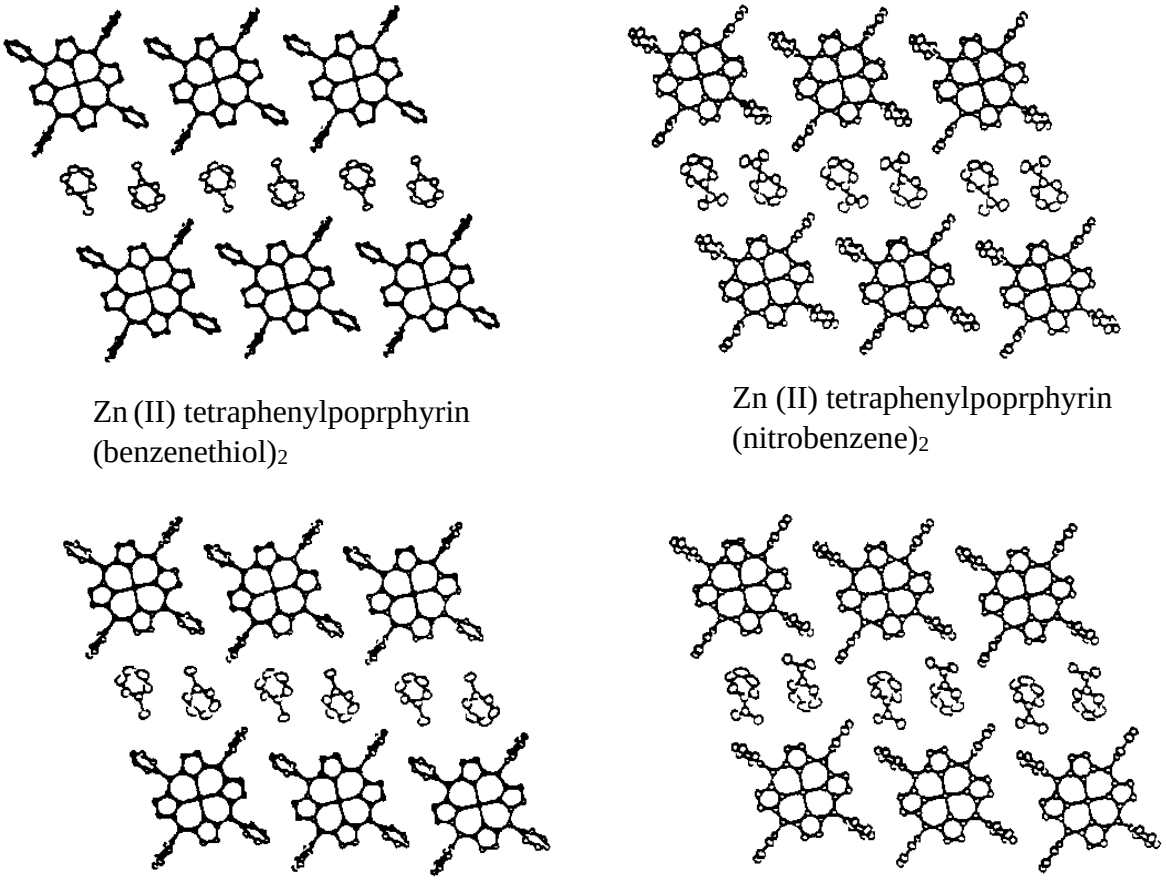

Figure 1. 1 Examples of porphyrin clathrates with guest having monosubstitued six membered rings.[30] Reused with permission from reference 30.

Molecular flasks were defined as hollow molecular structures that can encapsulate guest species within their cavities and influence their reactivity in a controlled fashion.[31] In initial studies discrete molecular cages such as cyclodextrins, carcerands, and hemicarcerands were the obvious choice to use as molecular flasks because of their robust framework and the ability to retain crystallinity while the guest species undergo a reaction. These hosts are typically composed of

rigid aromatic components connected by covalent, coordination or hydrogen bonds and have a molecular-sized empty cavity. However, in the past three decades, the preferences have shifted to self-assembled molecular hosts. Since self-assembled cages are extended structures in three dimensions (3D), even bulky guest molecules can penetrate through the pores of these networks.[32] The most popular self-assembled networks are porous coordination networks also known as metal-organic frameworks (MOFs). Their modular synthesis enables the size and nature of their pores to be easily altered. Most importantly, MOFs are highly crystalline and readily provide high-quality, robust single crystals. These unique features of MOFs have extended the scope of molecular flasks and driven the rapid progress in crystalline-state reactions. In 1997 Rebek Jr. and coworkers,[21] demonstrated that reversibly self-assembled hosts also function as molecular flasks, as shown in Figure 1.2. The molecular flask was assembled from two C-shaped halves, consisting of two glycoluril units connected by a linker. Complementary hydrogen bonding along the rim ensures that the two molecular halves afford a stable capsule in the presence of smaller guests. The room temperature Diels–Alder reaction of p-benzoquinone and cyclohexadiene at high dilution was significantly accelerated in the presence of a hydrogen-bonded host, the rate of reaction was increased because of the increase in the effective molarity. In 2002 Fujita and coworkers.[33] utilised self-assembled cages as molecular flasks to accelerate and significantly alter the rate of [2+2] photodimerization of olefins.

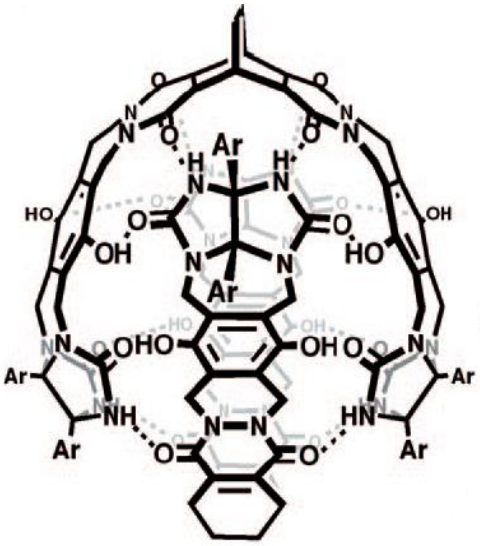

Figure 1. 2 Structure of the molecular flask used to accelerate Diels-Alder reaction.[21]

Reused with permission from reference 21

1.1.3 Host-guest interactions

The guest binding ability of the host framework is dependent on the non-bonding interactions between the guest and host. The most important of these interactions are defined briefly in this section.

Van der Waals Interactions

According to IUPAC van der Waals interactions can be defined as 'The attractive or repulsive forces between molecular entities (or between groups within the same molecular entity) other than those due to bond formation or to the electrostatic interaction of ions or ionic groups with one another or with neutral molecules. The term includes dipole-dipole, dipole-induced dipole and London (instantaneous induced dipole-induced dipole) forces. The term is sometimes used loosely for the totality of nonspecific attractive or repulsive intermolecular forces.'

Hydrogen bonding

IUPAC definition: 'An attractive interaction between a hydrogen atom from a molecule or a molecular fragment X–H in which X is more electronegative than H, and an atom or a group of atoms in the same or a different molecule, in which there is evidence of bond formation.'[34]

A hydrogen bond is generally observed as short contacts less than or equal to the sum of the van der Waals radii of the interacting atoms.[35] A hydrogen bond can be assigned to one of three classes; very strong (F–H–F), strong (O–H···O) or weak (C–H···O) according to the length of the interaction. However, this classification system is open to debate in the literature.[36]

Aromatic interactions

The π-system of the aromatic rings can be involved in three types of interactions involving the aromatic moieties: (i) π-π, (ii) cation-π and (iii) X–H-π.[37] Depending on the nature of the aromatic rings involved, their interactions give rise to three different types of geometries, namely, edge-to-face (T-shaped), face-to-face and parallel displaced (offset stacked) interactions.[38] It has been observed that most of the attractive orientations are T-shaped and the face-to-face orientation is rarely observed because of the unfavourable electrostatic repulsion forces between the two planar faces of the aromatic rings. In addition, there are various sub-types present under offset stacked interactions.[37]

1.2 Introduction to metal-organic frameworks (MOFs)

Metal-organic frameworks (MOFs) are constructed from inorganic and organic building units. The inorganic unit is comprised of metal-containing nodes or clusters which are coordinated to organic linkers through functional groups, such as carboxylates, pyridines, phosphates, sulphates and thus forming one-, two- or three-dimensional infinite networks (Figure 1.3).[39–41] MOFs provide high synthetic flexibility[42] and structural tunability,[43] which suggests that by a selection of appropriate combinations of metal nodes and the bridging organic spacers a wide range of designs in MOFs can and indeed have been obtained.[44] The nature of the two components and the type of connection between them plays a central role in the functionality of the MOFs, and therefore MOFs can be tailored according to the needs of the desired application.[45] For example, the pore size of MOFs can be tuned from several angstroms to several nanometres in size by simply changing the length of the rigid organic linkers. MOFs, because of their microporous character (<2 nm),[46] are useful for the adsorption of large gas molecules for separation purposes. Similarly, other framework functionalities can be enhanced by changing the metal components (e.g. magnetism, catalysis), and the organic linkers (e.g. luminescence, nonlinear optics, chirality).[47–49] As a consequence MOFs are emerging as a rapidly developing class of porous materials in chemical and material sciences and for the past two decades and attract tremendous attention from researchers. The reasons behind such popularity are their properties such as ultrahigh permanent porosity,[50] incredibly high internal surface areas,[51,52] crystalline nature, uniform pore sizes, and finely tuneable pore surface properties. These properties play a crucial role in functional applications such as gas adsorption and separation,[53,54] catalysis,[55] luminescence,[56,57] sensing,[58] protons,[59] electron conduction,[60] and drug delivery.[61]

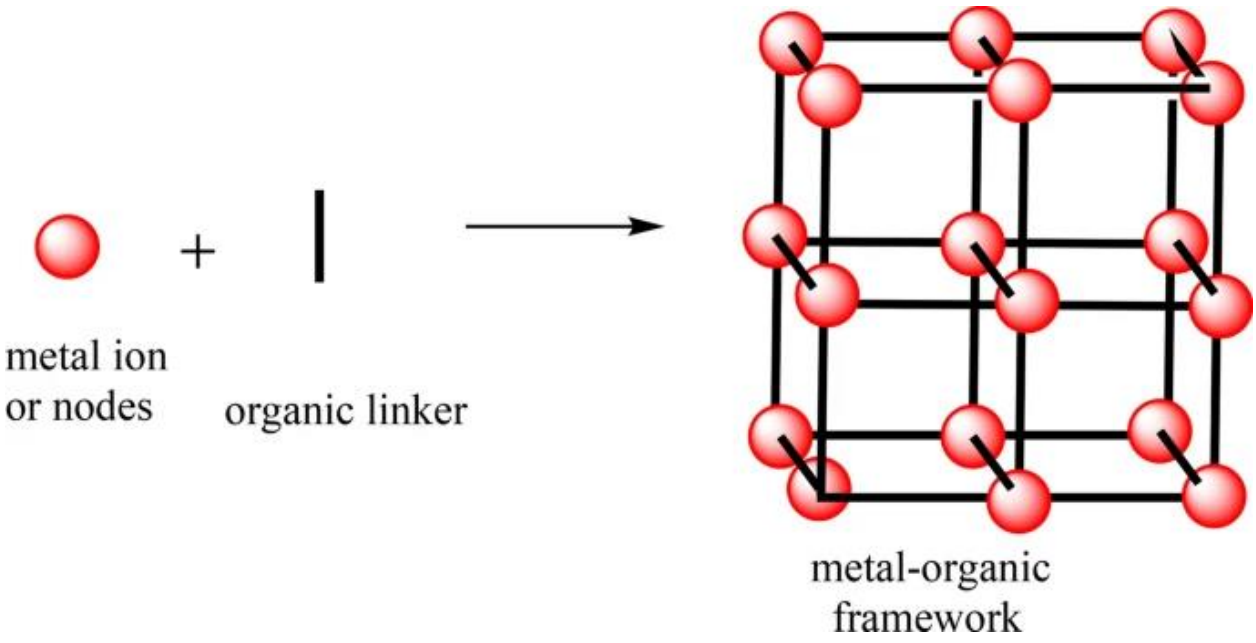

Figure 1. 3 Metal-Organic Framework.[161] Reused with permission from reference 161.

1.2.1 History of MOFs

In 1989 Robson and co-workers constructed an infinite 3D porous framework by a tetragonal ligand 4,4',4'',4'''-tetracyanotetraphenylmethane and Cu^{I} ions were considered the starting point for assembling porous frameworks. After synthesis, the pores were found filled with nitrobenzene and BF_4^- counterions.[62] In 1990 Kitagawa and co-workers reported 2D porous coordination polymers with the pyrazine ligand and copper and large hexagonal cavities were found occupied by acetone molecules.[63] In 1995, Yaghi and co-workers[64] first introduced the term MOFs for all the porous 2D and 3D coordination polymers. Since then, scientists have made tremendous efforts to synthesise MOFs with new designs and structures to optimise their functional properties. However, a disadvantage of MOFs was their inability to hold the porous structure in the absence of the guest molecules, a property called permanent porosity. In 1999 Yaghi and co-workers[65] published $[Zn_4O(bdc)_3]$ (bdc = terephthalate) MOF 5, (crystal structure shown in Figure 1.4) which remained crystalline and stable once fully desolvated on heating to 300 °C. Similarly, synthesis of HKUST-1,[66] $[Cu_3(tma)_2(H_2O)_3]_n$, (tma = benzene 1,3,5-tricarboxylate), Figure 1.5 showed a pore size of 1 nm and solvent accessible void of about 40% of unit cell volume and remained stable up to 240 °C. In 2005, MOF-74 (Zn_2(dhbdc), dhbdc = 2,5-dihydroxy-1,4-benzenedicarboxylate),

(structure shown in Figure 1.6) was reported to show permanent porosity and architectural stability in the evacuated framework.[67] The synthesis of these stable MOFs was a significant breakthrough in the field of MOF chemistry and opened opportunities for new applications in various fields.

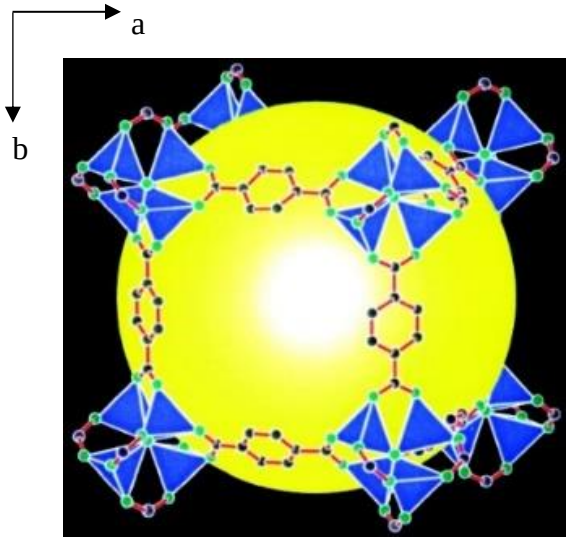

Figure 1. 5 Structure of MOF-5 framework [$Zn_4O(bdc)_3$], showing one of the cavity.[65] *Reused with permission from reference 65.*

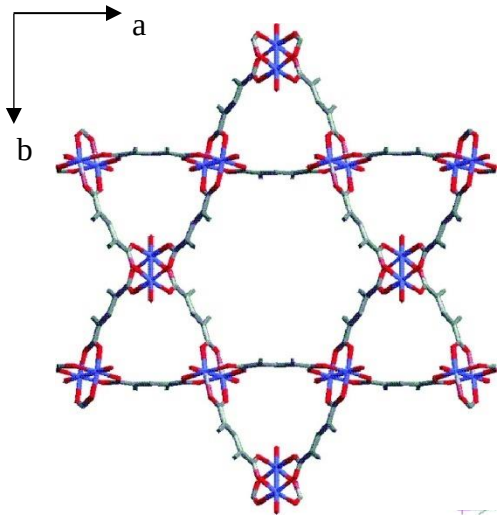

Figure 1. 4 HKUST-1 viewed along c axis showing a hexagonal-shaped pore.[66] *Reused with permission from reference 66.*

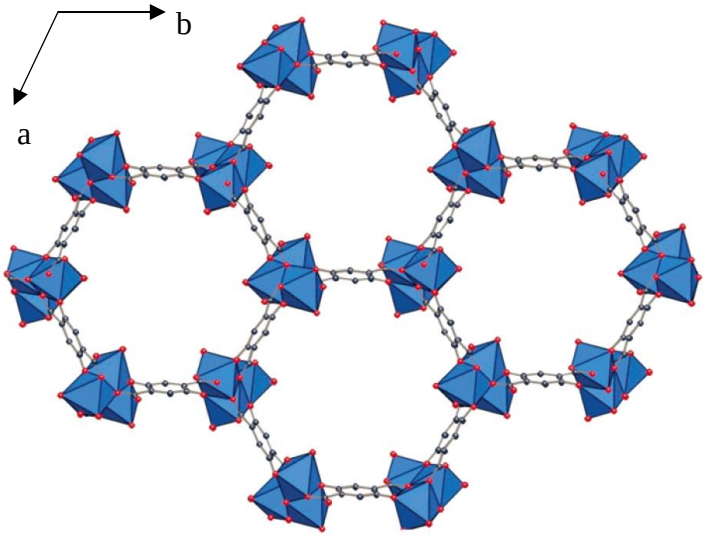

Figure 1. 6 Structure of MOF-74 viewed along the c-axis. [67] *Reused with permission from reference 67.*

1.2.2 Syntheses of crystalline MOFs: Strategies and Design

In the context of this thesis, only crystalline MOFs will be discussed. The synthetic procedure for the preparation of crystalline MOFs is challenging and is dependent on a large number of factors. This section will discuss strategies to synthesise and design crystalline MOFs to allow the development of materials with targeted properties and applications.

The design and synthesis of crystalline MOFs are highly impacted by various parameters such as the identity of the metal ions, length of the ligand, metal/ligand ratio, pH, solvent, and reaction conditions. In addition, there are supplementary components, such as templating agents, non-bonding guests, and counter anions, which can also influence the structure of MOFs. The coordination numbers and geometries of metal ions can also contribute to the final 3D structure of the MOFs. Therefore, for MOFs predictable structures based on desired properties have proven challenging. The combination of all the factors gives rise to a structure that is explicitly based on the number of binding sites the metal ion offers to the organic ligands. Many multidentate organic ligands such as carboxylates, bipyridine, and imidazole entities provide ample linking sites to metal ions and act as connectors to the network structure. The assembling of organic and inorganic building blocks generates the porous structure and the interactions existing between them play a crucial role in the strengthening of the porous framework. In literature, there are several synthetic methods commonly used for MOF construction, for example, the hydro/solvothermal, microwave-reaction, solvent evaporation, ionothermal, diffusion, and electrochemical approaches.[68] Different synthetic procedures can produce MOF with different structures and properties from the same reaction mixture. Moreover, the yield, crystal size, and morphology of the MOF products required for different applications can be modified from these different approaches. The maintenance of specific temperature conditions and modulation of reaction rates is essential to obtain good crystallinity with condensed or dense structures of MOFs. The advantage of MOF over previously prepared supramolecular polymers[69] is the ability to tune the dimensionality and pore properties, by choice of suitable organic ligands that bridge the metal ions. A good number of novel MOF structures were prepared by changing the molecular structure of the organic ligands.

1.2.3 Reticular synthesis

Despite all the challenges, targeted synthesis of MOF with predicted structures is highly desirable for specific applications, therefore reticular synthesis was introduced by Yaghi and co-workers.[70] to address the problem. Reticular synthesis is defined as the process of assembling judiciously selected molecular building blocks into an ordered structure. The orientation of organic linkers will result in the construction of MOFs with predetermined structural topologies. For example, in 2005 Yaghi and co-workers.[71] systematically designed isoreticular series with varying pore size and functionality based on the MOF-5 skeleton for methane storage. Isoreticular series is the term used when the framework topology remains the same, but the pore size varies. In this work the authors designed the series with ditopic carboxylate benzene linker with varying functionalities –Br, $–NH_2$, $–OC_3H_7$, $–OC_5H_{11}$, $–C_2H_4$, and $–C_4H_4$ and varying length of the linker biphenyl, tetrahydropyrene, pyrene, and terphenyl (Figure 1.7). Similarly, another isoreticular series was developed from a member of the MOF-74 family. Mg-MOF-74, was comprised of a phenylene unit of dhbdc (dhbdc = 2,5-dihydroxy-1,4-benzenedicarboxylate). This was then expanded to 2, 3, 4, 5, 6, 7, 9, and 11 phenylene units to produce isostructural analogues with pore apertures ranging from 14 to 98 Å. With these studies, the authors demonstrated the ability to control and direct the reticulation of building blocks into extended networks. In further studies to achieve targeted properties, the linker was kept the same and metal ions were varied. For example, the instability of carboxylate-based MOF-5 in the presence of water and high humidity was overcome by changing the metal ions from Zn to Be.[72] Two isostructural MOFs were obtained, and enhancement of the hydrothermal stability was observed.

Overall, the MOF research field is still growing not only by the escalating number of research papers published each year but also by the ever-expanding scope of applications. With the help of computational simulation and validation, novel structures and practical applications are continuously increasing. In addition, the above-mentioned control in tunability of MOFs for targeted properties is highly desirable for the development of the crystalline sponge method and can be tailored for particular guest encapsulation.

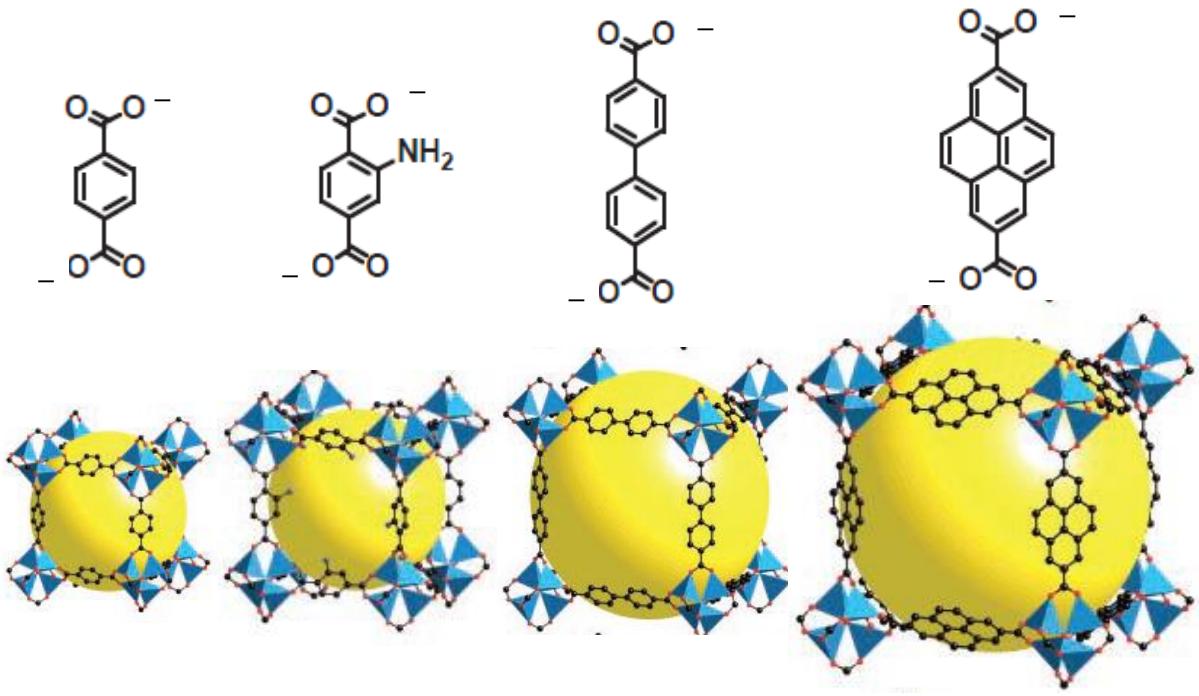

Figure 1. 7 Isoreticular series of MOF-5 with dicarboxylate organic linkers varying length.[70] *Reused with permission from reference 70.*

1.2.4 Potential applications of MOFs

Energy storage

The increasing amount of CO_2 in the atmosphere due to the burning of fossil fuels has pushed scientists to make use of rechargeable batteries and supercapacitors for energy storage such as lithium-ion batteries (LIBs). LIBs are widely used as energy storage devices in portable electronics and currently, industries are manufacturing LIB-based electric vehicles. However, the limited energy density and their high cost have motivated the exploration of better-performing electrode materials. Many researchers have demonstrated that MOFs with redox-active functionalities and high porosity, can play key roles as electrode materials in enhancing LIBs performance.[73,74] Song and coworkers.[75] have reported the polycarboxylate-based one-dimensional (1D) MOF nanowires as anode material for LIBs. These have, outstanding long-term cycling stability, of more than 1000 cycles, and a reversible lithiation/delithiation mechanism.

Protective fabric

Many MOFs are good adsorbents and are known to capture toxic industrial chemicals like NH_3 and H_2S and to remove SO_2, NO_x, CO, and CO_2 from flue gas.[76] Owing to MOFs capturing and catalytic properties, some examples have now been used for catalytic degradation of chemical warfare agents, for example, Nerve agent X (VX), Sarin, and Soman (Figure 1.8).[77] In particular, hexanuclear zirconium cluster-based MOFs (Zr-MOFs) have been explored as catalysts for the hydrolysis of nerve agents in aqueous alkaline solutions.[78] Recently, Farah and co-workers. collaborated with their industrial partners *NuMAT Technologies, Inc.* and have prepared a fabric coated with MOF-808/polyester as a protective layer against nerve agents. Capturing and slow diffusion of toxic chemicals within the MOF layer allow time for the destruction of these harmful agents and might be applied to the development of personal protective equipment, such as face masks and suits.

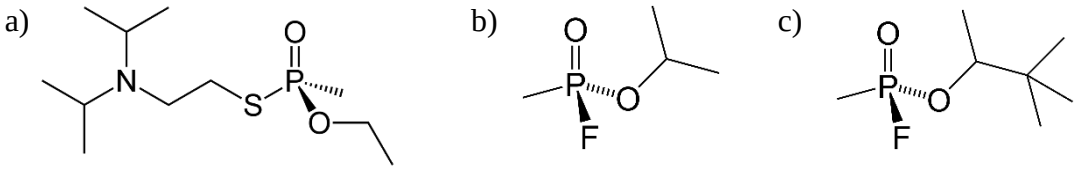

Figure 1. 8 Chemical structures of nerve agents a) VX: Ethyl ({2-[bis(propan-2 yl)amino]ethyl}sulfanyl)(methyl)phosphinate b) Sarin: (RS)-Propan-2-yl methylphosphonofluoridate c) Sonam: 3,3-Dimethylbutan-2-yl methylphosphonofluoridate[76]

Food packaging

MOFs have made the transition from the laboratory to their first commercial product as a material that keeps fruit and vegetables fresh and prevents them from ripening while in storage. Fresh fruits and vegetables over-ripen before reaching the consumer's fridge because of the release of plant growth hormone ethylene. In 2014 *Ducco*[79] and *MOF Technologies* companies built a MOF-based packaging material called TruPick which release 1-methylcyclepropene (1-MCP), a synthetic plant growth regulator that slows down the ripening process. The 1-MCP is stored in the pores of the MOF and slowly release to prolong the shelf life of fruits and vegetables.

Crystalline sponge

MOFs were used as the porous matrix for structure analysis of small molecules without actually crystallising them independently. Invented in 2013 in the laboratory of Makoto Fujita, a chemist at the University of Tokyo, Fujita and co-workers are now working to bring the crystalline sponge method to industrial partners, such as pharmaceutical, agrochemical, and fragrance producing companies. In addition, *Merck* and *Rigaku Corporation* have signed a joint development agreement to develop X-ray systems for highly innovative crystalline sponge technology.[16]

1.3 Foundation of the crystalline sponge method (CSM)

In 2013 Fujita and co-workers.[1] introduced the crystalline sponge method (CSM) for the structural determination of non-crystalline compounds by SCXRD. In this method, MOFs were used as a host 'crystalline sponges' to absorb non-crystalline compounds into its pores and through host-guest interactions arranged themselves in a regular pattern and thus capable of contributing to the Bragg peaks and a characteristic diffraction pattern. Interactions that are responsible for guest arrangements within the pores of the framework are π-π, CH-π, and charge-transfer interactions. These interactions are governed by the selection of ligands for the synthesis of the crystalline MOF. In Fujita's study, a large panel like tris(4-pyridyl)-1,3,5-triazine (TPT) ligand, shown in Figure 1.9, was used. TPT is electron-deficient and highly aromatic and can thus attract electron-rich molecules through π-π and CH-π interactions. In the initial study, two MOFs were synthesised with TPT, $[\{(Co(NCS)_2)_3(TPT)_4 \cdot x(solvent)_n]$[80] and $[\{(ZnI_2)_3(TPT)_2 \cdot x(solvent)_n]$.[81]

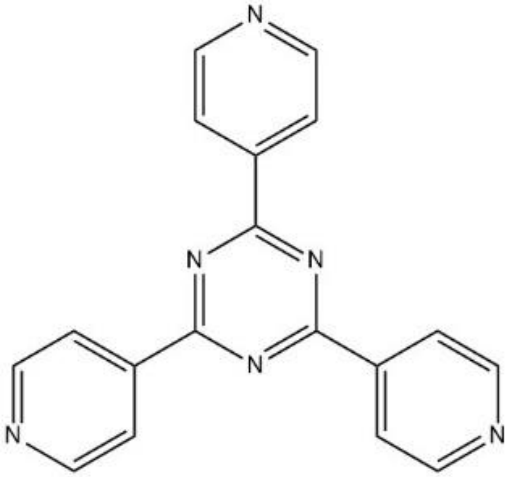

Figure 1. 9 tris(4-pyridyl) 1,3,5-triazine (TPT)

The $[\{(Co(NCS)_2)_3(TPT)_4 \cdot x(solvent)_n]$ porous crystalline network has an infinite array of octahedral M_6L_4 cages (M = $Co(NCS)_2$, L = TPT), in which each metal vertex is shared between two adjacent octahedra. The host framework occupies only 22% of the crystal volume, but it displays remarkably robust crystallinity. This crystalline network helped in separating C_{60} and C_{70} fullerenes from a toluene solution by the selective uptake of C_{70} in the pores.[80] However, this porous complex was not used as the crystalline sponge in later studies because it crystallises in the $Fm\bar{3}m$ space group, cubic system. The higher symmetry of the framework will provide more chances for the guest molecules to sit on a symmetry element and cause crystallographic disorders. As a consequence, $[\{(ZnI_2)_3(TPT)_2 \cdot x(solvent)_n]$ was used for the majority of the subsequent crystalline sponge studies.

The synthesis of complex $[\{(ZnI_2)_3(TPT)_2 \cdot x(solvent)_n]$ (**1**) was first reported in 2002 by Fujita and co-workers along with the remarkable guest exchange property. An interpenetrated $[\{(ZnI_2)_3(TPT)_2 \cdot 6(C_6H_5NO_2)\}_n]$[81] porous complex was synthesised with the ability to absorb and desorb guest molecules. Figure 1.10 shows the solvent-accessible voids present in the structure filled with partially disordered nitrobenzene (from the synthesis), which could exchange with other solvent molecules without losing crystallinity. For example, benzene was exchanged into the pores and ordered sufficiently to be refined isotropically. Interestingly, a non-interpenetrated $[\{(ZnI_2)_3(TPT)_2 \cdot 2(CHBr_3)_n]$ complex was obtained by replacing nitrobenzene with bromoform in the synthetic method and disordered bromoform molecules were observed occupying the channels, as shown in Figure 1.11. The guest exchanging property of sponge **1** was further studied and large molecules were successfully encapsulated in the pores, for example, triphenylene, anthracene, and perylene. In these inclusion complexes, donor-acceptor interactions were observed and found to be responsible for the host-guest close contacts.[82] In 2005 a biporous interpenetrating coordination network $[\{(ZnI_2)_3(TPT)_2(triphenylene)] \cdot x(nitrobenzene)_y(methanol)\}_n]$ was reported by Fujita and co-workers.[83] Triphenylene was intercalated within the framework because of the strong π-stacking with TPT, therefore it could not undergo the guest exchange process and is considered a part of the host framework. This framework has two distinct channels and was capable of selectively taking up a preferred guest in a specific channel. Guests such as naphthalene, nitrobenzene, and cyclohexane were shown to be separately included in the two different channels. This selective uptake property leads to the storage of incompatible compounds together in one framework, for example, an acid/base pair.

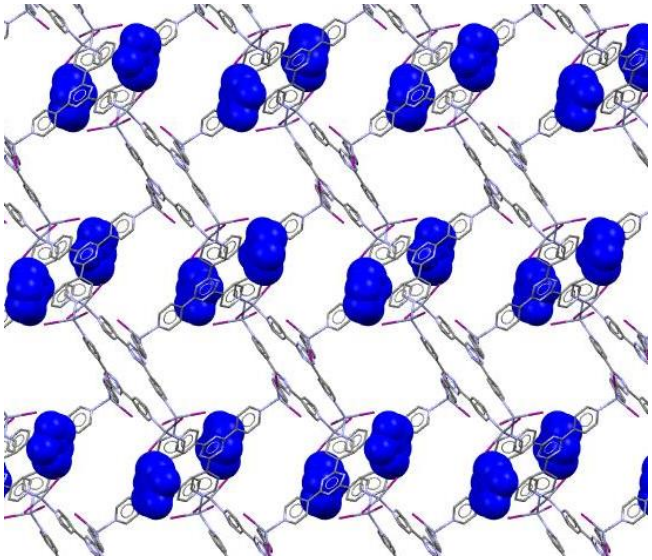

Figure 1. 10 The 3D network of [{(ZnI$_2$)$_3$(TPT)$_2$·6(C$_6$H$_5$NO$_2$)}$_n$]. Nitrobenzene molecules are shown in space-filling mode in blue.[81] *Redrawn with permission from reference 81.*

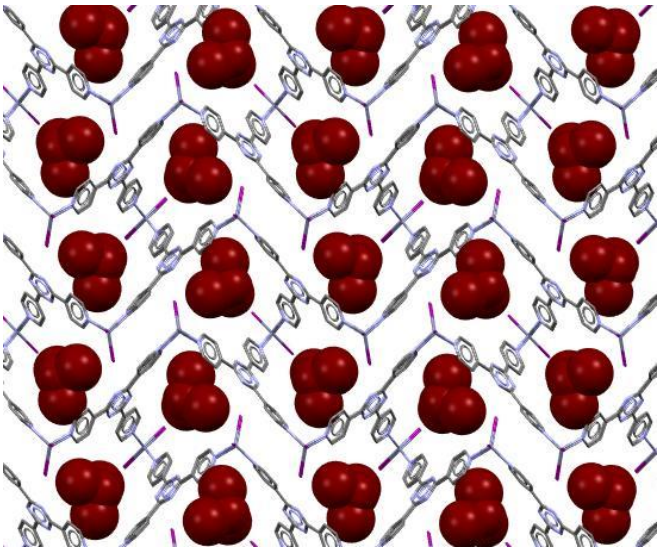

Figure 1. 11 The 3D network of [{(ZnI$_2$)$_3$(TPT)$_2$·2(CHBr$_3$)}$_n$]. Bromoform molecules are shown in space-filling mode in brown.[81] *Redrawn with permission from reference 81.*

All the above studies on [{(ZnI$_2$)$_3$(TPT)$_2$·6(solvent)}$_n$] (**1**) demonstrated that guest molecules absorbed into the pores of **1** showed host-guest interactions which make guests amenable to structural determination by SCXRD. As a result, in 2013 Fujita and co-workers.[1] proposed [{(ZnI$_2$)$_3$(TPT)$_2$·6(solvent)}$_n$] as a material used in the CSM; a technique for the structural

determination of non-crystalline compounds by SCXRD. The structure of liquid and volatile molecules was determined by the crystalline sponge method. Further work established that the method could be applied to the study of guests present in nanogram-microgram quantities and in determining the absolute structure of chiral compounds.

1.3.1 Synthetic improvements to the preparation of crystalline sponge **1**

In the original Fujita's report, single crystals of **1** were synthesised by layering ZnI_2 in methanol solution over a solution of TPT in nitrobenzene for 7 days at room temperature, followed by solvent exchange with cyclohexane for a further 7 days at 50 °C. However, in practice, this synthetic method resulted in crystal imperfections due to high temperature resulting in cracking of the crystals, incomplete solvent exchange, and long preparation time. Subsequently, Fujita and co-workers.[84,85] published guidelines and protocols to avoid problems with the methodology. However, several problems remained, and many researchers actively contributed to the field of CSM and optimised the synthetic procedure. Clardy and co-workers.[86] reported the modified synthesis of sponge **1** where $CHCl_3$ was used as the solvent instead of nitrobenzene, which produced an improved quality of crystals and reduced the preparation and encapsulation time from 14 to 3 days. This method avoided solvent interference in guest refinement after SCXRD since $CHCl_3$ was easily identified within the pores owing to the larger electron density associated with Cl. In addition, Clardy and co-workers.[87] synthesised analogous sponge **1** by replacing ZnI_2 with $ZnBr_2$ or $ZnCl_2$ thus improving the visibility of guest molecules within the pores. The Cl congener of **1** proved helpful in resolving the structure of many natural products. The variants of sponge **1** were also used to trap guaiazulene, trans-anethole, and (1*R*)-(−)-menthyl acetate and were studied by using synchrotron radiation. Furthermore, Santarsiero and co-workers.[88] introduced a microwell droplet approach for the synthesis of sponge **1** where high-quality crystals grew in just 10 h with a ≥90% yield, compared to Fujita's methods with a ≥5% yield.

1.4 Applications of the crystalline sponge method

The main application of the CSM is the structure determination of liquids, volatile materials, natural products, and unstable reaction intermediates. The CSM is often applicable even though the target material is present in nanogram-microgram quantities. In addition, reaction mechanisms can be studied within the pores of the sponge, and it also proved helpful in the absolute structure determination of chiral compounds. Furthermore, the CSM in combination with chromatographic

techniques can be used to identify components present in trace amounts in natural products. These overlapping areas are discussed in the four sections below.[89]

1.4.1 Studies of nanogram-microgram of guest

Fujita and co-workers.[1] in their original crystalline sponge paper demonstrated the use of the CSM for structure determination at the nano-microgram scale. They performed the encapsulation of guaiazulene in the crystal of **1** with a tiny ~1 µg crystal (60×60×70 μm^3) and placed it in a micro vial with 45 µl of cyclohexane / CH_2Cl_2 solution of the guest (500 ng, 5µl), which was added to the supernatant and the microvial was capped with a screw cap with a pinhole. After two days of incubation at 45 °C, the crystal turned dark blue indicating that guest exchange had occurred. When subjected to X-ray diffraction the presence of guaiazulene in the pores of **1** was observed with 60% occupancy. This indicated that only 26 ng of the guest was present in the pores, less than 10% of the quantity of the guest added. The experiment was then repeated with smaller quantities of guest (>80 ng) and XRD confirmed the presence of guest molecules in the pore.

1.4.2 Studies of liquid and volatile guests

Analysis of non-crystalline liquid guests was carried out by CSM where a single crystal of sponge **1** was brought into contact with a drop of cyclohexanone at room temperature and rapid guest penetration occurred. Two days later, the crystal was subjected to an X-ray diffraction experiment and the crystal data clearly showed the molecular structure of cyclohexanone packed within the cavity of the cage. Furthermore, Fujita and co-workers. demonstrated the use of CSM in the structural determination of highly volatile compounds. The volatile nature of such compounds inhibits crystal growth and therefore, little attention has been paid to X-ray diffraction as a technique for their structure determination. For example, isoprene[1] which has a melting point below −125 °C, was absorbed by the crystals of **1** and trapped within the voids of the crystals and the structure was determined by X-ray crystallography. However, this procedure did not work with other volatile compounds where the guest was not absorbed in the pores because of their rapid evaporation along with the solvent at 25 °C. Therefore, Fujita and co-workers[90] further developed two soaking methods for volatile compounds namely, direct inclusion from sample vapours and low-temperature soaking with low-boiling-point solvents.

1.4.3 Crystalline sponge method in combination with chromatographic/spectroscopic techniques.

Fujita and co-workers proposed structural determination in combination with chromatography where trace components are present as a mixture in the sample and can be separated by HPLC/GC and then directly subjected to the crystalline sponge method. They carried out the structure determination of several polymethoxyflavones (PMF) that are trace components in orange peel *Citrus unshiu* in combination with HPLC. The method involved 30 µg of PMFs, which were extracted from an air-dried piece of orange peel and separated by HPLC into three components. The crystals of **1** were then soaked in each of the components and subjected to X-ray diffraction for structure analysis revealing the structures shown in Figure 1.12. In addition, HPLC in combination with CSM (LC-CSD) was applied for the structure determination of metabolites produced from 1,1-*bis*(4-chlorophenyl)-2,2,2-trichloroethane (DDT), tetralone, and adrenosterone as a result of enzymatic reduction reaction by baker's yeast by CSM with absolute stereochemistries determined.[2] Furthermore, CSM combined with gas chromatography (GC) was applied to separate and identify the major and minor volatile components of peppermint oil.[90]

Figure 1. 12 Structure of three fractions of polymethoxyflavones extracted from citrus unshiu.[1] Reused with permission from reference 1.

Moreover, CSM was combined with several spectroscopic methods for structure determination and other applications. For example, CSM in combination with HPLC-NMR was used for the full characterisation of several natural products.[13,14,91–94] In addition, CSM combined with mass spectroscopy was used to understand the ionisation mechanism of matrix-assisted laser desorption ionization (MALDI)[95–97] and combined with ultra-high performance liquid chromatography and tandem mass spectroscopy (UPLC-MS) to optimise various soaking conditions.[98]

1.4.4 Study of reaction mechanisms of organic compounds within pores

Chemists have always been intrigued to study reaction mechanisms in crystalline states because of their unusual reaction pathways, high product selectivity, and the stabilisation of intermediate species. However, it is challenging to retain crystallinity during the reaction and observe any structural changes directly by SCXRD. In 2009 Fujita and co-workers observed a short-lived hemiaminal transient species by SCXRD trapped in the pores of complex **1**.[9] This short-lived hemiaminal intermediate was formed during the chemical transformations of an amine into an aldehyde and had only rarely been observed previously. It was kinetically trapped at 215K within the pores, as shown in Figure 1.13, and thus amenable to X-ray analysis and structure determination. This work suggested that the use of porous complexes could be further extended to provide mechanistic insight. Since 2013, with the introduction of the CSM, several chemical transformations were studied and structure analysis of unisolable intermediates and short-lived transient species was obtained.[99–103]

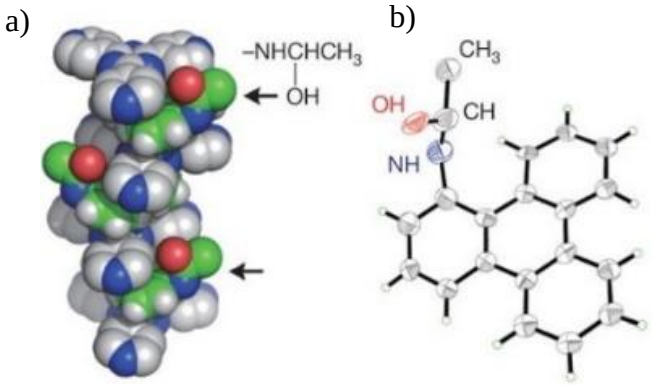

*Figure 1. 13 a) view of the columnar stack of hemiaminal and the triazine ligand. b) The transient hemiaminal intermediate, formed in situ by treating a crystal of **1** with acetaldehyde.[9] Reused with permission from reference 9.*

For example, an intermediate formed during Pd-mediated bromination of an aromatic compound was crystallographically studied in the pores of sponge **1** with the help of time-resolved X-ray diffraction.[10] Figure 1.14 illustrates the conversion of the intermediate to the final product and the mechanism of the reaction which was confirmed by the appearance and/or disappearance of electron density associated with Pd-Br and C-Br bonds. Similarly, various reaction mechanisms were confirmed by CSM.[104–107]

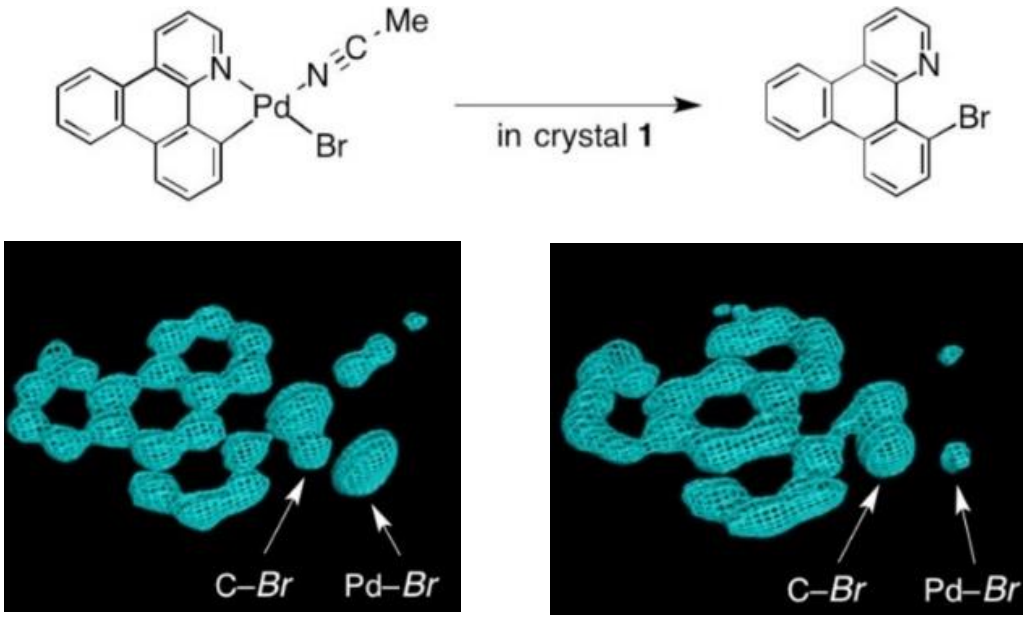

*Figure 1. 14 The palladium mediated bromination reaction performed in sponge **1**. Electron density maps (F_0) show the bromine atoms of disappearing Pd−Br and forming C−Br bonds.[10] Reused with permission from reference 10.*

Recently, the CSM was used to study biosynthesis involving biologically active compounds. Biocatalyst P450 mono-oxygenase, TleB which normally catalyses C─N bond formation was tested to study C-S bond formation. Figure 1.15 illustrates the reaction scheme of C─S intramolecular bond formation of the thiol-containing substrate. This reaction resulted in the formation of a sulfur-containing thio-indolactam V along with an unusual indole-fused 6/5/8 tricycle product. The crystal structures for both products were studied via the CSM. The CSM enabled the study of the unusual product formation and opened possibilities to study new skeletons created by biological P450 enzymes.[108]

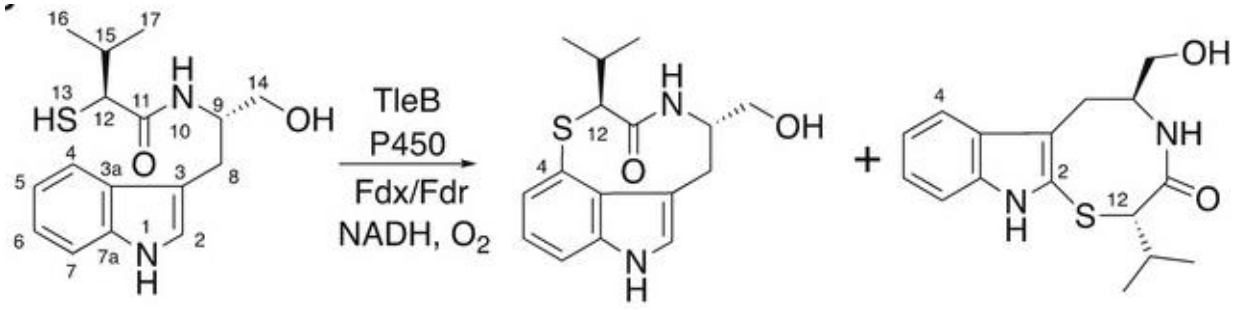

Figure 1. 15 Reaction scheme of C-S intermolecular bond formation of thiol substituted substrate catalysed by TleB.[108] Reused with permission from reference 108.

1.4.5 Absolute structure determination of chiral compounds

The ability to distinguish between the enantiomeric pairs of the chiral compound with a non-centrosymmetric structure is known as absolute structure determination. In the early 1900, the X-ray diffraction method was not supposed to determine absolute structure because they measure interatomic distances which were the same for model and inversion. In addition, Friedel's law states that the intensities of the *h,k,l,* and $\bar{h},\bar{k},\bar{l}$ reflections are equal irrespective of the direction of the diffraction, and the phase difference of the diffracted X-rays will be of equivalent magnitude. However, the introduction of anomalous scattering in X-ray diffraction made it possible to distinguish a non-centrosymmetric crystal structure from its inverted image. In this second-order effect, the phase lag was introduced by exciting the inner shell electrons of the heavy atom by using the incident X-ray wavelength resonating with the frequency of the electron and thus violating Friedel's law. J. M. Bijvoet in 1951 applied this technique to assign the absolute configuration of (+)-tartrate using its mixed sodium rubidium salt.[109]

Fujita and co-workers.[1] applied the CSM to determine the absolute structure of chiral compounds, the Bijvoet method can be used directly on inclusion complexes due to the presence of heavy elements (Zinc and Iodine) in the crystalline sponge **1** framework. The authors first applied the CSM for the structure determination of santonin, (Figure 1.16) an anthelminthic drug bearing four chiral centres. Sponge **1** crystallises in the achiral space group *C*2/*c* under normal circumstances. However, if a chiral guest is encapsulated in **1** then it would be expected that the space group would change to chiral. Therefore, after the encapsulation of santonin, the space group was observed to be $P2_1$ and the absolute structure was found in the pores of **1**.

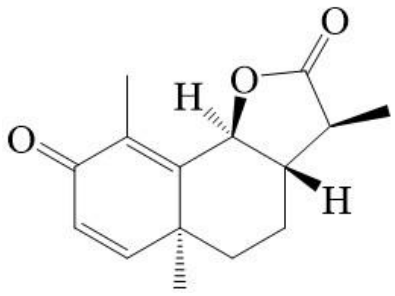

Figure 1. 16 Line diagram of santonin

Chiral molecules with axial and planar chirality do not have stereogenic centres, therefore their absolute configuration determination is even more troublesome. However, successful absolute structure determination has been demonstrated by the CSM for such molecules. An axially chiral biaryl compound was prepared by the aryl-aryl coupling reaction between 2,3 dimethylthiophene and 2-isopropyl-1-naphthylboronic acid via direct aryl C–H activation.[110,111] The racemic mixture of the biaryl compound was first subjected to HPLC separation and then the enantiopure compounds were treated with the CSM. The crystallographic analysis revealed the absolute configuration of both major and minor products as *S* and *R* respectively. Furthermore, several compounds were subjected to the CSM for absolute structure determination.[12,112] Another example of absolute structure determination of the chiral compounds, camphene α-pinene, and β-pinene was demonstrated by Gelder and co-workers.[113] Surprisingly when uptake of enantiopure (+)-camphene into the sponge was investigated, the space group remain unchanged. Therefore, it was argued that (−)-camphene was present as an impurity in the commercial (+)-camphene, which was, in this case, 90% pure. Figure 1.17 shows the structure of camphene in the asymmetric unit of sponge **1**. Recently, symmetry retention phenomenon upon encapsulation of chiral guest was also observed with chiral agrochemical metalaxyl-M and S-metolachlor.[18]

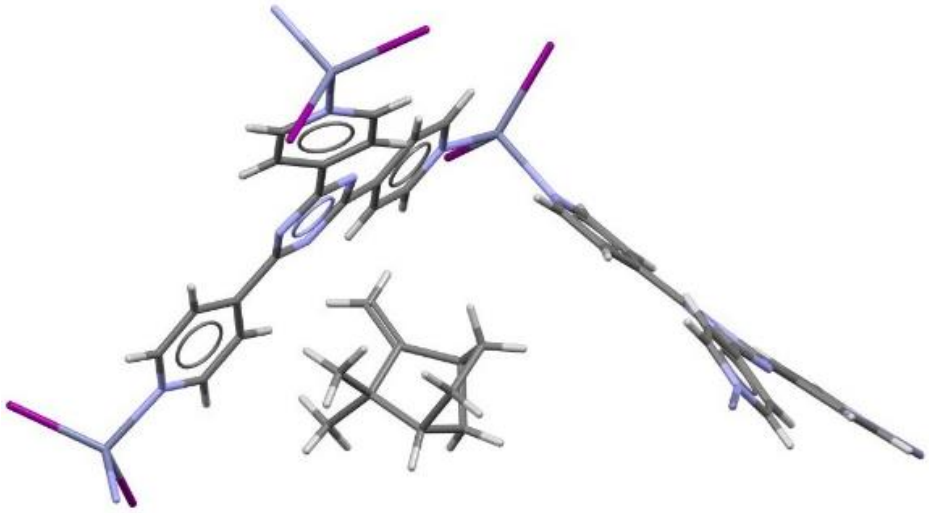

*Figure 1. 17 Structure of (+)-camphene in the asymmetric unit of sponge **1** which remained in C2/c spacegroup[113] Adapted with permission from reference 113.*

Furthermore, Fujita and co-workers.[114] applied the CSM for the analysis of non-enantiopure compounds often found in asymmetric synthesis studies. The studies revealed a new phenomenon in which a low *ee* compound was crystallised within the sponge lattice to give the unusual conglomerate of a chiral composite consisting of both enantiomers in an unequal ratio. For example, a chiral homoallylic bromide (synthesised in 88% *ee*) was encapsulated in pores of sponge **1**, in the space group *C*2. Eight independent guest molecules were observed in the asymmetric unit of the structure. Seven of them showed *R,R* configuration but, the eighth guest was observed with *S,S* configuration. The guest molecules thus form an unusual enantiomerically pure [$(RR)_7(SS)_1$] composite.

1.5 Limitations of the Fujita's crystalline sponge **1**

Although sponge **1** is the most successful and frequently used crystalline sponge it has a few limitations such as:

1) The stability of the crystalline sponge - as it remains stable in only a few solvents and exposure to the protic solvents and nucleophilic guests leads to deterioration in the crystallinity of the sponge.
2) Size of the pore - the commonly used crystalline sponge **1** has a pore size of 8 Å × 5 Å and guest molecules larger than this pore size cannot be encapsulated.
3) The environment of the pores - the pores are hydrophobic because of the electron-deficient TPT ligand and therefore, this sponge is limited to the encapsulation of hydrophobic guests only.

1.6 Alternative crystalline sponges

The limitations of the sponge **1** restrict the technique and preclude application to guests that are hydrophilic or nucleophilic in nature. Therefore, investigating new sponge candidates is crucial in the development of this technique and allows the encapsulations of a wider range of guests with different functionalities and sizes. To address such limitations several researchers have developed alternative crystalline sponges, which are not limited to MOFs.[115116] These crystalline sponge structures were often found in the existing literature, and some were even redesigned to recognise specific target molecules. Some of the alternative sponges published so far are discussed in this section.

1.6.1 A porous organic material

Porous organic materials (POMs) as an alternative crystalline sponge demonstrated advantages over the MOF based sponges. POMs are assembled from molecular components by weak intermolecular forces but lack coordination bonding and heavy metals hence the X-ray scattering from the framework would be reduced and guest visibility increased i.e., guest contribution to the diffraction pattern is more significant. Furthermore, the lack of labile metal−ligand bonds may make POMs amenable for nucleophilic and basic guests. Costa and co-workers.[117] have reported a crystalline porous organic material (POM) assembled from a semirigid macrocyclic tetraimine and ethyl acetate, as shown in Figure 1.18. The POM was synthesised via Schiff base condensation and crystallisation was achieved with a diamine and terephthaldehyde with a pore size of 12 × 9 $Å^2$. Figure 20 illustrates the encapsulation of guest *S*-(−)-nicotine in the pore of the POM which demonstrates the compatibility with nucleophilic guests. Furthermore, this POM was used to encapsulate diethyl phthalate.[117,118] Since the tetraimine POM has only light atoms, the chirality of *R*-(+)-limonene and *S*-(-)-nicotine was not determined because of the use of Mo Kα radiation. Yamaguchi and co-workers.[6] reported a cyclophane based POM synthesised by one-pot S_NAr reactions of disubstituted adamantanes having halophenol units and 3,6-dichlorotetrazine. The POM showed permanent porosity and adsorption of volatile compounds. Therefore, cis-3-hexen-1-ol and trans-2-hexenal, respectively known as leaf alcohol and leaf aldehyde were encapsulated and the molecular structures of these guests were elucidated. In 2021 Hong and co-workers.[119] reported a 9,9'-(5'-(4-(anthracene-9-yl)phenyl)-[1,1':3,1"-terphenyl]-4,4"-diyl)dianthracene based ultra-stable π–π stacked POM framework exhibiting permanent porosity, high thermal stability, and good chemical resistance. Small organic molecules with various functionalities were encapsulated, however, larger molecules were unable to penetrate the pore.

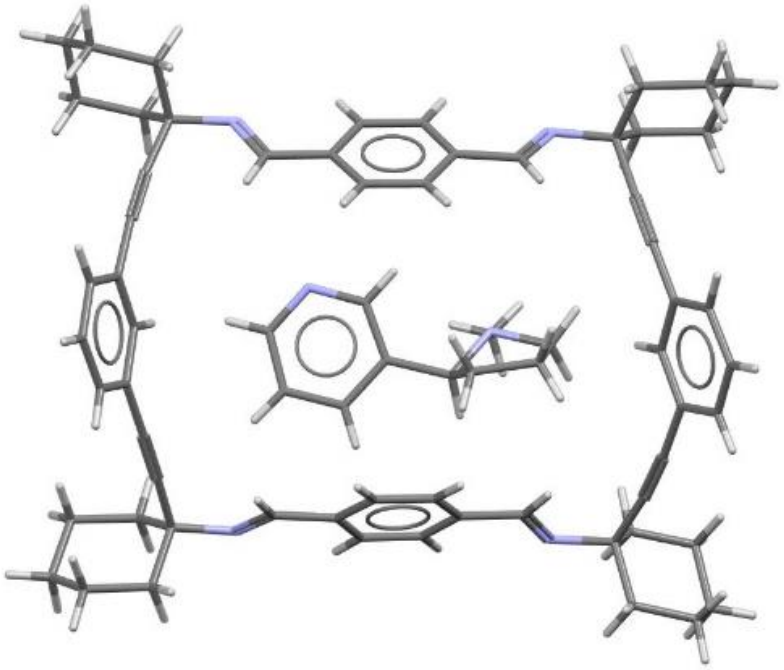

Figure 1. 18 Crystal structure of macrocyclic tetraimine and ethyl acetate POM with S-(−)-nicotine as guest.[117] *Adapted with permission from reference 117.*

1.6.2 Coordinative Alignment

The guest alignment in the pores of sponge **1** is mainly due to non-covalent weak interactions between host and guest that readily allow guest disorder. The coordinative alignment (CAL) method was developed to overcome this problem. In the CAL, guest molecules are covalently bonded to the metal centres of the MOFs thereby reducing the opportunities for the orientational disorder. In 2016 a chiral metal-organic framework, MOF-520, ($[Al_8(OH)_8(BTB)_4(HCO_2)_4]$) (BTB = 1,3,5-benzentribenzoate) was used by Yaghi and co-workers.[120] to coordinatively bind and align molecules of varying size, complexity, and functionality. MOF 520 was chosen as a crystalline sponge because of its high crystallinity and robustness. The framework has two types of pores that are approximately octahedral (10.01 Å × 10.01 Å × 23.23 Å) and tetrahedral (5.89 Å × 5.89 Å × 6.21 Å). The authors were successful in encapsulating 16 small molecules with alcohol and carboxylic acid functional groups. Figure 1.19 illustrates a molecule of 3,5-diaminobenzoic acid covalently bonded to the Al^{3+} ion via bridging of the carboxylate in the asymmetric unit of MOF-520. In 2019[121] MOF 520 was further used for the structure determination of azolates, sulfur oxoacids and phosphorus oxoacids. In addition, MOF 520 demonstrated enantiomeric

discrimination where two enantiomers of the chiral MOF selectively uptake *R* and *S* of the 2,3-dimethoxy-5,11,12,12a-tetrahydropyrazolo[3',4':4,5]pyrido[2,1-a]-isoquinolin-8(6H)-one from the racemic mixture. The *S* form coordinates to Δ-MOF-520 only, while the *R* form coordinates exclusively to Λ-MOF-520. It should be noted that with MOF-520 the X-ray data collection required synchrotron radiation and that guests without binding groups could not be studied. In contrast, Cohen and co-workers.[122] reported an Mn-based coordination porous framework – **5** (CPF-5) $(Mn_{21}(HCOO)_{18}(H_2O)_{12}(4\text{-tetrazolate-benzoate})_{12}$ as a crystalline sponge that binds several Lewis basic guests, such as pyridine and 3-aminopyridine, to the Mn^{2+} centre by coordinative alignment. Guest molecules without a binding group, for example, 1-aminoadamantane were stabilised in the hydrophilic pore by strong hydrogen bonding and good quality X-ray data was collected with an in-house diffractometer with Mo-Kα radiation.

Pelagatti and co-workers.[123] used a mesoporous Cu-based MOF $[Cu_6(H_2O)_6(TATB)_4 \bullet DMF \bullet 12H_2O]$ [TATB = 4,4',4"-(1,3,5-triazine-2,4,6-triyl) tribenzoic acid] for trapping nicotine by coordinative alignment. The X-ray analysis revealed the molecular structure of nicotine in which each Cu atom coordinates to the pyridine ring of the nicotine molecule. This contrasts with sponge **1** where nicotine severely damaged the crystals and therefore could not be analysed.[124]

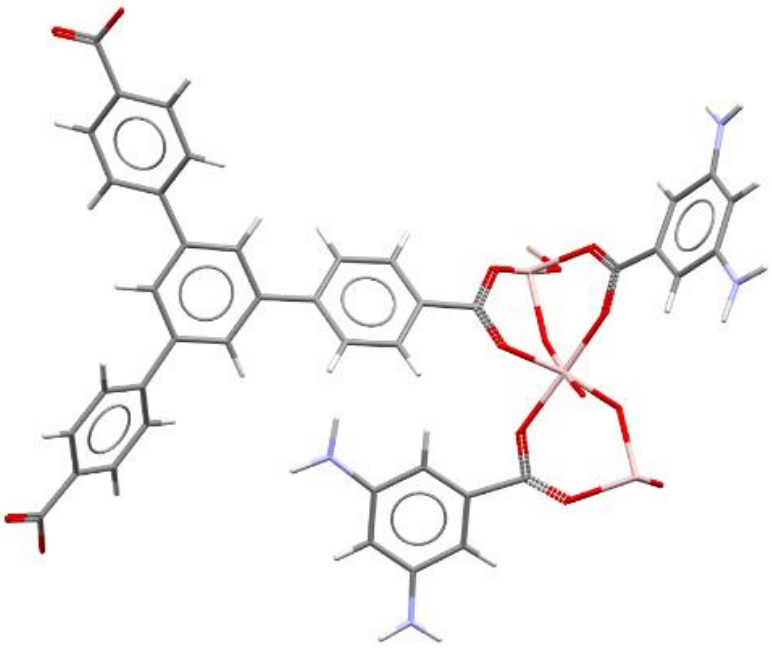

Figure 1. 19 The asymmetric unit of MOF-520 with 3,5-diaminobenzoic acid coordinated to Al^{3+} ion via bridging of carboxylates.[120] Adapted with permission from reference 120.

1.6.3 Hydrophilic MOF

Since sponge **1** is limited to encapsulation of hydrophobic guests, Fujita and co-workers.[125] developed a saccharide-based-crystalline sponge for the analysis of the hydrophilic compounds. The coordination network is composed of a *D*-mannose-based organic ligand and sodium ions. The pores are hydrophilic owing to multiple hydrogen bonding, however, too small in size (7.5 Å × 3.5 Å) to be useful for larger guest molecules. To address the incompatibility of sponge **1** with protic solvents Gelder and co-workers.[126] developed a crystalline sponge procedure in water where they used three Gd-based MOF, constructed from 1,3,5-benzenetribenzoic acid (H_3BTB) and 4,4',4''-(1,3,5-triazine-2,4,6-triyl)tribenzoic acid (H_3TATB) to trap guests. To investigate the stability, the new Gd-MOFs were exposed to various solvents such as methanol, water, *N*,*N*-dimethylformamide, acetonitrile and pyridine. It was observed that the Gd-MOFs remain stable whereas sponge **1** degraded. Both hydrophobic and hydrophilic guests were encapsulated into the host frameworks; one of the MOFs shows only van der Waals interactions with the guest molecules while the other two also have guest molecules coordinated to the metal centre. Examples of van der Waals interactions and coordinated guest molecules in Gd-MOFs are demonstrated in Figure 1. 20a,b. Carmalt and co-workers.[127] further demonstrated the capability of the Gd-MOF to encapsulate aromatic guests and a non-aromatic herbicide. Among the five guests, three of them were found coordinated to the metal atom of the framework and two guests were found in the pore, despite containing appropriate functional groups for coordination. In addition, the intermolecular interactions observed were found consistent with the original report.

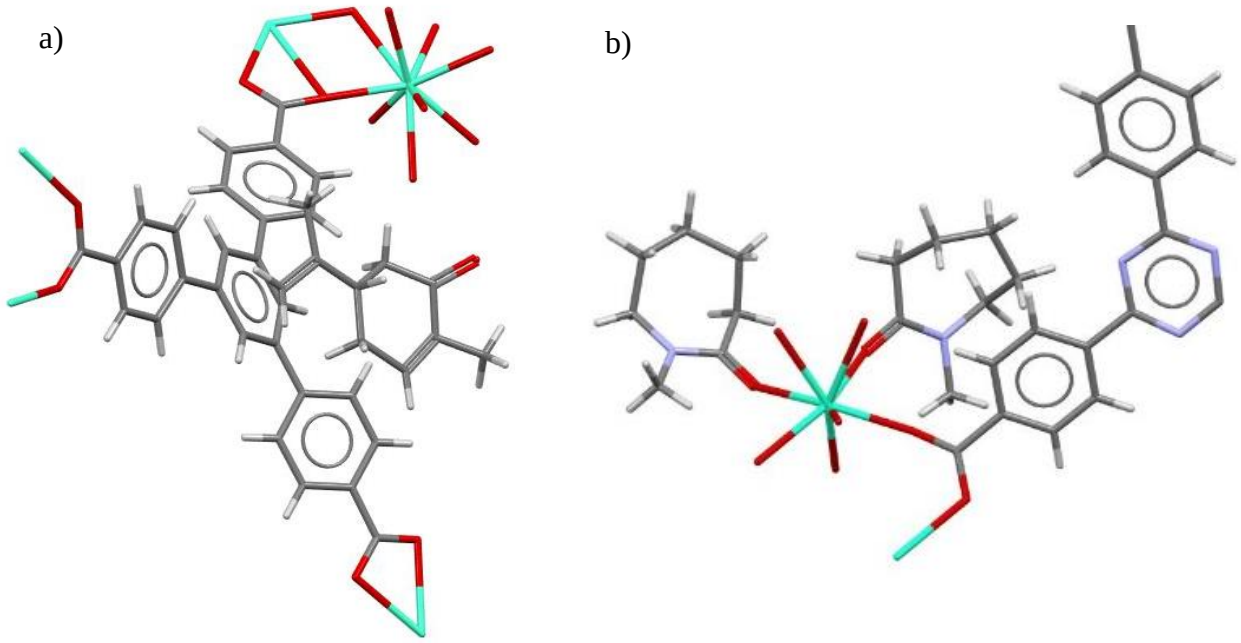

Figure 1. 20 a) Structure of carvone molecule ordered inside the pores of Gd-MOF via van der Waals interactions b) Asymmetric unit of Gd-MOF showing two molecules of ε-caprolactam coordinated to the Gd ion.[126] *Adapted with permission from reference 126.*

1.6.4 Chiral Metal-Organic Materials

Sponge **1** was successful in absolute configuration determination up to an extent, however, the incorrect stereochemistry assignment at C14 of miyakosyne A has been criticised.[128] Therefore, the development of chiral metal-organic materials as crystalline sponges was studied for the absolute structure determination of organic molecules. In this method, the guest chirality can be analysed by comparing its relative stereochemistry to the known chirality pre-installed in the host framework. Zaworotko and co-workers.[129] reported a pair of enantiomeric chiral metal−organic materials (CMOMs) based upon mandelate (man) and 4,4′- bipyridine (bpy) ligands combined with $Co(NO_3)_2 \cdot 6H_2O$. The enantiomeric pair of the framework $[Co_2(S\text{-man})_2(bpy)_3](NO_3)_2 \cdot$guest] and $[Co_2(R\text{-man})_2(bpy)_3](NO_3)_2 \cdot$guest] exhibit one-dimensional chiral channels of diameter 8.0 Å and the chiral surfaces were lined with nitrate anions and phenyl groups creating multiple binding sites for guest and/or solvent molecules. The guests encapsulated were 1-phenyl-1-propanol (PP), nitrobenzene, dichloromethane and cyclohexane. It was observed that the presence of the solvent molecules affected the availability of chiral binding sites and thus selectivity. For example, the *S* form of the framework with solvents prefer (*S*)-1-phenyl-1-propanol. Figure 1.21 shows the position of the (*S*)-1-phenyl-1-propanol in the asymmetric unit.

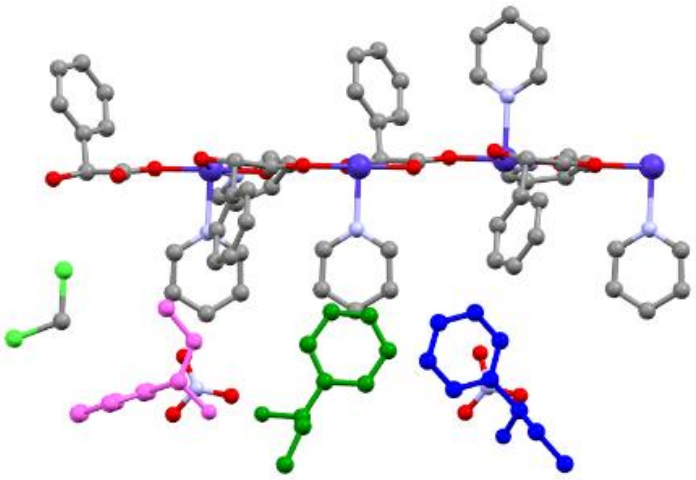

Figure 1. 21 The three (S)-1-phenyl-1-propanol molecules in the asymmetric unit (coloured magenta, green, and blue) in 1S·PP [129] *Adapted with permission from reference 129.*

Furthermore, Zaworotko and co-workers.[130] develop various variants of $[Co_2(man)_2(bpy)_3](NO_3)_2]$ for enantioselective separation/identification of racemic mixtures. The CMOM-3S variant was used as chiral stationary phase (CSP) in gas chromatography (GC) for chiral purification and enantiomeric identification. Similarly, chiral discrimination was studied with variants of CMOM-3S using a racemic mixture of phenyl propanol.[131] The CMOMs as crystalline sponges enabled the use of X-ray crystallography to provide detailed insight into the molecular recognition phenomena that impacted chiral separation.

In 2020 Fujita and co-workers.[132] reported a chiral metal-peptide porous complex $[(Ag\cdot 2\text{-aminoisobutylic acid})_2(OH)(PF_6)(EtOH)_m(H_2O)_l]_n$, which was used to study chiral alcohols and ketones. For example, the *S* configuration of (*S*)-1,2-propanediol was confirmed by comparing the relative stereochemistry with respect to the chiral peptide framework. Furthermore, Pardo and co-workers.[133] reported a chiral honeycomb-like three-dimensional (3D) calcium(II)–copper(II) network with the formula $\{Ca^{II}Cu_6^{II}$ [(*S*,*S*-serimox]$_3(OH)_2(H_2O)\}\cdot 39H_2O$ (serimox = *bis*[(*S*)-serine]oxalyl diamide). The channels of this MOF have hydroxyl groups pointing towards the accessible void space which provided a hydrophilic environment. Two vitamins [ascorbic acid (vitamin C) and pyridoxine (vitamin B6)], one anti-depressant (bupropion) and the primary female sex hormone (17-*β*-estradiol) were encapsulated. SCXRD revealed that strong hydrogen bonds were responsible for organising vitamins C and B6 in the pores. In contrast, the larger and less polar guest molecules bupropion and 17-*β*-estradiol were packed by very weak, but highly efficient C–H···O van der Waals interactions.

1.6.5 Other MOFs

Zhou and co-workers.[134] synthesised a MOF from a flexible thioether-based linker (1,3,5-tris(4-pyridylsulfanylmethyl)-2,4,6-trimethylbenzene and a stair-like $\{Cu_4I_4\}$ cluster. This flexible framework has an electron-rich pore environment that possesses a strong affinity for electron-deficient small molecules such as *N*,*N*-dimethylformamide which were observed within the pores of the framework. Su and co-workers.[135] used a flexible Cu-MOF synthesised from $Cu(NO_3)_2 \cdot 2.5H_2O$ and the fluorinated ligand (2,2′-bis(trifluoromethyl)-4,4′-biphenyldicarboxylic acid to encapsulate liquids such as *N*,*N*-dimethylacetamide. The suitable pore size, electron-rich channel environment, and low symmetry space group ($P2_1/c$) make it an ideal candidate for a crystalline sponge. The trifluoromethyl group from the ligand and H-bond receptor O atoms from the polar Cu─O chain possess a strong affinity towards the polar ends of the guest molecules, therefore, the major interactions observed between host and guest were H-bonding.

1.6.6 Coordination Cages

In the field of supramolecular chemistry, coordination cages are a popular area of investigation because of their ability to bind small-molecule guests in their cavities. The host-guest chemistry of such cages has been exploited in many ways, varying from fundamental studies of molecular recognition properties to catalysis. Coordination cages have recently been used for host-guest studies consistent with the CSM when trapping the guest within the cavity via cocrystallisation

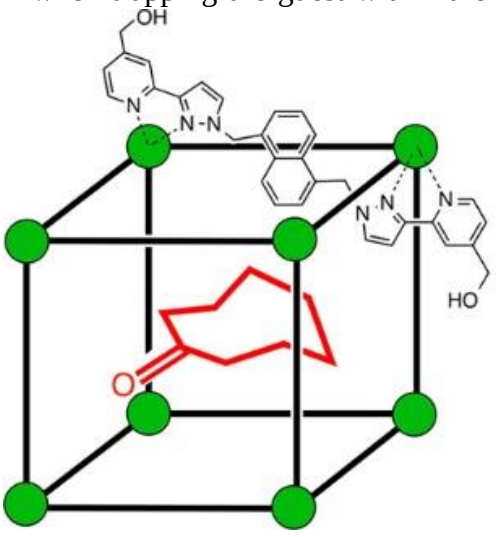

Figure 1. 22 The cubic host cage of $[Co_8L_{12}](BF_4)_{16}$. One bridging ligand on a cube edge is shown simultaneously chelating two Co^{+2} ions. Cycloundecanone sits inside the cavity.[136] *Reused with permission from reference 136.*

was unsuccessful. The host cage used as a crystalline sponge was a $[Co_8L_{12}](BF_4)_{16}$], based on bridging ligands that contain two chelating bidentate pyrazolyl-pyridine termini, connected to naphthalene-1,5-diyl spacer via flexible methylene units, as shown in Figure 1.22. It has a large enough cavity to bind an interesting range of guests and is, therefore, suitable as a crystalline sponge. In 2015 Ward and co-workers.[136] used this cage as a crystalline sponge for the structure determination of cycloundecanone and di(isopropyl)methyl phosphonate (Figure 1.22) since earlier attempts to isolate the host-guest complex via cocrystallization were unsuccessful. The successful result led to other studies using this cage, for example, the structure determination of adamantane-1-carboxylic acid[137] and alkyl-phosphonate chemical warfare agent simulants.[138] In 2020 Ward and co-workers.[139] performed a crystallographic investigation of a series of bicyclic compounds including coumarins using this cage and also demonstrated the guest binding ability to both the internal and external surfaces of this cage.[140]

1.6.7 Biological frameworks

Inspired by the macromolecule's binding abilities, some of the biologically based frameworks were used as a crystalline sponge, although only a few examples have been reported in the literature. Matsumoto and co-workers.[141] used a multidrug-resistance regulator protein (RamR) as a crystalline sponge for the structure determination of organic compounds. This has flexible and large binding pockets consisting of charged, polar, and hydrophobic residues. 4-((3-Chloro-4-fluorophenyl)amino)-7-methoxyquinazolin-6-ol was encapsulated in RamR which is an analogue of the synthetic intermediate of gefitinib (the active pharmaceutical ingredient of an anticancer agent). The crystal structure of RamR-gefitinib complex was successfully determined by SCXRD shown in Figure 1.23. Furthermore, Snow and co-workers.[142] selected a protein-based crystalline sponge with binding sites available for guest binding via chemical conjugation. The crystal structure of several active reagents was demonstrated via CSM.

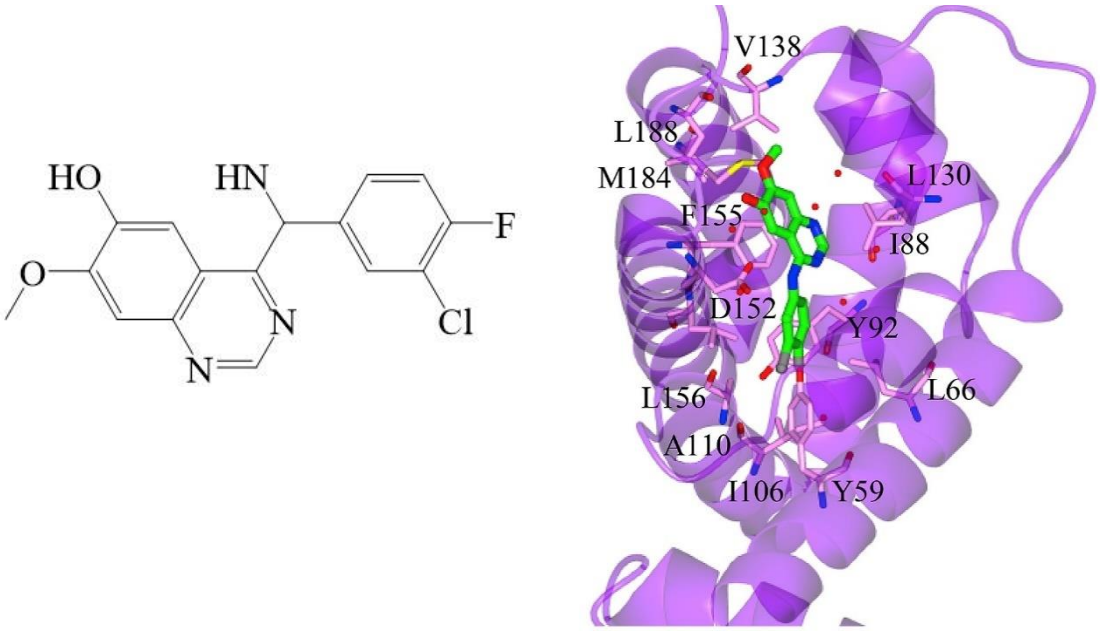

Figure 1. 23 a) Line diagram of gefitinib intermediate. Structure of the RamR−gefitinib Intermediate complex. The protein is represented as a purple ribbon diagram. Gefitinib Intermediate is shown in capped stick style.[141] *Reused with permission from reference 141.*

1.7 Limitations and Prospects

The CSM has proved successful in overcoming many of the limitations associated with traditional X-ray analysis and provided researchers with a new analytical technique for the analysis of the crystal structures of liquids and trace samples. The CSM has expanded rapidly in the last eight years and has been applied in various fields such as pharmaceuticals in drug discovery, agrochemicals, perfume, and aroma chemical companies for analyses of active ingredients, impurities, or metabolites. However, there are a few limitations of the technique which should be addressed and resolved. It is important to note that although the CSM provides crystal-free crystallography for target compounds the crystals of the sponge should be of high quality with no defects such as cracking and twinning and should be able to withstand different temperatures during encapsulations and a range of concentrations of the guest. This is particularly necessary since the trial-and-error approach is used to optimise the soaking conditions by varying numerous parameters. Even with the tremendous success in application to various fields, the CSM is still in its early stage of development. To expand CSM for the study of a wider range of guest molecules development of new sponges is essential, hence, researchers have developed a variety of crystalline sponges based on POMs, CMOM, coordination cages, and biological frameworks. It is clear that

there is not one perfect sponge that is suitable for all types of guest molecules, therefore the discovery and development of new sponges remain highly desirable. In this thesis, several MOFs with the appropriate pore size, hydrophilic/hydrophobic pore environment, and stability toward the guest were selected from the Cambridge Structural Database (CSD) and investigated as crystalline sponges.

ENCAPSULATION OF TERPENES 2

2.1 INTRODUCTION

This chapter describes the synthesis of the most successful crystalline sponge $[\{(ZnI_2)_3(TPT)_2 \cdot 6(CHCl_3)\}_n]$ (**1**) and its $ZnBr_2$ analogue $[\{(ZnBr_2)_3(TPT)_2 \cdot 6(CHCl_3)\}_n]$ (**2**) and novel encapsulations of terpenes. Sponge **1** and **2** were chosen as their applicability has been demonstrated in previous studies and was successful in the structure determination of complex structures. The guest molecules used in this study are of an appropriate size for inclusion in sponges **1** and **2**. Previous work by Carmalt and co-workers.[143,144] suggested that a small change in size and functionalities of guest molecules influenced ordering and orientations. Therefore, terpenes with different functional groups were encapsulated in crystal sponges **1** and **2** to study their structure and orientational interactions with the host framework.

Terpenes are naturally occurring organic chemicals produced by plants and some insects. Their strong aromatic qualities contribute to the perfume industry, agribusiness interested in their potential pesticidal properties, and their role in traditional herbal remedies interests pharmaceutical and biotechnology industries to guide the synthesis of potential drugs. With this motivation, the guest molecules selected for this research have medicinal properties such as anti-inflammation, anti-cell proliferation, selectively killing leukaemia cells, and function as metabolites in biosynthesis.[145–148]

2.1.1 Guests selection

Guests selected for this study were classified into two categories based on their functional groups.

Guest series **A**: geraniol, farnesol, and prenol, which have hydroxyl as the functional group (Figure 2.1).

Guest series **B**: α-ionone, β-ionone, and β-damascone, which have ketonic carbonyl functional groups (Figure 2.2).

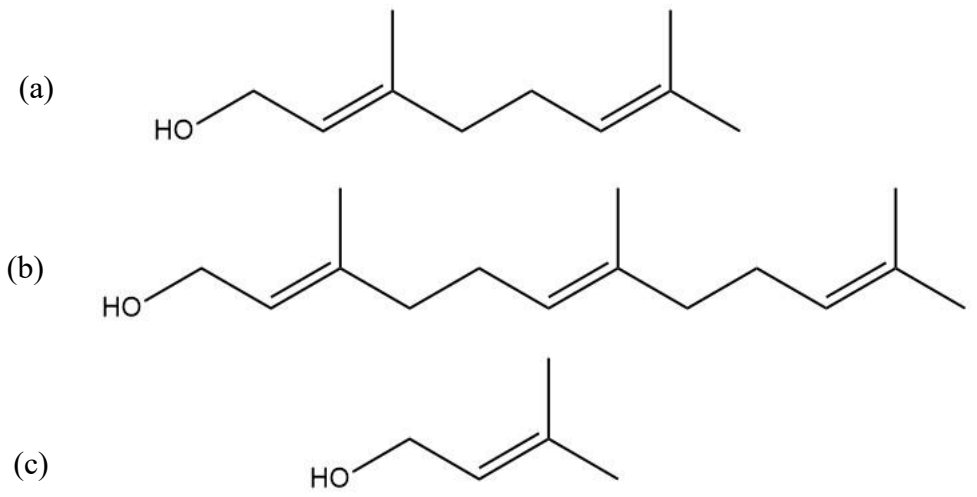

*Figure 2. 1 Guest series **A**: a) Geraniol b) Farnesol c) Prenol.*

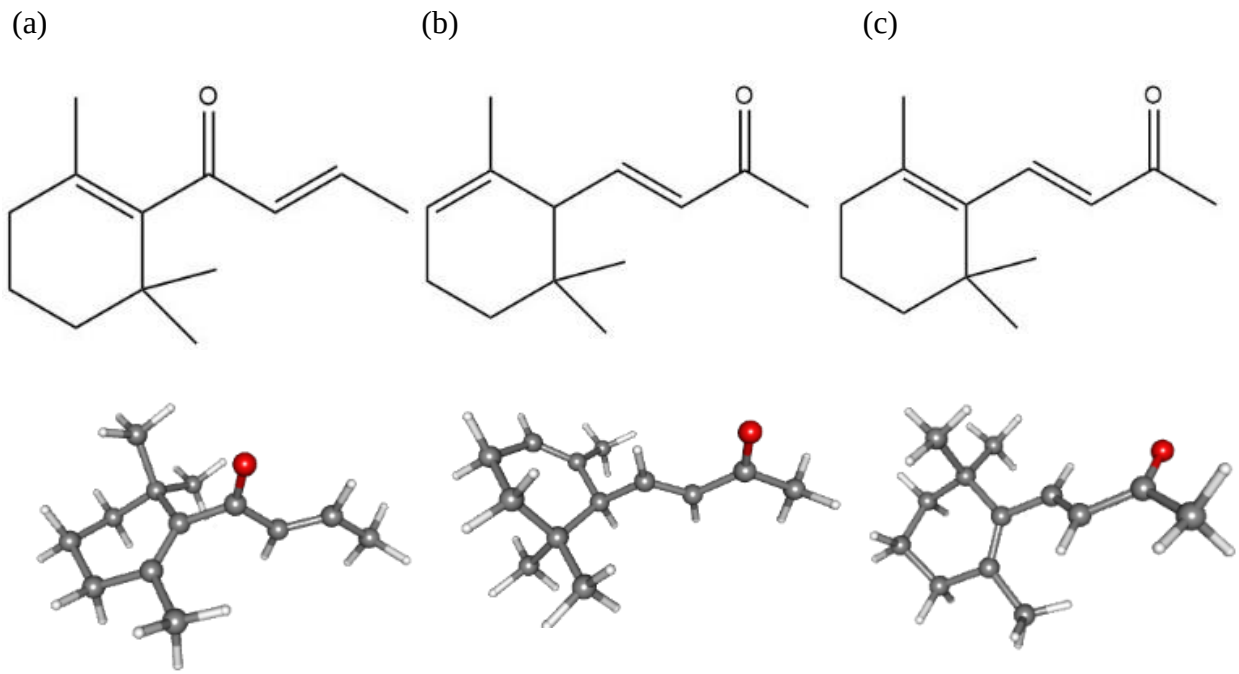

*Figure 2. 2 **.** Line diagrams of guest series **B** along with their 3D conformers: a) β-Damascone, b) α-Ionone, c) β-Ionone.*

2.2 RESULT AND DISCUSSION

2.2.1 Series **A**:

From series **A** encapsulation with geraniol and farnesol was successful and the structure of the guests was determined in the pores of the sponge **1**. Guest encapsulation was first attempted with neat liquids to obtain higher occupancies however, this resulted in cracking of the crystals, which were therefore not suitable for X-ray diffraction. Hence, a strategy was developed where the guest was dissolved in cyclohexane before soaking. Several soaking conditions were investigated, and optimisation of the parameters gave maximum occupancies as well as the best quality crystals for X-ray diffraction measurements. Details of the soaking experiments for geraniol and farnesol are given in Section 2.3 in Tables 2.2 and 2.3.

Inclusion complex with geraniol

Single crystal X-ray analysis showed the structure of geraniol within the pores of the framework of **1**.[149] The guest−host complex was found to crystallise in the centrosymmetric space group *C*2/*c*, showing a slight expansion in cell dimensions compared with the as-prepared crystalline sponge **1**. One guest molecule was found per asymmetric unit with a 20% occupancy, along with one well-characterised residual $CHCl_3$ molecule (from the synthesis of **1**). All the atoms of the guest were found and modelled. The packing diagram is displayed in Figure 2.3a and revealed that the guest molecule was positioned over the aromatic panel of the tris(4-pyridyl)-1,3,5-triazine (TPT) and was interacting with two of the pyridyl rings and a triazine ring Figure 2.3b and c. The formation of CH-π interactions and π-π interactions were observed between the guest and the framework. The $C_{geraniol}$—$centroid_{pyridine}$ interactions were 3.7 and 3.8 Å, $C_{geraniol}$—$centroid_{triazine}$ distance was 3.6 Å, and π-π interactions between $C{=}C_{geraniol}$ and the $centroid_{pyridine}$ of the framework was observed at 4.0 and 4.1 Å, as illustrated in Figure 2.3b,c. Since geraniol has a hydroxyl group it might be expected to form a hydrogen bond with the host framework, however, the length of $O_{geraniol}$—$C_{pyridine}$ interaction was 4.2 Å, larger than that normally expected between the two heavy atoms to form a hydrogen bond which would be ~2.7 – 3.3 Å.[34]

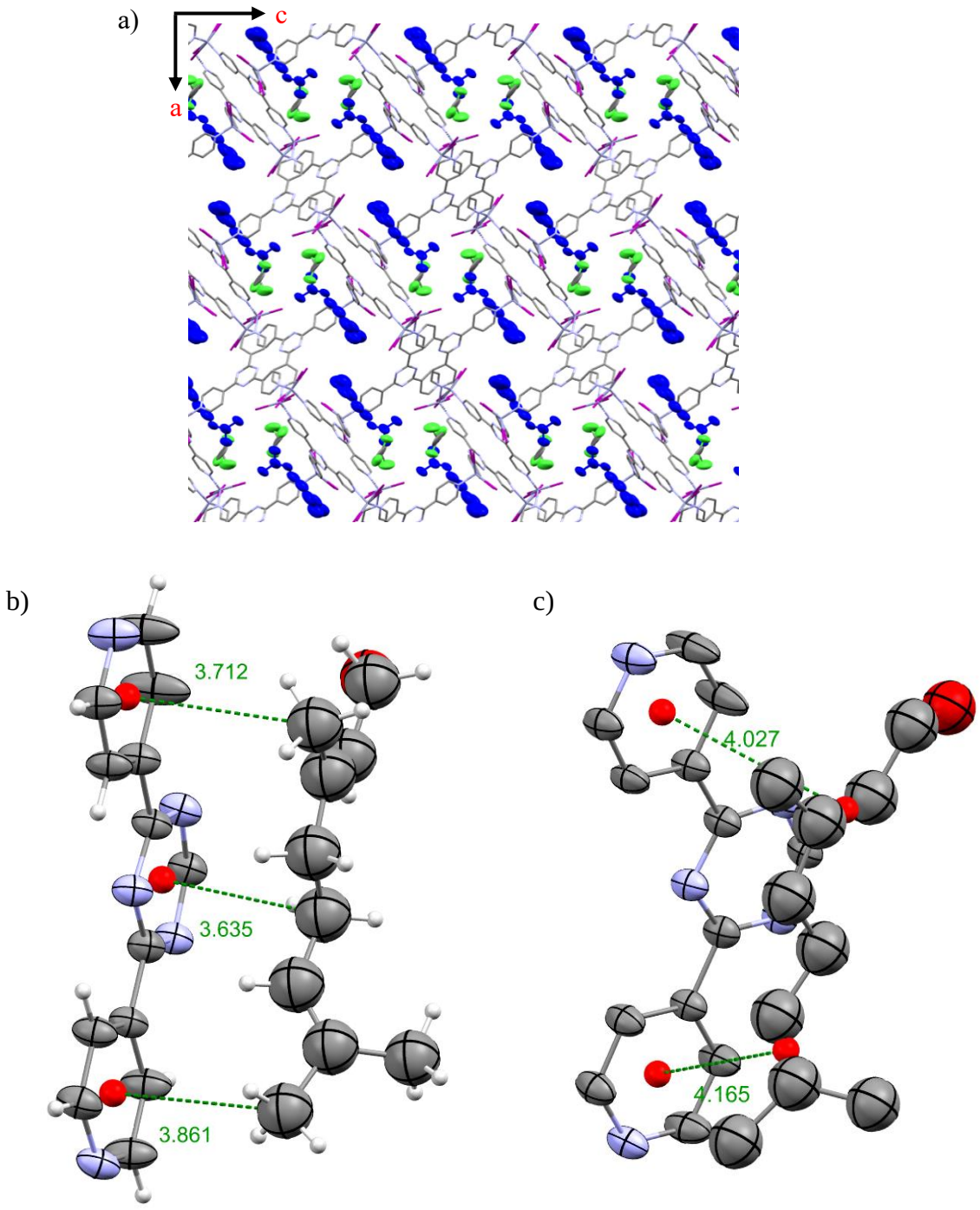

Figure 2. 3 Packing diagram of geraniol inclusion complex viewed down the b axis. Framework shown as capped stick model, geraniol as ellipsoids shown in blue, residual chloroform in green colour. Hydrogen atoms have been omitted for clarity; b) CH-π interactions between part of the host framework and geraniol c) π-π interactions of part of host framework and geraniol. Geraniol molecule displayed in ellipsoids at 50% probability. Reused with permission from reference 149

Inclusion complex with farnesol

The encapsulation complex of 1 with farnesol crystallised in the centrosymmetric space group *C*2/*c*.[149] One guest molecule was found per asymmetric unit with 15% occupancy and no residual solvent was refined. The guest molecule was found disordered about the crystallographic 2-fold axis. One of the methyl groups attached to C44 was severely disordered, therefore could not be modelled. Figure 2.4a shows a packing diagram with farnesol positioned over only one of the pyridine rings and appearing to be stabilised by several interactions with that unique pyridine ring of the host. Each farnesol molecule forms four CH-π and one π-π interaction with the unique pyridine. Each of the three C=C bonds in farnesol interacts with the host framework. The unique π-π interaction between a C=C of farnesol and the centroid of the pyridine ring was observed at 4.1 Å. The other two C=C of farnesol each take part in CH-π interactions and as displayed in Figure 2.4b were 3.0 Å, 3.8 Å, 3.6 Å, and 3.4 Å. Similarly, to geraniol, no H-bonding between the hydroxyl group of farnesol and the framework was observed, with the shortest Ofarnesol—Hpyridine distance being 3.2 Å. Since farnesol is similar in structure to geraniol but with a longer carbon chain, it was expected to show some similarity in positioning inside the pore as a previous study had suggested this was observed for related molecules.[143] However, in this case, these two guest molecules were found situated at different sites relative to the tris(4-pyridyl)-1,3,5-triazine), TPT linker of the framework. Geraniol interacted with two pyridyl rings and a triazine ring, whereas farnesol shows interaction with that unique pyridyl ring only since the ends of the chain are extended into the adjacent pores (see Figures 2.3b–2.4b).

From the literature, it was noted that other related guest molecules containing a hydroxyl group have been encapsulated in sponge **1**. For example, among the four guests, 2-azido-1-phenyl-ethanol and dimethyl L-(+)-tartrate were found interacting with the framework with a hydrogen bond.[150] In both cases, there were four molecules present in the asymmetric unit, however, only one molecule sitting in a unique site was interacting with the TPT panel through a hydrogen bond. The hydrogen bond distances were OH···$N_{triazine}$ 2.308 Å and OH···$HC_{pyridine}$ 2.425 Å respectively, which suggests that only specific sites allow hydrogen bonding interactions.

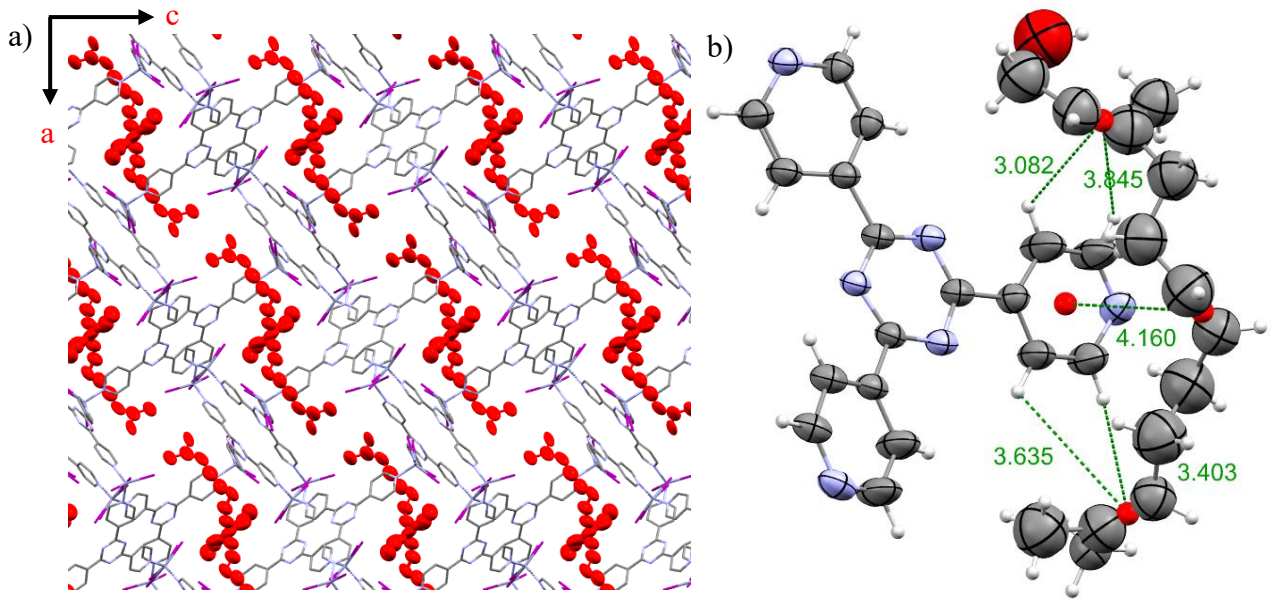

Figure 2. 4 a) Packing diagram of farnesol inclusion complex viewed down the b axis. Framework shown as capped stick model, farnesol as ellipsoids shown in red colour, Hydrogen atoms have been omitted for clarity; b) CH-π and π - π interaction between host framework and farnesol. Farnesol molecule displayed in ellipsoids with 50% probability. Reused with permission from reference. 149

Inclusion complex with prenol

Several soaking conditions with the neat and diluted guest were attempted with sponges **1** and **2** however, deterioration of the crystals was observed in each case and hence data collection was not performed. Details of different soaking conditions attempted to encapsulate prenol with sponges **1** and **2** are shown in Table 2.4.

2.2.2 Series **B**:

Among the three terpenes from this series, only one was successfully encapsulated. The optimisation conditions used to obtain high-quality crystal data for encapsulation complex with β-damascone are detailed in Section 2.3 in Table 2.5.

Inclusion complex with β-damascone

The crystals of β-damascone encapsulated into **1** were obtained in the *C*2/*c* space group with one guest molecule per asymmetric unit at 60% occupancy, along with one molecule of cyclohexane, and no disorder in the guest molecule was observed.[149] Figure 2.5a shows a packing diagram with β-damascone in the pores along with residual cyclohexane (from the solvent exchange). Figure

2.5b is showing the host−guest interactions. In this example, dominant interactions were found to be CH-π interaction with $CH_{\beta\text{-damascone}}$—$centroid_{pyridine}$ of 3.0 Å, $CH_{\beta\text{-damascone}}$—$centroid_{triazine}$ of 3.5Å and the carbonyl group of β-damascone interacting with the triazine ring forming a contact distance $C{=}O_{\beta\text{-damascone}}$—$N_{traizine}$ of 3.0 Å. Although two C=C bonds are present in β-damascone, no π-π interactions were observed because the orientation of the side chain containing the C=C bond was in the pore, as shown in Figure 2.5b. In addition, the shortest $C{=}O_{\beta\text{-damascone}}$—$H_{pyridine}$ distance was 4.0 Å, suggesting that the position and orientation of β-damascone in the pore did not allow hydrogen bond formation. A similar observation was found in a previous study,[143] where a *trans*-cinnamaldehyde molecule formed a hydrogen bond at one site in the pore, whereas on the other site a carbon chain containing the carbonyl group of *trans*-cinnamaldehyde extended too far into the pore, therefore not forming a hydrogen bond with the framework. Furthermore, a metabolite analysed from adrenosterone within sponge **1** showed C=O···H hydrogen bond interactions between only one guest molecule and the framework among the three guest molecules present in the asymmetric unit.[2] This unique guest molecule was positioned in a unique site compared to the other two molecules. Thus, the orientation and site of the guest inside the pore play an important role in the formation of a hydrogen bond.

The packing diagram is given in Figure. 2.5a, shows this guest molecule is interestingly positioned on a site similar to geraniol, with a slight rotational difference with respect to the TPT linker, which is evident by comparing CH-centroid distances. In Figures 2.3b and 2.5b, CH—$centroid_{triazine}$ distances are comparable because both the guests interact with the triazine ring and one of the CH—$centroid_{pyridine}$ interactions is also common to both the guests. However, the other CH—$centroid_{pyridine}$ distance was different since both guests were interacting with a different pyridyl ring. In addition, the guest molecule appears to occupy every alternate pore, unlike the other two encapsulation complexes discussed in this chapter. However, the number of guest molecules in the unit cell is the same in all three novel complexes. With closer examination of the packing diagram, it was revealed that β-damascone was positioned in such a manner that the carbon chain of the molecule is held within the same pore. In contrast, for geraniol and farnesol, the carbon chains extend into the adjacent pore, therefore geraniol and farnesol occupy a larger pore space compared to β-damascone.

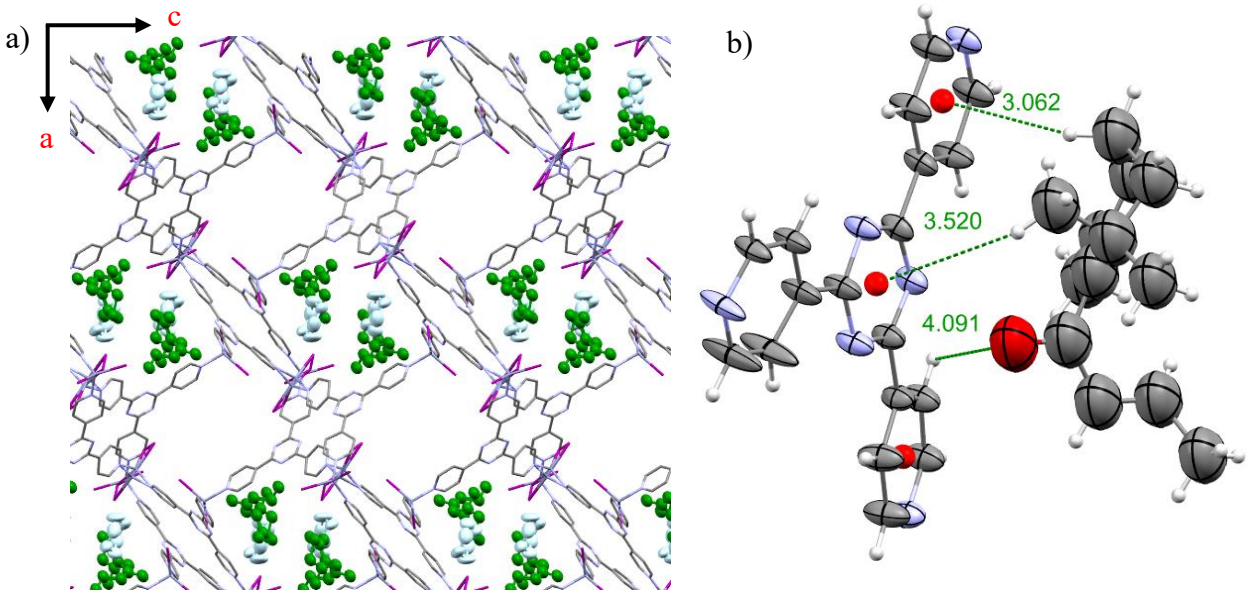

Figure 2. 5 a) Packing diagram of β-damascone inclusion complex viewed down the b axis. Framework shown as capped stick model, β-damascone as ellipsoids shown in green colour, residual cyclohexane in light blue colour. Hydrogen atoms have been omitted b) CH-π interaction between host framework and β-damascone. β-damascone molecule displayed in ellipsoids at 50% probability. Reused with permission from reference 149.

Inclusion complex with α-ionone and β-ionone

A partial guest was observed in the pores of **1** in both cases. In Section 2.3, Table 2.5 summarises the soaking conditions and observed results for α and β-ionones. After 6 days of the incubation period, a fragment of the guest structure of α-ionone was observed in the pores of sponge **1**. Similarly, with β-ionones partial guest molecules were observed after 7 days of the incubation period. Later attempts with an increase in the incubation time resulted in severely degraded crystals not being suitable for data collection. Observation of partial guest structures in the pores of sponge **1** was previously reported.[124] For example, the partial structure of nifedipine (a drug) was found in the pores sponge **1**. Similarly, for five other guests, only a partial structure was observed.

The dominant host-guest interactions in all three complexes discussed in this chapter were found to be similar to previously reported non-aromatic terpenes. Since the novel terpenes encapsulated in this study are non-aromatic the pi-electron density of an isolated double bond engages in π-π interactions with the centroid of the aromatic TPT panel. The π-π and CH-π distances were comparable to those previously reported for non-aromatic terpenes, as shown in Table 2.1. However, the relative strength of the host-guest interactions cannot be compared with other non-

aromatic guests as in CSM interactions are required only to be strong enough to regularly order the guest molecules in the pores and any discussion based on length is highly speculative. Additionally, this work was compared with the other functionalised terpenes encapsulated by Fujita and co-workers.[11] Terpene natural products extracted from *Laurencia pacifica* with a hydroxyl functional group were encapsulated and in no instance were any OH groups found to form hydrogen bonds with the framework. These comparisons suggest, since the ordering of the guests inside the pores was dominated by CH-π and π-π interactions, that the formation of hydrogen bonds was not favoured unless the guest has occupied a unique site and orientation was favourable for such a bond. This reflects the hydrophobic nature of the tris((4-pyridyl)-1,3,5-triazine)$_2$, TPT link.

Table 2. 1 Comparison of CH-π and π-π interaction between non-aromatic terpenes in the pores of the host framework. (†this work)

Guest	geraniol†	farnesol†	β-damascone†	rac-camphene[113]	rac. α-pinine[113]	β-pinine[113]	Astellifadiene[14]
CH-π	3.18 Å	3.1 Å	3.4 Å	3.3 Å	3.4 Å	3.3 Å	3.1 Å
π -π	4.1 Å	3.9 Å	-	4.9 Å	4.1 Å	4.4 Å	4.4 Å

2.2.3 Conclusions

Three novel inclusion complexes were synthesised with terpenes as guests through the crystalline sponge method, further validating the utility of this exciting new methodology and expanding the range of structures solved. The chosen guests have an important role in the biotech and agribusiness context, and further understanding of their non-crystalline low energy conformations could provide insights into biological mechanisms and potential analogue design. Along with the structure determination of the guests, their interactions with the host framework were studied.

These non-aromatic terpenes have comparable host-guest interactions to the other reported non-aromatic terpenes. That is CH-π and π-π were identified as the dominating interactions and no interactions between the functional group (hydroxyl or carbonyl) in the guests and the host framework were observed.

2.3 EXPERIMENTAL SECTION

2.3.1 Crystalline sponge synthesis

[{$(ZnI_2)_3$(tris(4-pyridyl)-1,3,5-triazine)$_2$·$(CHCl_3)$}$_n$] (**1**) was prepared following the modified procedure reported in the literature.[151] [{$(ZnI_2)_3$(tris(4-pyridyl)-1,3,5-triazine)$_2$ $(CHCl_3)$}$_n$] has pore dimensions of 8 Å × 5 Å and the solvent-accessible voids per unit cell were 4714 $Å^3$ which is 47.9% of the unit cell volume. Similarly, crystalline sponge **2** was synthesised with a modified literature procedure.[87]

2.3.2 Guest Encapsulation experiment

In initial guest encapsulation experiments crystals were soaked in neat liquid guests but the deterioration of the crystals was observed in each case. Therefore, a strategy was developed where guests were dissolved in a solvent, such as chloroform or cyclohexane, before soaking. Several soaking conditions were investigated to obtain the best quality crystal data and optimise guest occupancy. Parameters such as guest: solvent ratio, temperature, and length of incubation period were optimised in each case. All attempted soaking experiments with chloroform resulted in either deterioration of crystals or poor diffraction of the crystals on X-ray exposure. In contrast, soaking experiments with cyclohexane were successful and three encapsulation complexes were obtained with guests dissolved in cyclohexane. In addition, in all cases with longer incubation period crystals start to develop cracks making them unsuitable for X-ray diffraction experiments. Furthermore, in other cases, while crystals looked of good quality on optical examination, they did not show strong peaks when placed on the diffractometer. Experimental conditions are listed in the tables below.

Table 2. 2 Soaking conditions for inclusion complex with geraniol

Guest	Solvent/ Cyclohexane	Soaking temperature	Incubation period/days	Result
2 mL	-	25 °C	1	Crystals deteriorated
100 µL	2 mL	25 °C	17	Crystal changed colour to dark red but did not diffract
40 µL	2 mL	25 °C	3	Incomplete guest found in the pores with 25% occupancy
40 µL	2 mL	25 °C	7	Guest found in the pores with 40% occupancy
40 µL	2 mL	25 °C	13	Crystals optically look fine but are not diffract
40 µL	2 mL	50 °C	7	Crystals deteriorated
20 µL	2 mL	50 °C	7	Crystals deteriorated

Table 2. 3 Soaking conditions for inclusion complex with farnesol

Guest	Solvent/ Cyclohexane	Soaking temperature	Incubation period/days	Result
2 mL	-	25 °C	1	Crystals deteriorated
100 µL	2 mL	25 °C	6	Crystals optically look fine but did not diffract
40 µL	2 mL	25 °C	2	Crystals optically look fine but did not diffract
40 µL	2 mL	25 °C	6	Crystals optically look fine but did not diffract
20 µL	2 mL	25 °C	6	Crystals optically look fine but did not diffract
10 µL	2 mL	10 °C	10	Incomplete guest found
10 µL	2 mL	10 °C	12	Guest found with 30% occupancy
10 µl	2 mL	10 °C	18	Crystals optically look fine but did not diffract

Table 2. 4 Soaking conditions attempted to encapsulate prenol

Guest/Prenol	Solvent/ 1 mL	Soaking temperature	Incubation period/days	Result
2 mL	-	25 °C	1	Crystals deteriorated
1 mL	$CHCl_3$	25 °C	2	Crystals deteriorated
500 mL	$CHCl_3$	25 °C	3	Crystals deteriorated
100 mL	$CHCl_3$	25 °C	3	Crystals deteriorated
40 µL	$CHCl_3$	25 °C	3	Crystals deteriorated
10 µL	$CHCl_3$	10 °C	3	Crystals deteriorated
1 mL	C_6H_{12}	25 °C	2	Crystals deteriorated
500 µL	C_6H_{12}	25 °C	3	Crystals deteriorated
100 µL	C_6H_{12}	25 °C	3	Crystals deteriorated
40 µL	C_6H_{12}	25 °C	3	Crystals deteriorated
10 µL	C_6H_{12}	10 °C	3	Crystals deteriorated

Table 2. 5 Soaking conditions for inclusion complex with β-damascone

Guest	Solvent/ Cyclohexane	Soaking temperature	Incubation period/days	Result
2 mL	-	25 °C	1	Crystals deteriorated
20 µL	2 mL	25 °C	7	Crystals are diffracting guest not found
20 µL	2 mL	10 °C	7	Crystals deteriorated
40 µL	2 mL	25 °C	7	Crystals are diffracting guest found with 60% occupancy
40 µL	2 mL	25 °C	14	Crystals optically look fine but did not diffract
40 µL	2 mL	25 °C	30	Crystals deteriorated

Table 2.6 soaking conditions attempted to encapsulate α and β-ionone.

Host framework (Sponge)	Guest (µL)	Solvent	Soaking temperature	Incubation period	Result
α-ionone					
1	40 µL	C_6H_{12}	25 °C	4	guest not found
1	100 µL	C_6H_{12}	25 °C	6	partial guest structure found
1	100 µL	C_6H_{12}	25 °C	10	crystal deteriorated
1	40 µL	C_6H_{12} /2ml	25 °C	60	poorly diffracting
2	100 µL	$CHCl_3$/2ml	25 °C	15	poorly diffracting
2	40 µL	$CHCl_3$/2ml	25 °C	60	cracked crystals
β-ionone					
2	100 µL	$CHCl_3$	25 °C	7	partial guest found
2	100 µL	$CHCl_3$	25 °C	14	poorly diffracting
2	40 µL	$CHCl_3$	25 ˚C	7	poorly diffracting
2	40 µL	C_6H_{12}	25 ˚C	7	poorly diffracting

2.3.3 Crystallographic procedures

Crystals were placed in fomblin, and single crystals were selected and mounted onto nylon loops. X-ray diffraction data were recorded at 150 K on an Agilent Super Nova dual diffractometer (Agilent Technologies Inc., Santa Clara, CA) with Cu K_α radiation (λ = 1.5418 Å). Unit cell determination, data reduction, and absorption corrections were carried out using CrysAlisPro.[152] The structures were solved by direct methods and refined by full-matrix least-squares based on F^2 using SHELXL[153] within the OLEX 2.0[154] GUI. Generally, non-hydrogen atoms were refined anisotropically, and hydrogen atoms were included using a riding model but see individual reports on the refinement of guest molecules.

2.3.4 Structural analysis details

The structures were solved by direct methods and refined by full-matrix least-squares based on F^2 using SHELXL[153] within the OLEX 2.0[154] GUI. Non-hydrogen atoms of the framework were

refined anisotropically and hydrogen atoms were included using a riding model. The TPT and Zn components of the framework were freely refined without constraints or restraints. The iodine component of the framework displayed some disorder and where required atoms were modelled across two positions with a combined occupancy of 100%. DFIX was used to restrain the bond lengths of the Zn-I minor component of the framework. Refinement of guest species was first performed without any constraints/restraints and only if this was unsuccessful, they were added based on their known structures. The occupancy of each guest molecule was refined against its own free variable which in the final stages of refinement was fixed to values reported. Standard deviations for restraints used are as follows:

- DFIX S_1 = 0.02 Å S_2 = 0.01 Å S_3 = 0.005 Å
- DANG S = 0.04 Å
- SIMU S_1 = 0.04 $Å^2$ S_2 = 0.08 $Å^2$
- ISOR S_1 = 0.01 $Å^2$ S_2 = 0.001 $Å^2$

2.3.5 Refinements of individual guests in each inclusion complex

Geraniol

Anisotropic refinement of the non-hydrogen atoms of geraniol was performed by applying constraints/restraints to achieve a stable model. DFIX was used to fix bond lengths to obtain a realistic and acceptable geometry. DANG was applied to C39, SIMU and ISOR commands was used to restrain ADPs all non-hydrogen atoms. Hydrogen atoms were added by riding model. Hydrogens on C40, C45, and C46 show disorder due to freely rotating methyl groups and were fixed by using HFIX 137. At the end of the refinement large solvent accessible voids were detected, these would be filled with heavily disordered solvent or guest molecules that could not be refined in a way that makes chemical sense. Therefore, they were accounted for by the use of the SQUEEZE function. The solvent mask found one significant void within the asymmetric unit which was 2566.0 $Å^3$ in size containing 694 electrons.

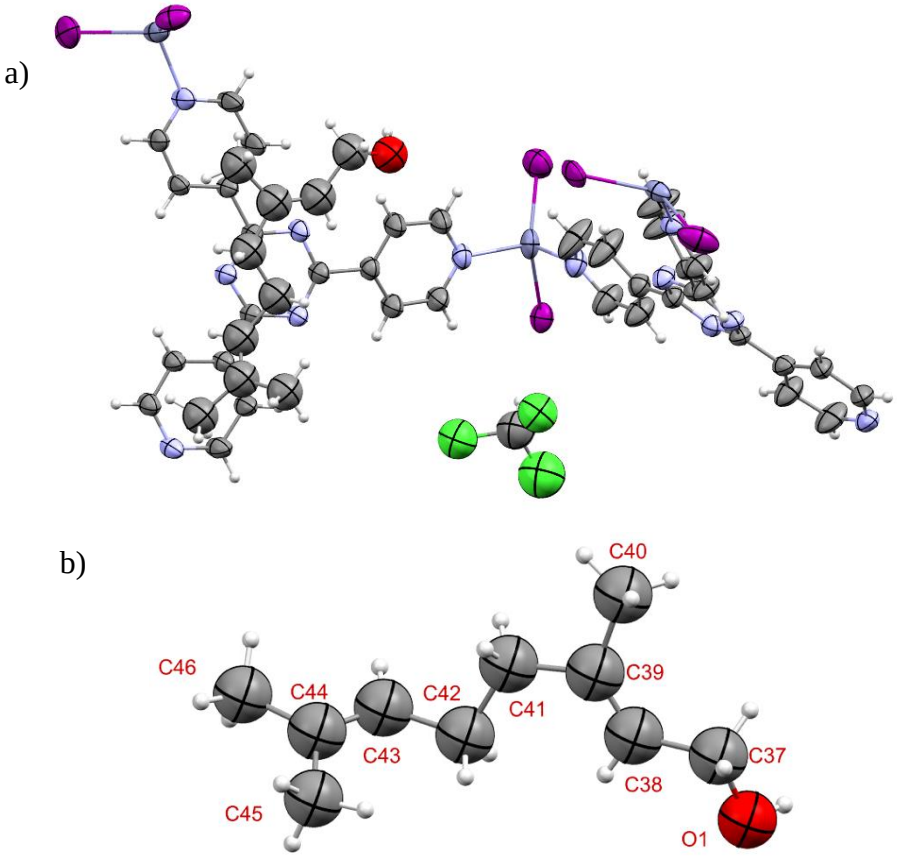

Figure 2. 6 a) Asymmetric unit of inclusion complex with geraniol showing only major component b) ORTEP diagram of geraniol molecule displayed as ellipsoids at 50% probability.

Farnesol

Anisotropic refinement of the non-hydrogen atoms of farnesol was performed by applying constraints/restraints to achieve a stable model. Farnesol's long carbon chain was severely disordered C39 and C41 show disorder about the crystallographic 2-fold rotational axis. DFIX and DANG were used to obtain realistic and acceptable geometry. SIMU and ISOR were used to restrain ADPs of all non-hydrogen atoms. Hydrogen atoms were added by riding model. Few hydrogens show disorder were fixed by using HFIX. At the end of the refinement large solvent accessible voids were detected and therefore, they were accounted for by the use of the SQUEEZE function. The solvent mask found one significant void within the asymmetric unit which was 3050.5 $Å^3$ in size containing 371 electrons.

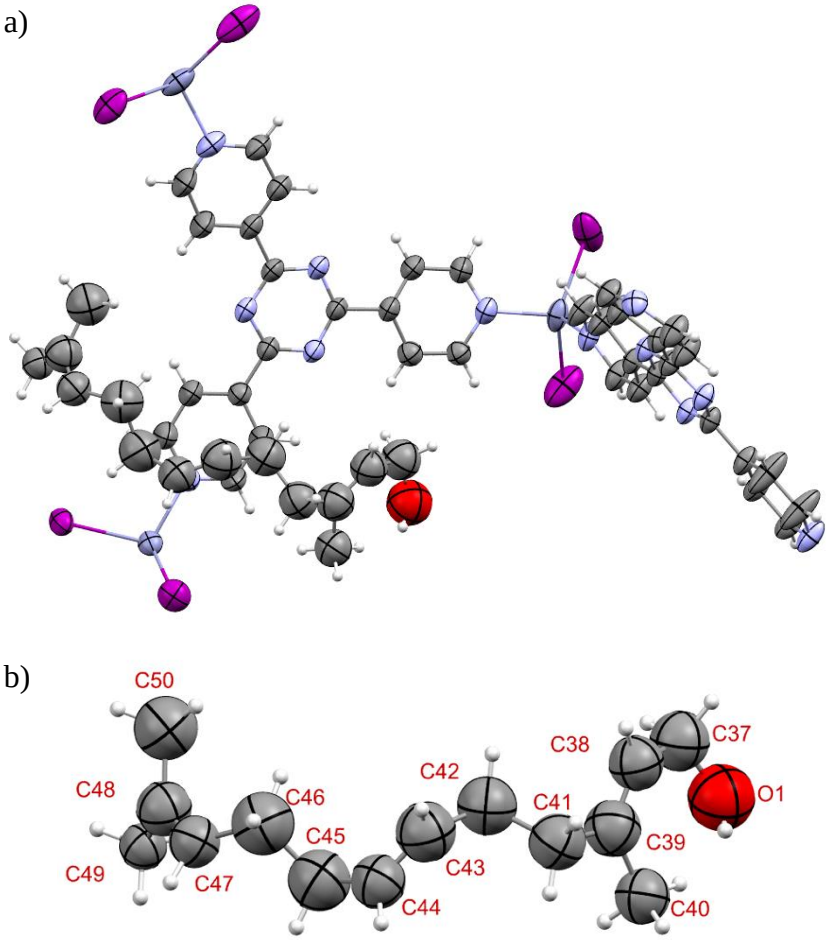

Figure 2. 7 a) Asymmetric unit of inclusion complex with farnesol showing only major component b) ORTEP diagram of farnesol molecule displayed as ellipsoids at 50% probability.

β-damascone

Anisotropic refinement of the non-hydrogen atoms of β-damascone was performed by applying restraints/constraints. DFIX was used to fix variations in the bond lengths. EADP was used to refine the anisotropic displacement parameters of all non-hydrogen atoms to a achieve stable model. Hydrogens were included with a riding model. A large residual peak 3.2 e/ Å was found near I1B on ZnI2 component. This peak is due to absorption and/or termination errors in Fourier calculations. Large solvent accessible voids were detected and therefore, they were accounted for by the use of the SQUEEZE function. The solvent mask found one significant void within the asymmetric unit which was 1155.9 $Å^3$ in size containing 211 electrons.

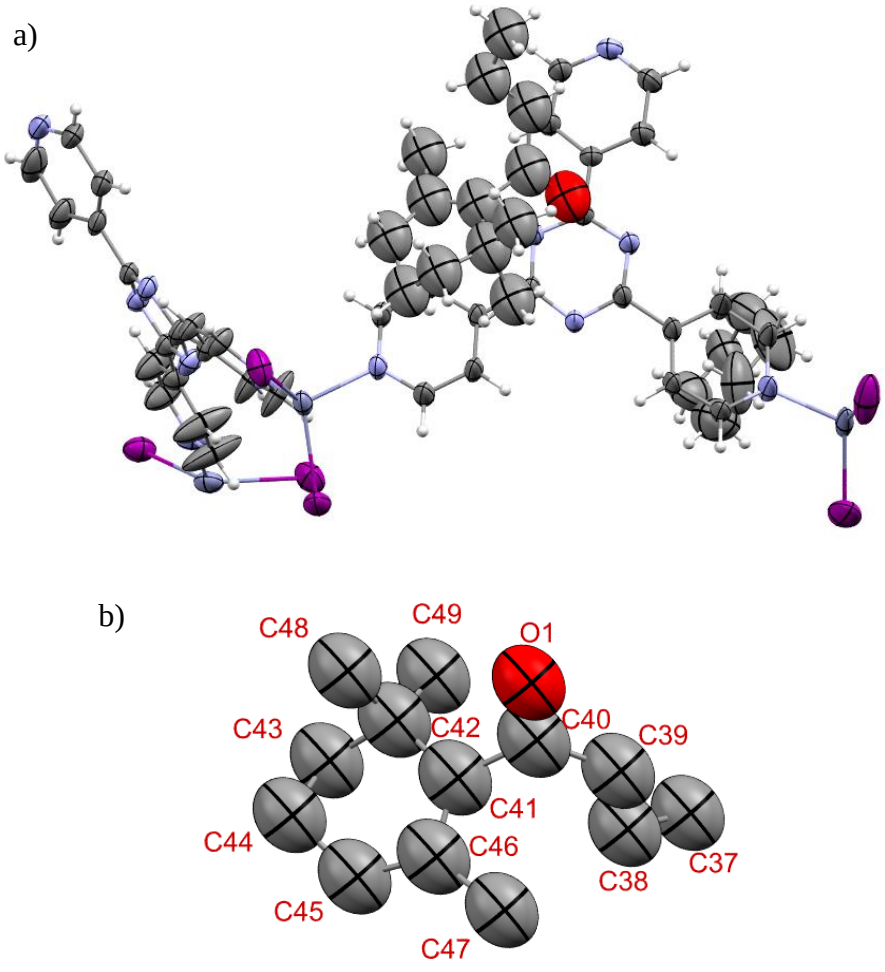

Figure 2. 8 a) Asymmetric unit of inclusion complex with β-damascone showing only major component b) ORTEP diagram of β-damascone molecule displayed as ellipsoids at 50% probability.

2.3.6 Crystallographic Tables

	Inclusion complex with geraniol	Inclusion complex with farnesol	Inclusion complex with β-damascone
Empirical formula	$C_{40.25}H_{24.25}Cl_{0.75}I_6N_{12}O_{0.4}Zn_3$	$C_{39.9}H_{24}I_6N_{12}O_{0.3}Zn_3$	$C_{49.8}H_{48}I_6N_{12}O_{0.6}Zn_3$
Formula weight	1636.90	1613.43	1781.71
Temperature/K	150(1)	150(1)	150(1)
Crystal system	monoclinic	monoclinic	monoclinic
Space group	*C*2/*c*	*C*2/*c*	*C*2/*c*
a/Å	35.4273(5)	35.3680(4)	35.8227(5)
b/Å	14.7790(2)	14.8449(2)	14.6554(2)
c/Å	31.6523(5)	31.6560(4)	32.5418(5)
α/°	90	90	90
β/°	102.0530(10)	102.1780(10)	103.4420(10)
γ/°	90	90	90
V/Å^3	16207.2(4)	16246.5(4)	16616.3(4)
Z	8	8	8
ρ_{calc}g/cm^3	1.342	1.319	1.424
μ/mm^{-1}	19.369	19.137	18.769
F(000)	6086	5995	6749
Crystal size/mm^3	0.24 × 0.22 × 0.15	0.18 × 0.13 × 0.12	0.23 × 0.18 × 0.17
Radiation	CuK_α (λ = 1.54184)	Cu K_α (λ = 1.54184)	Cu K_α (λ = 1.54184)
2Θ range for data collection/°	6.818 to 146.866	6.86 to 145.312	6.88 to 145.6
Index ranges	−36 ≤ h ≤ 43, −18 ≤ k ≤ 18,−37 ≤ l ≤ 39	−32 ≤ h ≤ 43, −17 ≤ k ≤ 18, −39 ≤ l ≤ 23	−43 ≤ h ≤ 29, −18 ≤ k ≤ 17, −39 ≤ l ≤ 40
Reflections collected	57499	56428	55278
Independent reflections	16021 [R_{int} = 0.0380, R_{sigma} = 0.0293]	15847 [R_{int} = 0.0303, R_{sigma} = 0.0237]	16232 [R_{int} = 0.0389, R_{sigma} = 0.0317]
Data/restraints/parameters	16021/134/694	15847/207/677	16232/11/647
Goodness-of-fit on F^2	1.044	1.065	1.071
Final R indexes [$I>=2\sigma(I)$]	R_1 = 0.0507, wR_2 = 0.1713	R_1 = 0.0554, wR_2 = 0.1703	R_1 = 0.0639, wR_2 = 0.1764
Final *R* indexes [all data]	R_1 = 0.0578, wR_2 = 0.1757	R_1 = 0.0585, wR_2 = 0.1760	R_1 = 0.0686, wR_2 = 0.1812
Largest diff. peak/hole / e Å^{-3}	1.69/−1.32	1.79/−1.69	3.20/−1.72

A Co-BASED SPONGE AND THE ENCAPSULATION OF PRIMARY ALCOHOLS

3

3.1 INTRODUCTION

This chapter describes the synthesis of $\{[Co_2(L)(H_2O)_3]\cdot(solvent)_x\}_n$ L = *bis*-(3,5-dicarboxy-pheny1)terephthalamide and investigates its potentiality as an alternative crystalline sponge. Though **1** is the most successful sponge to date, it has limitations as described in Section 1.5. Therefore, the development of new sponges is essential for the expansion of the CSM. Several researchers have developed a variety of crystalline sponges such as porous organic MOFs,[155] chiral metal-organic materials,[129] hydrophilic MOFs,[126] coordination cages,[136] and biological frameworks.[141] All of these alternative sponges were developed to overcome the limitation of sponge **1** and to target a particular type of guest encapsulation. For example, chiral metal-organic frameworks target the encapsulation of chiral guests. Hydrophilic MOFs were used as sponges because sponge **1** has a hydrophobic pore environment and does not allow encapsulation of hydrophilic guest molecules. However, it is clear that there is not one perfect sponge that is suitable for all types of guest molecules, therefore the development of the new sponges remains highly desirable.

A few hydrophilic sponges have been reported in the literature, as described in Section 1.6.3. For example, saccharide-based-crystalline sponge[125] consists of a *D*-mannose linker, which has free hydroxyl groups that contributes to the hydrophilic nature of the pore by forming a hydrogen bond with the incoming guests such as propyl alcohol. However, the pores were too small to accommodate larger guest molecules. Another example of a hydrophilic MOF was a Gd based MOF in which carboxylate groups of the 1,3,5- benzenetribenzoic acid linker were bound to the metal. Solvents molecules, such as DMF and water, which were coordinated to the metal were replaceable by the incoming guest or can serve as an anchoring site for hydrogen bond donors or acceptors. e-caprolactam and 2-pyrrolidone coordinated to the metal through a lone pair of the ketone group.[126] Similarly, in another report of the Gd based hydrophilic MOF, 2-phenylethanol and benzyl acetate were found coordinated to the metal via the hydroxyl group and the carbonyl

group present in the guest molecules, respectively.[127] The above examples from the literature show that for a successful hydrophilic MOF, the choice of host is dependent on the organic linker, coordination properties and functionality of the guest compound. In this chapter, a literature MOF was explored as an alternative crystalline sponge keeping the conditions into consideration.

3.1.1 Selection of $\{[Co_2(L)(H_2O)_3]\cdot(solvent)_x\}_n$ as an alternative sponge.

Fujita and co-workers.[156] reported the search and selection procedure of an appropriate MOF as a crystalline sponge from the CSD. The necessary features of a porous crystal to be used as a crystalline sponge are (1) stability of the crystals on guest soaking; (2) a flexible interpenetrated host framework that can induce effective host-guest interactions as observed in sponge **1**; (3) a low-symmetry space group to avoid trapping of guest molecules across symmetry planes or rotation axes, therefore, making them difficult to characterise and (4) the pores are non-confined and large enough to accommodate target molecules. To the given search parameters, the hydrophilicity of the MOF was also included to guide the search for hydrophilic MOF. For example, a MOF consisting of hydroxyl or carbonyl groups to participate in hydrogen bonding with the incoming guest molecules and with the coordination site available for guest exchange. Thus, a MOF which will meet all these criteria would be an appropriate candidate for a hydrophilic crystalline sponge.

From the search $\{[Co_2(L)(H_2O)_3]\cdot(solvent)_x\}_n$ meets all the criteria listed above for use as a crystalline sponge. The MOF has solvent-accessible voids of 21.5% of unit cell volume, pore size 11.0 × 5.3 $Å^2$ and low symmetry - Monoclinic $P2_1$. The ligand *bis*-(3,5-dicarboxy-pheny1)terephthalamide has free carbonyl groups for hydrogen bonding and water molecules coordinated to the metal which would be replaceable by the guest molecules. The ligand and the MOF were synthesised by a modified literature procedure,[157] the details of which are described in the experimental section.

3.1.2 Selection of guest molecules

To investigate the hydrophilic nature of the selected $\{[Co_2(L)(H_2O)_3]\cdot(solvent)_x\}_n$ MOF (hereafter referred to as sponge **3**), hydrophilic guest molecules were required. As mentioned in Section 3.1, the guest molecules with hydroxyl or carbonyl groups would align themselves via hydrogen bonding in the pores of the framework and at the coordination site. In addition, in MOF-520

various guest molecules containing primary alcohol and carboxylic acid bind themselves with the metal by replacing the coordination solvent. Keeping the given examples from the literature in consideration, four primary alcohols as guest molecules were selected. The selected guests were 3-phenylpropanol (3PP), 2-phenylethanol (2PE), prenol and geraniol (Figure 3.1). The four guest molecules containing hydroxyl groups would aid hydrogen bonding with the framework. It was expected given the functional group present that the guest would occupy the coordination site by replacing the water molecule. 3PP and 2PE are aromatic and similar in structure with the difference being in the chain length. Similarly, prenol and geraniol have similar structures with different chain lengths however, they are linear.

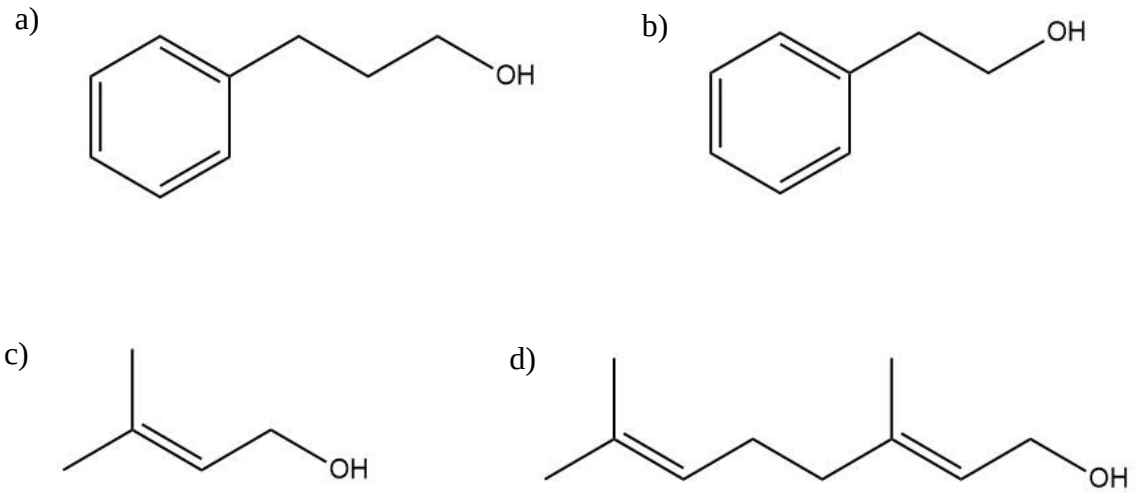

Figure 3. 1 Guest molecules. a) 3-phenylpropanol b) 2-phenylethanol c) prenol d) geraniol.

3.2 RESULTS AND DISCUSSION

3.2.1 Structure of sponge **3**

Sponge **3** was synthesised from the linker bis-(3,5-dicarboxy-pheny1)terephthalamide (BDTA) and $Co(NO_3)_2{\cdot}6H_2O$ following the modified literature procedure.[157] Purple needle-shaped crystals of sponge **3** were obtained, which crystallised in the non-centrosymmetric $P2_1$ space group. In addition, twinning was observed in the purple crystals. However, the reported crystals were blue

and block-shaped with no mention of twinning. A possible explanation for the observed morphological differences is due to changes in the experimental conditions. Since the literature procedure did not reproduce the same blue crystals. Figure 3.2 shows the packing diagram of sponge **3** with channels clearly shown running parallel to the *b*-axis. The structure of obtained crystals of sponge **3** was found to be consistent with the structure reported in the literature with some differences present. The asymmetric unit of the reported and the obtained structure consisted of one linker molecule and two Co-ions. Co1 ion is surrounded by six oxygen atoms from four different carboxylates. In the reported structure, the Co^{2+} 2 ion is occupied by four oxygen atoms from two different carboxylates and two water molecules. However, in the obtained structure it was observed that one of the water molecules was replaced by the DMF molecule (present during synthesis). In both the structures, water molecules were observed in the pore. In addition, the unit cell parameters of the obtained structure were observed with shorter *b* and larger β in comparison with the reported structure. The presence of an additional DMF molecule in the obtained structure caused these slight differences in the unit cell parameters. For example, it was commonly observed in sponge **1**, that the change of solvent molecules caused slight differences in the unit cell parameters.

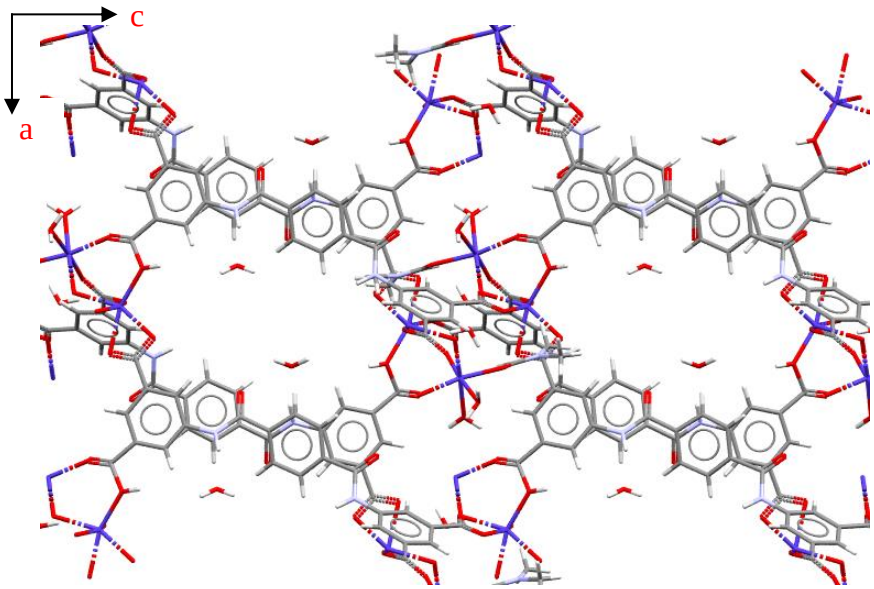

Figure 3. 2 Packing diagram of 3 viewed down the b-axis

3.2.2 Solvent exchange and successful guest encapsulations

For the successful guest encapsulation, it was essential to remove DMF molecules from the coordination site and water molecules from the pores. This is because their presence may reduce the chance of a guest molecule occupying the same site as the solvent molecules and could inhibit guest exchange. In addition, it has been reported previously that the presence of solvent molecules increases the challenge of structure refinement.[85] Therefore, solvent exchange with ethanol, methanol, propanol, chloroform, water and acetone was performed. The crystals of **3** remained stable in ethanol, methanol and propanol, however, the structure was obtained only for the crystals exchanged with propanol (details and results of solvent exchange in Section 3.4.5). The result shows the removal of water molecules from the pore, however, the propanol molecule was not refined in the pores. In addition, DMF remained coordinated to Co^{2+} 2 ion. A longer soaking period with propanol was also attempted which resulted in the deterioration of the crystals. As a result, the most appropriate solvent to store crystals in was DMF. Therefore, as-synthesised crystals of **3** were stored in a screw-capped vial submerged in DMF. The vial was kept in an incubator maintained at 25 °C and the crystals remained stable for up to 1 month. Since the crystals were stored in DMF, additional DMF molecules were observed in the pore in the inclusion complexes. Guest encapsulations were first attempted with neat liquids to obtain higher occupancies, however, this resulted in the cracking of the crystals which were therefore not suitable for X-ray diffraction. Hence, a strategy was developed where the guest was dissolved in cyclohexane before soaking. Cyclohexane was chosen as a pore solvent because of the lack of functional groups and aromaticity given that solvents with functional groups used in solvent exchange resulted in the deterioration of the crystals. In addition, previous studies also suggested that cyclohexane does not interact with the framework and therefore, reduces the challenge of guest identification.[85] Several soaking conditions were investigated, and optimisation of the parameters gave maximum occupancies as well as the best quality crystals for X-ray diffraction measurement. Details of the soaking experiments are given in Tables 3.1 to 3.5 in the experimental section.

3.2.2 Inclusion complex with 3-phenylpropanol (3PP)

Single crystal X-ray analysis shows the structure of 3PP within the pores of the sponge **3**. The inclusion complex crystallised in the space group $P2_1$. The unit cell parameters were observed with

longer *b*, shorter *c* and smaller *β* in comparison with the as-synthesised structure (Section 3.3.8). One guest molecule was found per asymmetric unit with 50% occupancy. In addition, four DMF molecules were observed, two of the DMF molecules were coordinated to a Co atom and the other two were found in the pore each forming hydrogen bonds with the framework. Strong hydrogen bonds formed between the amide carbonyl group of the DMF and hydrogens from the phenyl ring and amide group from the framework $C{=}O_{(DMF)}{—}NH_{(framework)}/CH_{(framework)}$, 2.0, 2.2, 2.6, 2.0 Å (Figure 3.6). Since the DMF molecules were fixed because of these hydrogen bonds the incoming guest molecules were unable to replace them from these sites. Figure 3.3a shows the packing diagram and it was observed that the position of the guest molecule was such that the carbon chain within the hydroxyl group approaches the Co-O coordination centre. Figure 3.3b shows host-guest interaction in which the hydroxyl group of the guest forms a hydrogen bond with one of the O atoms coordinated to Co atom $OH_{(guest)}\cdots Co\text{-}O_{(framework)}$, 2.8 Å. A second hydrogen bond was observed between the hydroxyl group of the guest and the carboxylate carbonyl group of the framework $OH_{(guest)}\cdots C{=}O_{(framework)}$, 2.8 Å. The rest of the guest molecule was fixed by various CH-π interactions. The distances of $CH_{(guest)}\cdots Centroid_{(framework)}$ were 3.8, 3.2, 2.6, and 2.8 Å. The orientation of the guest molecule was such that the distance $centroid_{(guest)}\cdots centroid_{(framework)}$ was 4.5 Å. Given the interactions observed it is reasonable to conclude that the hydrogen bonding is primarily responsible for the positioning of the guest in the pore.

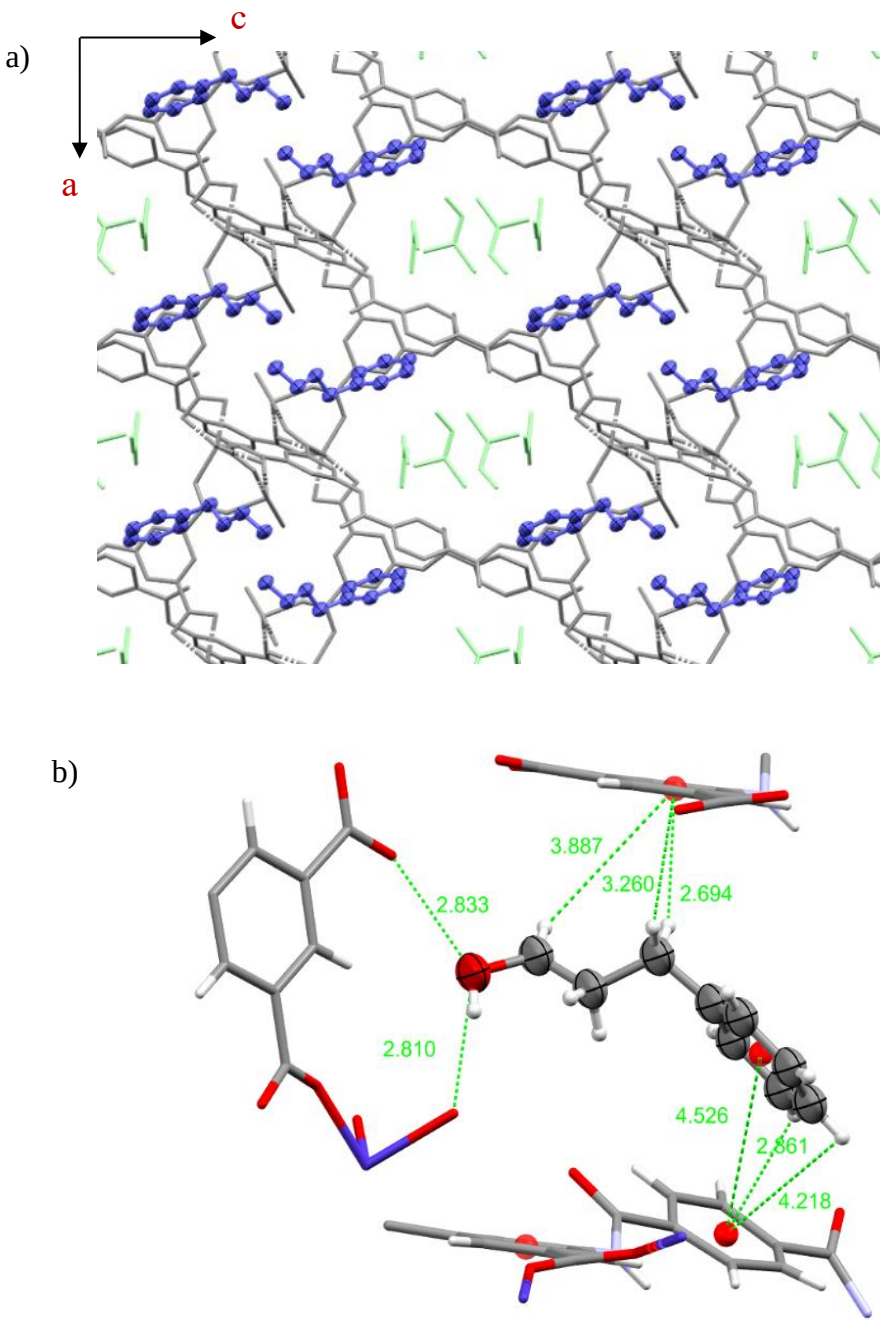

Figure 3. 3 a) Packing diagram of inclusion complex with 3PP viewed down the b-axis. Framework shown as capped stick and 3-PP as ellipsoids in blue, residual DMF molecules in light green. b) Non-bonding interactions between host framework and 3PP. Centroids are displayed as red spheres, and interactions are represented as dotted lines. Interaction distances are displayed in angstroms. Guest molecules displayed in ellipsoids at 50% probability.

3.2.3 Inclusion complex with 2-phenylethanol (2PE)

The inclusion complex with 2PE was crystalised in space group $P2_1$. Two guest molecules were found per asymmetric unit with 100% and 50% occupancy along with four DMF molecules. Similar to the inclusion complex with 3PP the unit cell parameters were observed with longer *b* length, shorter *c* length and shorter β in comparison with the as-synthesised structure (Section 3.3.8). Two DMF molecules were found coordinated to a Co^{2+} ion and one was refined in the pore which formed a hydrogen bond with the framework $C{=}O_{(DMF)}\cdots NH_{(framework),}$ 2.1 Å (Figure 3.7). Figure 3.4a shows the packing diagram of the inclusion complex revealing the positions occupied by the two guest molecules. Figure 3.4 b,c shows details of host-guest interactions. The guest molecule at site 1 (illustrated by pink colour in Fig 3.4a) was surrounded by three phenyl rings from the framework and was mainly stabilised by the hydrogen bonds. The distance of the hydrogen bonds observed were $OH_{(guest)}\cdots C{=}O_{(framework)}$ 1.9 Å, $OH_{(guest)}\cdots CH_{(framework)}$ 2.6 Å and $OH_{(guest)}$—Co-$O_{(framework)}$ 2.8 Å. Along with the hydrogen bonds, weaker CH-π interactions were also observed. Another guest molecule present at site 2 (illustrated by orange colour in Figure. 3.4a) was also surrounded by three phenyl rings of the framework and the phenyl ring of the guest was interacting with the centroids of the framework by CH-π interactions. The observed distances between $Centroid_{(framework)}\cdots CH_{(guest)}$ were 2.8, 3.6, 3.3, 2.8 and 3.3 Å. In addition, the orange guest molecule was oriented in such a manner that the hydroxyl end of the guest molecule was extended in the pore and away from the framework therefore weaker hydrogen bonding was observed with the framework, $OH_{(guest)}\cdots NH_{(framework)}$ 3.3 Å. However, the hydroxyl group of the guest molecule shows hydrogen bonding with the DMF in the pore via $OH_{(guest)}\cdots C{=}O_{(DMF)}$ 2.6 Å. In this case, there was no dominant hydrogen bonding with the framework and this guest molecule was fixed via unique CH-π interactions and weaker hydrogen bonds. (Figure 3.4c).

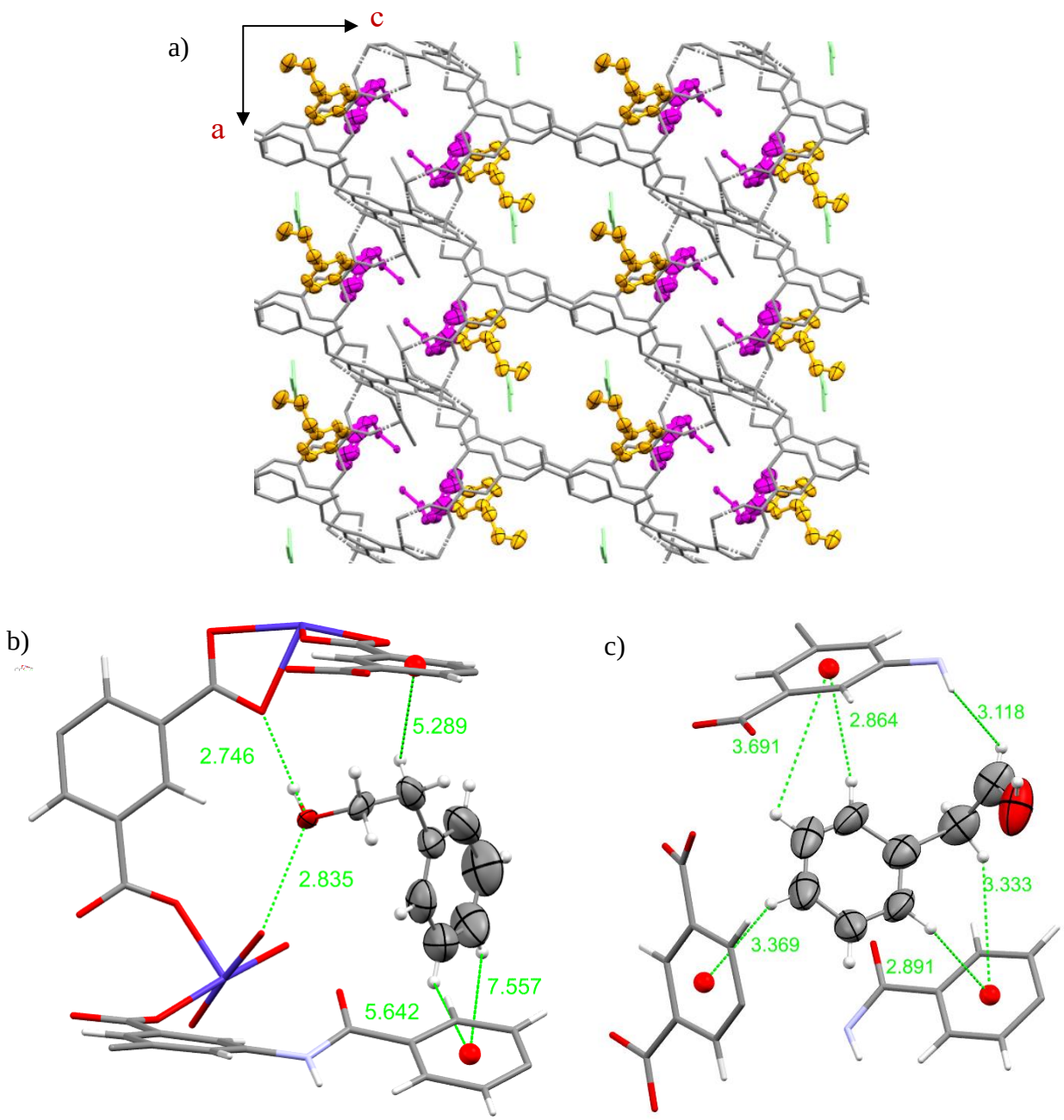

Figure 3. 4 a) Packing diagram of inclusion complex with 2PE viewed along the b-axis. Framework shown as capped stick model and 2PE as ellipsoids in pink at site 1 and in orange at site 2. colour, residual DMF molecules in light green colour. b) Non-bonding interactions between host framework and 2PE present at site 1,c) Non-bonding interactions between host framework and 2PE present at site 2. Centroids are displayed as red spheres, and interactions are represented as dotted lines. Interaction distances are displayed in angstroms. Guest molecules displayed in ellipsoids at 50% probability.

The inclusion complex with 2PE has been previously reported with Gd-based hydrophilic MOF (discussed in Section 3.1).[127] It was observed that 2PE was coordinated to the Gd ion as well as found in the pore. In sponge **3**, 2PE was only observed in the pores because incoming guest molecules were unable to replace the DMF molecules from the coordination site. In the Gd-MOF the DMF solvent was replaced by methanol before guest encapsulation. However, attempts at the solvent exchange with sponge **3** were unsuccessful, therefore existing DMF molecules inhibited the guest exchange at the coordination site. In addition, similarities between the non-bonding interactions of 2PE with sponge **3** and with the Gd-MOF were observed. In both the examples, 2PE was stabilised by hydrogen bonding and several CH-π interactions. In the Gd-MOF hydroxyl groups of both the guest molecules aligned towards the coordination centre. However, in sponge **3** only the pink molecule was closer to the coordination centre. This is likely due to the coordination sites near the pink molecule being occupied and does not allow further bonding. Thus, the guest molecule oriented itself such that the hydroxyl group of the molecule was stabilised by a hydrogen bond with the amide group of the DMF in the pore as well as with the amide group of the framework. (Figure 3.3c)

Furthermore, the pink molecule of 2PE was also compared to the 3PP molecule in sponge **3**. Although these molecules were not situated at the same sites, some similarities and differences were observed. Both the molecules were closer to the coordination site and form hydrogen bonds with the Co—O and the carboxylates of the framework. However, a difference in the orientation was observed for both the molecules. The phenyl ring of 2PE was observed roughly parallel to the *b* axis and thus it interacted with the phenyl ring of the framework in an 'edge to face' manner. In contrast, the phenyl ring of the 3PP was observed roughly parallel to the *c* axis and an 'offset stacked' type of interaction was observed. This is due to an extra carbon atom in 3PP helping the molecule to propagate in the pore while in 2PE the molecule bends and were aligned parallel to the *b* axis (see Figures 3.2b and 3.3b). Such an observation was previously reported, where a longer carbon chain affected the orientation of the molecule, resulting in differences in the observed interaction with the framework.[143]

3.2.4 Inclusion complex with prenol

The inclusion complex with prenol crystallised in space group $P2_1$. After 3 weeks of soaking one guest molecule per asymmetric unit was identified in the pore with 35% occupancy. The guest

molecule was found sitting on the 2-fold rotational axis, thus, a severe disorder in the molecule was observed. In addition, there was no DMF molecule refined in the pore as well not being found coordinated to the cobalt ion. This is likely due to the poor crystal and data quality, therefore lower occupancy of the guest molecule and difficulty in the identification of the solvent molecules was observed. Several attempts were made to improve the crystal and data quality by optimising the soaking conditions. Details of optimisation conditions and refinement of the structure are in the experimental section.

3.2.5 Inclusion complex with geraniol

The inclusion complex with geraniol crystallised in space group $P2_1$. After 3 weeks of soaking one guest molecule per asymmetric unit was identified in the pore with 30% occupancy. All the atoms of the guest molecule were refined however, severe disorders were observed. In addition, disorders in the framework were observed with no DMF molecule refined in the pore as well as not being found coordinated to the cobalt ion. Similar to the prenol inclusion complex, the crystal and data quality for this structure was also poor. Several attempts were made to improve the crystal and data quality by optimising soaking conditions. Details of optimisation conditions and refinement of the structure are in the experimental section.

3.2.6 Conclusions

The MOF **3** was identified from the literature as a candidate to be used for the CSM and was studied in this chapter. An alternative crystalline sponge was selected from the literature and tested. Two novel inclusion complexes were synthesised with aromatic alcohols as guests. The formation of inclusion complexes confirmed the utility of $\{[Co_2(L)(H_2O)_3]\cdot(solvent)_x\}_n$ as an alternative sponge to Fujita's sponge. The host-guest interactions observed proved the hydrophilic pore environment was suitable to accommodate polar solvents. The guest molecules were anchored at the sites mainly by hydrogen bonding. In addition, comparison between the two inclusion complexes shows similarities in the observed value of hydrogen bonds. However, the small difference in the structure of the guest molecules led to different orientations for the phenyl rings and hence disparities in the host-guest interaction. In conclusion, sponge **3** was suitable as an alternative crystalline sponge and preferred to utilise hydrogen bonding to anchor guest molecules, although weaker CH-π interactions were also observed.

3.3 EXPERIMENTAL SECTION

3.3.1 Synthesis of ligand L = bis-(3,5-dicarboxy-pheny1)terephthalamide

Ligand bis-(3,5-dicarboxy-pheny1)terephthalamide was synthesised by the reported literature procedure.[157] Terephthaloyl chloride (3.05 g) was added to a solution of 5-amino isophthalic acid (5.62 g) and triethylamine (1 mL) in DMF (60 mL). The mixture was stirred for 16 hrs, and then water (500 ml) was added. A white precipitate formed which was filtered off and the solid was washed with acetone, water, methanol, and finally diethyl ether and then further dried in a vacuum. The product was characterised by NMR and mass spectroscopy. ^{1}H NMR (DMSO-d_6, δ ppm): 13.35 (broad peak, COOH), 10.76 (s, 2H, CONH), 8.71 (s, 4H, ArH), 8.24 (s, 2H, ArH), 8.16 (s, 4H, ArH), *m/z* 491.

3.3.2 Synthesis of $\{[Co_2(L)(H_2O)_3]\cdot(solvent)_x\}_n$

The crystals of $\{[Co_2(L)(H_2O)_3]\cdot(solvent)_x\}_n$ were synthesised by a modified literature procedure.[157] A solvothermal reaction of $Co(NO_3)_2\cdot 6H_2O$ (0.0322 g) and ligand (0.0240 g) in DMF (6 mL) with H_2O (1 mL) was performed at 85 °C for 5 days. The purple rod-shaped crystals of sponge **3** were obtained. The crystals were kept immersed in DMF in a 25 °C incubator until required for the guest encapsulation experiment.

3.3.3 Solvent exchange

SCXRD analysis of **3** shows that DMF molecules from the synthesis were coordinated to the Co atom. Several attempts were made to remove DMF from the pores by solvent exchange with methanol, ethanol, propanol, chloroform, water and acetone. Exchange with, chloroform, water and acetone resulted in the deterioration of the crystals. The crystals survived in methanol, ethanol and propanol. Details of solvent exchange are represented in Table 3.1.

Table 3. 1 Solvent exchanged to replace DMF

Solvent	Incubation period/days	Result
Acetone	2	Crystals deteriorated
Chloroform	immediately	Crystals deteriorated
Water	immediately	Crystal deteriorated
Ethanol	7	Crystals deteriorated as soon as removed from the solvent therefore data could not be collected
Methanol	7	Crystals deteriorated as soon as removed from the solvent therefore data could not be collected
Propanol	21	Crystals diffracted but propanol was not observed in the pores and DMF molecules were still coordinated to Co^{2+} ion.

3.3.4 Guest encapsulation experiment

In initial guest encapsulation experiments crystals were soaked in neat liquid guests but deterioration of the crystals was observed in each case. Dilution of the guests with ethanol or propanol resulted in unsuccessful guest diffusion. After two weeks of the incubation period, no guest molecules were found in the pore and longer incubation resulted in the deterioration of the crystals. Therefore, a strategy was developed where guests were dissolved in cyclohexane before soaking. Several soaking conditions were investigated to obtain the best quality crystal data and optimise guest occupancy. Parameters such as guest: solvent ratio, temperature, and length of incubation period were optimised for each guest. Details of encapsulation conditions are given in the Tables below.

Table 3. 2 Soaking conditions for the inclusion complex with 3PP

Guest	Solvent/ Cyclohexane	Soaking temperature	Incubation period/days	Result
2 mL	-	25 °C	1	Crystals deteriorated
100 µL	2 mL	25 °C	7	Crystals deteriorated
50 µL	2 mL	25 °C	3	Crystal deteriorated
30 µL	2 mL	25 °C	7	Crystal deteriorated
20 µL	3 mL	25 °C	4	Guest found in the pores with 50% occupancy
20 µL	3 mL	25 °C	7	Crystals optically look fine but did not diffract
20 µL	3 ml	10 °C	4	Crystals optically look fine but did not diffract
20 µL	3 ml	10 °C	2	Crystals optically look fine but did not diffract
20 µL	3 ml	50 °C	1	Crystal deteriorated

Table 3. 3 Soaking conditions for inclusion complex with 2PE

Guest	Solvent/ Cyclohexane	Soaking temperature	Incubation period/days	Result
2 mL	-	25 °C	1	Crystals deteriorated
100 µL	2 mL	25 °C	7	Crystals deteriorated
50 µL	2 mL	25 °C	2	Crystal deteriorated
40 µL	2 mL	25 °C	5	Crystal deteriorated
20 µL	3 mL	25 °C	5	Two guest molecules were found in the pores with 100% occupancy
20 µL	3 mL	25 °C	8	Crystals optically look fine but did not diffract
20 µL	3 ml	10 °C	2	Crystals optically look fine but did not diffract
20 µL	3 ml	10 °C	2	Crystals optically look fine but did not diffract
20 µL	3 ml	50 °C	1	Crystal deteriorated

Table 3. 4 Soaking conditions for inclusion complex with prenol

Guest	Solvent/ Cyclohexane	Soaking temperature	Incubation period/days	Result
2 mL	-	25 °C	1	Crystals deteriorated
100 µL	2 mL	25 °C	1	Crystals deteriorated
50 µL	2 mL	25 °C	3	Crystal deteriorated
40 µL	2 mL	25 °C	3	Crystal deteriorated
20 µL	2 mL	25 °C	5	Crystal deteriorated
10 µL	2 mL	25 °C	15	Crystals diffracted but the guest was not found
10 µL	2 ml	25 °C	21	Guest found in the pore with 35% occupancy
10 µL	2 ml	25 °C	30	Crystal deteriorated
10 µL	2 ml	10 °C	7	Crystals optically look fine but do not diffract
20 µL	2 ml	50 °C	1	Crystal deteriorated
10 µL	2 ml	50 °C	1	Crystal deteriorated

Table 3. 5 Soaking conditions for inclusion complex with geraniol

Guest	Solvent/ Cyclohexane	Soaking temperature	Incubation period/days	Result
2 mL	-	25 °C	1	Crystals deteriorated
100 µL	2 mL	25 °C	1	Crystals deteriorated
50 µL	2 mL	25 °C	3	Crystal deteriorated
40 µL	2 mL	25 °C	5	Crystal deteriorated
20 µL	2 mL	25 °C	7	Crystal deteriorated
10 µL	2 mL	25 °C	12	Crystals diffracted but guest was not found
10 µL	2 ml	25 °C	25	Guest found in the pore with 35% occupancy
10 µL	2 ml	25 °C	30	Crystal deteriorated
10 µL	2 ml	10 °C	4	Crystal deteriorated
20 µL	2 ml	50 °C	1	Crystal deteriorated
10 µL	2 ml	50 °C	1	Crystal deteriorated

3.3.5 Crystallographic procedures

Using the same procedure as described in Section 2.3.3

3.3.6 Structural analysis details

The non-hydrogen atoms of the framework were refined anisotropically and hydrogen atoms were included using a riding model. The BDTA and Co components of the framework were freely refined and only if necessary, constraints/restraints were applied. Refinement of guest species was first performed without any constraints/restraints and only if this was unsuccessful, were these added based on their known structures. The occupancy of each guest molecule was refined against its free variable which in the final stages of refinement was fixed to values reported. Standard deviations for restraints used are as described in chapter 2 section 2.3.4.

3.3.7 Refinements details of as-synthesised **3** and of individual guests in each inclusion complex

Sponge **3**

Anisotropic refinement of the non-hydrogen atoms of sponge **3** was performed by applying constraints/restraints to achieve a stable model. DFIX and DANG were used to fix bond lengths and bond angles to obtain a realistic and acceptable geometry. SIMU, ISOR was used to restrain the ADPs. Hydrogen atoms were added by the riding model. At the end of the refinement large solvent accessible voids were observed which were then accounted for using SQUEEZE function. The solvent mask found one significant void within the asymmetric unit which was 1932 $Å^3$ in size and containing 688 electrons. Flack parameter for the structure is 0.496(5) due to the poor quality of crystals and twinning in the crystals.

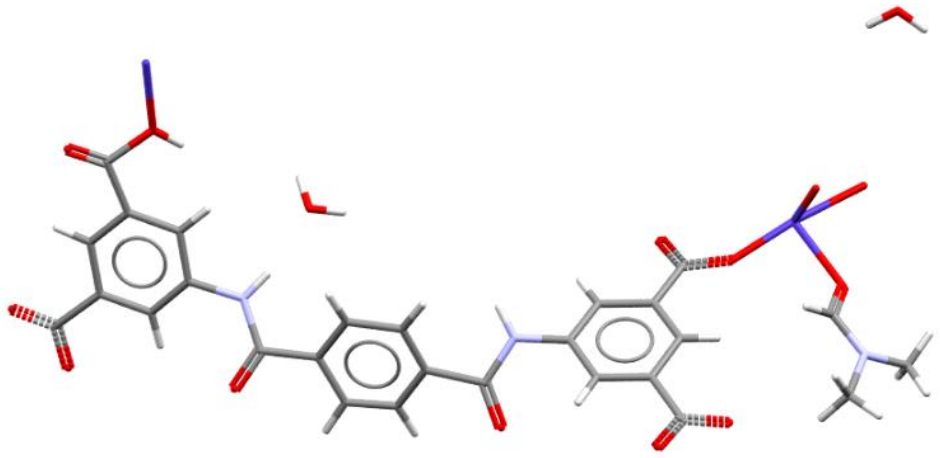

Figure 3. 5 Asymmetric unit of Sponge 3

3PP

Anisotropic refinement of the non-hydrogen atoms of 3PP was performed by applying constraints/restraints to achieve a stable model. DFIX was used to fix bond lengths to obtain a realistic and acceptable geometry. EADP was used to refine the anisotropic displacement parameters of all non-hydrogen atoms to a achieve stable model. Hydrogen atoms were added by the riding model. At the end of the refinement large solvent accessible voids were observed which were then accounted for using SQUEEZE function. The solvent mask found one significant void within the asymmetric unit which was 989 $Å^3$ in size and containing 251 electrons. Flack parameter is 0.286(3) for this structure. This is because of the observed twinning and poor quality of the crystals.

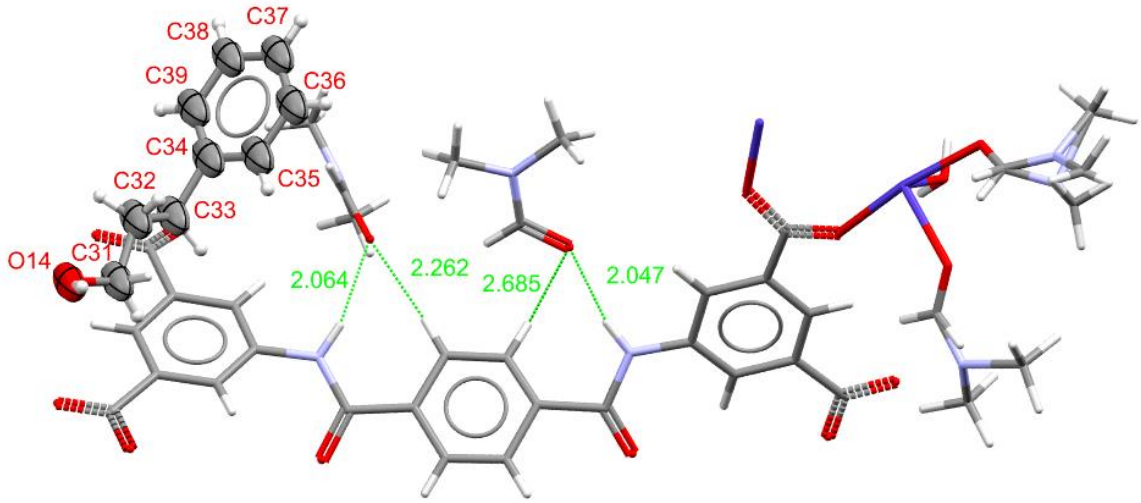

Figure 3. 6 Asymmetric unit of inclusion complex with 3PP.

2PE

Anisotropic refinement of the non-hydrogen atoms of 2PE was performed without applying any constraints/restraints to achieve a stable model. Hydrogen atoms were added by the riding model. At the end of the refinement large solvent accessible voids were observed which were then accounted for using SQUEEZE function. The solvent mask found one significant void within the asymmetric unit which was 924Å^3 in size and containing 123 electrons. The value of the flack parameter in this example is 0.068(7). Therefore, this structure refinement has given the correct configuration.

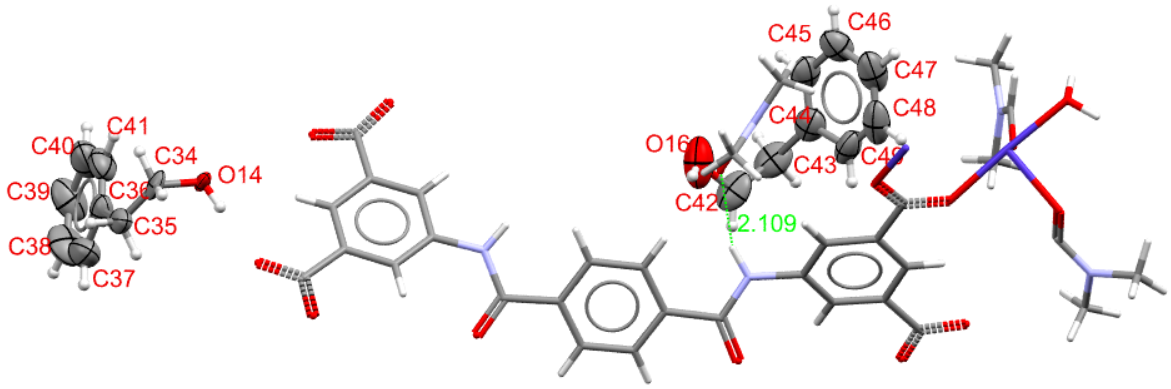

Figure 3. 7 Asymmetric unit of inclusion complex with 2PE

3.3.8 Crystallographic Tables

	Sponge **3**	Inclusion complex with 3PP	Inclusion complex with 2PE
Empirical formula	$C_{27}H_{28}Co_2N_3O_{15}$	$C_{37.5}H_{35.3}Co_2N_5O_{14.8}$	$C_{45}H_{50}Co_2N_5O_{15.5}$
Formula weight	732.29	812.45	1042.90
Temperature/K	150(1)	150(1)	150(1)
Crystal system	monoclinic	monoclinic	monoclinic
Space group	$P2_1$	$P2_1$	$P2_1$
a/Å	10.0994(3)	10.1071(2)	10.06930(10)
b/Å	16.3790(10)	17.3785(5)	17.4461(3)
c/Å	18.3265(6)	18.1448(4)	18.0468(3)
α/°	90	90	90
β/°	95.217(3)	92.559(2)	91.2840(10)
γ/°	90	90	90
V/Å^3	3019.0(2)	3183.89(13)	3169.49(8)
Z	2	2	2
ρ_{calc}g/cm^3	0.806	0.984	1.076
μ/mm^{-1}	4.648	4.508	4.572
F	738	976.0	1066.0
Crystal size/mm^3	0.22 × 0.15 × 0.13	0.26 × 0.13 × 0.12	0.25 × 0.16 × 0.14
Radiation	CuK_α (λ = 1.54184)	CuK_α (λ = 1.54184)	Cu$K\alpha$ (λ = 1.54184)
2Θ range for data collection/°	7.252 to 145.226	7.04 to 145.42	7.048 to 145.146
Index ranges	−12 ≤ h ≤ 12, −20 ≤ k ≤ 18, −22 ≤ l ≤ 15	−12 ≤ h ≤ 9, −21 ≤ k ≤ 21, −22 ≤ l ≤ 21	−11 ≤ h ≤ 11, −20 ≤ k ≤ 19, −19 ≤ l ≤ 21
Reflections collected	13005	23584	21819
Independent reflections	9177 [R_{int} = 0.0460, R_{sigma} = 0.0687]	11923 [R_{int} = 0.0458, R_{sigma} = 0.0573]	9371 [R_{int} = 0.0620, R_{sigma} = 0.0706]
Data/restraints/parameters	9177/192/275	11923/8/511	9371/151/649
Goodness-of-fit on F^2	1.626	1.034	1.040
Final R indexes [I>=2σ (I)]	R_1 = 0.1464, wR_2 = 0.3818	R_1 = 0.1136, wR_2 = 0.3001	R_1 = 0.0944, wR_2 = 0.2426
Final R indexes [all data]	R_1 = 0.1568, wR_2 = 0.3997	R_1 = 0.1171, wR_2 = 0.3047	R_1 = 0.1010 wR_2 = 0.2519
Largest diff. peak/hole / e Å^{-3}	1.69/−1.70	1.37/−0.66	171./−1.00
Flack parameter	0.496(5)	0.297(3)	0.013(7)

A NEW Cd-BASED SPONGE AND STUDIES ON THE ENCAPSULATION OF POLAR SOLVENTS

4

4.1 INTRODUCTION

Sponge **3** described in Chapter 3 addressed one of the limitations of **1** namely the hydrophobic pore environment. This chapter aims to explore a new versatile MOF which addresses all three limitations of **1** described previously, that is instability in the presence of polar solvents and nucleophilic guests,[124] small pore size, and the hydrophobic environment. The hydrophobicity issue was addressed by several researchers in previous studies and hydrophilic sponges were developed as described in Section 3.1. However, relatively less attention has been paid to the compatibility of crystalline sponges with polar solvents and nucleophilic guests. For example, the crystals of sponge **1** are severely damaged when exposed to nicotine and therefore cannot be studied by SCXRD.[124] A few sponges have been reported which remain stable when exposed to polar solvents and nucleophilic guests. For example, a porous organic material (POM) synthesised from a semirigid macrocyclic tetraimine and ethyl acetate demonstrates the compatibility with nucleophilic guests by the encapsulation of *S*-(−)-nicotine.[155] Another example is the Mn-based coordination porous framework – **5** (CPF-5) ($Mn_{21}(HCOO)_{18}(H_2O)_{12}$(4-tetrazolate-benzoate)$_{12}$, a crystalline sponge that binds several Lewis base guests, including pyridine and 3-aminopyridine to the Mn centre by coordinative alignment.[122] Furthermore, in a mesoporous Cu-based MOF [$Cu_6(H_2O)_6(TATB)_4 \cdot DMF \cdot 12H_2O$] [TATB = 4,4',4''-(1,3,5-triazine-2,4,6-triyl) tribenzoic acid] the Cu^{2+} ions coordinate to the pyridine ring of nicotine.[123] In addition, the hydrophilic [$Gd(DMF)_2(H_3BTB) \cdot 3DMF \cdot 2H_2O$] [$H_3BTB$ = 1,3,5-Benzenetribenzoic acid] (Gd-MOF) also demonstrated stability in polar solvents.[126] As it is clear from previous studies, to develop the crystalline sponge method and expand the guest range a large variety of new crystalline sponges are required. In particular, a crystalline sponge stable in polar solvents is highly desirable. This chapter describes the synthesis of {[$Cd_7(BTA)_4(H_2O)_x(DMF)_n] \cdot (solvent)_m$} BTA = 4,4'4''-[1,3,5-benzenetriyltris(carbonylimino)]-trisbenzoic acid and investigates its potential as an alternative crystalline sponge and studies its compatibility with polar solvents and nucleophilic guests.[158]

4.1.1 Selection of $\{[Cd_7(L)_4(H_2O)_x(DMF)_n]\cdot(solvent)_m\}$ as an alternative sponge.

The search and selection procedure described in section 3.1.1 was followed to find an appropriate MOF for use as a crystalline sponge from the CSD. Along with more general criteria, a hydrophilic pore environment and a pore size larger than sponge **1** were also criteria in the search. For example, a MOF containing some hydroxyl or carbonyl groups, to participate in hydrogen bonding with the incoming guest molecules, and with a metal-based coordination site available for guest exchange would be appropriate for polar solvents.

From the search, a few MOFs synthesised with the BTA linker meet all the criteria mentioned above. The MOF $\{[Cd_7(BTA)_4(H_2O)_x(DMF)_n]\cdot(DMF)_m\}$, which has solvent-accessible voids, pore size 11.0 Å × 9.2 Å, and low symmetry - Triclinic $P\bar{1}$ was selected as an ideal choice.[158] The ligand 4,4'4''-[1,3,5-benzenetriyltris(carbonylimino)]-trisbenzoic acid has free carbonyl groups for hydrogen bonding and water molecules coordinated to the metal could be replaceable by the guest molecules. Thus, it was expected that this MOF would be stable in polar solvents. The ligand and the MOF were synthesised by a modified literature procedure, the details of which are described in the experimental sections 4.3.1 and 4.3.2

4.2 RESULTS AND DISCUSSION

4.2.1 Structure of $\{[Cd_7(BTA)_4(H_2O)_x(DMF)_n]\cdot(DMF)_m\}$

$\{[Cd_7(BTA)_4(H_2O)_x(DMF)_n]\cdot(DMF)_m\}$ (hereafter referred to as sponge **4**) was synthesised from the linker 4,4'4''-[1,3,5-benzenetriyltris(carbonylimino)]-trisbenzoic acid and $Cd(NO_3)_2\cdot6H_2O$ following the modified literature procedure. Colourless single crystals were obtained. The literature procedure was modified to a simpler and direct synthetic route for synthesising single crystals of **4**. This is because the CSM is a post crystallisation method and high-quality single crystals are required repeatedly for guest encapsulation experiments. In the modified synthetic procedure maintenance of the reaction conditions was much simpler. In contrast, the published procedure involves, for example, crystallisation under high pressure in a sealed tube.[158] Therefore, to routinely obtain good qualities of single crystals for the CSM, a simpler synthetic route was the efficient approach.

Since the synthetic procedure followed in this thesis was different from the reported procedure, changes in the structure were expected. Interestingly, different synthetic procedure led to a new MOF structure and the crystal structure was also found different from that reported previously. It was observed that sponge **4** was crystallised in the monoclinic $P2_1/n$ space group instead of triclinic $P\bar{1}$. The original structure was a two-dimensional framework generated from the linking of trimeric cadmium clusters with BTA^{3-} bridges.[158] The asymmetric unit consisted of one BTA linker and two Cd ions, and each Cd ion was six coordinate. One DMF molecule was coordinated to Cd1 and another DMF was observed in the pores. However, the structure obtained in this work exhibited a two-fold interpenetrating three-dimensional honeycomb framework. In addition, on closer examination, it was observed that the structure obtained for sponge **4** was similar to another BTA-based MOF synthesised with $CoCl_2 \cdot 6H_2O$ reported in the same literature.[158] The unit cell diagram of sponge **4** is illustrated in Figure 4.1 and shows channels down the *a*-axis.

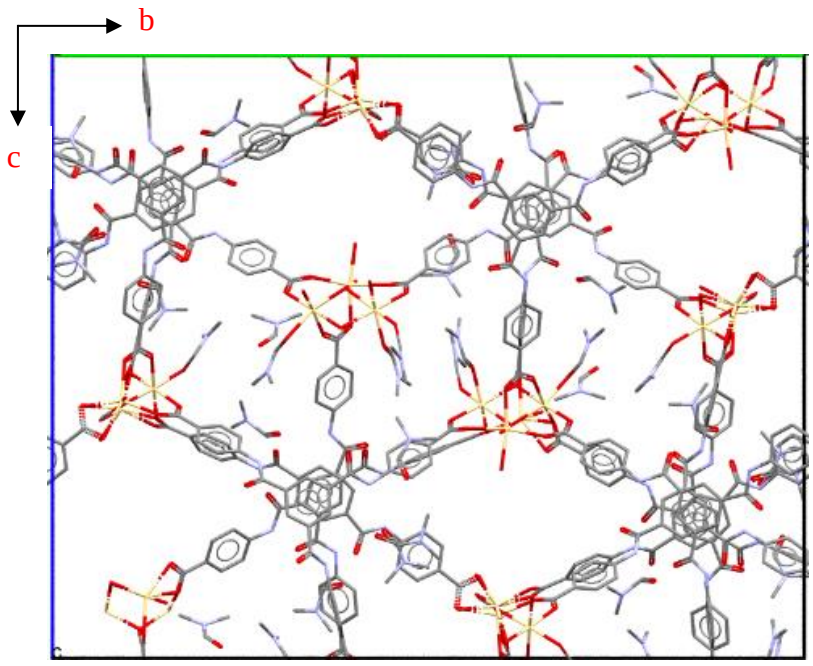

*Figure 4. 1 Illustration of unit cell of sponge **4** viewed down the a-axis.*

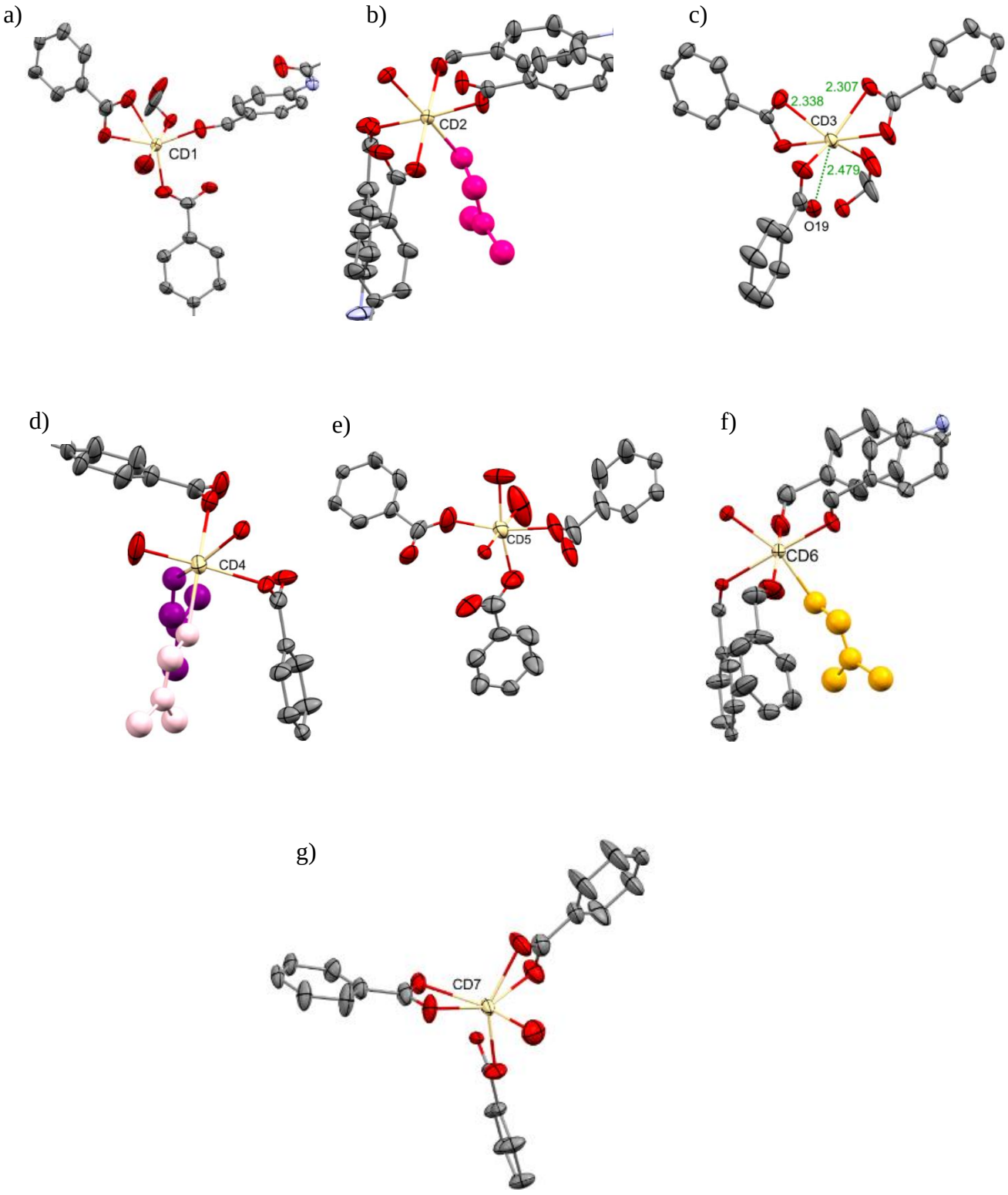

Figure 4. 2 a)-g) Geometry of Cd1-Cd7 ions surrounded by linker molecules, bridging oxygens, water molecules and DMF molecules. DMF molecules are coloured according to their positional equivalence. DMF molecules are displayed in ball and stick model.

The asymmetric unit of the previously reported structure with $CoCl_2 \cdot 6H_2O$ consisted of two linker molecules, one O^{2-} ligand and one coordinated DMF molecule and three metal ions. The three cobalt ions in the asymmetric unit were bridged by one oxygen atom and six carboxylate groups. Co1 was found to adopt a tetrahedral coordination environment involving three oxygen atoms from three different carboxylate groups and one bridging oxygen. Co2 was six-coordinated with an octahedral geometry, surrounded by four oxygen atoms from four carboxylate groups from the linker, one bridging oxygen atom, and one DMF oxygen atom. Similar to Co2, Co3 was also six-coordinated with octahedral coordination geometry completed by four oxygen atoms from three different carboxylate groups from linker molecules, one bridging oxygen and one water molecule. However, the asymmetric unit of sponge **4** consists of seven Cd ions, four linker molecules, two O^{2-} ligand, four coordinated DMF molecules and three coordinated water molecules. In addition, six DMF molecules were identified and refined in the pores of the new structure. Figure 4.2 illustrates the geometry of the Cd ions. Cd3 of **4** (Figure 4.2c) is distorted octahedral geometry due to the non-bonding interaction between Cd3 and O19. The remaining six Cd ions of the sponge **4** are six coordinate with an octahedral geometry bonded to six oxygen atoms. The source of oxygen atoms coordinated to the Cd ions varied in the structure. For example, in Cd6 (Figure 4.2f) two oxygen atoms are from the two different BTA linker molecules, two from the bridging O^{2-} ligand and the remaining two were from coordinated water and DMF. On the other hand, Cd5 (Figure 4.2e) is connected to three oxygen atoms from the BTA linker, two water molecules, and one O^{2-} bridging ligand. This difference is probably a function of the number of solvent molecules coordinated to Cd ions. For example, Cd6 only binds to two linker molecules because three coordination sites are taken up by the solvent molecules. In contrast, Cd5 is coordinated to three BTA linker molecules, since only two water molecules are coordinated. Each cadmium cluster bridges three BTA linker molecules, and each BTA linker molecule further connects three neighbouring cadmium clusters to form a three-dimensional, double interpenetrated honeycomb framework, as shown in Figure 4.1a. Sponge **4** has solvent-accessible voids of 18.5% of unit cell volume, 3892 $Å^3$ and pore dimension 10 Å × 16 Å. All the above-mentioned structural information of sponge **4** suggests that it is geometrically different from the reported MOF and therefore a new MOF.

The packing diagram of sponge **4**, shown in Figure 4.3, was studied to understand the positions and orientations occupied by the DMF molecules in the pore and at the coordination site on the Cd

ions. In the asymmetric unit of sponge **4**, there were six DMF in the pores identified in blue, turquoise, red, green, dark pink, and brown colour. Four DMF molecules were identified coordinated to Cd^{2+} ions. DMF identified in magenta is coordinated to Cd2 (Figure 4.2b), purple and light pink to Cd4 (Figure 4.2d), and light orange Cd6 (Figure 4.2f). It is important to recognise these favourable sites and identify the type of intermolecular interaction between the host and DMF molecules. Knowing the nature of the host-guest interactions may assist in the selection of guest molecules with appropriate functionality. Figure 4.4a-e illustrates the intermolecular interactions between the host framework and DMF molecules. Guest molecules were coloured according to the positional equivalence in the structure and across all the structures described in this chapter to facilitate structure comparisons. It was observed that the DMF molecules identified in blue, turquoise, red and green are strongly bonded to the framework via hydrogen bonds. These particular sites were consistently occupied either by the DMF molecules or replaced by the incoming guest in the inclusion complexes described later. In addition, extra stabilisation was often provided by CH-π interactions. Figure 4.4e shows the purple and light pink molecules are interacting with each other via hydrogen bonds. The above observations indicated that sponge **4** behaved as a hydrophilic sponge and hydrogen bonding was identified as the dominant host-guest interaction. Therefore, it was expected that sponge **4** may accommodate a number of polar solvents with different functionality.

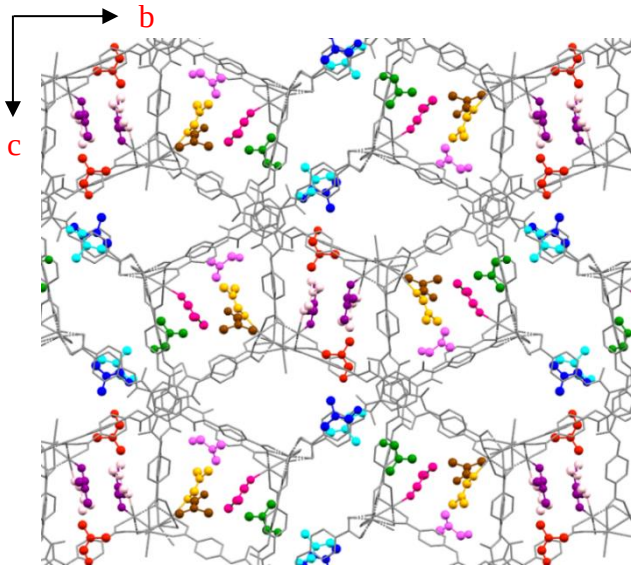

*Figure 4. 3 Packing diagram of sponge **4** viewed down the a-axis. DMF molecules are coloured according to the positional equivalence. Framework shown in capped sticked. Hydrogens are omitted for clarity.*

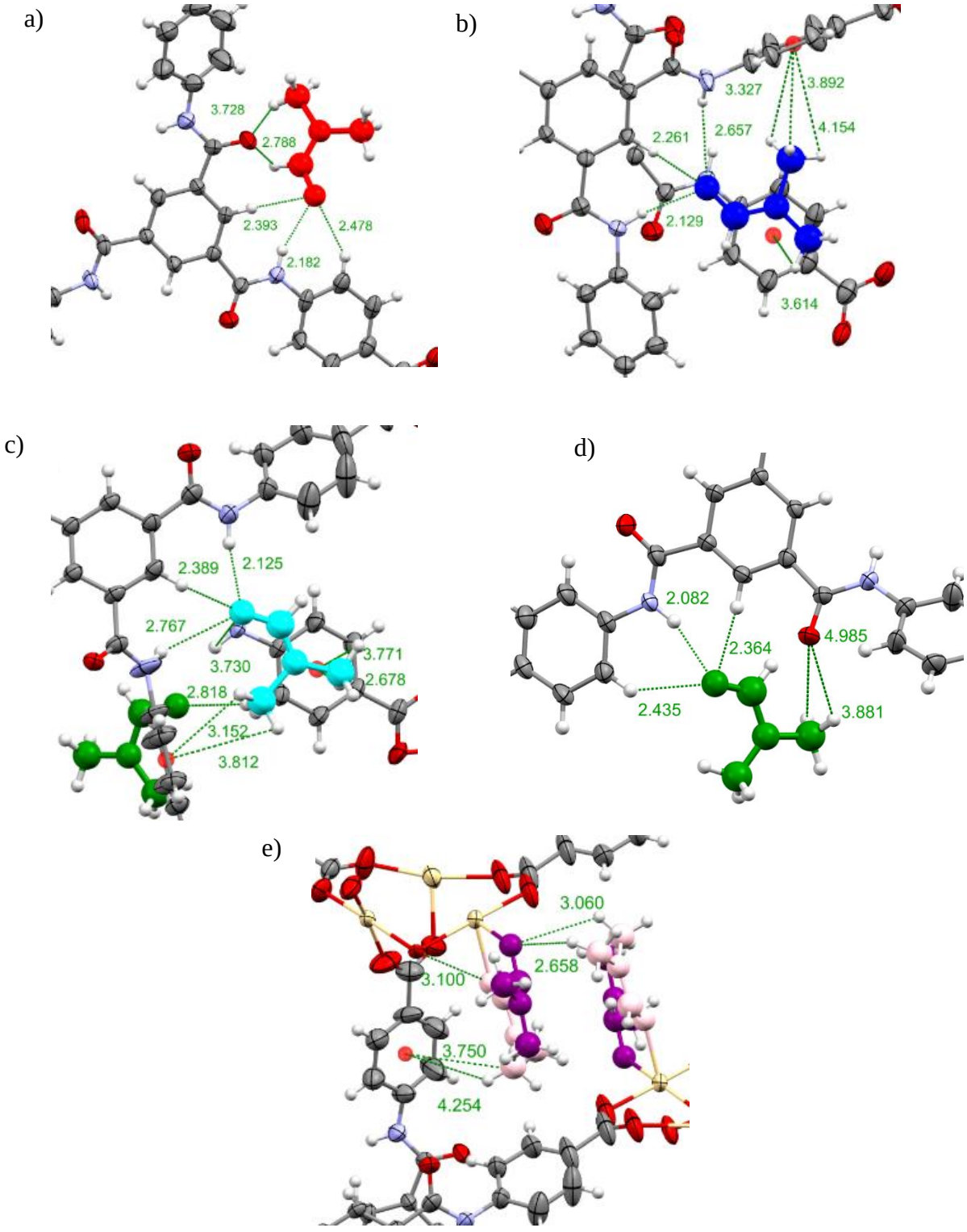

Figure 4. 4 a)-e) Intermolecular interactions between DMF molecules shown in a) red, b) blue, c) turquoise, d) green, e) purple and pink and the host framework. DMF molecules were shown in ball and stick and are coloured according to the symmetry equivalence. Interaction distances are displayed in angstroms.

4.2.2 The stability of sponge **4** in polar solvents

In a recent study,[159] Fujita demonstrated the importance of polar solvents in the ordering of the guest molecules in the pores of sponge **1**. Using acetone to dissolve the guest compound for soaking, instead of an inert solvent, results in efficient co-crystallisation of acetone molecules by interacting with the host framework. Hence, tight packing of the guest molecules with fewer disorders was observed.[159] The result of this study contrasts with the previous work with sponge **1** where crystals deteriorate in polar solvents. In this case, crystals survived because only 50 µL of acetone was used for dissolving the guest compound and the incubation period was 12 hours. Thus, sponge **1** is still at the risk of deterioration in polar solvents and therefore, a more stable crystalline sponge is required.

The stability of sponge **4** was investigated by exposing it to a variety of solvents containing different chemical functionalities. The results are summarised in Table 4.1, which are also compared with the reported solvent stability of sponge **1** and the Gd-MOF.[126] Since the Gd-MOF was reported with better stability than sponge **1**, it is reasonable to compare the results and obtain a better understanding regarding the relative stability of sponge **4**. If the host crystals survived after exposure to the solvent and a crystal structure was obtained, then it was considered to be stable in that solvent. In contrast, if the crystals were damaged and did not diffract, then instability with regard to that solvent was concluded. The length of the incubation period of sponge **4** crystals with each solvent is given in Table 4.2. The results revealed that sponge **4** is stable in most of the solvents studied except methanol and chloroform. In the case of methanol, the crystals remained stable in the solvent, based on optical examination but readily degraded once removed for data collection. It was suspected that methanol was readily lost from the pores of **4**, resulting in the deterioration of the crystals. When longer chain alcohols were used, the crystal structures were obtained successfully.

It was clear that sponge **4** outperformed sponge **1** in terms of stability and demonstrated stability in polar solvents and basic solvents similar to that of the Gd-MOF. Even though the crystals of **4** deteriorated in two solvents, they proved sufficiently stable in many solvents for the application of the CSM. The superior stability of **4** extends the potential to encapsulate polar and nucleophilic guest molecules.

*Table 4. 1 Stability of sponge **4** in polar solvents in comparison with sponge **1** and Gd-MOF*

Solvent	Sponge 4	Sponge 1	Gd-MOF
Methanol	Deteriorated	Deteriorated	Survived
Ethanol	Survived	Not reported	Not reported
Isopropanol	Survived	Not reported	Not reported
Acetone	Survived	Survived (in diluted acetone)	Not reported
Chloroform	Deteriorated	Survived	Survived
DMF	Survived	Deteriorated	Survived
Acetonitrile	Survived	Deteriorated	Survived
Pyridine	Survived (in diluted Pyridine)	Deteriorated	Survived

4.2.3 Successful solvent exchange

The key purpose of solvent exchange experiments was to investigate the stability of sponge **4** in solvents with different functionalities. The second objective was to remove DMF and water molecules from the pore and the Cd coordinated sites. It was important to remove DMF and water molecules to facilitate successful guest exchange and to make sure that the maximum number of sites were available for the incoming guests to occupy. The crystals of **4** were stable in solvents acetonitrile (**A**), acetone (**B**), isopropanol (**C**), ethanol (**D**), and pyridine (**E**). The inclusion complexes obtained with them were named **4A**, **4B**, **4C**, **4D** and **4E**. The soaking experiments were performed at 25 °C with neat solvents (hereafter referred to as guests) to obtain high occupancies. The crystals of **4** remained stable for up to 1 month without showing any cracks and other signs of deterioration in guests **A**, **B**, **C**, and **D**. The soaking period was optimised (reduced)

to give the maximum occupancies as well as the best quality crystals for X-ray diffraction measurements. Soaking **4** in neat pyridine led to rapid loss of all crystalline material, which was presumably due to nucleophilic substitution at many (all) of the Cd coordination sites. Therefore, pyridine was diluted with DMF before soaking resulting in the formation of good quality crystals. SCXRD revealed that only at a few coordination sites had pyridine replaced DMF. Since the presence of DMF molecules was in large quantities exchange with pyridine was unsuccessful. Therefore, acetone was used instead of DMF for dilution and SCXRD revealed all coordinated DMFs were replaced by pyridine molecules. Details of solvent exchange and optimisation conditions are represented in Table 4.2 in the experimental section 4.3.3.

4.2.4 The structure of inclusion complexes with solvents as guest molecules

This section describes the crystal structures obtained with solvent as guest molecules in sponge **4**. Inclusion complexes **4A-4E** were studied to understand the host-guest interactions to aid further selection of guest molecules for encapsulation in sponge **4**. Since the polar solvents were used it was expected that the solvent molecules would arrange themselves in the pores of sponge **4** via hydrogen bonds and would replace DMF molecules. SCXRD analysis of inclusion complexes **4A, 4B, 4C** and **4D** revealed that guest molecules partially removed DMF from the pores but not from the metal coordination sites. Only in **4E** were all DMF molecules replaced from the coordination site, however, DMF was still observed in the pores.

Inclusion complex with acetonitrile **4A**

The structure of inclusion complex **4A** with seven Cd^{2+} ions and four BTA linkers was unchanged from **4**. MOF **4A** crystallised in the $P2_1/n$ space group, the same as **4**, but with shorter *a*, longer *b* and larger β in comparison with **4**. In the asymmetric unit of inclusion complex **4A** consisted of five coordinated DMFs, two DMFs in the pore with 100% occupancy and two guest molecules with occupancy of 50 and 100%. Figure 4.6a illustrates the packing diagrams of **4A**, which are also compared with the packing diagram of **4**. DMF molecules are identified in magenta, purple, and light orange and were observed coordinated to Cd2, Cd4 and Cd6 respectively, similar to **4**. In addition, a DMF molecule identified in black was also observed coordinated to Cd5. This site was previously occupied by a water molecule in **4**. The DMF molecule identified in purple colour coordinated to a Cd ion in **4A** showed rotational differences when compared with **4**. In **4** this molecule was roughly parallel to the *a*-axis and was hydrogen-bonded with the pink DMF (Figure

4.4e). Since pink DMF was absent in **4A**, no hydrogen bonds existed which were probably holding it in that particular orientation. Therefore, this rotation might have taken place to become parallel to the *b*-axis to seek stabilisation from CH-π interactions and hydrogen bonds with the framework, $CH_{3(DMF)}\cdots C{=}O_{(framework)}$ 2.4 Å, as shown in the Figure 4.5a. Two DMF molecules in the pores, identified in red and blue, occupied the same site as in **4** and a few other DMF molecules identified in dark pink, green, and brown colour from **4** were not observed in **4A**. However, as always with solvent molecules in the pores, there could be several explanations for this (genuine absence, low symmetry, low occupancy). The DMF shown in turquoise in the pore was replaced by **A** and the similarities in the interactions with the framework can be observed by comparing Figure 4.4c with Figure 4.5b. Both the molecules were bonded with the framework mainly by the hydrogen bonds: $H_{framework}\cdots O{=}C_{DMF}$ 2.3, 2.1, 2.7 Å and $H_{framework}\cdots N{\equiv}C_{\mathbf{A}}$ 2.2, 2.3, 3.2 Å. However, extra stabilisation of the molecule was obtained by additional CH-π interactions to hold the acetonitrile molecule in this particular site. A slightly longer hydrogen bond was observed in **4A**, which was probably due to the orientational difference that arises because **A** is less sterically demanding than DMF. The second molecule of **A** was found at the site which was previously occupied by the DMF molecule shown in pink in **4,** as depicted in Figure 4.4e. In **4** and **4A** both molecules were aligned roughly parallel to the *c* axis. Despite being able to replace DMF from the site, **A** did not coordinate to the Cd ion. The nitrile group forms only weak bonds with the framework: $N{\equiv}C_{\mathbf{A}}\cdots H_{framework}$ 3.6, 3.5 Å. However, the methyl group is engaged in a hydrogen bond with the carboxylate of the framework: $CH_{3\mathbf{A}}\cdots O{=}C_{framework}$ 2.860 Å. Since the intermolecular interactions in sponge **4** are dominated by hydrogen bonding, it is likely that **A** preferred the $CH_{3\mathbf{A}}\cdots O{=}C_{framework}$ bond for stabilisation. In addition, it is reported in the literature that guest molecules with an appropriate binding functional group do not necessarily coordinate to the metal and may stabilise themselves in the pores.[126,127]

a)

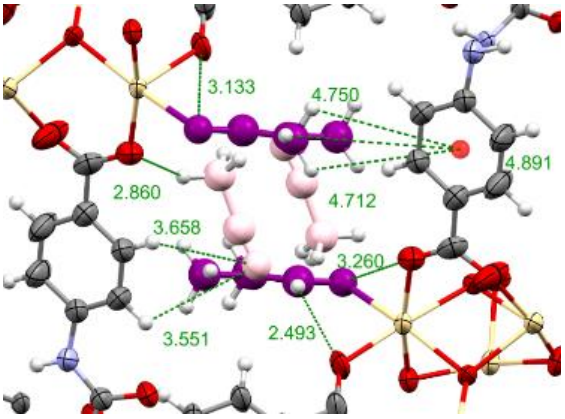

b)

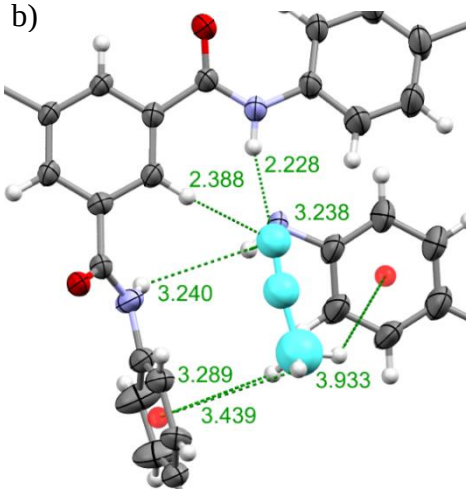

Figure 4. 5 a) Intermolecular interaction between turquoise acetonitrile and the host framework b) Intermolecular interaction between pink acetonitrile and the host framework. Acetonitrile molecules were coloured according to their positional equivalence similar to the DMF molecules in sponge ***4****. Acetonitrile molecules were displayed in ball stick. Interaction distances are displayed in angstroms.*

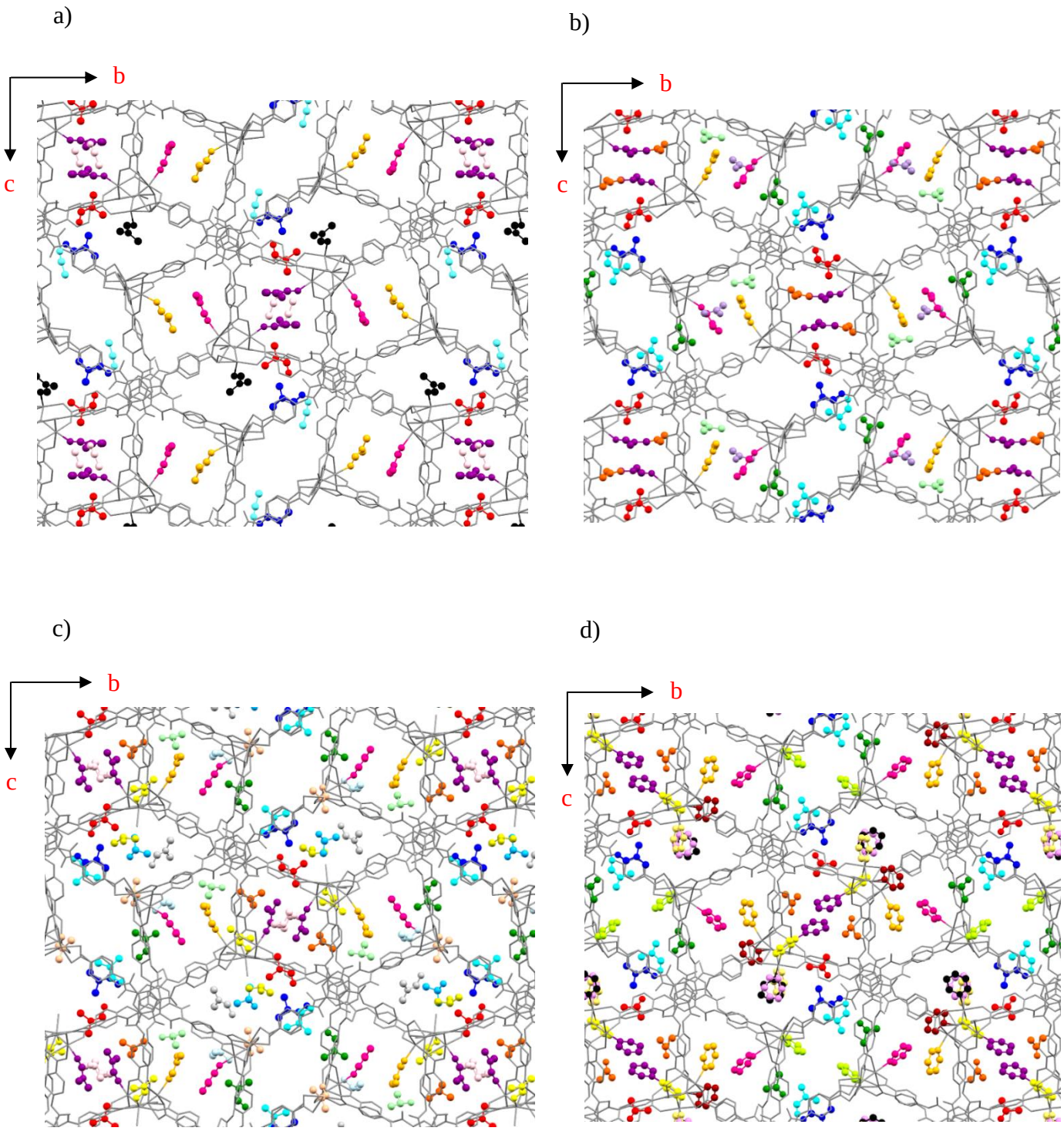

Figure 4. 6 Packing diagram of inclusion complexes viewed down the a-axis. a) acetonitrile, b) acetone, c) isopropanol, d) pyridine. Framework is displayed in capped stick and guest molecules in ball and stick. Colours of the molecules are according to the positional equivalence.

Inclusion complex with acetone **4B**

The structure of inclusion complex **4B** with seven Cd^{2+} ions and four BTA linkers was unchanged from **4**. Inclusion complex **4B** crystallised in the $P2_1/n$ space group, the unit cell parameters are similar to **4A**. In the asymmetric unit of inclusion complex **4B**, six DMF molecules, three coordinated with 100% occupancy and three were in the pores with 75 and 100% occupancy. Four acetone molecules were observed in the pores with 30-100% occupancy. Figure 4.6b illustrates the packing diagrams of **4B**, which are compared with the packing diagram of **4,** displayed in Figure 4.3. DMF identified in magenta, purple, and light orange were observed coordinated to Cd2, Cd4 and Cd6 respectively, similar to **4** and **4A**. DMF molecules in the pore identified in blue, turquoise and red colour were present at the same site as **4**. The red DMF molecules were observed with a slight rotation difference in comparison with **4**. This can be explained by the formation of hydrogen bonds with the **B** molecule which was missing in **4**. The DMF molecule identified in green in **4** is replaced by a molecule of **B** in **4B**. A closer examination of Figure 4.7a shows that both the DMF and acetone molecules are interacting with the framework via almost the same hydrogen bond distances, $H_{framework}\cdots O{=}C_{DMF}$ 2.0, 2.3, 2.4 Å and $H_{framework}\cdots O{=}C_{acetone}$ 2.1, 2.3, 2.4 Å. The methyl group of **B** forms a hydrogen bond with the framework $O{=}C_{framework}\cdots H_3C_{acetone}$ 2.5Å, whereas the methyl group of the DMF molecule forms only weaker interaction with the same carboxylate group of the framework $O{=}C_{framework}\cdots H_3C_{DMF}$ 3.8Å. The remaining three acetone molecules in the pore occupied unique positions shown in lilac, light green, and orange which was not observed in **4** or **4A**. The acetone molecule shown in lilac is oriented such that the C=O group is extending in the pore along the *a*-axis, hence not involved in the hydrogen bonding. The light green molecule of acetone is hydrogen-bonded with the framework of 2.378 Å and via CH-π with the framework of 3.8 Å, as shown in Figure 4.7b. In the orange molecule, the C=O is parallel to the *b*-axis extending in the pore and away from the framework, hence no hydrogen bonding with the framework was observed. However, one of the methyl groups of the acetone molecule shown in orange is engaged in hydrogen bonding with the carboxylate group of the framework and the other one is forming CH-π interaction with the centroid of the phenyl ring of the framework. In addition, C=O of orange acetone forms a hydrogen bond with the red DMF molecule 2.7 Å, due to its proximity. These different orientations acquired by **B** were explained by its polar nature. The carbonyl group of **B** is polar and aprotic therefore it orients itself to face a nearby hydrogen donor

to form hydrogen bonding with the framework. These observations further support the hydrophilic nature of the sponge **4**.

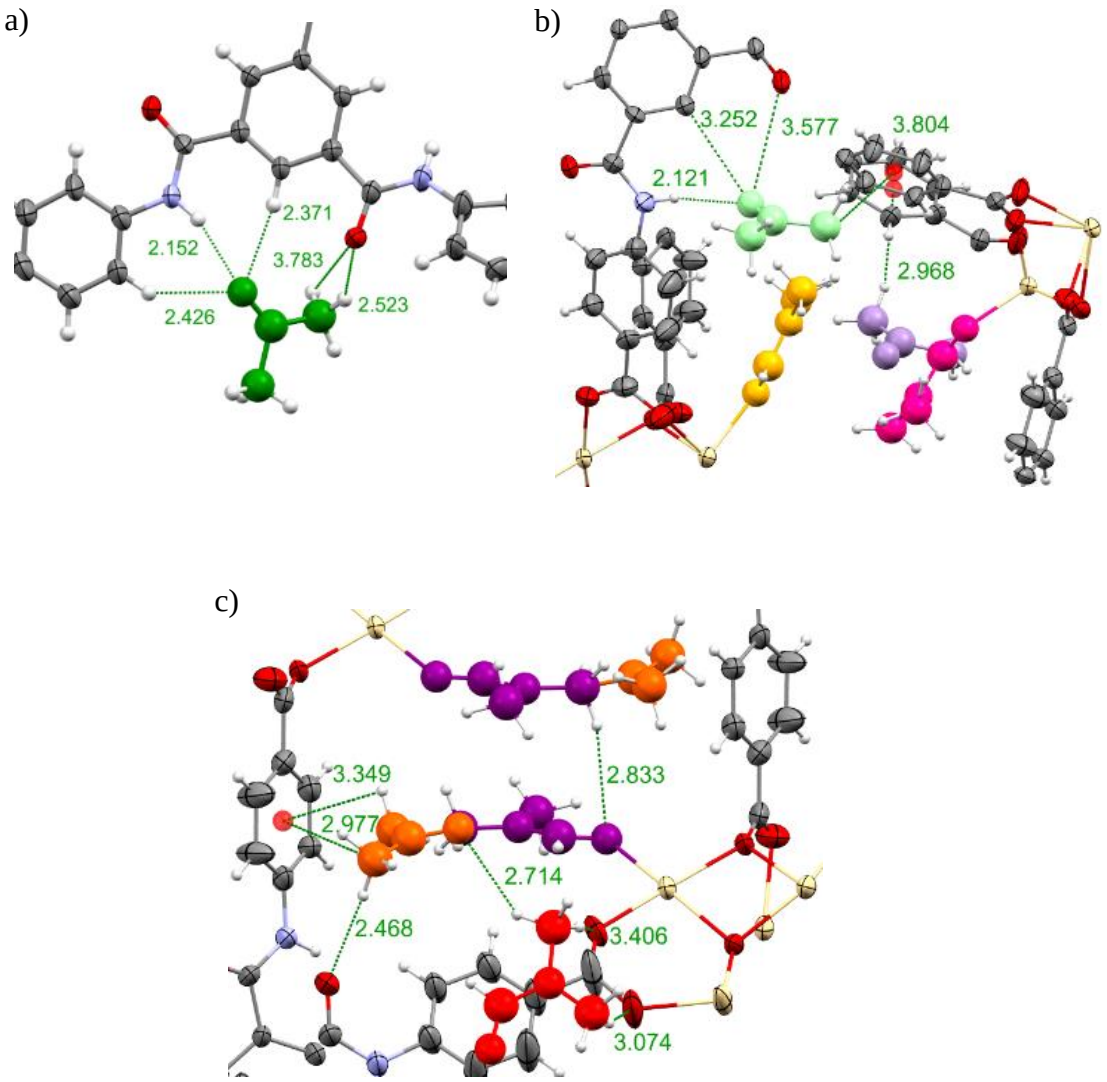

*Figure 4. 7 Intermolecular interactions between acetone a) green b) light green and lilac c) orange with the host framework. Guest molecules were coloured according to their positional equivalence similar to the DMF molecules in sponge **4**. Acetone molecules were displayed as ball stick models. Interaction distances are displayed in angstroms.*

Inclusion complex with isopropanol **4C**

The structure of inclusion complex **4C** with seven Cd^{2+} ions and four BTA linkers was unchanged from **4**. Inclusion complex **4C** crystallised in the $P2_1/n$ space group same as **4** with larger β in comparison with **4**. In the asymmetric unit of inclusion complex **4C**, five DMF molecules were coordinated to Cd ions with 100% occupancy. Three DMF molecules, identified in magenta, purple, and light orange, were observed coordinated to Cd2, Cd4 and Cd6 respectively, similar to **4**, **4A** and **4B**. The remaining two DMF molecules, identified in yellow and peach, were coordinated to Cd1 and Cd2. These sites were occupied by the water molecules in the previous structures. Five DMF molecules were observed in the pores identified in red, blue, turquoise, and green along with one unique position in grey colour with occupancy 100%. The grey DMF molecule was also fixed in the pore via hydrogen bonding with the framework, as shown in Figure 4.8c.

Six isopropanol molecules were observed in the pores with 50 and 75% occupancy. Figure 4.6c illustrates the packing diagrams of **4C**. Comparison with the packing diagram of **4**, displayed in Figure 4.2, shows that the pink molecule of **C** occupied the same position as pink DMF in **4**. Although not coordinated, a similar observation was made in **4A**. The molecule of **C** at the pink position is oriented such that the hydroxyl group is roughly parallel to the *a*-axis that is it is extending in the channel. This hydroxyl group is interacting with the framework via a hydrogen bond of 2.9 Å. Since **C** is more polar than **A** such differences in non-bonding interactions were expected. Furthermore, molecules of **C** identified in light green and orange occupied the same position common to both **4B** and **4C**, as shown in Figures 4.7c and 4.8b. However, molecules of **C** in **4C** were oriented differently than **B** from **4B**. This is because light green- and orange-coloured molecules of **C** share a unique hydrogen bond of 2.726 Å, which was not observed between **B** molecules in **4B**. In addition, a few unique positions were occupied by isopropanol molecules, as coloured in olive, light blue and cyan (Figure 4.8 c,d,e). The hydroxyl groups of the olive and light blue coloured **C** molecule forms a hydrogen bond with the carboxylates of the framework of 2.6 Å and 2.8 Å, respectively. Due to the proximity of the light blue molecule of **C** with the framework, a few CH-π were also observed. In contrast, the olive molecule has extended far into the pore thus no more interaction with the framework was observed. Similarly, the cyan coloured **C** molecule was stabilised in the pore via a hydrogen bond with the nearby blue DMF molecule 2.5 Å. These

unique positions are mainly fixed in the pore due to the presence of donor atom of the hydroxyl group. Since **A** and **B** are aprotic solvents and lack that group, these sites were not observed in **4A** or **4B**.

Inclusion complex with ethanol **4D**

The structure of inclusion complex 4D with seven Cd^{2+} ions and four BTA linkers was unchanged from **4.** The asymmetric unit of inclusion complex with ethanol 4D, consists of two ethanol molecules with an occupancy of 20%, three DMF molecules in the pores and two coordinated to the Cd ion with occupancy ranging from 50-100%. Although the structure shows similarities with the other inclusion complexes the data was of low quality and will not be discussed in detail. Several positions common to the other structures were identified however, with DMF molecules identified in blue and turquoise colour being observed in **4D**. The red coloured DMF molecule from **4** was replaced by the ethanol molecule and found hydrogen-bonded with the framework similar to all the other inclusion complexes. The other ethanol molecule was found at the site similar to the cyan molecule of isopropanol in **4C**.

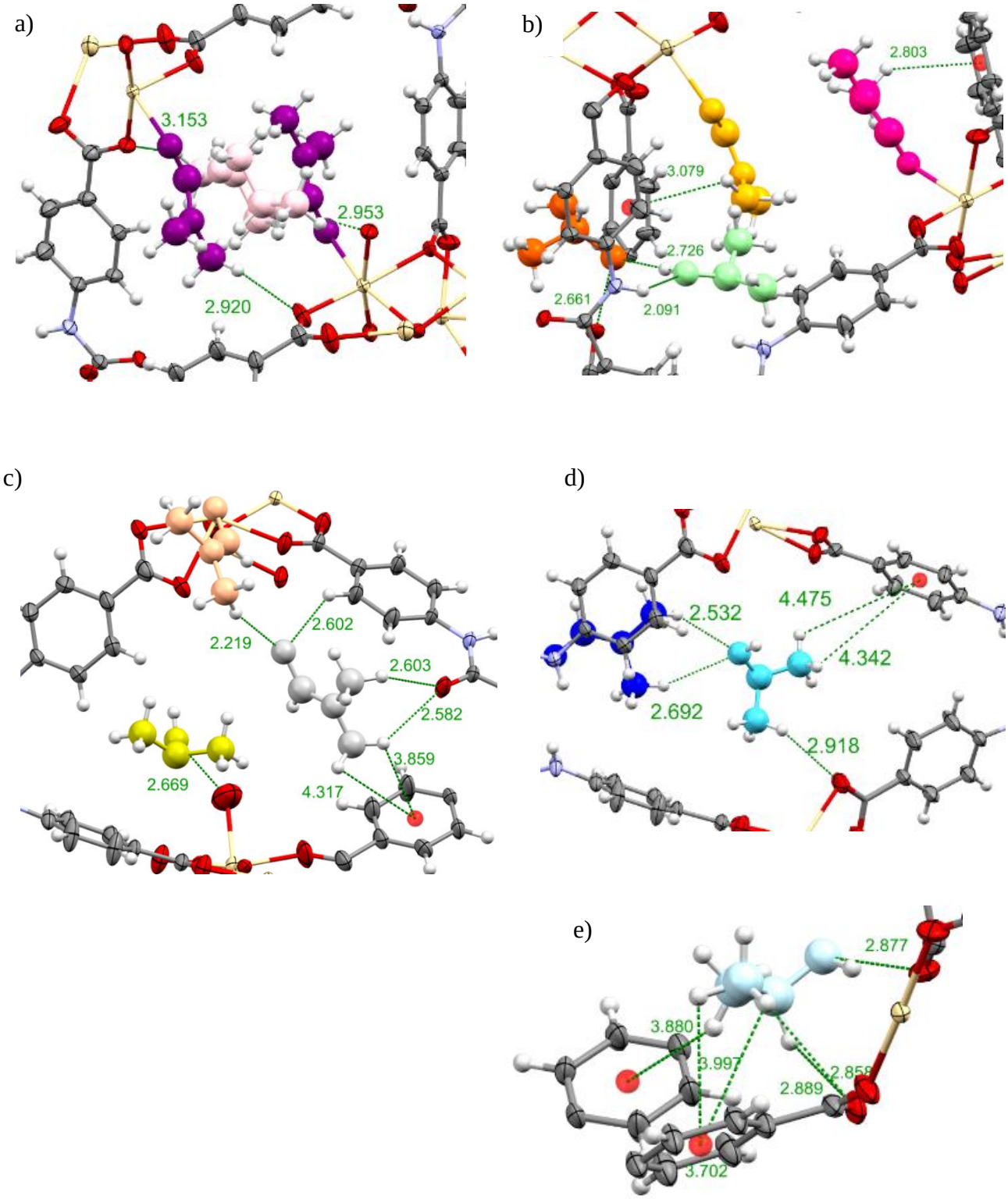

Figure 4. 8 Intermolecular interactions between isopropanol a) pink b) light green and orange c) olive d) cyan e) light blue and host framework. Guest molecules were coloured according to their positional equivalence similar to the DMF molecules in sponge ***4****. isopropanol molecules were displayed as ball and stick model. Interaction distances are displayed in angstroms.*

Inclusion complex with pyridine **4E**

The structure of inclusion complex **4E** with seven Cd^{2+} ions and four BTA linkers is different from **4**. This is because pyridine was found coordinated to the Cd ions replacing all the coordinated DMF from **4** and hence the structure of sponge **4E** is different and now referred to as **4'**. Inclusion complex **4'** crystallised in the $P2_1/n$ space group, same as **4**, but with shorter *a*, longer *b* and larger β in comparison with **4**. In the asymmetric unit, there are nine pyridine molecules observed. Eight of them are coordinated to Cd ions with 100% occupancy and one was observed in the pore with 50% occupancy. Two DMF molecules with occupancy 75 and 100% and three acetone molecules with occupancy ranging from, 25 to 100% (used for diluting pyridine for soaking) were found in the pore.

Among eight coordinated pyridines, five were bonded to Cd1, Cd2, Cd4, Cd6, and Cd7, where each Cd ion has one coordinated pyridine molecule identified in lime, magenta, purple, light orange, and maroon respectively. The remaining three pyridine molecules were bonded to Cd5 identified in black, light purple and yellow. A few sites, shown in purple, orange and magenta on their respective Cd ions, are constantly observed in all the inclusion complexes previously described on the same Cd ion. The black and yellow position on Cd5 was observed in **4B** and **4C** respectively and was occupied by DMF. The unique positions occupied by pyridine that appeared only in **4'** are shown in lime, light purple and maroon. In the previous structure, these sites were occupied by water molecules, O^{2-} ligand or BTA linker molecules. One pyridine in the pore was observed and is shown in gold colour in Figure 4.9a. This pyridine is very close to Cd7 but did not coordinate. In addition, the distance between Cd7 and the nitrogen atom of the pyridine shown in gold was 2.8 Å, which is longer than observed between the coordinated pyridine to Cd ion distances, which ranged from 2.2 to 2.3 Å. However, a short contact between the N of gold pyridine with the carboxylate of the framework was observed at 2.6 and 2.7 Å. Furthermore, Figure 4.9 illustrates the geometry of all the Cd^{2+} ions of **4'** and was compared to the geometry of **4** shown in Figure 4.2. It was observed that the Cd^{2+} ions in **4'** were also six coordinate with octahedral geometry except for Cd3 which has distorted octahedral geometry (Figure 4.9c). Cd ions in **4'** are now surrounded by nitrogen atoms from the pyridine molecule along with the oxygen atoms from the linker molecules and the bridging oxygen. For example, Cd5 is now coordinated to three pyridine molecules identified in black, light purple, and yellow (Figure 4.9e). In contrast, Cd5 in

4, these sites were occupied by two water molecules and one carboxylate from the linker (Figure 4.2e).

The DMF molecules identified in blue and turquoise persisted from the synthesis and could not be exchanged because they were strongly bonded to the framework via hydrogen bond as observed in previous complexes **4A**-**4C** (see Figure 4.5). Among the three acetone molecules observed in **4'**, two were found at green and orange sites which were common to the structure of **4B** (Figure 4.7). The green acetone molecule in both the complexes **4'** and **4B** was found at the same location as evident from the bond distances in Figures 4.7a and 4.10a. However, the orange acetone molecule in both the complexes even though sharing the same site, a difference in orientation was observed. Compared to the molecule in **4B**, the orange acetone molecule in **4'** is now oriented such that the C=O group is roughly parallel to the *c*-axis. In contrast to the **4B**, no hydrogen bond was observed in **4'** (Figure 4.7c and 4.10b). Furthermore, the third acetone molecule occupying a red position in **4'**, was previously occupied by the DMF molecule in **4B**, although no interaction between red and orange molecules was observed in **4'** as observed in **4B** (Figure 4.7c and 4.10b). The reason for these observed differences is probably due to the change in the structure of **4'** caused by the presence of pyridine instead of DMF. Pyridine is less polar than DMF, therefore, does not attract acetone molecules to form hydrogen bonds, as evident from the non-bonding interaction. The accommodation of pyridine molecules through coordinative alignment is indicative of the stability of **4** in the nucleophilic guests. This result is consistent with previous literature reports described in section 4.1 where pyridine molecules bind to the framework via coordinative alignment. Moreover, in **4'** even after accommodating pyridines on the Cd, 5% of the unit cell volume 1018 $Å^3$ is still available to accommodate more guest molecules.

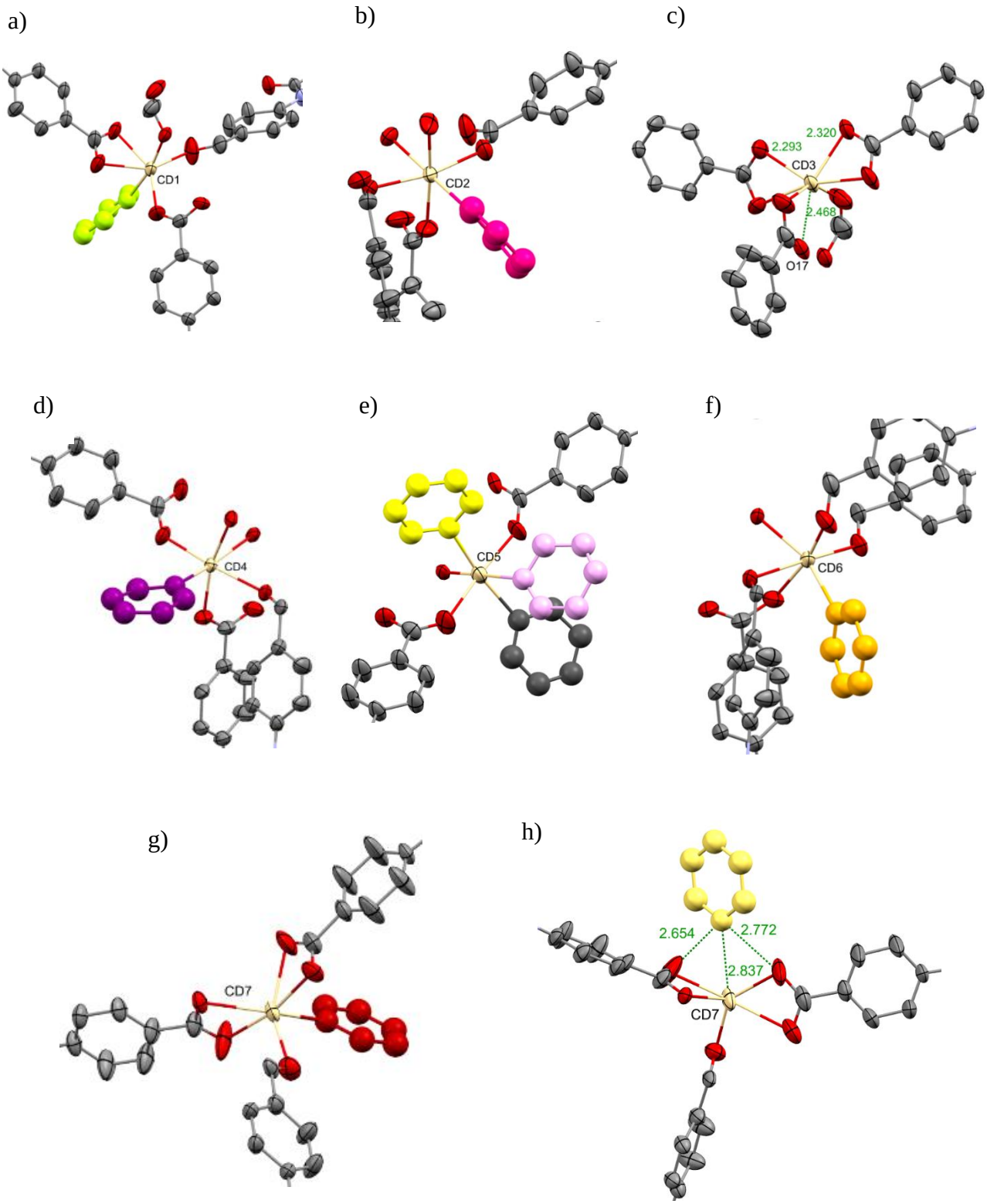

Figure 4. 9 a)-g) Geometry of Cd1-Cd7 ions surrounded by linker molecules, bridging oxygens and pyridine molecules. h) Pyridine in the pore and interaction with the framework. Guest molecules were coloured according to their positional equivalence like the DMF molecules in sponge ***4****. Pyridine molecules were displayed in ball and stick model. Interaction distances are displayed in angstroms.*

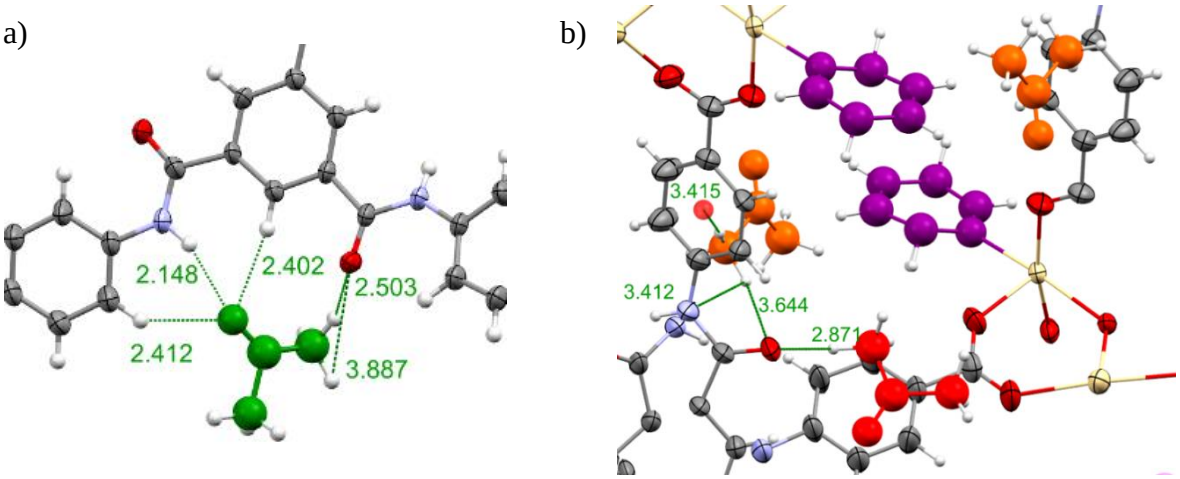

*Figure 4. 10 Intermolecular interactions between acetone a) green b) orange, red molecule, and host framework. Guest molecules were coloured according to their positional equivalence like the DMF molecules in sponge **4**. Acetone molecules were displayed in ball stick. Interaction distances are displayed in angstroms.*

4.2.5 Conclusions

Attempts to generate {[$Cd_7(BTA)_4(H_2O)_x(DMF)_n$]·$(DMF)_m$}, by a modified literature procedure led to a new MOF **4** that was used in all subsequent studies. Sponge **4** was stable in a variety of solvents, polar aprotic, polar protic and Lewis bases. The results show that sponge **4** has outstanding stability and outperformed sponge **1** in this report. Detailed analysis of inclusion complexes generated from **4** further demonstrates the hydrophilic nature of the sponge **4**. Hydrogen bonding was observed as the dominant non-bonding host-guest interaction and was the rationale for solvent molecules occupying different orientations. Moreover, DMF molecules were strongly held in the sponge **4** via hydrogen bond at particular sites in all inclusion complexes. Sponge **4** shows versatility in accommodating guest molecules in the pores as well as via coordinative alignment. The formation of the **4'** complex demonstrates the opportunities to accommodate a variety of Lewis bases via coordinative alignment. In conclusion sponge **4** is a successful alternate crystalline sponge that has overcome all the limitations of Fujita's sponge. This sponge is highly recommended for use in CSM, particularly to accommodate Lewis bases and nucleophile guests.

4.3 EXPERIMENTAL SECTION

4.3.1 Synthesis of ligand L = 4,4'4''-[1,3,5-benzenetriyltris(carbonylimino)]-trisbenzoic acid

Ligand 4,4'4''-[1,3,5-benzenetriyltris(carbonylimino)]-trisbenzoic acid was synthesised by the reported literature procedure.[160] 1,3,5-benzenetricarboxylic acid chloride (3.98 g, 15.0 mmol) was added to a solution of 4-amino-benzoic acid (6.18 g, 45.1 mmol) and triethylamine (3.62 mL, 26.0 mmol) in *N*,*N*-dimethylacetamide (DMA) (80 mL). The mixture was stirred for 16 h at room temperature and then water (300 mL) was added. A white precipitate was formed which was filtered off and the solid was washed with acetone, water, and methanol. The product was then air-dried and characterised by NMR and mass spectroscopy. ^{1}H NMR (DMSO-d_6, δ ppm): 12.81 (broad peak, 3H, COOH), 10.89 (s, 3H, CONH), 8.75 (s, 3H, ArH), 7.98 (s, 12H, ArH), *m/z* 567.13.

4.3.2 Synthesis of $\{[Cd_7(L_4)(H_2O)_x(DMF)_n]\cdot(solvent)_m\}$ (sponge **4)**

The crystals of $\{[Cd_{27}(L_4)(H_2O)_x(DMF)_n]\cdot(solvent)_m\}$ were synthesised by a modified literature procedure.[158] A solvothermal reaction of $Cd(NO_3)_2\cdot 6H_2O$ (0.033 g) and BTA (0.013 g) in DMF (2ml) with H_2O (4-5 drops) was performed at 85 °C for 3 days in a screw-capped pyrex vial. The colourless rod-shaped crystals of sponge **4** were obtained. The crystals were kept immersed in DMF in an incubator at 25 °C until required for the solvent exchange and guest encapsulation experiments.

4.3.3 Solvent exchange and synthesis of sponge **4'**

SCXRD analysis of **4** shows that DMF molecules from the synthesis were coordinated to the Cd ions. Several attempts were made to remove DMF from the pores as well from the coordination site by solvent exchange with methanol, ethanol, isopropanol, chloroform, acetonitrile, acetone, and pyridine. Exchange with neat chloroform and neat methanol resulted in the deterioration of the crystals. The crystals survived in neat ethanol, acetone, isopropanol, and acetonitrile. SCXRD analysis revealed that solvents partially removed DMF from the pores however DMF remained bonded to the metal ions.

Synthesis of sponge **4'**

Sponge **4'** was obtained when crystals of **4** were exchanged with diluted pyridine. When neat pyridine was used the crystal dissolved therefore pyridine was diluted with DMF. SCXRD analysis

revealed that pyridine molecules replaced DMF from the coordination site but one coordinated DMF was remaining. Therefore, acetone for dilution was selected and results revealed that pyridine successful replaced DMF from all the coordination sites which is the formation of sponge **4'**. Details of solvent exchange are represented in Table 4.1.

*Table 4. 2 Soaking conditions of crystals **4** in various solvents*

Solvent	**Composition**	**Incubation period/days**	**Results**
Methanol	neat	2	Crystals deteriorated as soon as removed from the solvent therefore data could not be collected
Chloroform	neat	2	Crystals deteriorated
Ethanol	neat	2	Crystals remain stable. SCXRD analysis showed ethanol molecules in the pores along with a few DMF molecules.
Ethanol	neat	14	Crystals optically look fine but do not diffract.
Isopropanol	neat	8	Crystals remain stable. SCXRD analysis showed isopropanol molecules in the pores along with a few DMF molecules.
Isopropanol	neat	21	Crystals optically look fine but do not diffract.
Acetonitrile	neat	3	Crystals remain stable. SCXRD analysis showed acetonitrile molecules in the pores along with DMF molecules.
Acetonitrile	neat	30	Crystals remain stable. SCXRD analysis showed acetonitrile molecules in the pores along with a few DMF molecules.
Acetone	neat	7	Crystals remain stable. SCXRD analysis showed acetone molecules in the pores along with a few DMF molecules
Acetone	neat	30	Crystals remain stable. SCXRD analysis showed acetone molecules in the pores along with a few DMF molecules
Pyridine	neat	1	Crystal dissolved
Pyridine	Pyridine (50 µL) DMF (3 mL)	7	Out of 6 Coordinated DMF molecules, pyridine replaced 5 DMF molecules. However, one DMF was still coordinated to the Cd.
Pyridine	Pyridine (50 µL) Acetone (3 mL)	14	All coordinated DMF molecules were replaced by the pyridine molecules. Acetone and DMF molecules were observed in the pores.

4.3.4 Crystallographic procedures

Using the same procedure as described in Section 2.3.3

4.3.5 Structural analysis details

The non-hydrogen atoms of the framework were refined anisotropically and hydrogen atoms were included using a riding model. The BTA and Cd components of the framework were at first freely refined without applying any constraints/restraints. However, the BTA, Cd and coordinated DMF components of the framework showed some disorder and where required atoms were modelled across two positions with a combined occupancy of 100% were used. DFIX and EADP were used to obtain a stable model. Refinement of solvent species was first performed without any constraints/restraints and only if this was unsuccessful, were these added based on their known structures. The occupancy of each solvent molecule was refined against its free variable which in the final stages of refinement was fixed to values reported. In addition, some disorders were observed in the DMF molecules (coordinated and in the pores) and the guest solvent molecules in the pores were modelled across two positions with a combined occupancy of 100% were used. In all the structures it was not possible to assign all the residual density peaks in a way that makes chemical sense, these peaks belong to heavily disordered guests or solvent molecules, and these were taken into account by the use of a solvent mask in the OLEX2 GUI[154]. On occasion a large residual density peak remained near the cadmium metal of the host framework this is due to absorption and/or termination errors in Fourier calculation. Standard deviations for restraints used are as described in Chapter 2 section 2.3.4.

4.3.6 Refinements details of as synthesised **4** and of individual guests in each inclusion complex

Sponge **4**

The asymmetric unit of four consists of four BTA linkers, seven Cd ions, four coordinated DMF molecules and six DMF molecules in the pore. Anisotropic refinement of the non-hydrogen atoms of sponge **4** was performed by applying constraints/restraints to achieve a stable model. ISOR and EADP was used to constrain the atomic displacement parameters of the coordinated DMF molecules to similar values. DFIX and SIMU were used to fix bond lengths of DMF molecules in the pores to obtain a realistic and acceptable geometry. Hydrogen atoms were added by the riding model. However, for a few DMF molecules hydrogens were required to be placed in fixed positions. The solvent mask detected one significant void 71104 $Å^3$ in size containing 1584 electrons. A large residual peak (5.4 e/Å) was found closer to Cd ion, this is due absorption.

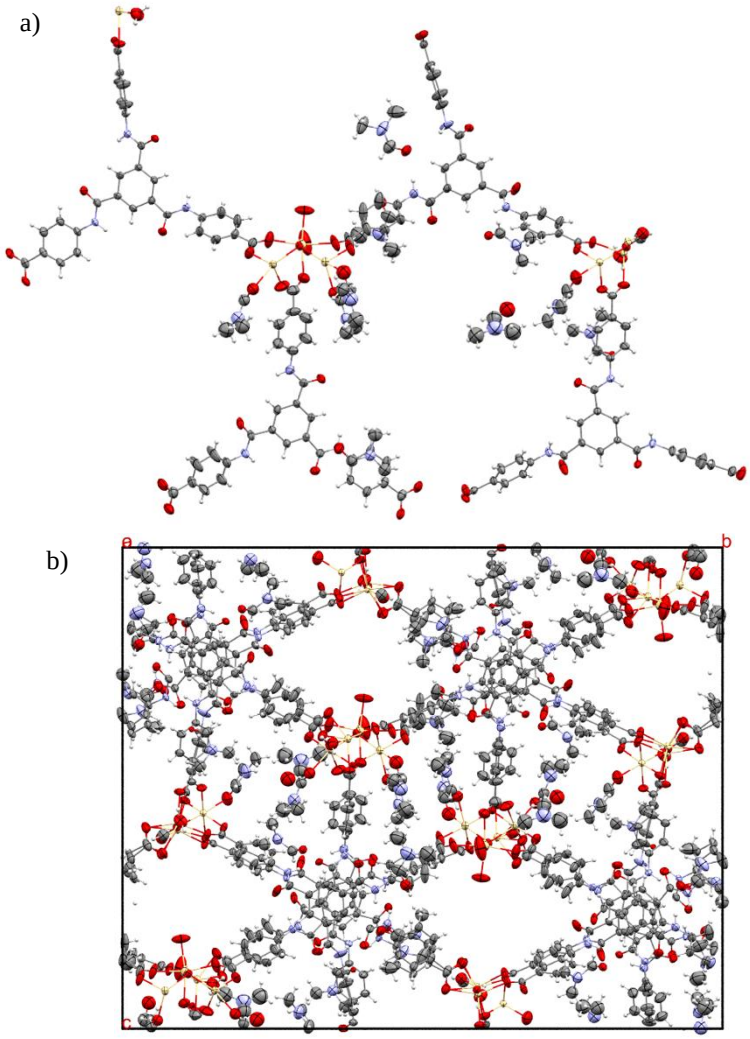

*Figure 4. 11 a) The asymmetric unit of Sponge **4.** b) Unit cell of Sponge **4***

Inclusion complex **4A**

The asymmetric unit of **4A** four consists of four BTA linkers, seven Cd ions, four coordinated DMF molecules, two DMF molecules in the pore and two acetonitrile molecules in the pore. Anisotropic refinement of the non-hydrogen atoms of the framework was performed by applying constraints/restraints where necessary. Acetonitrile molecules were refined anisotropically and where necessary DFIX was applied to achieve acceptable geometry and a stable model. ISOR and EADP were applied to restrain the ADPs. Hydrogen atoms were added by the riding model. However, for some molecules hydrogens were required to be placed in fixed positions. The solvent mask detected one significant void 6864 $Å^3$ in size containing 1510 electrons. A large residual peak (4.5 e/ Å) was found closer to O20, this peak could not be assigned in a way that makes any chemical sense.

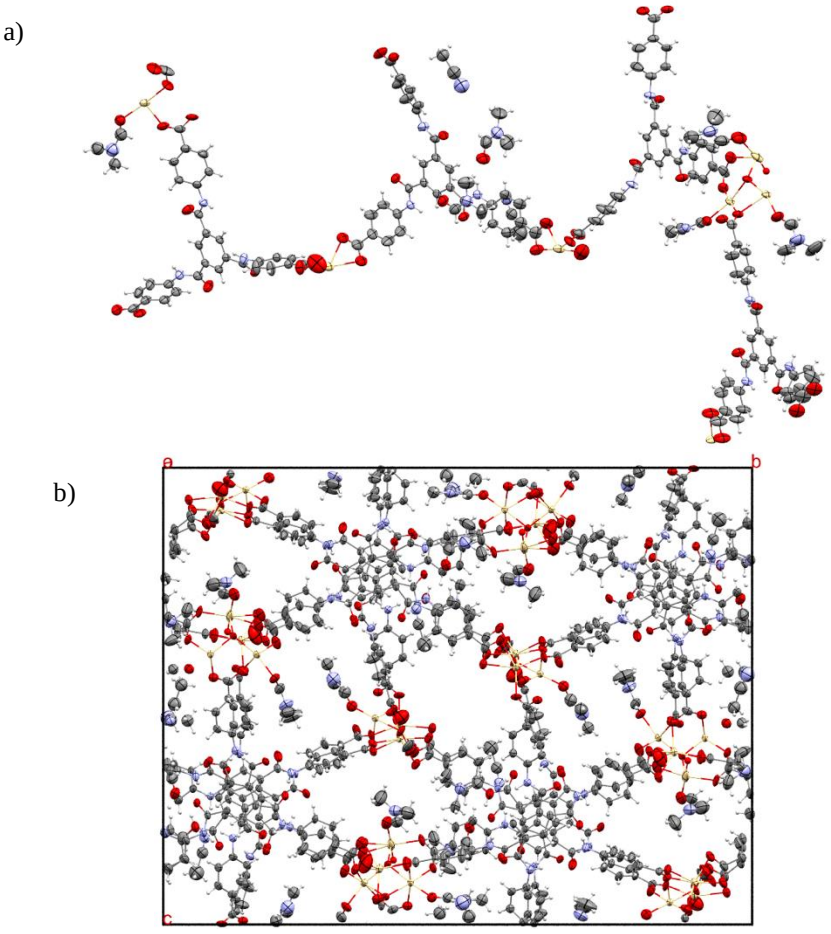

*Figure 4. 12 a) The asymmetric unit of complex **4A**, showing major components of disorder only. b) Unit cell of inclusion complex **4A**.*

Inclusion complex **4B**

The asymmetric unit of **4B** four consists of four BTA linkers, seven Cd ions, three coordinated DMF molecules, three DMF molecules in the pore and four acetone molecules in the pore. Anisotropic refinement of the non-hydrogen atoms of the framework was performed by applying constraints/restraints where necessary. Acetone molecules were refined anisotropically and where necessary DFIX, ISOR and EADP was applied to achieve a stable model. Hydrogen atoms were added by the riding model. However, for some molecules hydrogens were required to be placed in fixed positions. The solvent mask detected one significant void 6257 $Å^3$ in size containing 1435 electrons. A large residual peak (3.9 e/Å) was found closer to Cd ion, this is due absorption and/or termination errors in the Fourier calculations.

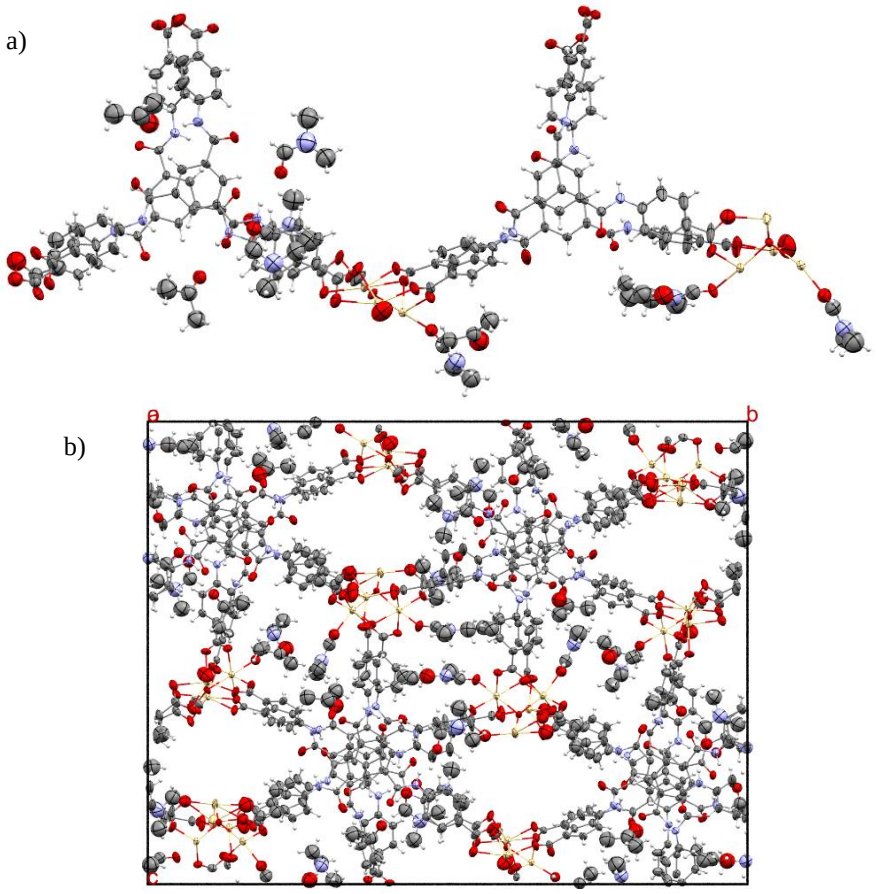

*Figure 4. 13 a) The asymmetric unit of complex **4B**, showing major components of disorder only. b) Unit cell of complex **4B**.*

Inclusion complex **4C**

The asymmetric unit of **4C** four consists of four BTA linkers, seven Cd ions, five coordinated DMF molecules, five DMF molecules in the pore and six isopropanol molecules in the pore. Anisotropic refinement of the non-hydrogen atoms of the framework was performed by applying constraints/restraints where necessary by using DFIX and EADP. Isopropanol molecules found in the pores were refined anisotropically and where necessary DFIX, ISOR and EADP were applied to achieve a stable model. Hydrogen atoms were added by the riding model. However, for some molecules hydrogens were required to be placed in fixed positions. The solvent mask detected two significant voids 769 $Å^3$ and 472 $Å^3$ in size containing 188 and 127 electrons respectively. A large residual peak (9.8 e/Å) was found closer to Cd ion, this is due absorption and/or termination errors in the Fourier calculations.

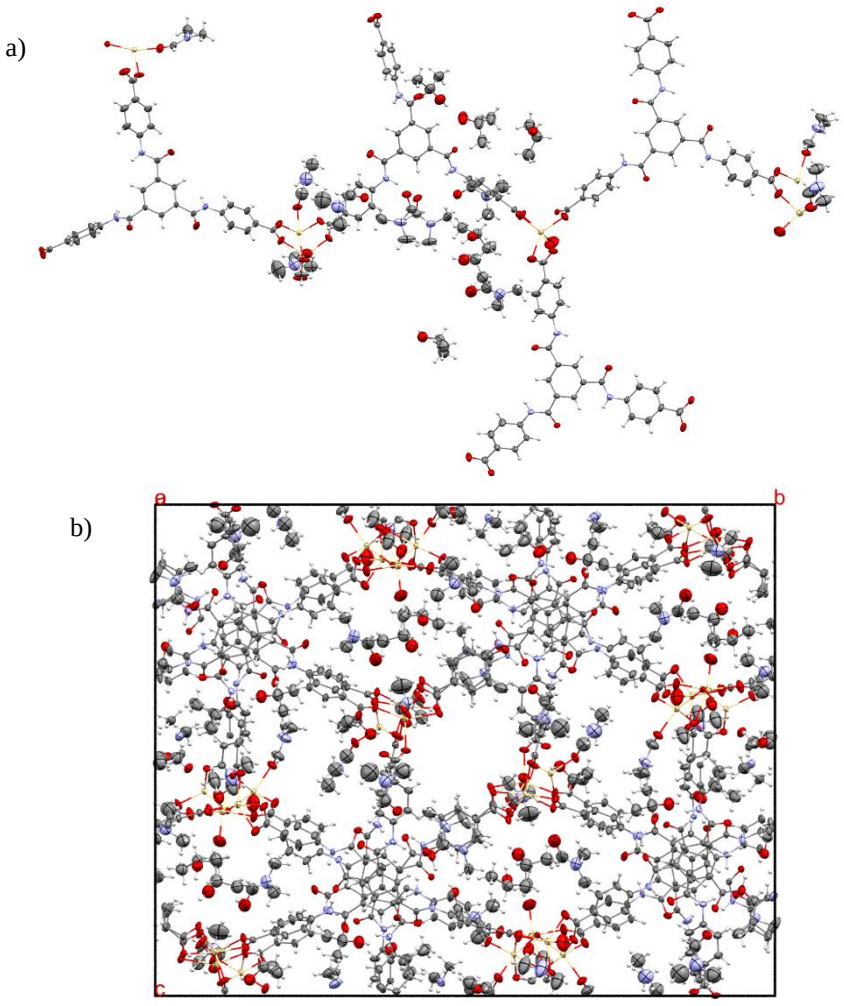

*Figure 4. 14 a) The asymmetric unit of complex **4C**, showing major components of disorder only. b) Unit cell of complex sponge **4C.***

Inclusion complex **4'**

The asymmetric unit of **4'**, four consists of four BTA linkers, seven Cd ions, and seven coordinated pyridine molecules. In the pore two DMF molecules, three acetone molecules and one pyridine molecule were observed. Anisotropic refinement of the non-hydrogen atoms of the framework was performed by applying constraints/restraints where necessary. In this complex pyridine molecules are part of the framework. Disordered pyridine molecules were observed and where necessary atoms were modelled over the two positions with combined occupancies of 100%. DFIX was applied to fix the bond lengths, and AFIX was used to make the pyridine ring rigid. On several pyridine molecules EADP and ISOR were used to constrain the atomic displacement parameter to similar values. Hydrogen atoms were added by the riding model. The solvent mask detected two significant voids 1662 $Å^3$ and 355 $Å^3$ in size containing 406 and 71 electrons respectively. A large residual peak (2.6 e/Å) was found closer to N11, this peak could not be assigned in a way that makes any chemical sense.

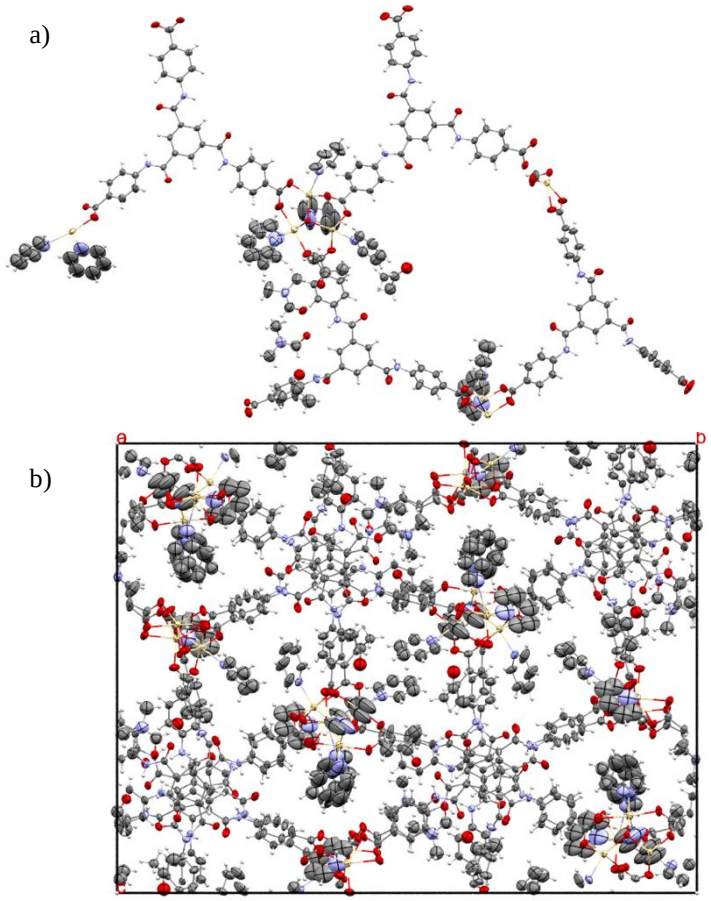

*Figure 4. 15 a) The asymmetric unit of complex **4'**, showing major components of disorder only. b) The unit cell of complex **4'**.*

4.3.7 Crystallographic Table

Inclusion complexes	**4**	**4A**	**4B**	**4C**	**4'**
Empirical formula	$C_{148.5}H_{135.5}Cd_7N_{21}O_{52}$	$C_{142.2}H_{124.2}Cd_7N_{19.5}O_{47}$	$C_{142.23}H_{121.47}Cd_7N_{17}O_{47.32}$	$C_{159.73}H_{162.49}Cd_7N_{21.75}O_{54}$	$C_{168.79}H_{137.80}Cd_7N_{21}O_{42.88}$
Formula weight	3833.07	3645.00	2890.27	2691.77	2621.86
Temperature/K	150(1)	150(1)	150(1)	150(1)	150(1)
Crystal system	monoclinic	monoclinic	monoclinic	monoclinic	monoclinic
Space group	$P2_1/n$	$P2_1/n$	$P2_1/n$	$P2_1/n$	$P2_1/n$
a/Å	14.6954(2)	13.6817(2)	13.9475(2)	14.52210(10)	14.02999(14)
b/Å	42.2913(4)	43.2808(4)	43.3134(4)	42.7754(2)	43.3663(3)
c/Å	33.8929(4)	33.7646(4)	33.5321(4)	33.9548(2)	33.7009(2)
α/°	90	90	90	90	90
β/°	91.6490(10)	95.3182(14)	94.4569(11)	93.4290(10)	94.3810(8)
γ/°	90	90	90	90	90
V/Å^3	21055.3(4)	19907.9(5)	20195.9(4)	21054.6(2)	20444.7(3)
Z	4	4	4	4	4
ρ_{calc}g/cm^3	1.61	1.212	1.224	1.273	1.307
μ/mm^{-1}	6.143	6.289	6.376	6.177	6.322
F(000)	7128	7269	7466	8156	8096
Crystal size/mm^3	0.28 × 0.13 × 0.06	0.24 × 0.12 × 0.08	0.27 × 0.15 × 0.06	0.25 × 0.15 × 0.05	0.24 × 0.13 × 0.06
Radiation	CuK_α (λ = 1.54184)	CuK_α (λ = 1.54184)	CuK_α (λ = 1.54184)	CuK_α (λ = 1.54184)	CuK_α (λ = 1.54184)
2Θ range for data collection/°	6.818 to 145.824	7.074 to 146.946	6.996 to 147.07	7.082 to 147.072	6.656 to 147.438
Index ranges	−18 ≤ h ≤ 12, −52 ≤ k ≤ 49, −41 ≤ l ≤ 40	−16 ≤ h ≤ 16, −38 ≤ k ≤ 53, −41 ≤ l ≤ 28	−17 ≤ h ≤ 15, −51 ≤ k ≤ 53, −41 ≤ l ≤ 40	−17 ≤ h ≤ 16, −52 ≤ k ≤ 52, −39 ≤ l ≤ 42	−17 ≤ h ≤ 17, −53 ≤ k ≤ 53, −41 ≤ l ≤ 41
Reflections collected	160787	81548	148527	166701	378169
Independent reflections	41170 [R_{int} = 0.0586, R_{sigma} = 0.0457]	38920 [R_{int} = 0.0478, R_{sigma} = 0.0556]	40073 [R_{int} = 0.0671, R_{sigma} = 0.0513]	41795 [R_{int} = 0.0486, R_{sigma} = 0.0351]	40915 [R_{int} = 0.0836, R_{sigma} = 0.0315]
Data/restraints/parameters	41170/381/2066	38920/148/2052	40073/466/2091	41795/239/2221	40915/530/2102
Goodness-of-fit on F^2	1.017	1.077	1.021	1.040	1.042
Final R indexes [I>=2σ (I)]	R_1 = 0.0751, wR_2 = 0.2019	R_1 = 0.0757, wR_2 = 0.2108	R_1 = 0.0840, wR_2 = 0.2194	R_1 = 0.0686, wR_2 = 0.2034	R_1 = 0.0781, wR_2 = 0.2130
Final R indexes [all data]	R_1 = 0.0946, wR_2 = 0.2235	R_1 = 0.0906, wR_2 = 0.2280	R_1 = 0.1078, wR_2 = 0.2446	R_1 = 0.0737, $wR2$ = 0.2124	R_1 = 0.0877, $wR2$ = 0.2235
Largest diff. peak/hole / e Å^{-3}	5.45/−2.70	4.5/−1.91	3.29/−2.17	9.80/−3.38	2.59/−2.09

ENCAPSULATION OF PYRIDINE DERIVATIVES IN SPONGE 4 VIA COORDINATIVE ALIGNMENT

5

5.1 INTRODUCTION

The previous chapter clearly shows that sponge **4** was stable in the presence of polar solvents and nucleophiles and could accommodate pyridine on the cadmium ions. This chapter aims to attempt encapsulation of N-containing molecules in **4**. The guests may be accommodated in **4** via coordinative alignment (CAL). This is because it is commonly observed in the literature that N-containing guest molecules incorporate themselves in a crystalline sponge via CAL. For example, in MOF-520($[Al_8(OH)_8(BTB)_4(HCO_2)_4]$) (BTB = 1,3,5-benzentribenzoate), azolates ions were bonded to the Al^{3+} centres.[120] Similarly, in the mesoporous Cu-based MOF $[Cu_6(H_2O)_6(TATB)_4 \cdot DMF \cdot 12H_2O]$ [TATB = 4,4',4"-(1,3,5-triazine-2,4,6-triyl) tribenzoic acid], nicotine was bonded to Cu^{2+} ions.[123] In addition, the Mn-based MOF (CPF-5) $(Mn_{21}(HCOO)_{18}(H_2O)_{12}$(4-tetrazolate-benzoate)$_{12}$, was shown to accommodate several Lewis base guests, such as pyridine and 3-aminopyridine bonded to Mn^{2+} centres.[122] In contrast while sponge **1** accommodated N-containing guests in the pores, severe damage to the crystals was observed because of the instability of sponge **1** in the presence of nucleophilic guest molecules.[124]

5.1.1 Selection of guest molecules

In this chapter, the CAL approach for the accommodation of guests is explored with five N-containing nucleophilic guests. In particular, pyridine derivatives were chosen for encapsulation in **4**, namely 4-aminopyridine (**F**), 3,5-lutidine (**G**), 3-bromopyridine (**H**), 4-acetylpyridine (**I**) and 4,4'-bipyridine (**J**) (Figure 5.1). Accommodation of pyridine in **4** generated **4'** and changed the structure of **4** (section 4.2.4), hence similar changes are expected in the inclusion complexes generated from the guests **F**-**J**. Furthermore, in the guest molecules, except for **J**, an additional functional group is present on the pyridine ring which might allow further interactions with the framework structure. Comparisons with **4'** will allow an assessment of the importance of the functional group in determining the overall structures.

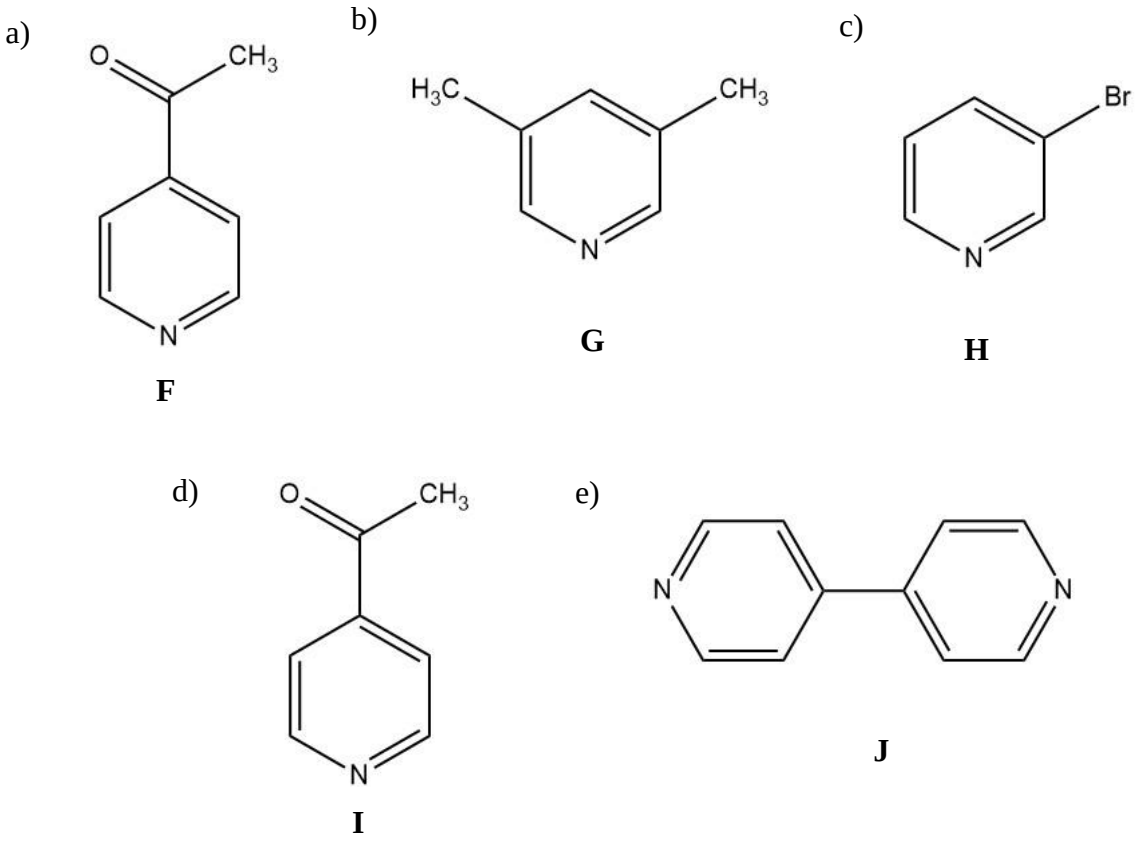

*Figure 5. 1 Guest molecules a) 4-aminopyridine (**F**) b) 3,5-lutidine (**G**) c) 3-bromopyridine (**H**) d) 4-acetylpyridine (**I**) e) 4,4'bipyridine (**J**).*

5.2 RESULTS AND DISCUSSION

5.2.1 Soaking experiments

Guests 3,5-lutidine (**G**), 3-bromopyridine (**H**) and 4-acetylpyridine (**I**) are liquid at room temperature, therefore, soaking experiments with neat guests at 25 °C were performed to obtain high occupancies. The crystals of **4** remained stable in neat 3,5-lutidine, however, with neat 3-bromopyridine and 4-acetylpyridine cracking of the crystals was observed. Therefore, these guests were diluted with acetone before soaking. Guests 4-aminopyridine (**F**) and 4,4'-bipyridine (**J**) are solid at room temperature therefore they were dissolved in acetone before soaking. The saturated solution resulted in quick deterioration of the crystals and hence several dilution conditions for soaking were attempted to obtain inclusion complexes (Table 5.1). Acetone was chosen for dilution of guests because crystals of **4** are stable in acetone and this solvent does not coordinate to the Cd^{2+} ions, as described in section 4.2.4. In addition, dilution with acetone resulted in the

successful replacement of DMF from all the coordination sites subsequently occupied by pyridine (Chapter 4).

Guests 4-aminopyridine (**F**), 3,5-lutidine (**G**) and 3-bromopyridine (**H**) successfully replace from DMF bonded to the Cd^{2+} ions, coordinating to these ions, in their respective inclusion complexes. Table 5.1 provides the optimised soaking conditions for the inclusion complexes **4F, 4G** and **4H**. In contrast, guests 4-acetylpyridine (**I**) and 4,4'-bipyridine (**J**) only occupied a few sites at the Cd^{2+} ions, where they replaced the DMF molecules. At the remaining coordination sites, DMF was present. In the case of 4-acetylpyridine, several soaking conditions were investigated to replace all DMF molecules bonded to the Cd^{2+} ions with 4-acetylpyridine. However, at the optimum soaking condition, only three molecules of 4-acetylpyridine were observed bonded to Cd^{2+} ions and three DMF were still bonded to the Cd^{2+} ions. In the case of 4,4'-bipyridine, the optimum soaking condition resulted in two molecules of 4,4'-bipyridine bonded to the Cd ions. In addition, at two positions only one pyridine ring of 4,4'-bipyridine was identified bonded to Cd ions. Using a higher guest concentration, a longer incubation period and a lower temperature tended to deteriorate the crystals. The soaking conditions and optimisation of the parameters gave maximum occupancies as well as the best quality crystals for X-ray diffraction measurement. Details of the soaking experiments are given in Table 5.1 in the experimental section 5.3.

5.2.2 The structure of inclusion complexes with pyridine derivatives

This section describes the structures obtained when using pyridine derivatives as guest molecules in sponge **4**. The SCXRD analysis of inclusion complexes **4F**-**4J** revealed that the guest molecules were accommodated via the CAL mechanism as expected. In each of the inclusion complexes **4F**, **4G**, and **4H** all the coordination sites initially occupied by DMF were found to be occupied by the new N-containing guests. However, in **4I** and **4J** only a few positions on Cd^{2+} ions were replaced by the guest molecules, and some were still occupied by the DMF molecules. Furthermore, molecules of 3,5-lutidine and 3-bromopyridine were identified in the pores, as well as on the Cd^{2+} ions in their respective inclusion complexes. Some DMF and acetone molecules were also observed in the pores which were then compared with occupied positions in **4** and **4'** to identify the similarities and differences. In the inclusion complexes, the N-containing guests bonded to the Cd^{2+} were observed with disorders. In some cases, N-containing guests were refined across two positions with a combined occupancy of 100%. However, in several N-containing molecules, the

minor components of the disorder could not be resolved successfully. All five inclusion complexes **4F-4J** described in this chapter crystallised in the $P2_1/n$ space group with similar unit cell parameters as observed for **4'**. This also implies that unit cell parameters of **4F-4J** were different to **4** in the same way as **4'** such that they had the same unit cell lengths but larger β angle in comparison with **4**. Section 5.3.5 provides details of the unit cells.

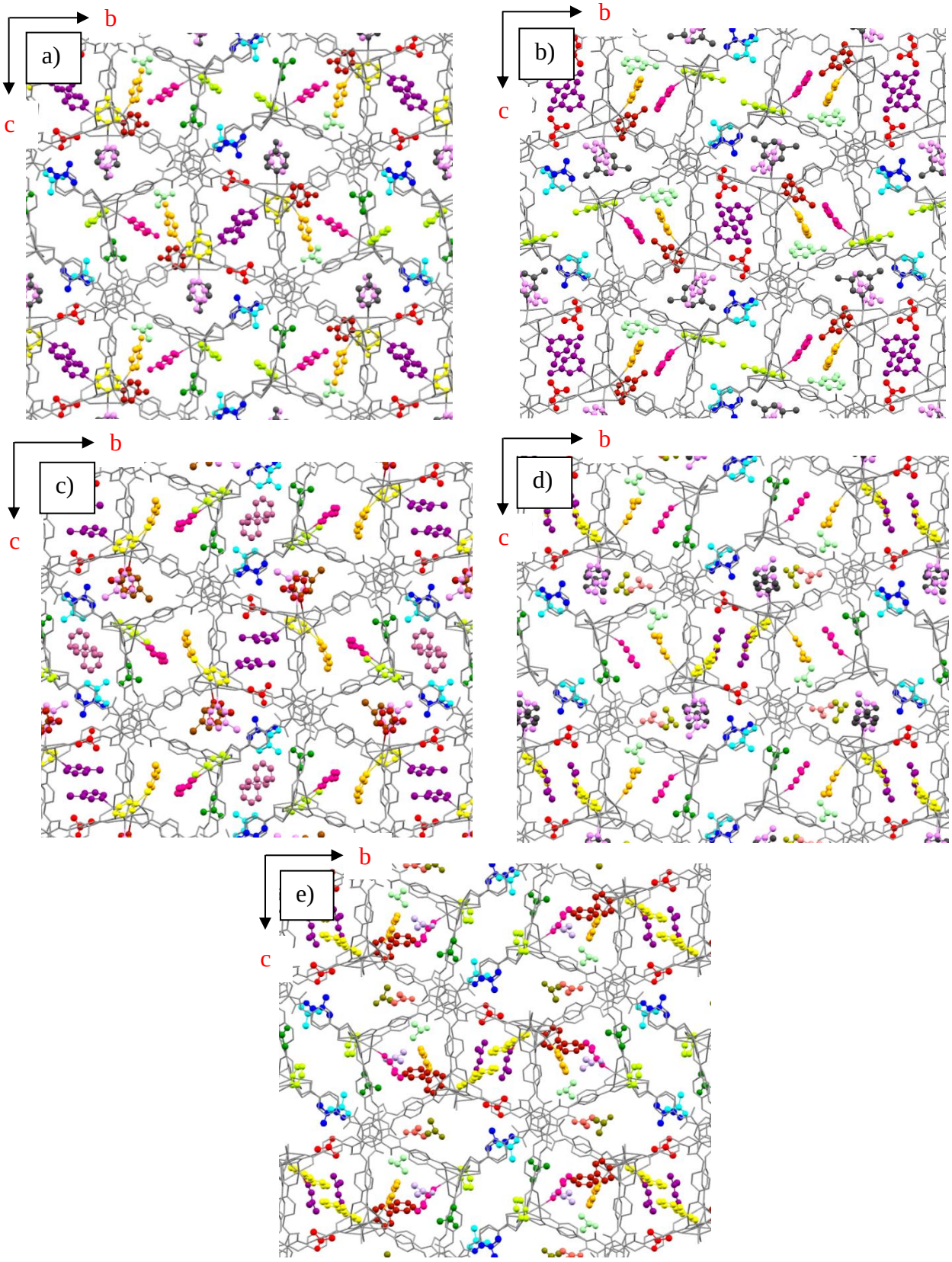

Figure 5. 2 Packing diagrams of complexes viewed down the a-axis. a) ***4F****, 4-aminopyridine b)* ***4G****, 3,5-lutidine c)* ***4H****, 3-bromopyridine d)* ***4I****, 4-acetylpyridine e)* ***4J****, 4,4'-bipyridine. Guest molecules were coloured according to their positional equivalence to those sponge* ***4'****. Framework displayed as capped stick and guest molecules as ball and stick representations.*

Inclusion complex with 4-aminopyridine (**4F**)

The structure of inclusion complex **4F** was different to **4** as 4-aminopyridine replaced all the coordinated DMF molecules from **4** in **4F**. In the asymmetric unit, eight molecules of 4-aminopyridine were identified bonded to Cd ions with 100% occupancy and none were in the pores. A DMF molecule with 100% occupancy and four acetone molecules with 50 and 75% occupancy were identified in the pore.

Eight molecules of 4-aminopyridine were observed bonded to Cd ions. Each Cd1, Cd2, Cd4, Cd6, and Cd7 has one coordinated guest molecule shown in lime, magenta, purple, light orange, and maroon in Figures 5.3a-e and Figure 5.4b. In contrast, Cd5 was bonded to three molecules of 4-aminopyridine. This result is consistent with the inclusion complex with pyridine **4'**. Comparing the packing diagram of **4F** (Figure 5.2a) with that of **4'** (Figure 4.6d) similarities in the positions of the guest molecules with only slight rotational differences were observed. Guest molecules were coloured according to the positional equivalence to the pyridine molecules in **4'**. Figure 5.3 shows the geometry of Cd ions in the **4F** inclusion complex, namely six-coordinate with octahedral geometry. However, Cd3 has distorted octahedral geometry, which is caused by the non-bonding interaction observed between O6 from the carboxylates of the framework and Cd3, with a Cd—O bond distance of 2.484 Å (Figure 5.4a). A non-bonding interaction was observed between Cd7 and O17 from the carboxylates of the framework with a particularly long Cd—O distance of 2.811 Å, therefore, distorting the geometry of the Cd7 ion (Figure 5.4b). Similar distorted octahedral geometry of only Cd3 was observed in **4** and **4'** (see sections 4.2.1 and 4.2.4).

The 4-aminopyridine molecule on Cd4 showed rotational disorder and atoms were refined across two positions (Figure 5.5a). The 4-aminopyridine molecules also interacted with the framework *via* hydrogen bonding. For example, the amino group of the 4-aminopyridine molecule shown in purple can be seen to be interacting with the carboxylates of the framework *via* a hydrogen bond, $H_{guest}\cdots C{=}O_{framework}$ 2.0 Å, as shown in Figure 5.5b. Similarly, the molecule shown in black formed hydrogen bonds with the framework, $H_{guest}\cdots C{=}O_{framework}$ 2.2 and 2.0 Å (Figure 5.5c). Furthermore, the molecule shown in light orange formed hydrogen bonds with the framework $H_{guest}\cdots C{=}O_{framework}$ 2.5 and 2.6 Å, as shown in Figure 5.5d. Such interactions were expected because of the hydrophilic nature of the framework. This result was compared with the inclusion complex of Mn-based MOF (CPF-5) with 3-aminopyridine. In the Mn complex, 3-

aminopyridine[122] was bonded to Mn^{2+} ions via CAL and formed hydrogen bonds with other molecules of 3-aminopyridine but not with the framework. In contrast, 4-aminopyridine in the inclusion complex **4F** was engaged in hydrogen bonding only with the framework. Interaction with another guest molecule was not observed in complex **4F** because of the large channels and spacing between the guest molecules. It is likely that this is probably the reason that the other five 4-aminopyridine molecules bonded to Cd ions do not form hydrogen bonds with the framework. On analysing the packing diagram, it was observed that these molecules were isolated in the channel. Therefore, hydrogen bonding with the framework was not favourable.

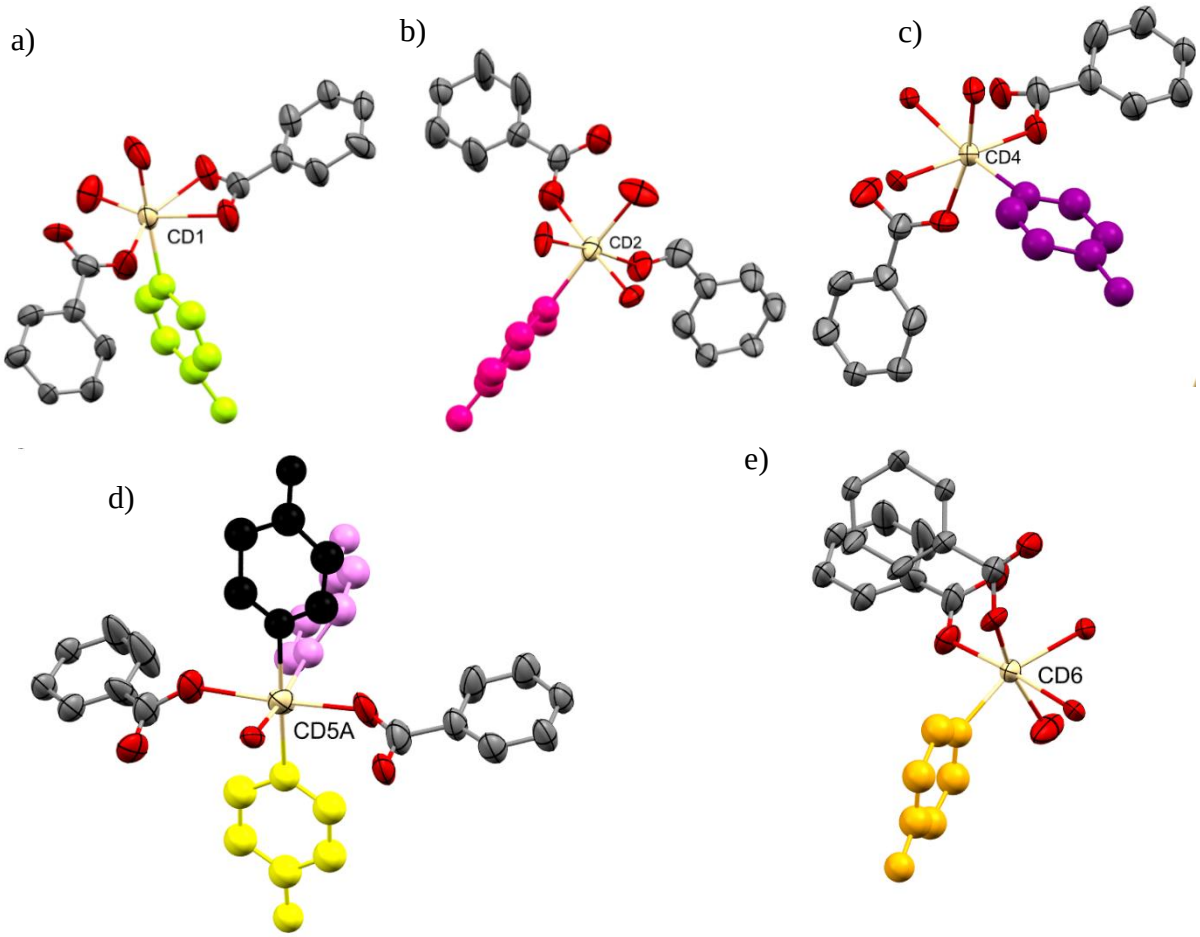

*Figure 5. 3 Geometry of Cd ions surrounded by linker molecules, bridging oxygen of carboxylates and 4-aminopyridine a) Cd1 b) Cd2 c) Cd4 d) Cd5 e) Cd6. Guest molecules were coloured according to their positional equivalence to the pyridine molecules in sponge **4'**. Guest molecules displayed as ball and stick model.*

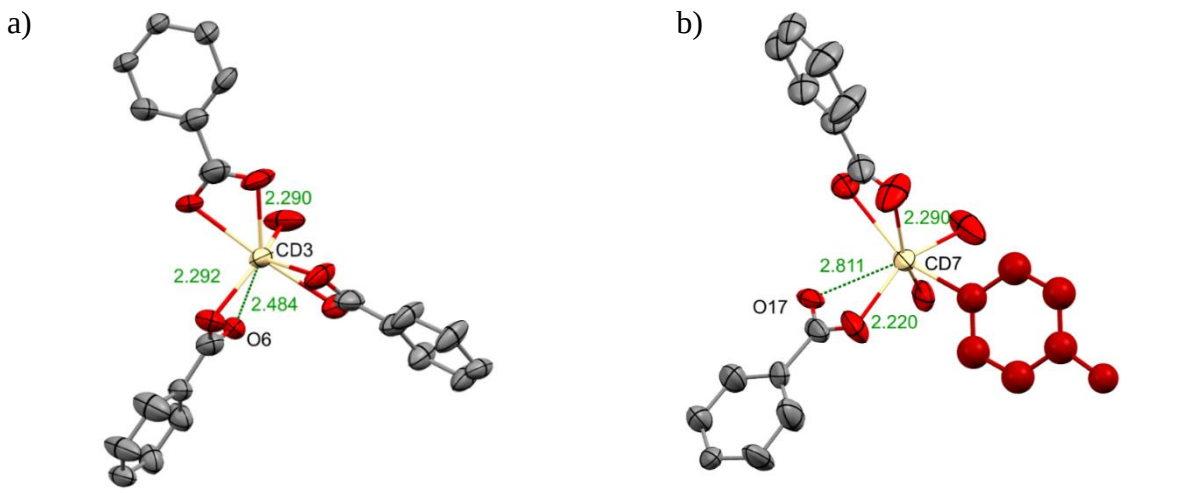

Figure 5. 5 Geometry of Cd ions a) Cd3 b) Cd7. Guest molecule displayed as ball and stick model. Interaction distances are displayed in angstroms.

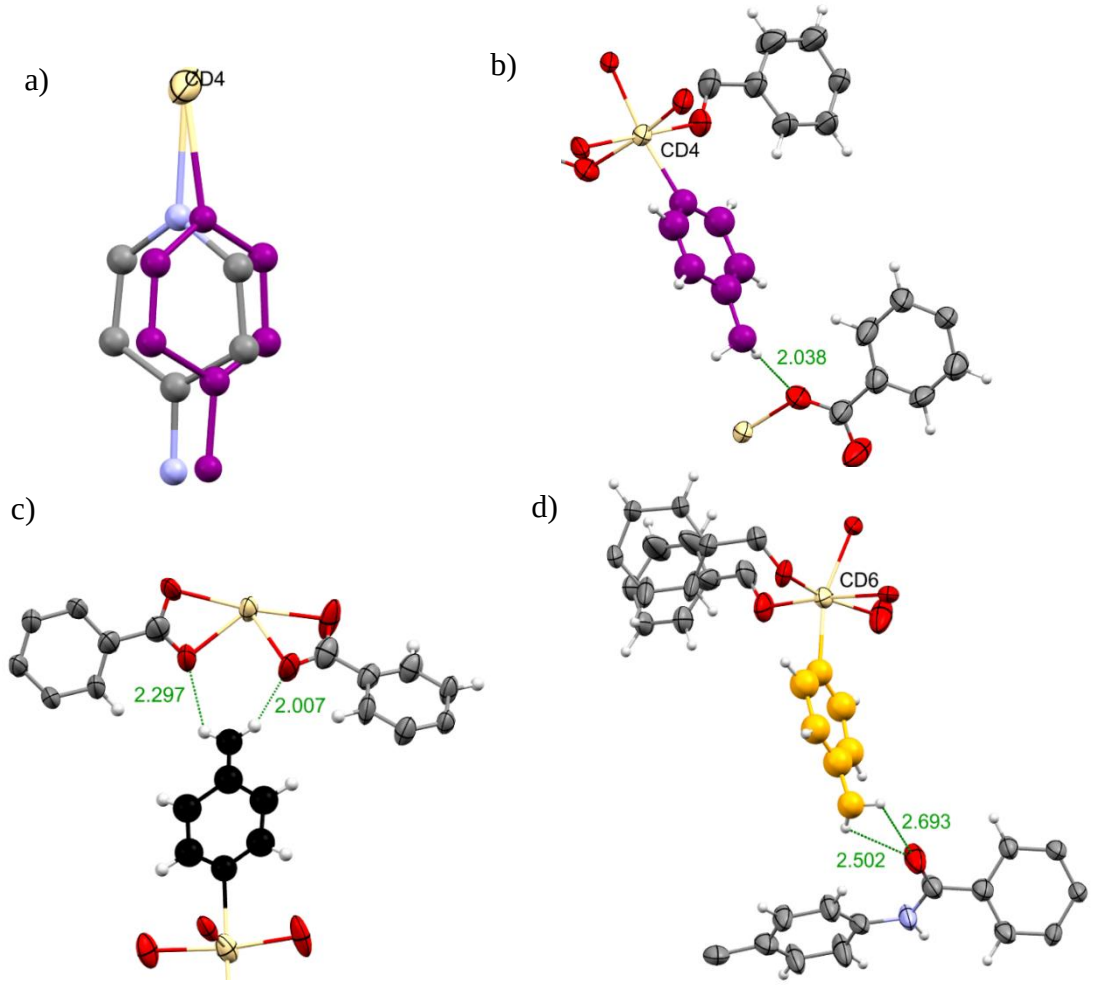

Figure 5. 4 Intermolecular interactions between molecules of 4-aminopyridine a) purple b) black c) light orange and the host framework. Guest molecules displayed as ball and stick model. Interaction distances are displayed in angstroms.

A single DMF molecule was observed in the pore at one of the favourable sites shown in blue. Acetone molecules observed in the pore are shown in turquoise, red and green (Figure 5.2a). These sites were previously identified as commonly occupied by the solvent molecules (guest molecules of chapter 4) in the pore and discussed in detail in section 4.2. The non-bonding intermolecular interactions observed between acetone or DMF molecules with the framework were consistent with the observation previously made in Chapter 4, such that these solvent molecules were fixed in these favourable sites by hydrogen bonding.

Inclusion complex with 3,5-lutidine (**4G**)

The structure of inclusion complex **4G** was observed different from **4** because all the coordinated DMF molecules from **4** were replaced by 3,5-lutidine in **4G**. In the asymmetric unit, eight 3,5-lutidine molecules were identified in the structure. Seven of them were bonded to Cd^{2+} ions with 100% occupancy and one molecule of 3,5-lutidine was observed in the pore with 100% occupancy. Three DMF molecules with a 50 to 100% occupancy range were observed in the pore. No acetone molecules were found in the pore for this structure because the soaking experiment was performed in the neat guest.

Seven molecules of 3,5-lutidine were observed bonded to the Cd^{2+} ions. Each Cd1, Cd2, Cd4, Cd6, and Cd7 has one guest molecule bonded, as shown in lime, magenta, purple, light orange, and maroon in Figure 5.6 which also illustrates the geometry of Cd1, Cd2, Cd4, Cd6, and Cd7. Each of these Cd^{2+} ions was six-coordinate. One difference was identified at Cd5 as in this structure two guest molecules were clearly identified, whereas in **4'** and **4F** there were three guest molecules bonded to Cd5. However, there is a significant electron density, which appears to be from a highly disordered 3,5-lutidine molecule which would be a sixth coordination site on Cd5. All attempts to model this were unsuccessful. On comparing the geometry of Cd5 from **4G** and **4F**, it was observed that both Cd ions have octahedral geometry with an O—Cd—O angle of 90°. Figures 5.7a and 5.7b illustrate the distorted octahedral geometry for Cd3 in **4G**, as also observed in **4'** and **4F**. Cd3 do not have any guest molecules bonded to it. However, two non-bonding interactions with O2 and O17 from the carboxylates of the framework with Cd—O bond distances of 2.5 and 2.5 Å respectively cause Cd3 to remain formally five-coordinate, as was the case in **4F**.

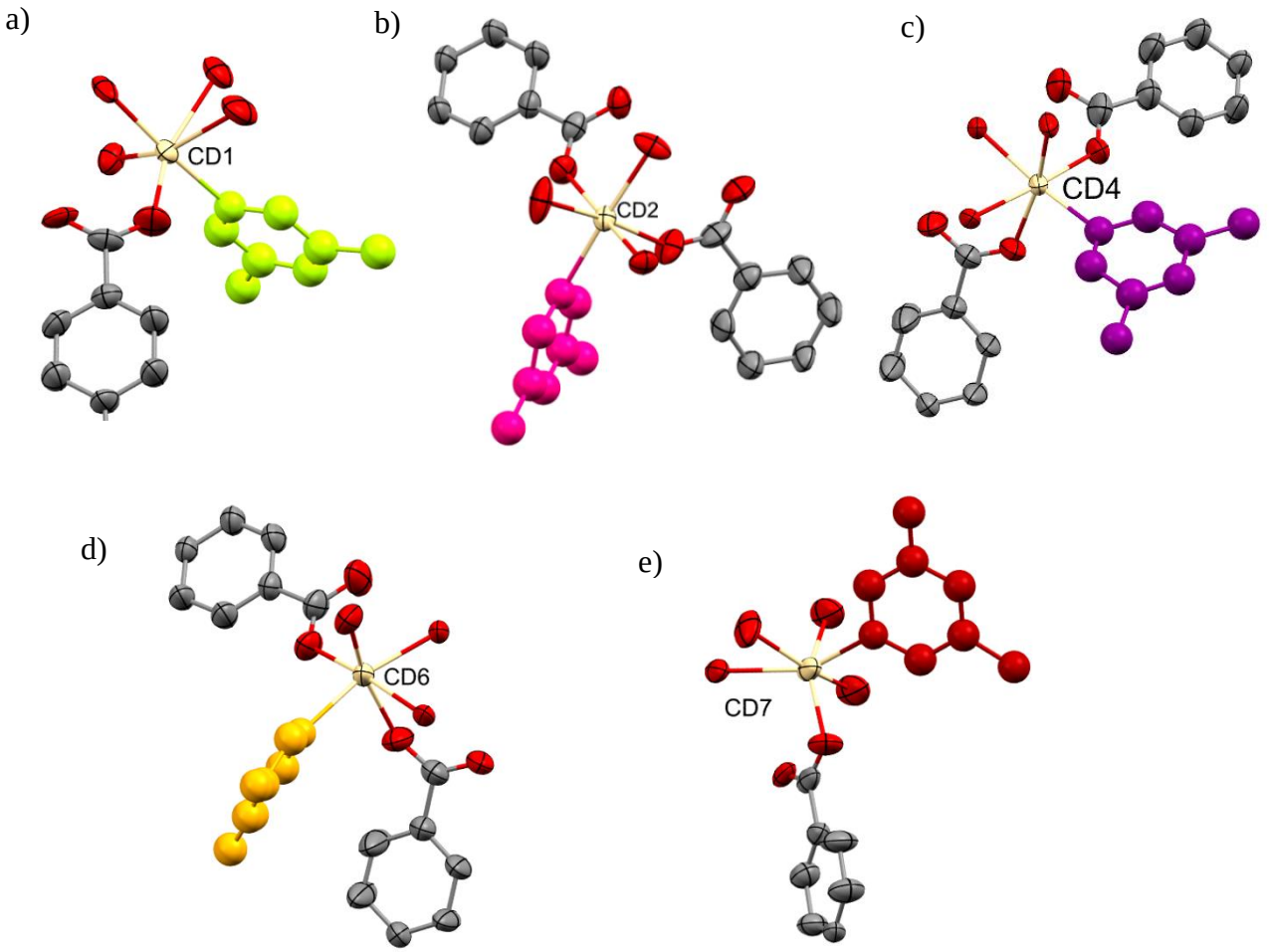

*Figure 5. 6 Geometry of Cd ions surrounded by linker molecules, bridging oxygen and 3,5-lutdine a) Cd1 b) Cd2 c) Cd4 d) Cd6 e) Cd7. Guest molecules were coloured according to their positional equivalence to the pyridine molecules in sponge **4'**. Guest molecules displayed as ball and stick model.*

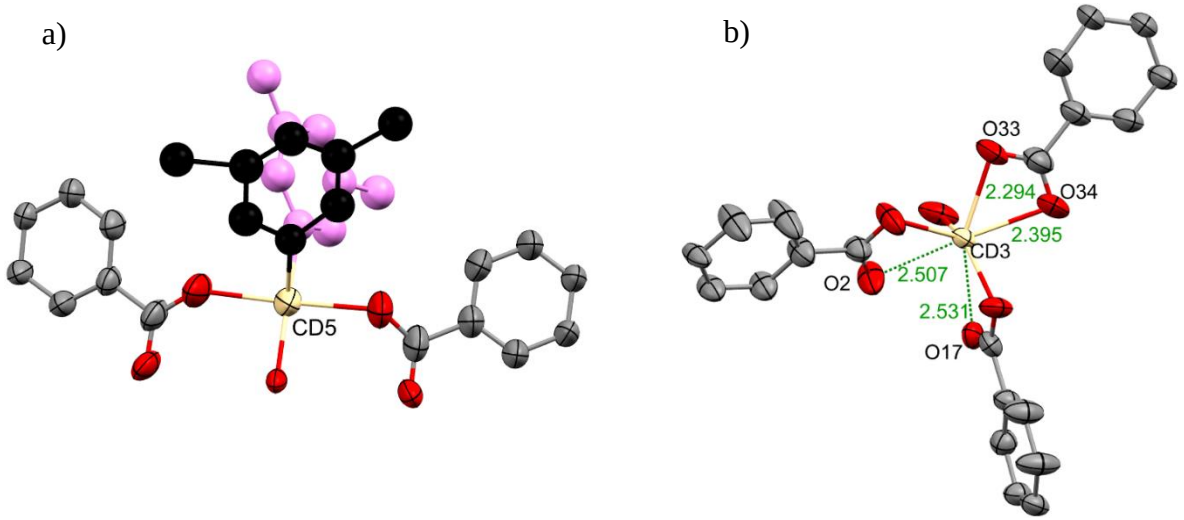

*Figure 5. 7 Geometry of Cd ions a) Cd5 and b) Cd3 of **4G**. Guest molecules are coloured according to the positional equivalence to the pyridine molecules in sponge **4'**. Guest molecules displayed in ball and stick model. Interaction distances are displayed in angstroms.*

The 3,5-lutidine molecules bonded to Cd5, as shown in black and light purple showed orientational disorder and were refined across two positions (Figure 5.8a, b). Similarly, the 3,5-lutidine molecule bonded to Cd2 showed orientational disorder (Figures 5.9) In other molecules of 3,5-lutidine, some disorder was observed, which was not resolved successfully.

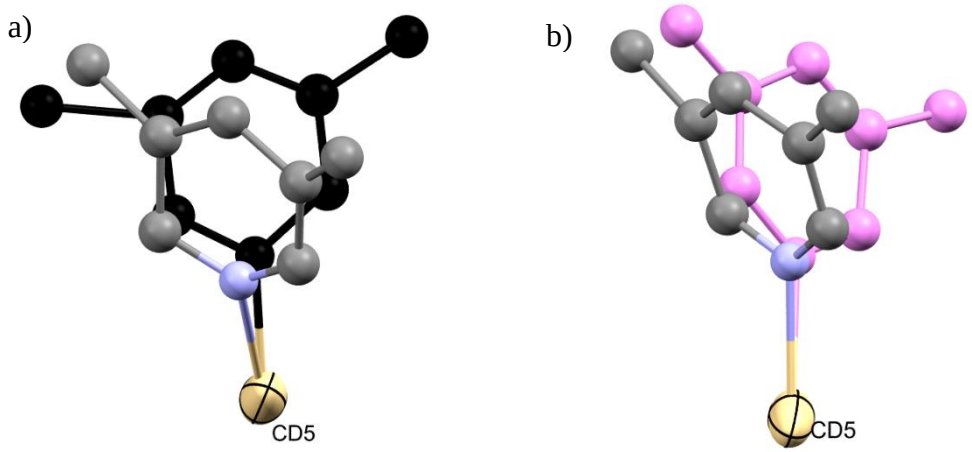

*Figure 5. 8 Disorder in the molecules of 3,5 lutidine bonded to Cd5. a) black b) light purple. Major component is coloured according to the position equivalence to pyridine molecule in sponge **4'**. Minor component is shown in elemental colours*

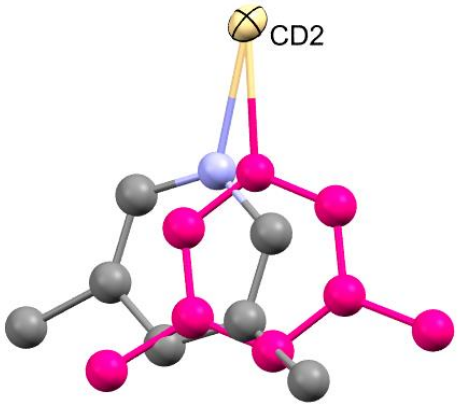

Figure 5. 9 Disorder in the 3,5 lutidine molecule bonded to Cd2.

The guest molecules exhibited CAL in the **4G** inclusion complex, however, one additional molecule of 3,5-lutidine was observed in the pore (shown in light green Figure 5.10). This site was occupied by an acetone molecule in inclusion complex **4B**. In **4B**, the acetone molecule was fixed at this position by a hydrogen bond with the framework. Similarly, the nitrogen of the 3,5-lutidine forms a hydrogen bond with the framework, $N_{guest}\cdots H_{framework}$ 2.0 Å in **4G**. This result supports the idea that the hydrophilicity of sponge **4** was also a strong reason for the accommodation of Lewis bases.

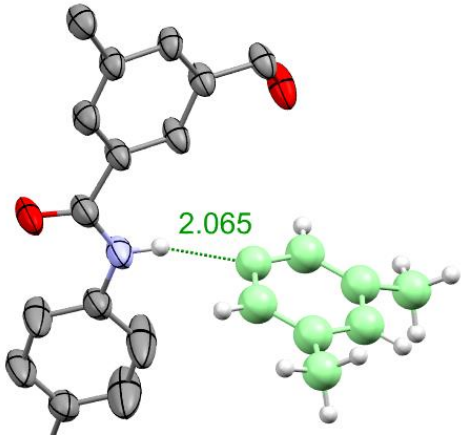

Figure 5. 10 3,5 lutidine shown in light green. Guest molecule displayed as ball and stick model. Interaction distance is displayed in angstroms.

Three DMF molecules in the pores (Figure 5.2 b) were identified at the most favourable sites common to the other structures, shown in blue, red and turquoise and described in Section 4.2.

Inclusion Complex with 3-bromopyridine (**4H**)

In the inclusion complex **4H,** the 3-bromopyridine molecules replaced the DMF molecules from **4** therefore the structure is different from **4**. In the asymmetric unit, seven 3-bromopyridine molecules were observed bonded to Cd^{2+} ions with a 100% occupancy range. In addition, two 3-bromopyridine molecules were observed in the pore with 50 and 100% occupancy. In the pores, two DMF molecules with 100% occupancy and two acetone molecules with 100% occupancy were identified.

Seven molecules of 3-bromopyridine were observed bonded to Cd^{2+} ions. The sites Cd1, Cd2, Cd4, Cd6, and Cd7 each have one guest molecule bonded shown in lime, magenta, purple, light orange, and maroon in Figure 5.11. In **4H** all Cd ions were clearly six-coordinate. On comparing

the packing diagram of **4H**, shown in Figure 5.2c, with previous inclusion complexes **4'**, **4F**, **4G** with coordinated guests, similarities in the structure were observed. For example, similar to the **4G** inclusion complex, Cd5 in **4H** was bonded to only two guest molecules shown in yellow and light purple, Figure 5.11d. However, in **4H**, unlike **4G**, Cd5 was six-coordinate. In addition, Cd3 in **4H** was also observed forming a distorted octahedral geometry similar to **4'**, **4F** and **4G**. There is an additional non-bonding interaction with O8 from the carboxylates of the framework with a Cd—O bond distance of 2.4 Å (Figure 5.12).

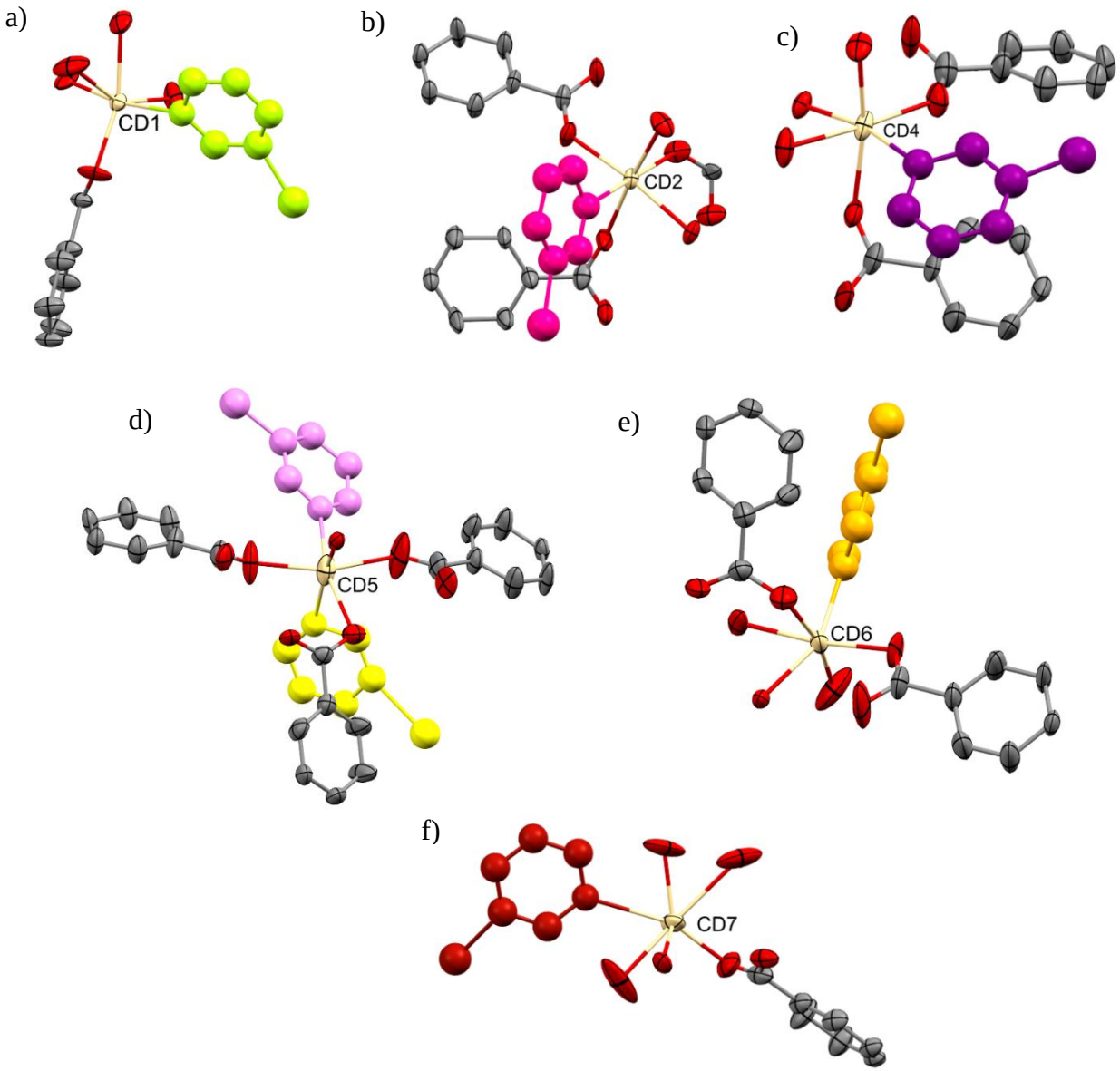

*Figure 5. 11 Geometry of Cd ions surrounded by linker molecules, bridging oxygen of the carboxylates and 3-bromopyridine a) Cd1 b) Cd2 c) Cd4 d) Cd5 e) Cd6 f) Cd7. Guest molecules were coloured according to their positional equivalence to the pyridine molecules in sponge **4'**. Guest molecules displayed as ball and stick model.*

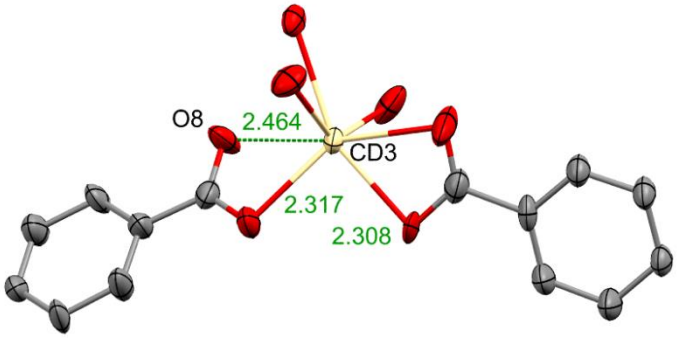

*Figure 5. 12 Geometry of Cd3 ion from inclusion complex **4H**. Interaction distance shown in angstroms.*

Two molecules of 3-bromopyridine were observed in the pore at unique sites shown in brown and mauve colour in Figure 5.13. These sites were not observed to be occupied in any previous structures. In the packing diagram Figure 5.2c, it appeared that the molecule shown in brown may be close to Cd5, however, the Cd-O bond distance was 3.877Å. In addition, the bromine atom of the brown molecule forms a hydrogen bond with the framework $Br_{guest}\cdots H_{framrework}$ 2.8Å, Figure 5.13a. The second 3-bromopyridine molecule in the pore shown in mauve colour in Figure 5.13b formed hydrogen bonds with the carboxylate of the framework, $H_{guest}\cdots C{=}O_{framework}$ 2.1Å. Among coordinated 3-bromopyridine molecules, a light purple molecule, bonded to Cd5 (Figure 5.13a) formed a hydrogen bond with a DMF molecule present in the pore with a distance of 2.9Å. No other additional hydrogen bonding between coordinated 3-bromopyridine and the framework was observed. These guest molecules were oriented such that they were isolated in the channel. Thus, short contacts between guest molecules and the frameworks were >3.5Å. Rotational disorder in the 3-bromopyridine molecule bonded to Cd6 was observed, as shown in Figure 5.13a. The bromine atom of the 3-bromopyridine molecule bonded to Cd1 showed disorder and was refined across two positions, as shown in Figure 5.14. Other molecules of 3-bromopyridine also showed disorder, however, this could not be resolved successfully.

The DMF molecules in the pores were identified, as shown in blue and turquoise. Acetone molecules occupied common sites, shown in red and green (Figure 5.2c). These sites are the most favourable in the pores because the solvent molecules were bonded to the framework *via* hydrogen bonds. (Section 4.2)

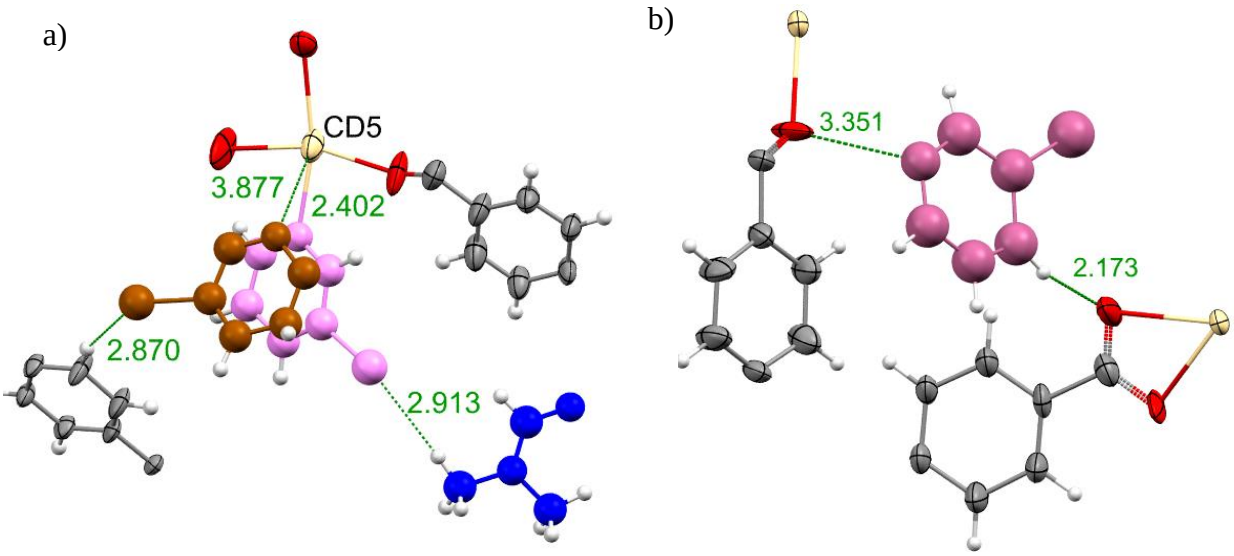

*Figure 5. 13 Intermolecular interactions between guest molecules a) brown and violet b) mauve. Colour of the guest molecule is according to the positional equivalence to pyridine molecules in sponge **4'**. Guest molecule displayed as ball and stick model. Interaction distances are displayed in angstroms.*

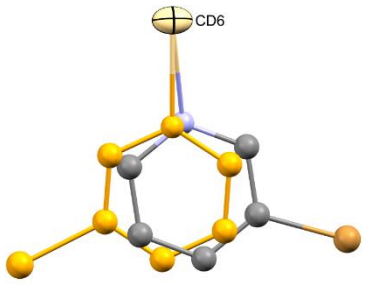

Figure 5. 14 Disorder in the 3-bromopyridine molecules orange molecule bonded to Cd6

Inclusion complex with 4-acetylpyridine (**4I**)

In the inclusion complex **4I,** 4-acetylpyridine only replaced some of the coordinated DMF molecules. In the asymmetric unit, three 4-acetylpyridine molecules were observed bonded to Cd ions with 100% occupancy with none in the pore. Five DMF molecules, with 100% occupancy, were observed, three of which were bonded to Cd^{2+} ions and the remaining two DMF molecules were observed in the pore. Four acetone molecules were identified in the pore with occupancy of 33 and 50%.

All three guest molecules were bonded to the Cd5. Figure 5.15a shows the geometry of Cd5A (the major component) and only two molecules of 4-acetylpyridine (light purple and yellow) were bonded. The molecule in black is bonded to Cd5B (the minor component), as shown in Figure 5.15b. These positions were previously occupied by guest molecules in **4', 4F, 4G,** and **4H**. Comparing the packing diagram of **4I**, shown in Figure 5.2d, with **4'** shows the similarity in the orientation of the guest molecules between the structures. Among the three 4-acetylpyridine molecules bonded to Cd5, the acetyl group of the molecule in light purple molecule was coplanar with the aromatic ring. The acetyl group of the molecule in black was not coplanar with the aromatic ring to which it is attached and formed a torsion angle of 46.91°, hence has a short contact with the carboxylate of the framework, $O_{guest}\cdots C{=}O_{framework}$ 3.0Å (Figure 5.15b). However, the acetyl group of the molecule in yellow was also not coplanar with the aromatic ring and formed a torsion angle of 38.19°, with no short contact with the framework.

Three coordinated DMF molecules were present on Cd2, Cd4 and Cd6, as shown in magenta, purple and light orange. These sites were observed occupied by DMF molecules in previous structures **4A-4C** and by pyridine in **4'**, as described in Section 4.2.4. In the pore, DMF is shown in blue and turquoise. Again, these are the commonly observed sites in previous structures. Four acetone molecules were identified in the pore. Two of them were previously observed at sites shown in green, and light green and two were at new sites shown in moss green and light red in **4I**, Figure 5.2d. All of the sites occupied by the acetone involved hydrogen bonding with the framework.

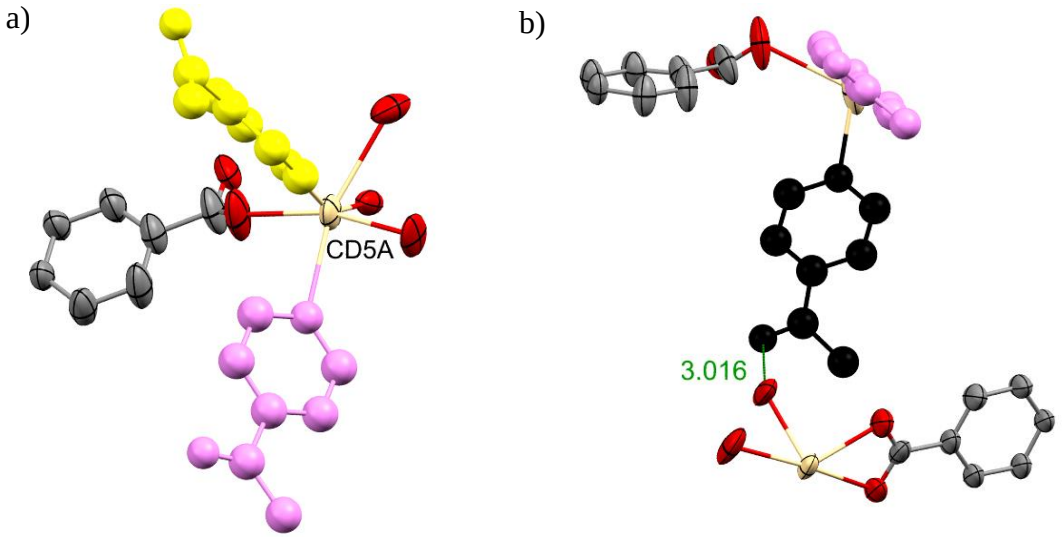

*Figure 5. 15 a) Geometry of Cd5A major component of the disorder of Cd5 b) Intermolecular interactions between guest molecule shown in black and the host framework. Guest molecules were coloured according to their positional equivalence to the pyridine molecules in sponge **4'**. Guest molecules displayed as ball and stick model. Interaction distance displayed in angstroms.*

Inclusion complex with 4',4''-bipyridine (**4J**)

The structure of inclusion complex **4J** was observed to be different from **4** as four coordinated DMF molecules were replaced by 4',4''-bipyridine. In the asymmetric unit, two complete molecules of 4',4''-bipyridine were observed bonded to Cd ions with 100% occupancy and two partial molecules of 4',4''-bipyridine with 100% occupancy containing only one pyridine ring bonded to Cd ions. Three DMF molecules with 100% occupancy were observed, two of which were bonded to Cd ions and the third DMF molecule was observed in the pore. Seven acetone molecules were identified in the pore with occupancy ranging from 25 to 100%.

The two complete guest molecules observed in the structure were bonded to the Cd5 and Cd7 ions, shown in yellow and maroon respectively in Figure 5.16. Comparison of the inclusion complex **4J** with **4'** revealed the similarity in the orientation of the guest molecules present at Cd5 and Cd7 in their respective complexes. For example, the yellow molecule of 4,4''-bipyridine in **4J** and the yellow pyridine molecule of **4'** both were bonded to Cd5 and extended into the pore along the *b*-axis. Similarly, maroon guest molecules from both inclusion complexes extended along the *a*-axis. Figure 5.16 shows the geometry of Cd ions Cd1, Cd6 and Cd7, which were octahedral as observed

in the previous structures. However, as observed in the previous complex, the geometry of Cd3 was distorted octahedral due to the non-bonding interaction observed between O9 from the carboxylate of the framework and Cd3, with a Cd—O distance of 2.4 Å (Figure 5.16a). Figure 5.16b show the Cd5 geometry, which was six-coordinate and clearly not octahedral because of the non-bonding interaction with the oxygen of the carboxylate from the framework with a Cd—O bond distance of 2.6 Å.

Furthermore, two partial guest molecules each showing only one pyridine ring were observed, bonded to Cd1 and Cd6, shown in lime and light orange respectively. Comparing **4J** and **4'**, both the **J** and pyridine molecules at Cd6 were oriented similarly, roughly parallel to the *c*-axis. However, a slight orientational difference was observed in the lime molecules at Cd1. Observation of partial structures was reported in the literature, particularly with N-containing/nucleophilic guest molecules. For example, in sponge **1**, several inclusion complexes with partial guest structures were reported. This is because encapsulation of nucleophilic guests caused degradation in the quality of the crystals. Similarly, encapsulation of 4,4'–bipyridine caused some degradation in the quality of the crystals resulting in the observation of partial guest molecules. Although, sponge **4** is compatible with N-containing guest molecules incomplete encapsulation was observed with 4,4'bipyridine. It was observed that diffusion of **J** into the sponge **4** was very slow. Therefore, to increase the diffusion rate, higher concentration and higher temperatures were applied but this resulted in the degradation of the crystals. Details of soaking conditions are summarised in Table 5.2 in the experimental section 5.3.1. Hence, the inclusion complex **4J** described was obtained within the best-optimised condition with two complete guest molecules along with two partial guests. It may be that with a more intense X-ray source e.g., synchrotron, then the missing pyridyl rings might reveal themselves.

The coordinated DMF molecules were observed on Cd2 and Cd4 shown in magenta and purple respectively. The third DMF molecule was observed in the pore at the blue site in previous structures. Of the seven acetone molecules in the pores, five molecules, shown in turquoise, red, green, lilac, and light green were previously observed and discussed in detail in section 4.2. In addition, two new sites are shown in moss green and light red were common to **4I** Figure 5.2e

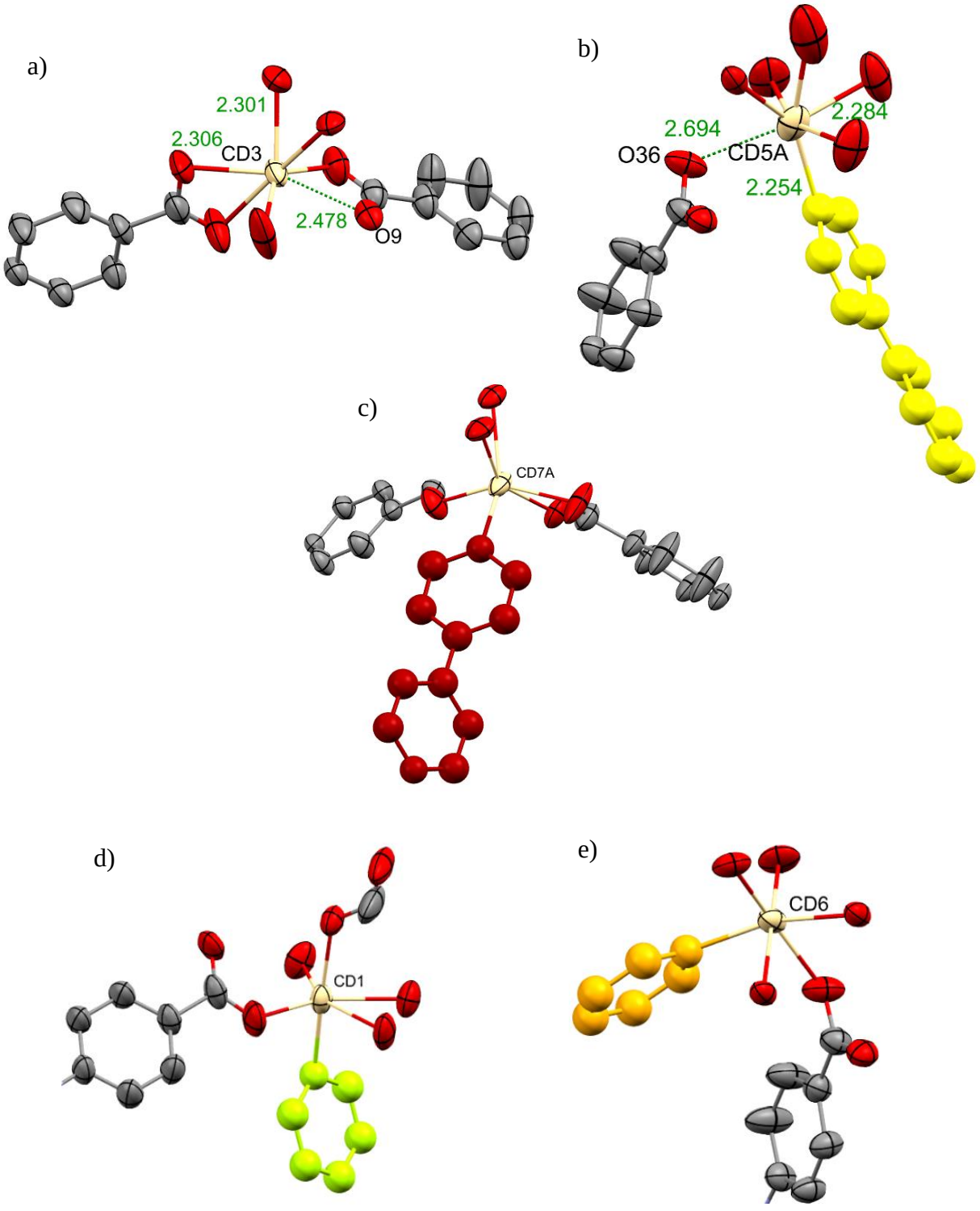

*Figure 5. 16 Geometry of Cd ions surrounded by linker molecules, bridging oxygen and 4,4'-bipyridine a) Cd3 b) Cd5 c) Cd7 d) Cd1 e) Cd6. Guest molecules were coloured according to their positional equivalence to the pyridine molecules in sponge **4'**. Guest molecules displayed as ball and stick model.*

5.2.3 Conclusions

In this chapter, the utility of sponge **4** for encapsulation of N-containing nucleophilic compounds was investigated. The results show that sponge **4** can accommodate nucleophilic compounds via CAL as had been hoped. In a few cases, guest molecules were also observed in the pores, fixed by hydrogen bonding to the framework. In inclusion complexes, **4I** and **4J**, incomplete inclusion of guests was observed and hence some Cd^{2+} ions are bonded to DMF ligands. Although incomplete inclusion was observed, each Cd^{2+} carries either DMF or guest molecules. Both DMF and guest bonded to the same Cd^{2+} ion was not observed in **4I** and **4J**. DMF and acetone molecules were repeatedly identified at the favourable sites in the pores. In conclusion, sponge **4** is suitable to encapsulate N-containing nucleophilic compounds. The use of sponge **4** in the crystalline sponge method is therefore highly advantageous, in particular for the structure determination of active pharmaceutical ingredients as they were commonly N-containing compounds. [3,124]

5.3 EXPERIMENTAL SECTION

5.3.1 Soaking experiment

Guest molecules except for 3,5-lutidine (**G**) were diluted with acetone before soaking. Neat guests produced cracks in the crystals therefore diluted solutions were used for soaking the crystals of **4** in the presence of guests **H** and **I**. Solid guests **F** and **J** were dissolved in acetone before soaking. Details of solvent exchange are given in Table 5.1.

Guest	Concentration	Incubation period	Temperature	Results
4-aminopyridine (**F**)	Saturated solution in acetone	1 day	25 °C	Crystal deteriorated
4-aminopyridine (**F**)	0.02 g in 2 mL acetone	8 days	25 °C	2 guest molecules were observed bonded to Cd ions
4-aminopyridine (**F**)	0.05 g in 2 mL acetone	1 week	25 °C	8 guest molecules were observed bonded to Cd ions
3,5-lutidine (**G**)	neat	11 days	25 °C	7 guest molecules were observed bonded to Cd ions and 1 molecule in the pore
3-bromopyridine (**H**)	neat	1 day	25 °C	Crystal deteriorated
3-bromopyridine (**H**)	100 µL in Acetone	1 week	25 °C	Crystals were fine optically but do not diffract
3-bromopyridine (**H**)	50 µL in Acetone	1 week	25 °C	7 Guest molecules observed bonded to Cd ions and two molecules in the pore
4-acetylpyridine **(I**)	neat	1 day	25 °C	Only 2 guest molecules observed bonded to Cd ions along with coordinated DMF.
4-acetylpyridine **(I**)	neat	2 days	25 °C	Crystal dissolved
4-acetylpyridine **(I**)	50 µL in 2 mL acetone	2 weeks	25 °C	1guest molecule along with one partial guest molecule was observed bonded to Cd ions
4-acetylpyridine **(I**)	50 µL in 2 mL acetone	3 weeks 3 days	25 °C	3 guest molecules observed bonded to Cd ions
4-acetylpyridine **(I**)	100 µL in 2 mL acetone	2 weeks	25 °C	Crystals were fine optically but do not diffract
4-acetylpyridine **(I**)	100 µL in 2 mL acetone	1 week	15 °C	Crystals were fine optically but do not diffract
4-acetylpyridine **(I**)	100 µL in 2 mL acetone	3 days	15 °C	Crystals were fine optically but do not diffract
4-acetylpyridine **(I**)	75 µL in 2 mL acetone	3 days	15 °C	Crystals were fine optically but do not diffract
4,4'-bipyridine (**J**)	Saturated solution in 1 mL acetone	1 day	25 °C	Crystals deteriorated
4,4'-bipyridine (**J**)	0.25 g in 2 mL acetone	2 weeks	25 °C	1guest molecule observed bonded to Cd ions
4,4'-bipyridine (**J**)	0.40 g in 2 mL acetone	1 week	25 °C	2 complete guest molecules and two partial guest molecules were observed bonded to Cd ions
4,4'-bipyridine (**J**)	0.40 g in 2 mL acetone	2 weeks	50 °C	Crystals were fine optically but do not diffract
4,4'-bipyridine (**J**)	0.50 g in 2 mL acetone	1 weeks	50 °C	Crystals were fine optically but do not diffract
4,4'-bipyridine (**J**)	Saturated solution in 1 mL acetone	1 day	25 °C	Crystals deteriorated

*Table 5. 1 Soaking conditions of 4-aminopyridine (**F**), 3,5-lutidine (**G**), 3-bromopyridine (**H**), 4-acetylpyridine (**I**) and 4,4'-bipyridine (**J**).*

5.3.2 Crystallographic procedures

Using the same procedure as described in Section 2.3.3

5.3.3 Structural analysis details

The non-hydrogen atoms of the framework were refined anisotropically and hydrogen atoms were included using a riding model. The BTA and Cd components of the framework were at first freely refined without applying any constraints/restraints. However, the BTA, Cd and coordinated guest components of the framework showed some disorder and where required atoms were modelled across two positions with a combined occupancy of 100%. DFIX and EADP were used to obtain a stable model. Refinement of pore solvent species was first performed without any constraints/restraints and only if this was unsuccessful, were these added based on their known structures. The occupancy of each guest molecule was refined against its free variable, which in the final stages of refinement was fixed to values reported. In all the structures it was not possible to assign all the residual density peaks in a way that makes chemical sense, these peaks belong to heavily disordered guests or solvent molecules, and these were taken into account by the use of a solvent mask in the OLEX2 GUI[154]. On occasion a large residual density peak remained near the cadmium metal of the host framework this is due to absorption and/or termination errors in Fourier calculation. Standard deviations for restraints used are as described in chapter 2 section 2.3.4. Refinements for the N-containing guests coordinated as well in the pores are detailed in section 5.3.4.

5.3.4 Refinements details of individual N-containing guests in each inclusion complex

Inclusion complex with 4-aminopyridine (**4F)**

The asymmetric unit of **4F** consists of four BTA linkers and seven Cd ions. Eight guest molecules bonded to Cd ions. One DMF molecule and three acetone molecules are in the pore. Anisotropic refinement of the non-hydrogen atoms of 4-aminopyridine was performed by applying constraints/restraints where necessary. DFIX, AFIX, ISOR and EADP were applied to 4-aminopyridine molecules to achieve acceptable geometry and a stable mode. DMF and acetone molecules were refined anisotropically where necessary DFIX, ISOR and EADP was applied. Hydrogen atoms were added by the riding model. The solvent mask detected one significant void 5883 $Å^3$ in size containing 1072 electrons.

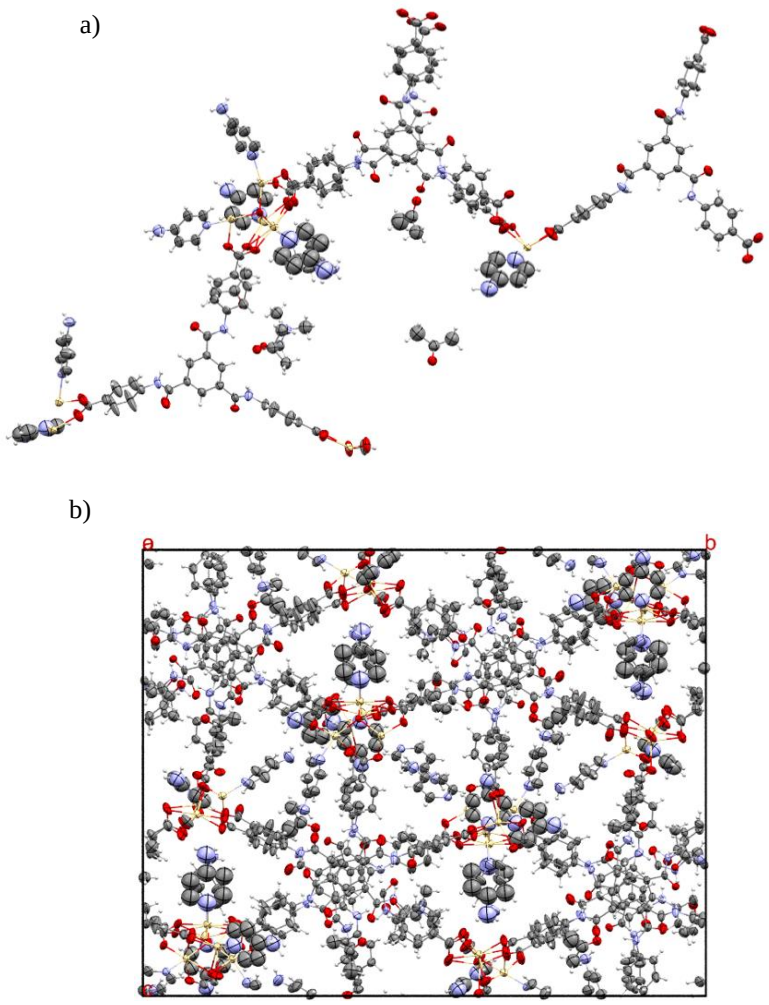

*Figure 5. 17 a) Asymmetric unit of inclusion complex **4F** showing major components of the disorders only. b) Unit cell of complex **4F.***

Inclusion complex with 3,5-lutidine (**4G)**

The asymmetric unit of **4G** consists of four BTA linkers and seven Cd ions. Seven guest molecules bonded to Cd ions. One guest molecule was in the pore along with three DMF molecules. All non-hydrogen atoms of 3,5-lutidine molecules bonded to Cd^{2+} and in the pore were refined anisotropically by applying DFIX, AFIX and EADP where necessary, to achieve acceptable geometry and a stable model. DMF molecules were refined anisotropically, and restraint/constraints were applied where necessary. Hydrogen atoms were added by the riding model. The solvent mask detected one significant void 2220 $Å^3$ in size containing 505 electrons. A large residual density peak (7.3 e/Å) was observed closer to Cd ion, this is due to absorption and/or termination error in Fourier calculations.

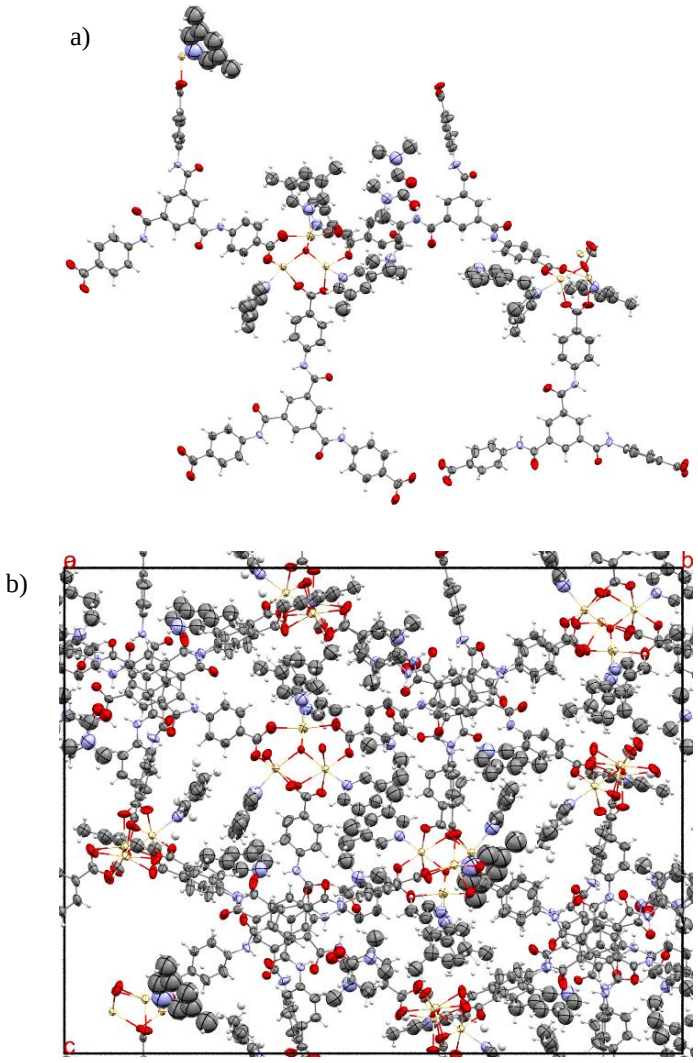

*Figure 5. 18 a) Asymmetric unit of inclusion complex **4G** showing major components of the disorders only. b) Unit cell of complex **4G.***

Inclusion complex with 3-bromopyridine (**4H)**

The asymmetric unit of **4H** consists of four BTA linkers, seven Cd ions and seven 3-bromopyridine molecules bonded to Cd^{2+} ions together with two 3-bromopyridine molecules in the pore. Two DMF and two acetone molecules were in the pore. All 3-bromopyridine molecules bonded to Cd^{2+} ions were anisotropically refined by applying DFIX, AFIX, ISOR and EADP where necessary. 3-bromopyridine molecules in the pore were also refined anisotropically by applying DFIX and AFIX to achieve acceptable geometry and a stable model. DMF and acetone molecules in the pore were also refined anisotropically and where necessary DFIX and EADP were applied. Hydrogen atoms were added by the riding model. The solvent mask detected two significant voids 1822 $Å^3$ and 250 $Å^3$ in size containing 309 and 103 electrons. A large residual density peak (7.0 e/Å) was observed closer to Br6, this peak could not be assigned in a way that can make any chemical sense.

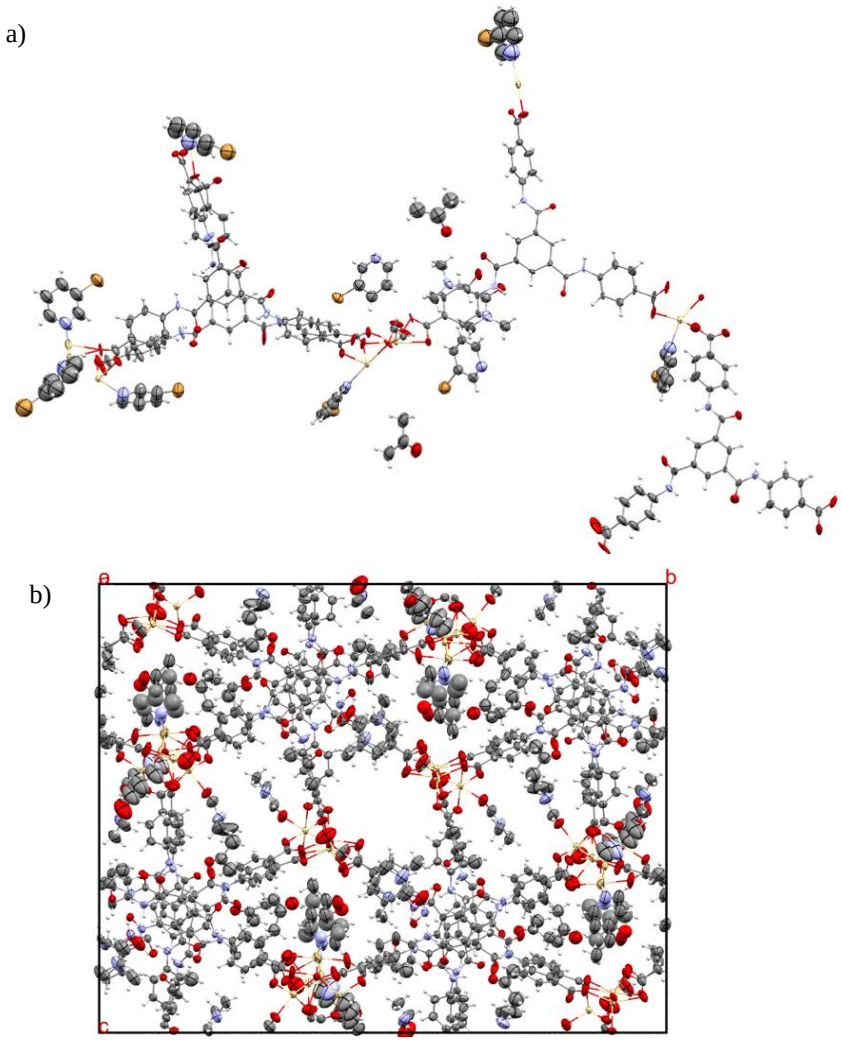

*Figure 5. 19 a) Asymmetric unit of inclusion complex **4H** showing major components of the disorders only. b) Unit cell of complex **4H**.*

Inclusion complex with 4-acetylpyridine (**4I)**

The asymmetric unit of **4I** consists of four BTA linkers, seven Cd ions, three molecules of 4-acetylpyridine bonded to Cd ions and three coordinated DMF molecules. In the pore two DMF molecules and four acetone molecules were found. 4-acetylpyridine molecules, two were anisotropically refined by applying DFIX, DANG, AFIX and EADP constraints/restraints to achieve acceptable geometry and a stable mode. Three DMF bonded to Cd^{2+} ions and two DMF molecules in the pore were refined anisotropically and where necessary DFIX and EADP were applied. Four acetone molecules in the pore were refined anisotropically and constrains/restrains were applied where necessary. Hydrogen atoms were added by the riding model. The solvent mask detected one significant void 2781 $Å^3$ in size containing 473 electrons. A large residual density peak (2.9 e/Å) was observed closer to Cd ion, this is due to absorption and/or termination error in Fourier calculations.

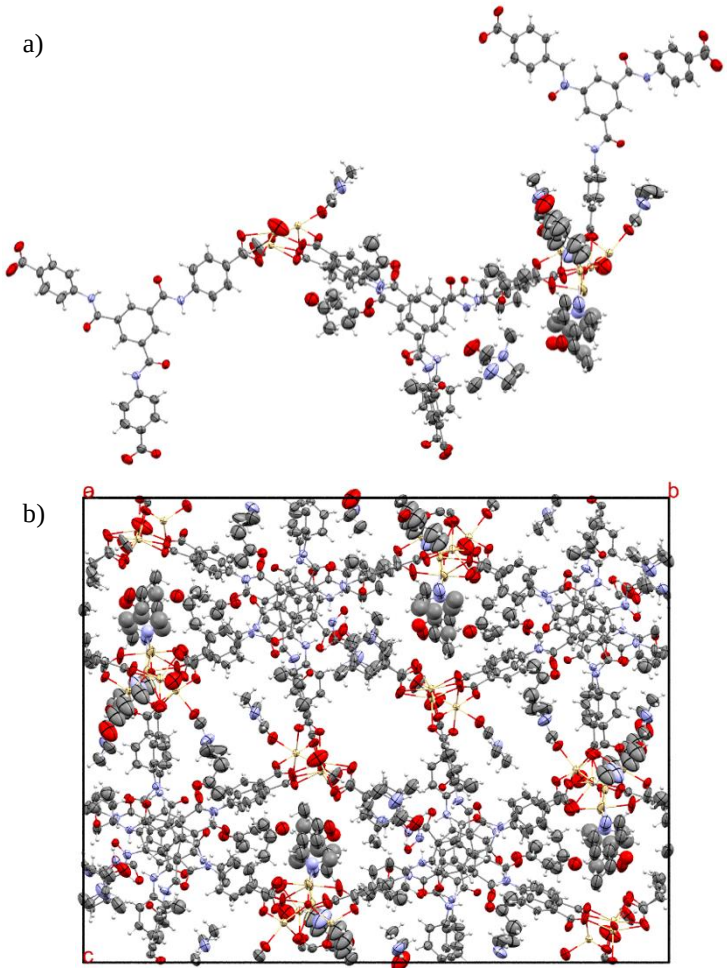

*Figure 5. 20 a) Asymmetric unit of inclusion complex **4I** showing major components of the disorders only. b) Unit cell of complex **4I**.*

Inclusion complex with 4,4'-bipyridine **4J**

The asymmetric unit of **4J** four consists of four BTA linkers, seven Cd ions, two complete 4,4'-bipyridine molecules and two half 4,4'-bipyridine molecules were bonded to Cd^{2+} ions together with two coordinated DMF molecules. In the pore one DMF molecule and seven acetone molecules were present. Anisotropic refinement of the non-hydrogen atoms of one of the two 4,4'-bipyridine molecules was performed by applying AFIX and EADP and the other one has refined anisotropically without constraints/restraints. Anisotropic refinement for half 4,4'-bipyridine molecules (only one pyridine ring) was refined by applying AFIX and EADP. Two DMF molecules were bonded to Cd^{2+} ions as well as one DMF in the pore, which was refined anisotropically without applying any constraints/restraints. Seven acetone molecules were refined anisotropically and DFIX was applied to all acetone molecules to achieve acceptable geometry and a stable model and ISOR was used to restrain the ADPs. Hydrogen atoms were added by the riding model. The solvent mask detected two significant void 1552 $Å^3$ and 506 $Å^3$ in size containing 208 and 81electrons respectively. A large residual density peak (3.2 e/Å) was observed closer to Cd ion, this is due to absorption and/or termination error in Fourier calculations

a)

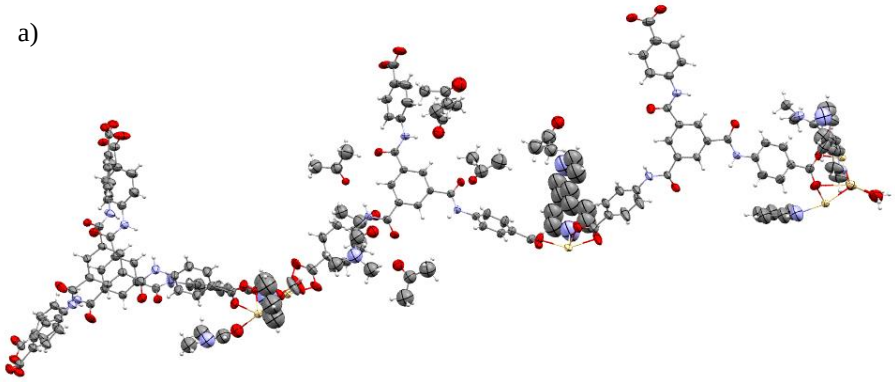

b)

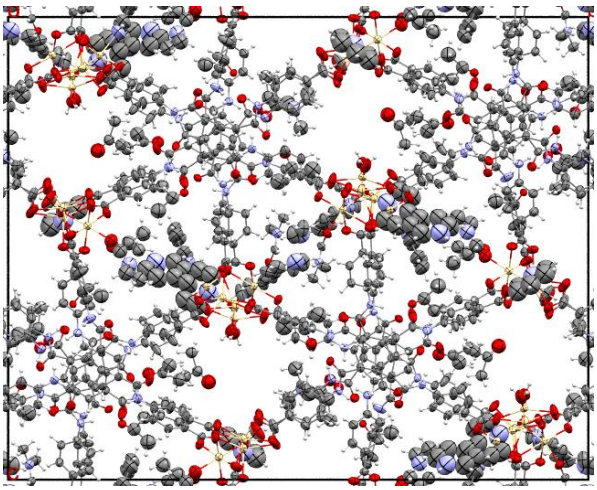

*Figure 5. 21 Asymmetric unit of inclusion complex **4J** showing major components of the disorders only. b) Unit cell of complex **4J**.*

5.3.5 Crystallographic table

Inclusion complex	**4F**	**4G**	**4H**	**4I**	**4J**
Empirical formula	$C_{155.65}H_{124.75}Cd_{6.9}N_{23.2}O_{42.15}$	$C_{178.65}H_{153.04}Cd_7N_{21.55}O_{41.29}$	$C_{169}H_{125.25}Br_7Cd_7N_{21.25}O_{42.75}$	$C_{152.95}H_{137.29}Cd_7N_{18.49}O_{58.19}$	$C_{165.4}H_{143.4}Cd_{7.1}N_{19.5}O_{47.8}$
Formula weight	3770.09	2699.58	4565.09	2548.08	3967.03
Temperature/K	150(1)	150(1)	150(1)	150(1)	150(1)
Crystal system	monoclinic	monoclinic	monoclinic	monoclinic	monoclinic
Space group	$P2_1/n$	$P2_1/n$	$P2_1/n$	$P2_1/n$	$P2_1/n$
a/Å	14.9412(2)	14.75582(16)	14.4839(2)	14.7831(16)	14.8231(2)
b/Å	42.7238(4)	42.9510(3)	43.3847(5)	42.6675(3)	42.5479(5)
c/Å	33.8725(4)	33.8388(3)	33.4003(3)	33.8751(2)	33.9598(4)
α/°	90	90	90	90	90
β/°	93.6969(14)	93.4415(9)	94.6441(13)	93.3844(8)	93.2426(11)
γ/°	90	90	90	90	90
V/Å^3	21577.4(5)	21407.6(3)	20919.2(5)	21329.8(3)	21383.9(4)
Z	4	4	4	4	4
ρ_{calc}g/cm^3	1.192	1.287	1.443	1.193	1.258
μ/mm^{-1}	5.896	6.048	7.861	6.056	6.063
F(000)	7770	8386	8964	7691	8152
Crystal size/mm^3	0.25 × 0.063 × 0.02	0.24 × 0.05 × 0.03	0.15 × 0.08 × 0.02	0.20 × 0.07 × 0.02	0.19 × 0.07 × 0.03
Radiation	Cu K_α (λ = 1.54184)	Cu K_α (λ = 1.54184)	Cu K_α (λ = 1.54184)	Cu K_α (λ = 1.54184)	Cu K_α (λ = 1.54184)
2Θ range for data collection/°	6.948 to 147.034	7 to 146.954	7.164 to 146.838	6.99 to 147.062	6.968 to 147.02
Index ranges	−18 ≤ h ≤ 17, −53 ≤ k ≤ 44, −35 ≤ l ≤ 42	−15 ≤ h ≤ 18, −52 ≤ k ≤ 51, −39 ≤ l ≤ 41	−17 ≤ h ≤ 16, −51 ≤ k ≤ 53, −40 ≤ l ≤ 41	−18 ≤ h ≤ 16, −46 ≤ k ≤ 52, −42 ≤ l ≤ 42	−18 ≤ h ≤ 13, −52 ≤ k ≤ 50, −42 ≤ l ≤ 37
Reflections collected	170415	163450	87829	156026	92612
Independent reflections	42835 [R_{int} = 0.0514, R_{sigma} = 0.0380]	42568 [R_{int} = 0.0486, R_{sigma} = 0.0357]	40840 [R_{int} = 0.0427, R_{sigma} = 0.0513]	42249 [R_{int} = 0.0446, R_{sigma} = 0.0333]	41735 [R_{int} = 0.0510, R_{sigma} = 0.0592]
Data/restraints/parameters	42835/424/2084	42568/965/2178	40840/407/2064	42249/204/1972	41735/1842/2058
Goodness-of-fit on F^2	1.060	1.059	1.887	1.023	1.032
Final R indexes [I>=2σ (I)]	R_1 = 0.1097, wR_2 = 0.2818	R_1 = 0.0921, wR_2 = 0.2367	R_1 = 0.1497, wR_2 = 0.4181	R_1 = 0.0793, wR_2 = 0.2307	R_1 = 0.0869, wR_2 = 0.2523
Final R indexes [all data]	R_1 = 0.1177, wR_2 = 0.2881	R_1 = 0.1038, wR_2 = 0.2480	R_1 = 0.1599, wR_2 = 0.4350	R_1 = 0.0958, wR_2 = 0.2543	R_1 = 0.1078, wR_2 = 0.2798
Largest diff. peak/hole / e Å^{-3}	1.92/−1.30	7.34/−1.82	7.05/−23.66	2.87/−2.36	3.17/−1. 57

COMPARISON OF ENCAPSULATED GUESTS IN THE PORE OF SPONGE **4** VS SPONGE **4'**

6

6.1 INTRODUCTION

In previous chapters, sponge **4** demonstrated the ability to accommodate guests in the pore and via the CAL method. It was noted that the structure of all the inclusion complexes generated from **4**, were closely similar to sponge **4**. For example, sponge **4** and inclusion complex **4'** only differ in having DMF and pyridine bonded to the Cd^{2+} respectively. This chapter attempts to compare sponges **4** and **4'** by encapsulating the same pair of guest molecules in both the frameworks and to look for any differences in the interaction with the framework. In previous chapters, it was observed that pore solvent molecules, DMF and acetone, repeatedly occupied sites common in all the inclusion complexes **4A**-**4J** and hydrogen bonding was the dominant interaction. Therefore, it is expected that the guest molecules in **4** might occupy the previously identified sites and be fixed by hydrogen bonding. However, for **4'**, it is hoped that due to the presence of pyridine, guest molecules might align themselves to form π-π interactions with the pyridine ring and hence it would be interesting to observe what sites guest molecules in **4'** would occupy.

6.1.1 Selection of guest molecules

Two guest molecules were selected for this chapter namely, *N*,*N*-dimethylaniline (**K**) and propiophenone (**L**). These molecules were selected as guests which would not coordinate to the metal centres of the sponges. For example, in *N*,*N*-dimethylaniline, the lone pair of electrons on nitrogen are not available for coordination. Therefore, it is expected that this guest will align itself in the pore. Propiophenone has a ketone group present, however, previous inclusion complex **4B** with acetone shows no coordination with the metal centres of **4** (Chapter 4). Therefore, it is likely that propiophenone molecules will align themselves in the pores of both the sponges. In contrast, in the literature, a few guest molecules containing the carbonyl/keto group were reported coordinated to metal centres. For example, *e*-caprolactam, *N*-methylcaprolactam[126] and benzyl acetate[127] were observed bonded to the Gd centre via the lone pair on the keto group or carbonyl

group of the guest molecules. Therefore, it would be interesting to observe how propiophenone molecules will align themselves in the pores of sponges **4** and **4'**.

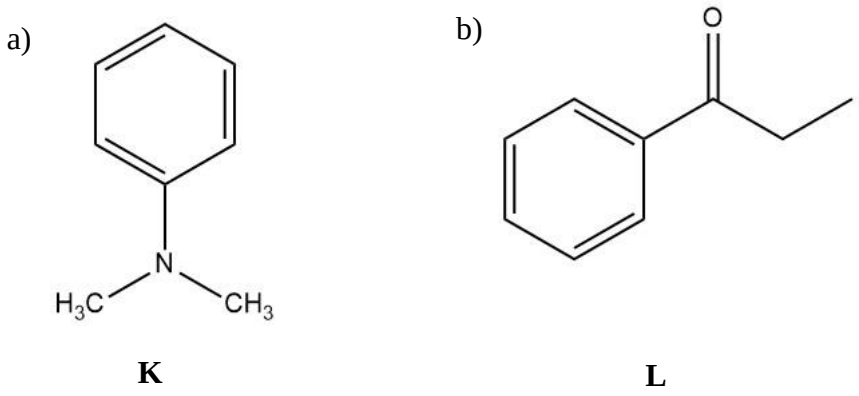

K **L**

Figure 6. 1 Guest molecules a) N,N-dimethylaniline b) Propiophenone

6.2 RESULTS AND DISCUSSION

6.2.1 Soaking experiment

Both guests *N*,*N*-dimethylaniline (**K**) and propiophenone (**L**) are liquid at room temperature, therefore, soaking experiments with neat guests at 25 °C were performed to obtain high occupancies with crystals of **4** to form **4K** and **4L**. However, crystals of **4'** deteriorated rapidly in the neat guests. Therefore, soaking experiments with a solution of **K** and **L** in acetone were used to obtain **4'K** and **4'L**.

Surprisingly when crystals of **4** were soaked in diluted guests the inclusion complexes from this soaking experiment have no guest molecules in the pores. Thus, the same soaking conditions do not work for both **4** and **4'**. Details of the soaking experiments are given in Table 6.1 in Experimental Section 6.3.

6.2.2 Inclusion complexes with **K** and **L**

This section describes the inclusion complexes obtained when **K** and **L** were encapsulated in **4** and **4'**. The SCXRD reveals that these guests were aligned in the pores as expected. All four inclusion complexes **4K**, **4L**, **4'K** and **4'L** crystallise in the $P2_1/n$ space group with very similar unit cell constants.

6.2.2a Comparison of inclusion complexes obtained with *N*,*N*-dimethylaniline (**4K** and **4'K**)

The structure of **4K** was similar to that of **4** because DMF was bonded to Cd^{2+} ions in both structures. On comparing the unit cell dimensions of **4K** with **4**, it was observed that both have similar unit cell lengths but **4K** has a large β angle. In addition, **4'K** unit cell parameters are indistinguishable from those of **4'**. This result is consistent with all the inclusion complexes discussed in previous chapters.

In inclusion complex **4K**, two molecules of *N*,*N*-dimethylaniline were observed in the asymmetric unit, shown in teal and mustard colour in Figure 6.2a, with occupancy of 20% and 35% respectively. On the other hand, the inclusion complex **4'K** was only able to accommodate one molecule of the *N*,*N*-dimethylaniline showed in mustard colour with occupancy of 25% in Figure 6.2b. This is might be because the diluted solution of *N*,*N*-dimethylaniline was used to obtain **4'K** compared to neat *N*,*N*-dimethylaniline used to obtain **4K**. A range of dilution conditions were used in an attempt to increase the number or the occupancy of guest molecules in **4'K**, however, all attempts were unsuccessful. In addition, it was observed that the solvent-accessible void space of **4** was 18.6% and of **4'** was 9% of the unit cell volume. This may provide a rational as to why **4'** accommodates fewer guests than **4**.

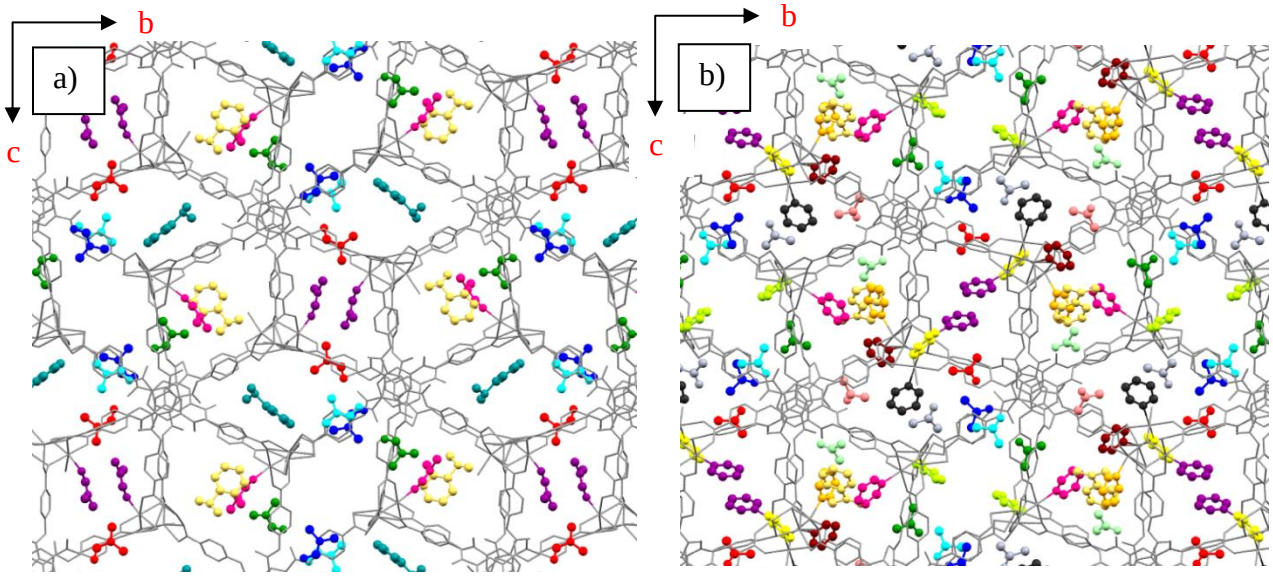

Figure 6. 2 Packing diagrams of complexes viewed down the a-axis. a) ***4K****, N,N-dimethylaniline in* ***4*** *b)* ***4'K*** *N,N-dimethylaniline in* ***4'****, Guest molecules were coloured according to their positional equivalence to those in sponge* ***4****. Framework displayed as capped stick and guest and solvent molecules as ball and stick representations.*

In inclusion complex **4K** the *N*,*N*-dimethylaniline molecule in teal colour was engaged in a CH-π interaction with the centroid of the aromatic ring of the framework, $CH_{guest}\cdots\cdots centroid_{framework}$ 2.7 Å, and a weak hydrogen bond with a carboxylate of the framework, Figure 6.3a. However, the molecule in mustard colour was isolated in the pore and had no interaction with the framework structure. Similarly, in inclusion complex **4'K**, the molecule in mustard colour was also isolated in the pore and thus no interaction with the framework was observed. Figures 6.3b and c illustrate the orientation of the mustard coloured molecule of *N*,*N*-dimethylaniline in **4K** and **4'K**, which is quite different in both cases. Interestingly, these sites occupied by the molecules of *N*,*N*-dimethylaniline in both the frameworks are unique and were not identified in previous structures. Surprisingly, in **4** the hydrogen bonding was not dominant as it was hoped. In **4'** the pyridine on Cd^{2+} extends into the pore space and it was hoped that it would provide a chance of π-π bonding to aromatic guests. However, unfortunately, that was not observed in practice. In literature, the inclusion of aniline in a POM based crystalline sponge was reported.[119] In this sponge, aniline molecules were also isolated in the pore and no hydrogen bonding with the framework was observed.

In **4K**, four DMF molecules in the pore were identified shown in blue, red, turquoise, and green as observed in Chapters 4 and 5. In **4'K** seven acetone molecules were observed in the pores shown in blue, red, turquoise, green, light red, light green and dark grey. Among these seven acetone molecules, only the dark grey position occupied by acetone is new and was not observed in previous structures. All these molecules are fixed in these positions by hydrogen bonding described in detail in Chapters 4 and 5.

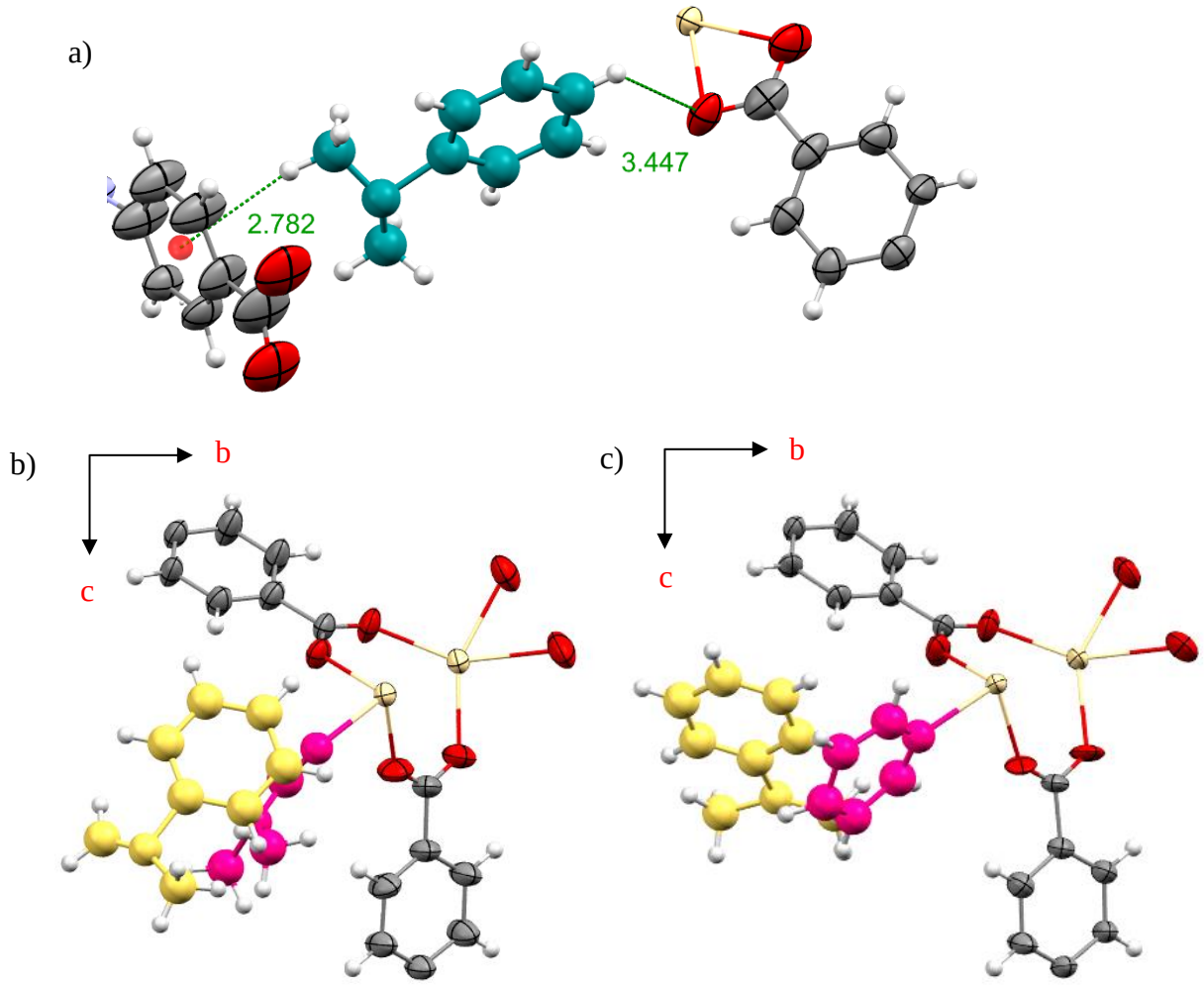

Figure 6. 3 a) Intermolecular interactions between molecules of N,N-dimethylaniline in teal colour with framework ***4*** *b) mustard coloured N,N-dimethylaniline in the pore of framework* ***4*** *c) mustard coloured N,N-dimethylaniline in the pore of framework* ***4'****. Guest molecules displayed as ball and stick model. Interaction distances are displayed in angstroms.*

6.2.2b Comparison of inclusion complexes obtained with Propiophenone (**4L** and **4'L**)

The inclusion complexes **4L** and **4'L** have similar structures as sponges **4** and **4'** respectively. Unsurprisingly the unit cell dimensions of **4L** are similar to those of **4**, and the dimension of **4'L** is similar to **4'**. This result is consistent with **4K** and **4'K** and all the inclusion complexes discussed in Chapters 4 and 5.

In the inclusion complex **4L**, four molecules of propiophenone were observed shown in black, mustard, violet and light green colour. Three molecules of propiophenone were refined with 50 to 80% occupancy range, Figure.6.4a. In contrast, the inclusion complex **4'L** has only one propiophenone molecule in the pore, with 50% occupancy, as shown in Figure 6.4b. In this case, also a smaller number of guest molecules in **4'** can be explained as described in section 6.2.2a. That is to obtain the inclusion complex **4'L**, propiophenone was diluted with acetone before soaking the **4'** crystals whereas crystals of **4** were soaked in neat propiophenone. Thus, fewer molecules of propiophenones were available to diffuse into the pore of **4'** compared to **4**. Moreover, solvent-accessible void space of **4** is larger (18.6% of the unit cell volume) than **4'** (9% of the unit cell volume). Thus, sponge **4** can accommodate more guest molecules in the pore than **4'**.

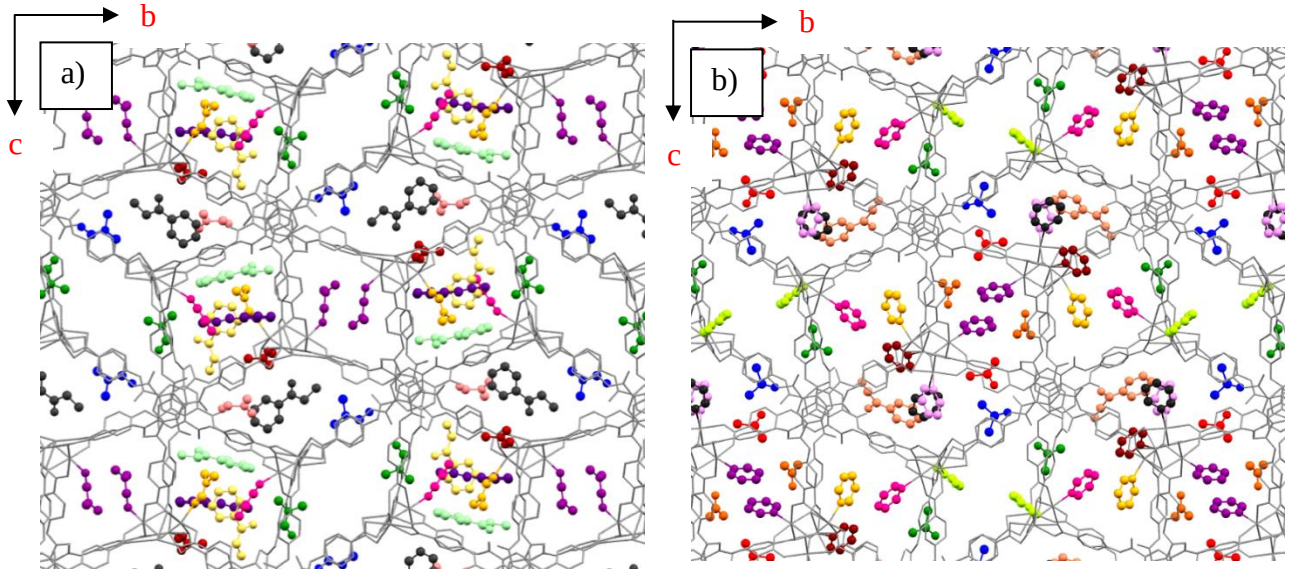

*Figure 6. 4 Packing diagrams of complexes viewed down the a-axis. a) **4L**, Propiophenone in **4** b) **4'L** Propiophenone in **4'**, Guest molecules were coloured according to their positional equivalence to those in sponge **4**. Framework displayed as capped stick and guest molecules as ball and stick representations.*

In the inclusion complex **4L**, the molecule shown in black was observed near the Cd5 ion, as shown in Figure 6.5a. This molecule was assigned black colour because of the position equivalence with the DMF molecule at this site in inclusion complex **4A**. However, unlike the black coloured DMF molecule in **4'**, the propiophenone molecule in black was not coordinated to Cd5, $Cd_{framework}\cdots O{=}C_L$ 3.6 Å. Due to its proximity with the framework carbonyl group of propiophenone, it is interacting with the carboxylates of the framework with $C{=}O_L\cdots O{=}C_{framework}$ 2.8 Å. In addition, hydrogen bonding between the hydrogen of propiophenone with the carbonyl of the framework, $H_L\cdots O{=}C_{framework}$ 2.4 Å, was observed. Figure 6.5b shows the non-bonding interaction of the second propiophenone molecule in light green colour with the framework. It was observed that this site was occupied by an acetone molecule in inclusion complex **4B** (Chapter 4). Similar to the acetone molecule in **4B** (see Figure 4.7b), the keto group of the propiophenone molecule forms three hydrogen bonds with the hydrogens of the framework, $C{=}O_L\cdots H_{framework}$ 2.4, 2.2, 2.6 Å. In addition, this site was also occupied by an isopropanol molecule in **4C** (See Figure 4.8b). The third propiophenone molecule observed in the pore, shown in violet, was oriented such that it was roughly parallel to the *b* axis. Probably because of this orientation, the keto group of this propiophenone molecule forms hydrogen bonds with the framework, $C{=}O_L\cdots H_{DMF}$ 2.5 and 2.4 Å, Figure 6.5c. The fourth molecule shown in mustard was observed at the same site as the molecules of *N*,*N*-dimethylaniline in **4K** and **4'K**. However, the orientation of the propiophenone molecule in mustard in **4L** (Figure 6.5d) was different than the *N*,*N*-dimethylaniline molecules in mustard in **4K** and **4'K** (Figure 6.3b,c). The difference was evident by the interaction between the propiophenone molecule and the DMF (Figure 6.5d) in green which was not observed in **4K** and **4'K**. This difference is probably because propiophenone has a keto group which can form a hydrogen bond with the closely located DMF molecule unlike *N*,*N*-dimethylaniline. In addition, the molecules of *N*,*N*-dimethylaniline observed at this site were isolated in the pore (Figure 6.3b). In contrast, the propiophenone molecule was engaged in hydrogen bonding with the framework, $C{=}O_L\cdots H_{DMF}$ 2.3, 2.4 Å and $H_L\cdots O{=}C_{framework}$ 2.8, 2.5 Å. An extensive study was performed with sponge **1**, on the difference in the host-guest interaction with the change in the functional groups and the change in the size of the guest molecules.[143,144] These studies reported that small changes in the functionality and size of guest molecules may affect their orientation and ordering within the sponge framework. Hence, the results in this chapter are consistent with the literature report.

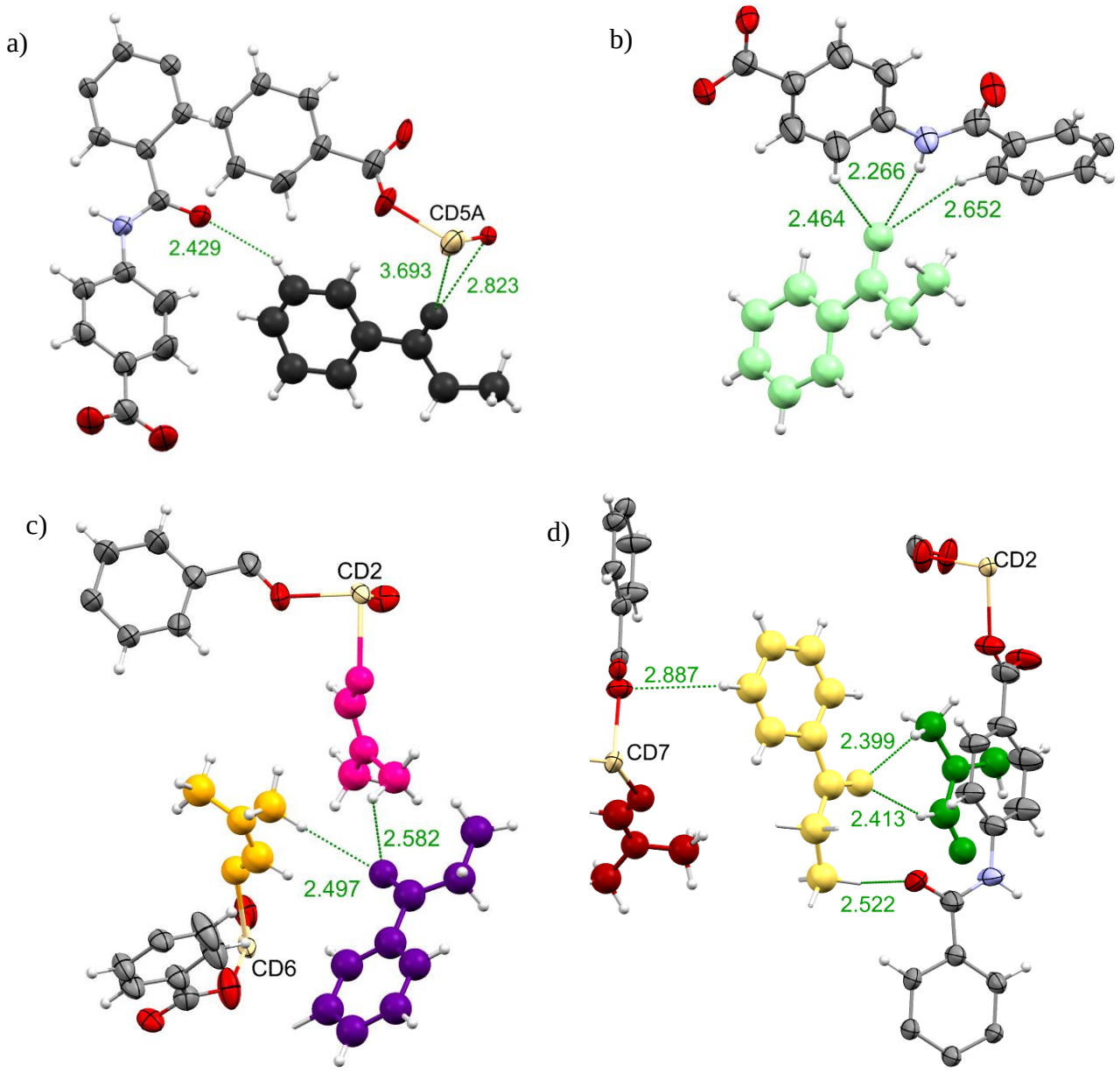

*Figure 6. 5 Intermolecular interactions between molecules of Propiophenone a) black b) light green c) violet d) mustard with framework **4**. Guest molecules displayed as ball and stick model. Interaction distances are displayed in angstroms.*

In the inclusion complex **4'L** only one molecule of propiophenone was observed in the pore, shown in light red Figure 6.6. The propiophenone molecule is fixed at this site via hydrogen bonding, $C{=}O_L{\cdots\cdots}H_{framework}$ 2.7, 2.0, 2.5 Å. This light red coloured site was also observed in **4L,** occupied by a DMF molecule (Figure 6.4a), and in Chapter 5 acetone molecules were observed at this site in inclusion complexes **4I** and **4J** (Figure 5.2 d,e). All guest molecules observed at this site were fixed in this position by the hydrogen bonding.

Furthermore, in the inclusion complex **4L**, seven DMF molecules were identified in the structure. Among them, four were bonded to Cd ions shown in light orange, magenta, maroon and purple and three molecules were in the pore shown in blue, green, and light red. In **4'L** four acetone molecules were observed in the pores shown in green, blue, red, and dark orange. All of these sites have been previously identified in the structures described earlier in this thesis.

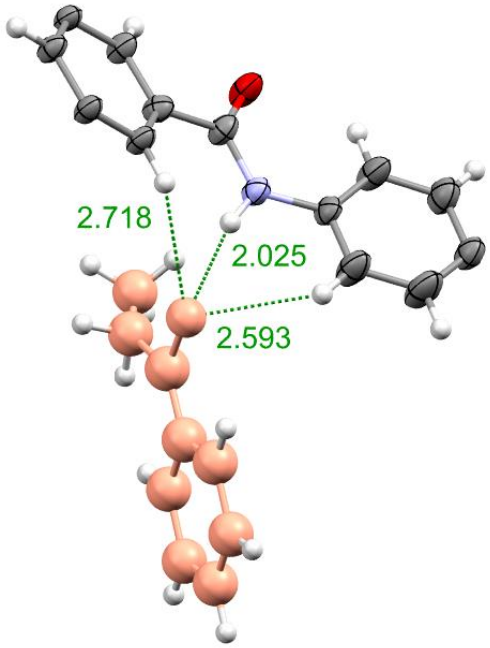

*Figure 6. 6 Intermolecular interactions between light red Propiophenone molecule with the framework **4'**. Guest molecule displayed as ball and stick model. Interaction distances are displayed in angstroms.*

6.2.3 Conclusions

In this chapter, it was hoped to make a direct comparison between the inclusion complexes derived from **4** and **4'**. However, this was not possible because different preparative methods had to be used, thus different occupancies. In inclusion complexes with *N*,*N*-dimethylaniline **4K** and **4'K** guest molecules occupy unique sites which were not fixed by the hydrogen bonding. In contrast, inclusion complexes with propiophenone **4L** and **4'L** guest molecules occupy previously identified sites and a unique site in **4L** was also observed and hydrogen bonding was the dominant interaction in these complexes. In inclusion complexes generated from **4'**, despite being hoped that guest binding would be via π-π interactions with pyridine bonded to Cd^{2+} however, this was not observed. In conclusion, insights of host-guest interaction from inclusion complexes generated from sponges **4** and **4'** suggested that usually, hydrogen bonding is the dominant interaction. However, in some cases, hydrogen bonding was not responsible for fixing the guest molecule in the pore. It is interesting to note that in the hydrophilic crystalline sponge, guest molecules can align themselves without an appropriate functional group to form a hydrogen bond.

6.3 EXPERIMENTAL SECTION

6.3.1 Soaking experiment

Guest molecules *N*,*N*-dimethylaniline and propiophenone are liquid at room temperature. Therefore, neat guests were used for soaking crystals of **4** to obtain inclusion complexes **4K** and **4L**. Soaking of crystals of **4** with diluted guests were also attempted however, guest molecules were not observed in the pores. To obtain inclusion complexes **4'K** and **4'L**, crystals of **4'** were first soaked in neat guests, however, deterioration of the crystals were observed. Therefore, guests were diluted with acetone prior to soaking. Details of soaking experiments are given in Table 6.1.

Guest	**Sponge**	**Guest dilution conditions**	**Solvent (1ml)**	**Incubation period**	**Results**
N,*N*-dimethylaniline (**K**)	**4**	neat	-	1 week	2 guest molecules in the pore (**4K**)
N,*N*-dimethylaniline (**K**)	**4**	neat	-	2 weeks	Crystals look fine optically but do not diffract
N,*N*-dimethylaniline (**K**)	**4**	100 µL	DMF	3 days	No guest was observed in the pore
N,*N*-dimethylaniline (**K**)	**4**	50 µL	DMF	3 days	No guest was observed in the pore
N,*N*-dimethylaniline (**K**)	**4'**	neat	-	1 day	Crystal deteriorated
N,*N*-dimethylaniline (**K**)	**4'**	50 µL	Acetone	3 days	1 guest molecule in the pore (**4'K**)
N,*N*-dimethylaniline (**K**)	**4'**	50 µL	Acetone	1 week	Crystals look fine optically but do not diffract
N,*N*-dimethylaniline (**K**)	**4'**	100 µL	Acetone	3 days	1 disordered guest molecule in the pore
Propiophenone (**L**)	**4**	neat	-	1 day	4 guest molecules in the pore (**4L**)
Propiophenone (**L**)	**4**	100 µL	DMF	10 days	No guest was observed in the pore
Propiophenone (**L**)	**4'**	neat	-	1 day	Crystals deteriorated
Propiophenone (**L**)	**4'**	100 µL	Acetone	10 days	1 guest molecule in the pore (**4'L**)
Propiophenone (**L**)	**4'**	500 µL	Acetone	10 days	1 guest molecule in the pore

*Table 6. 1 Soaking conditions for N,N-dimethylaniline and Propiophenone in sponge of **4** and **4'**.*

6.3.2 Crystallographic procedures

Using the same procedure as described in Section 2.3.3

6.3.3 Structural analysis details

The non-hydrogen atoms of the framework were refined anisotropically and hydrogen atoms were included using a riding model. The BTA and Cd components of the framework were at first freely refined without applying any constraints/restraints. However, on some occasions the BTA, Cd and coordinated guest components of the framework showed some disorder and where required atoms were modelled across two positions with a combined occupancy of 100%. DFIX and EADP were used to obtain a stable model. Refinement of solvent species (DMF and acetone) was first performed without any constraints/restraints and only if this was unsuccessful, were these added based on their known structures. The occupancy of each guest molecule was refined against its free variable which in the final stages of refinement was fixed to the values reported. In all the structures it was not possible to assign all the residual density peaks in a way that makes chemical sense, these peaks belong to heavily disordered guests or solvent molecules, and these were taken into account by the use of a solvent mask in the OLEX2 GUI[154]. On occasion a large residual density peak remained near the cadmium metal of the host framework this is due to absorption and/or termination errors in Fourier calculation. Standard deviations for restraints used are as described in chapter 2 section 2.3.4.

6.3.4 Refinements details of individual guests in each inclusion complex

Inclusion complex with *N*, *N*-dimethylaniline in **4** (**4K**)

The asymmetric unit of **4K** consists of four BTA linkers, seven Cd ions, two molecules of DMF bonded to Cd^{2+} ions and four molecules of DMF in the pore together with two molecules of *N*,*N*-dimethylaniline in the pores. Non-hydrogen atoms of both the molecule were refined anisotropically and DFIX, AFIX and EADP were applied to the molecule to achieve acceptable geometry. Four DMF molecules in the pores were refined anisotropically by applying DFIX and EADP where necessary. Hydrogen atoms were added by the riding model, though, for some DMF molecules hydrogens were required to be placed in fixed positions. The solvent mask detected one significant void 3770 $Å^3$ in size containing 735 electrons respectively. A large residual density peak (3.8 e/Å) was observed closer to Cd ion, this is due to absorption and/or termination error in Fourier calculations.

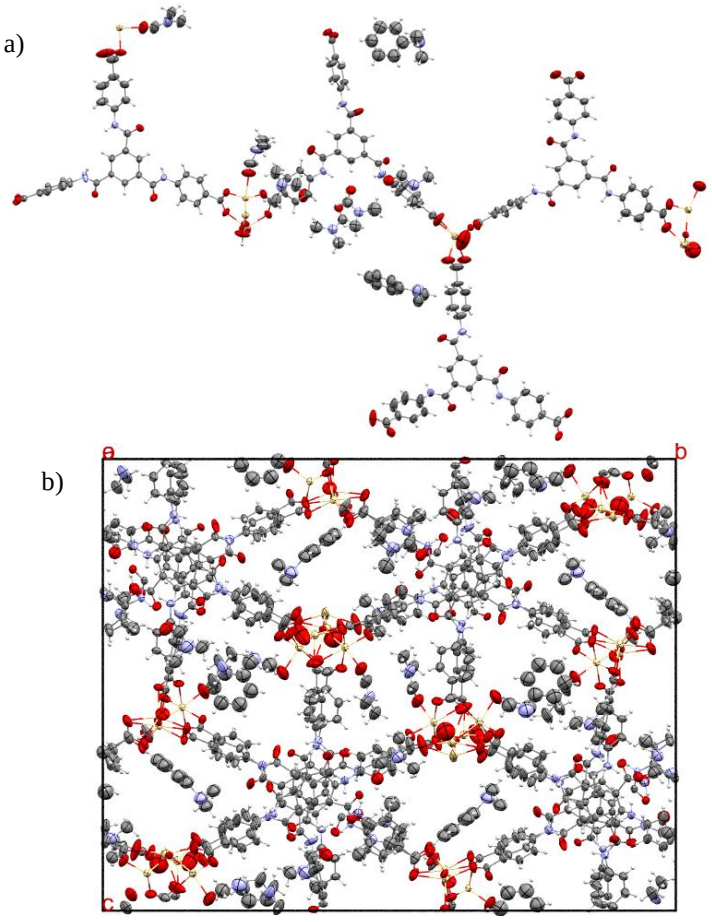

*Figure 6. 7 Asymmetric unit of the inclusion complex **4K** showing major components of the disorders only. b) Unit cell of complex **4K**.*

Inclusion complex with *N*,*N*-dimethylaniline in **4' (4'K)**

The asymmetric unit of **4'K** consists of four BTA linkers, seven Cd ions and seven pyridine ligands bonded to Cd^{2+} ions, and one molecule of *N*,*N*-dimethylaniline and seven molecules of acetone in the pores. The *N*,*N*-dimethylaniline molecule was refined anisotropically with DFIX and AFIX applied to the molecule to achieve acceptable geometry. Seven acetone molecules refined in the pores were anisotropically refined. DFIX and EADP were applied on acetone molecules where necessary. Hydrogen atoms were added by the riding model. The solvent mask detected three significant voids 598 $Å^3$, 443 $Å^3$ and 289 $Å^3$ in size containing 102, 103 and 64 electrons respectively. A large residual density peak (5.1 e/Å) was observed closer to N10, this peak could not be assigned in a way that makes any chemical sense.

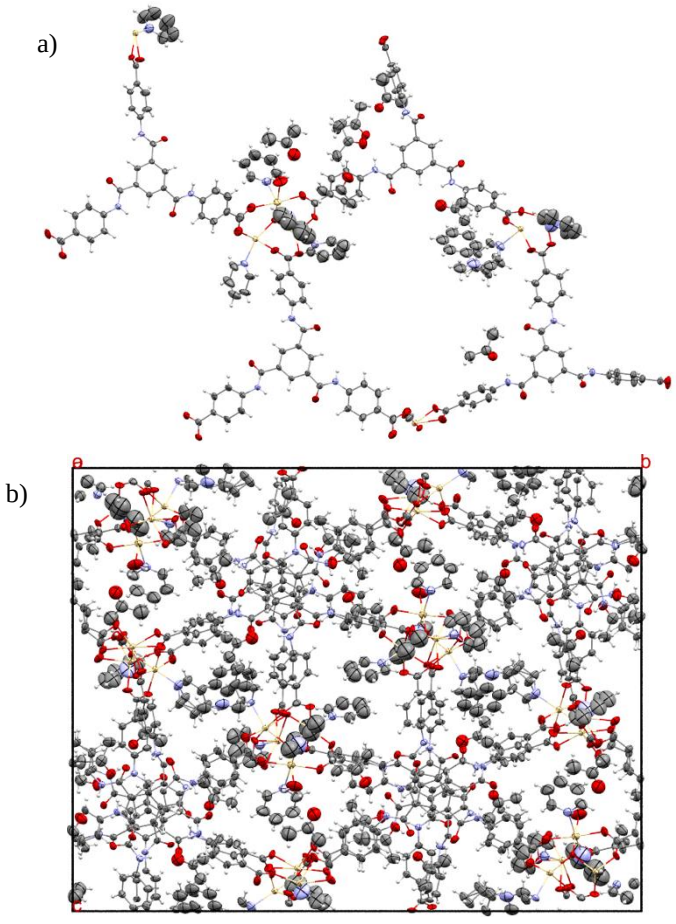

*Figure 6. 8 Asymmetric unit of the inclusion complex **4'K** showing major components of the disorders only. b) Unit cell of complex **4'K**.*

Inclusion complex with propiophenone in **4** (**4L**)

The asymmetric unit of **4L** consists of four BTA linkers, seven Cd ions, four molecules of DMF bonded to Cd^{2+} ions and three DMF molecules in the pore together with four molecules of propiophenone in the pores. Three molecules of propiophenone were refined anisotropically. DFIX, AFIX and EADP were applied to the propiophenone molecules to achieve acceptable geometry and a stable mode. Three DMF molecules in the pores were refined anisotropically by applying DFIX and EADP where necessary. Hydrogen atoms were added by the riding model. The solvent mask detected one significant void 2395 $Å^3$ in size containing 640 electrons. A large residual density peak (2.4 e/Å) was observed closer to Cd ion, this is due to absorption and termination error in Fourier calculations.

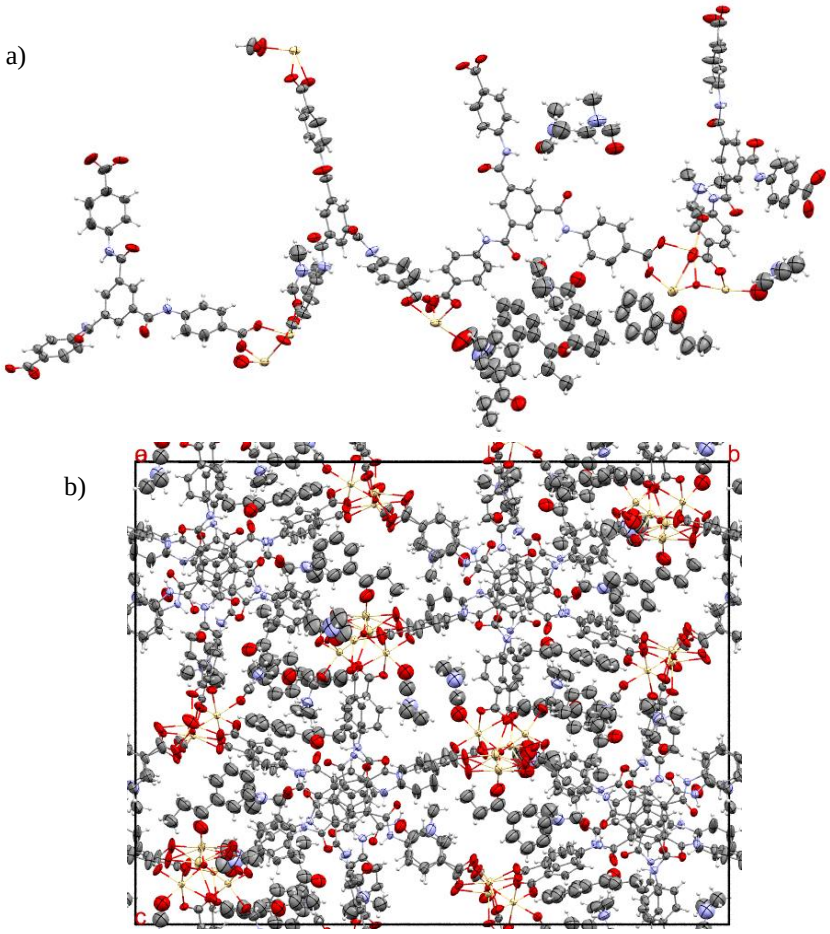

*Figure 6. 9 Asymmetric unit of the inclusion complex **4L** showing major components of the disorders only. b) Unit cell of complex **4L**.*

Inclusion complex with propiophenone in **4' (4'L)**

The asymmetric unit of **4'L** consists of four BTA linkers, seven Cd ions, and seven molecules of pyridine bonded to Cd^{2+} ions and four acetone molecules in the pore together with one molecule of propiophenone in the pore. Propiophenone molecule was refined anisotropically with 50% occupancy and DFIX, AFIX and EADP were applied to this molecule to achieve acceptable geometry. Acetone molecules in the pore were refined anisotropically and constrain/restrain applied where necessary. Hydrogen atoms were added by the riding model. The solvent mask detected one significant void 5221 $Å^3$ in size containing 1204 electrons. A large residual density peak (2.6 e/Å) was observed closer to Cd ion, this is due to absorption and termination error in Fourier calculations.

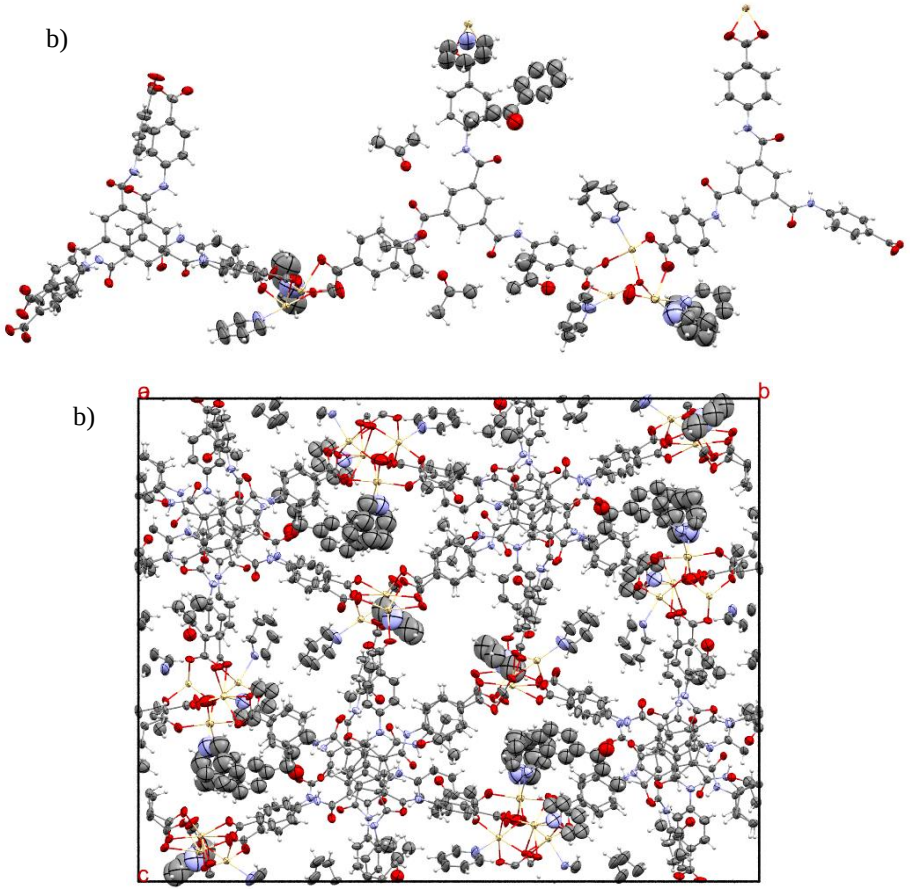

*Figure 6. 10 a) Asymmetric unit of the inclusion complex **4'L** showing major components of the disorders only. b) Unit cell of complex **4'L**.*

6.3.5 Crystallographic table

Inclusion complex	**4K**	**4'K**	**4L**	**4'L**
Empirical formula	$C_{148.3}H_{126}Cd_7N_{18.85}O_{49}$	$C_{172.5}H_{145.33}Cd_7N_{19}O_{45.83}$	$C_{168.19}H_{147.50}Cd_7N_{18.49}O_{49.54}$	$C_{168}H_{127.99}Cd_7N_{19}O_{44.50}$
Formula weight	2945.91	4004.52	2284.01	2606.78
Temperature/K	150(1)	150(1)	150(1)	150(1)
Crystal system	monoclinic	monoclinic	monoclinic	Monoclinic
Space group	$P2_1/n$	$P2_1/n$	$P2_1/n$	$P2_1/n$
a/Å	14.6869(11)	14.1427(3)	14.61500(10)	14.05890(12)
b/Å	42.8432(3)	43.1990(6)	43.0674(3)	43.1549(2)
c/Å	33.8507(2)	33.7991(4)	33.6023(2)	33.7222(2)
α/°	90	90	90	90
β/°	93.1111(7)	94.7053(16)	93.6760(10)	94.5246(7)
γ/°	90	90	90	90
V/Å^3	21268.7(3)	20580.0(6)	21106.8(2)	20395.9(2)
Z	4	4	4	4
ρ_{calc}g/cm^3	1.150	1.299	1.260	1.256
μ/mm^{-1}	6.049	6.288	6.140	6.312
F(000)	7371	8104	8060	7724
Crystal size/mm^3	0.25 × 0.05 × 0.01	0.23 × 0.05 × 0.04	0.15× 0.08 × 0.03	0.22× 0.05 × 0.03
Radiation	Cu K_α (λ = 1.54184)	Cu K_α (λ = 1.54184)	Cu K_α (λ = 1.54184)	Cu K_α (λ = 1.54184)
2Θ range for data collection/°	7.306 to 146.934	6.906 to 147.472	7.068 to 147.292	6.948 to 147.066
Index ranges	−18 ≤ h ≤ 15, −43 ≤ k ≤ 53, −41≤ l ≤ 37	−17 ≤ h ≤ 17, −50 ≤ k ≤ 52, −23 ≤ l ≤ 41	−12 ≤ h ≤ 18, −52 ≤ k ≤ 48, −41 ≤ l ≤ 41	−17 ≤ h ≤ 17, −53 ≤ k ≤ 53, −41 ≤ l ≤ 40
Reflections collected	148791	83443	152041	368403
Independent reflections	42145 [R_{int} = 0.0422, R_{sigma} = 0.0340]	40194 [R_{int} = 0.0625, R_{sigma} = 0.0792]	41905 [R_{int} = 0.0407, R_{sigma} = 0.0320]	40647 [R_{int} = 0.0712, R_{sigma} = 0.0310]
Data/restraints/parameters	42145/244/1900	40194/250/2101	41905/1797/2022	40647/280/1915
Goodness-of-fit on F^2	1.031	1.034	1.058	1.046
Final R indexes [I>=2σ (I)]	R_1 = 0.0795, wR_2 = 0.2335	R_1 = 0.0886, wR_2 = 0.2398	R_1 = 0.0759, wR_2 = 0.2081	R_1 = 0.0797, wR_2 = 0.2062
Final R indexes [all data]	R_1 = 0.0878, wR_2 = 0.2433	R_1 = 0.1102, wR_2 = 0.2594	R_1 = 0.0822, wR_2 = 0.2138	R_1 = 0.0954, wR_2 = 0.2236
Largest diff. peak/hole / e Å^{-3}	3.84/−2.29	5.11/−2.44	2.44/−1.69	2.62/−1.42

7 CONCLUSIONS AND PERSPECTIVES

7.1 CONCLUSIONS

The aim of this thesis was to expand the CSM to a wider range of guest molecules by synthesising novel inclusion complexes and developing alternative crystalline sponges. Initially, to become familiar with the CSM techniques and methodology, the most common crystalline sponge $[\{(ZnI_2)_3(TPT)_2 \cdot 6(CHCl_3)\}_n]$ (**1**) was used to synthesise three novel inclusion complexes with terpenes as guest molecules. Geraniol, farnesol and β-damascone were selected for this study because they have an important role in the biotech and agribusiness context, and the knowledge of their structure could provide insights into biological mechanisms. Although the molecular structures were previously known. The structure of these guests were determined in the pore and their interactions with the host framework were studied. In this work, CH-π and π-π were identified as the dominant interactions which confirm the hydrophobic pore environment of sponge **1**.

Although sponge **1** was the most common and successful crystalline sponge, it has practical limitations such as a hydrophobic pore environment, small pore size and instability in the presence of polar solvents and nucleophiles. Therefore, the range of guest molecules for sponge **1** is limited. Hence, to expand the CSM to a wider range of guest molecules, the development of an alternative crystalline sponge is essential. In the literature, various alternative crystalline sponges were developed to overcome the above-mentioned limitations. In this thesis, two previously synthesised MOFs were selected and their potential as alternative crystalline sponges was investigated. The MOF $\{[Co_2(L)(H_2O)_3] \cdot (solvent)_x\}_n$ L = *bis*-(3,5-dicarboxy-pheny1)terephthalamide (**3**), proved to perform well as an alternative crystalline sponge and two inclusion complexes with 3-phenylpropranol and 2-phenylethanol were synthesised. The guest molecules were fixed at the sites mainly by hydrogen bonding and established the hydrophilic pore environment for sponge **3**. Thus, **3** was suitable to accommodate polar solvents.

The MOF $\{[Cd_7(BTA)_4(H_2O)_x(DMF)_n]\cdot(solvent)_m\}$ BTA = 4,4'4''-[1,3,5-benzenetriyltris(carbonylimino)]-trisbenzoic (**4**), with pore size 10 × 16 $Å^2$, was investigated for its utility as a crystalline sponge. Results show excellent performance of sponge **4** as a crystalline sponge which was stable in a variety of solvents (polar aprotic and polar protic) and Lewis bases. In all the inclusion complexes with these solvent molecules, hydrogen bonding was observed as the dominant host-guest interaction. In addition, **4** was stable in the presence of nucleophiles and several N-containing molecules were accommodated in the sponge **4** via the CAL mechanism. Sponge **4** shows versatility in accommodating guest molecules in the pores as well as via coordinative alignment and thus, this is a successful alternative crystalline sponge, that has overcome all the limitations of Fujita's sponge. However, in a few inclusion complexes, partial guests and incomplete inclusion of guest molecules were observed, for example in the case of 4,4'-bipyridine. This is due to imperfections developed in the crystals after the inclusion of the guest compound. It is important to note that the crystals of the host framework should be able to withstand various soaking conditions such as different temperatures and different concentrations of the guest in a variety of solvents. Therefore, any damage to the host crystals can be kept to a minimum. Despite the degradation in the quality of the crystals of **4** at the best-optimised condition, two complete molecules of 4,4-bipyridine were successfully identified. In the end, a study was conducted to compare two closely similar structures of sponges **4** and **4'**. Results revealed that sponge **4'** has a relatively smaller void space to accommodate guest molecules in the pore than **4**. Perhaps surprisingly Pyridine molecules bonded to Cd^{2+} ions in **4'** do not form π-π interactions with the incoming guests as was hoped. The same pair of guest molecules were encapsulated in both the sponges **4** and **4'** and similarities and differences in the guest binding to the framework were documented. In conclusion sponge **4** was a successful alternative sponge to **1** and is highly recommended for use in CSM, particularly to accommodate Lewis bases, nucleophile guests and for the structure determination of active pharmaceutical ingredients as they commonly are N-containing compounds.[98,124]

7.2 FUTURE WORK AND PROSPECTS

Even with the tremendous success in application to various fields such as the pharmaceutical industry, agribusiness, and perfume companies, the CSM is still in its early stage and needs further development. This thesis contributed to the CSM technology by developing a versatile crystalline sponge **4**. The performance of sponge **4** as a crystalline sponge was well established in the presence

of polar solvents and nucleophiles. Although the pore size of sponge **4** is relatively large than sponge **1,** this work didn't explore the advantages of bigger pore size. The maximum recommended guest size for sponge **1** is 500 molecular weight. For future work, it would be interesting to encapsulate heavier guest molecules in CSM and establish the maximum guest size for sponge **4**. One of the limitations of CSM is that guest molecules in the pore are often disordered and have lower occupancies. This is also observed in sponge **4** along with observation of partial structures for example in **4I** and **4J** inclusion complexes. The crystals of these inclusion complexes should be exposed to high-intensity X-ray sources such as synchrotron and hopefully better data should reveal the remaining parts of the guest molecule. In addition, *Merck group* and *Rigaku Corporation* have signed a joint development agreement to improve X-ray crystallographic analyses both in terms of the software and hardware for highly innovative crystalline sponge technology[16] which would overcome this limitation of CSM.

8

REFERENCES

1 Y. Inokuma, S. Yoshioka, J. Ariyoshi, T. Arai, Y. Hitora, K. Takada, S. Matsunaga, K. Rissanen and M. Fujita, *Nature*, 2013, **495**, 461–466.

2 Y. Inokuma, T. Ukegawa, M. Hoshino and M. Fujita, *Chem. Sci.*, 2016, **7**, 3910–3913.

3 L. Rosenberger, C. von Essen, A. Khutia, C. Kühn, K. Urbahns, K. Georgi, R. W. Hartmann and L. Badolo, *Drug Metab. Dispos.*, 2020, **48**, 587–593.

4 K. Ohara and K. Yamaguchi, *Anal. Sci.*, 2020, **37**, 167–175.

5 K. Ohara, M. Kawano, Y. Inokuma and M. Fujita, *J. Am. Chem. Soc.*, 2010, **132**, 30–31.

6 M. Tominaga, T. Hyodo, Y. Maekawa, M. Kawahata and K. Yamaguchi, *Chem. – Eur. J.*, 2020, **26**, 5157–5161.

7 T. Haneda, M. Kawano, T. Kawamichi and M. Fujita, *J. Am. Chem. Soc.*, 2008, **130**, 1578–1579.

8 S. Yoshioka, Y. Inokuma, V. Duplan, R. Dubey and M. Fujita, *J. Am. Chem. Soc.*, 2016, **138**, 10140–10142.

9 T. Kawamichi, T. Haneda, M. Kawano and M. Fujita, *Nature*, 2009, **461**, 633–635.

10 K. Ikemoto, Y. Inokuma, K. Rissanen and M. Fujita, *J. Am. Chem. Soc.*, 2014, **136**, 6892–6895.

11 N. Wada, R. D. Kersten, T. Iwai, S. Lee, F. Sakurai, T. Kikuchi, D. Fujita, M. Fujita and J.-K. Weng, *Angew. Chem. Inter. Ed.*, 2018, **57**, 3671–3675.

12 S. Urban, R. Brkljača, M. Hoshino, S. Lee and M. Fujita, *Angew. Chem. Inter. Ed*, 2016, **55**, 2678–2682.

13 R. Brkljača, J. M. White and S. Urban, *J. Nat. Prod.*, 2015, **78**, 1600–1608.

14 Y. Matsuda, T. Mitsuhashi, S. Lee, M. Hoshino, T. Mori, M. Okada, H. Zhang, F. Hayashi, M. Fujita and I. Abe, *Angew. Chem. Inter. Ed*, 2016, **55**, 5785–5788.

15 A. D. Cardenal and T. R. Ramadhar, *ACS cent. Sci.*, 2021, **7**, 404–414.

16 Https://www.merckgroup.com/en/research/science-space/envisioning-tomorrow/future-of-scientific-work/crystalline-sponge-technology.html,.

17 H. Sato, A. Yamano, *Rigaku Journ*al, 2013, **35**, 1–3.

18 R. D. J. Lunn, D. A. Tocher, P. J. Sidebottom, M. G. Montgomery, A. C. Keates and C. J. Carmalt, *Crys. Growth Des.*, 2021, **21**, 3024–3036.

19 M. Fujita, *Chem. Soc. Rev.*, 1998, **27**, 417–425.

20 D. J. Cram, *Nature*, 1992, **356**, 29–36.

21 J. Kang and J. Rebek, *Nature*, 1997, **385**, 50–52.

22 J. W. Steed and J. L. Atwood, *Supramolecular Chemistry*, Wiley, Chichester, 3nd ed., 2022.

23 J. M. Lehn, *Acc. Chem. Res.*, 1978, **11**, 49–57.

24 G. W. Gokel, *Introduction and Overview of Supramolecular Receptor Types*, Elsevier, 2nd ed., 2017, vol. 1, ch. 1, pp, 1-10.

25 G. T. Williams, C. J. E. Haynes, M. Fares, C. Caltagirone, J. R. Hiscock and P. A. Gale, *Chem. Soc. Rev.*, 2021, **50**, 2737–2763.

26 N. Ahmad, H. A. Younus, A. H. Chughtai and F. Verpoort, *Chem. Soc. Rev.*, 2015, **44**, 9–25.

27 S. B. Carneiro, F. Í. C. Duarte, L. Heimfarth, J. D. S. S. Quintans, L. J. Quintans-Júnior, V. F. D. V. Júnior and Á. A. N. de Lima, *Int. J. Mol. Sci.*, 2019, **20**, 1–23.

28 M. Fujita, S. Washizu, K. Ogura and Y. J. Kwon, *J. Am. Chem. Soc.*, 1994, **116**, 1151–1152.

29 M. P. Byrn, C. J. Curtis, S. Khan, P. A. Sawin, R. Tsurumi and C. E. Strouse, *J. Am. Chem. Soc.*, 1990, **112**, 1865–1874.

30 M. P. Byrn, C. J. Curtis, I. Goldberg, Y. Hsiou, S. I. Khan, P. A. Sawin, S. Kathleen Tendick and C. E. Strouse, *J. Am. Chem. Soc.*, 1991, **113**, 6549–6557.

31 Y. Inokuma, M. Kawano and M. Fujita, *Nat. Chem.*, 2011, **3**, 349–358.

32 M. Yoshizawa, J. K. Klosterman and M. Fujita, *Angew. Chem. – Int. Ed.*, 2009, **48**, 3418–3438.

33 M. Yoshizawa, Y. Takeyama, T. Kusukawa and M. Fujita, *Analysis*, 2002, 1347–1349.

34 E. Arunan, G. R. Desiraju, R. A. Klein, J. Sadlej, S. Scheiner, I. Alkorta, D. C. Clary, R. H. Crabtree, J. J. Dannenber, P. Hobza, H. G. Kjaergaard, A. C. Legon, B. Mennucci and D. J. Nesbitt, *Pure App. Chem.*, 2011, **83**, 1637–1641.

35 J. Emsley, *Chem. Soc. Rev.*, 1980, **9**, 91–124.

36 G. A. Jeffrey, *Acta Crystallogr. Sect. B: Struct. Sci.*, 2000, **56**, 333–334.

37 R. Anjana, M. Kirti Vaishnavi, D. Sherlin, S. Pavan Kumar, K. Naveen, P. Sandeep Kanth and K. Sekar, *Bioinformation*, 2012, **8**, 1220–1224.

38 M. L. Waters, *Curr. Opin. Chem. Biol.*, 2002, **6**, 736–741.

39 H.-C. Joe Zhou and S. Kitagawa, *Chem. Soc. Rev.*, 2014, **43**, 5415–5418.

40 Q. L. Zhu and Q. Xu, *Chem. Soc. Rev.*, 2014, 43, 5468–5512.

41 Y. He, B. Li, M. O'Keeffe and B. Chen, *Chem. Soc. Rev.*, 2014, **43**, 5618–5656.

42 Z.-J. Lin, J. Lü, M. Hong and R. Cao, *Chem. Soc. Rev.*, 2014, **43**, 5867–95.

43 W. Lu, Z. Wei, Z.-Y. Gu, T.-F. Liu, J. Park, J. Park, J. Tian, M. Zhang, Q. Zhang, T. Gentle III, M. Bosch and H.-C. Zhou, *Chem. Soc. Rev.*, 2014, **43**, 5561–5593.

44 M. Eddaoudi, D. B. Moler, H. Li, B. Chen, T. M. Reineke, M. O'Keeffe and O. M. Yaghi, *Acc. Chem. Res.*, 2001, **34**, 319–330.

45 V. Guillerm, D. Kim, J. F. Eubank, R. Luebke, X. Liu, K. Adil, M. S. Lah and M. Eddaoudi, *Chem. Soc. Rev.*, 2014, **43**, 6141–6172.

46 S. L. James, *Chem. Soc. Rev.*, 2003, **32**, 276–288.

47 J. Rocha, L. D. Carlos, F. A. A. Paz and D. Ananias, *Chem. Soc. Rev.*, 2011, 40, 926–940.

48 M. D. Allendorf, C. A. Bauer, R. K. Bhakta and R. J. T. Houk, *Chem. Soc. Rev.*, 2009, **38**, 1330–1352.

49 S. M. Xie, Z. J. Zhang, Z. Y. Wang and L. M. Yuan, *J. Am. Chem. Soc.*, 2011, **133**, 11892–11895.

50 H. Furukawa, N. Ko, Y. B. Go, N. Aratani, S. B. Choi, E. Choi, a O. Yazaydin, R. Q. Snurr, M. O'Keeffe, J. Kim and O. M. Yaghi, *Science*, 2010, **329**, 424–428.

51 H. K. Chae, D. Y. Siberio-Pérez, J. Kim, Y. Go, M. Eddaoudi, A. J. Matzger, M. O'Keeffe and O. M. Yaghi, *Nature*, 2004, **427**, 523–527.

52 S. Chester, A. W. Clement, P. & Han, *US patent 6,136,291A*.

53 M. D. and J. R. L. Leslie J. Murray, *Chem. Soc. Rev.*, 2009, **38**, 1294–1314.

54 N. L. Rosi, J. Eckert, M. Eddaoudi, D. T. Vodak, J. Kim, M. O'Keeffe and O. M. Yaghi, *Science*, 2003, **300**, 1127–1129.

55 L. Zhu, X. Q. Liu, H. L. Jiang and L. B. Sun, *Chem. Rev.*, 2017, 117, 8129–8176.

56 J. Rocha, L. D. Carlos, F. A. A. Paz and D. Ananias, *Chem. Soc. Rev.*, 2011, 40, 926–940.

57 L. Ma, C. Abney and W. Lin, *Chem. Soc. Rev.*, 2009, **38**, 1248–1256.

58 L. E. Kreno, K. Leong, O. K. Farha, M. Allendorf, D. Van Richard P. and J. T. Hupp, *Chem. Rev.*, 2012, **112**, 1105–1125.

59 P. Ramaswamy, N. E. Wong and G. K. Shimizu, *Chem. Soc. Rev.*, 2014, **43**, 5913–5932.

60 L. Sun, M. G. Campbell and M. Dinca, *Angew. Chem. – Int. Ed.*, 2016, **55**, 3566–3579.

61 P. Horcajada, T. Chalati, C. Serre, B. Gillet, C. Sebrie, T. Baati, J. F. Eubank, D. Heurtaux, P. Clayette, C. Kreuz, J.-S. Chang, Y. K. Hwang, V. Marsaud, P.-N. Bories, L. Cynober, S. Gil, G. Ferey, P. Couvreur and R. Gref, *Nat. Mater.*, 2010, **9**, 172–178.

62 B. F. Hoskins and R. Robson, *J. Am. Chem. Soc*, 1990, **112**, 42.

63 S. Kitagawa, M. Munakata and T. Tanimura, *Inorg. Chem*, 1992, **31**, 1714–1717.

64 O. M. Yaghi and H. Li, *J. Am. Chem. Soc.*, 1995, **117**, 10401–10402.

65 H. Li, M. Eddaoudi, M. O'Keeffe and O. M. Yaghi, *Nature*, 1999, **402**, 276–279.

66 S. S.-Y. Chui, S. M.-F. Lo, J. P. H. Charmant, A. G. Orpen and I. D. Williams, *Science*, 1999, **283**, 1148–50.

67 N. L. Rosi, J. Kim, M. Eddaoudi, B. Chen, A. Michael O'Keeffe and Omar M. Yaghi, *J. Am. Chem. Soc.*, 2005, **127**, 1504–1518.

68 C. Dey, T. Kundu, B. P. Biswal, A. Mallick and R. Banerjee, *Acta Crystallogr., Sect. B: Struct. Sci., Crys. Eng. Mater*, 2014, **70**, 3–10.

69 J. M. Lehn, *Polymer Int.*, 2002, **51**, 825–839.

70 O. M. Yaghi, M. O'Keeffe, N. W. Ockwig, H. K. Chae, M. Eddaoudi and J. Kim, *Nature*, 2003, **423**, 705–714.

71 M. Eddaoudi, J. Kim, N. Rosi, D. Vodak, J. Wachter, M. O'Keeffe and O. M. Yaghi, *Science*, 2002, **295**, 469–472.

72 L. Bellarosa, S. Calero and N. López, *Phys. Chem. Chem. Phys.*, 2012, **14**, 7240–7245.

73 T. Mehtab, G. Yasin, M. Arif, M. Shakeel, R. M. Korai, M. Nadeem, N. Muhammad and X. Lu, *J. Energy Storage*, 2019, **21**, 632–646.

74 A. E. Baumann, D. A. Burns, B. Liu and V. S. Thoi, *Commun. Chem.*, 2019, **2**, 1–14.

75 Y. Yue, Y. Li, Z. Bi, G. M. Veith, C. A. Bridges, B. Guo, J. Chen, D. R. Mullins, S. P. Surwade, S. M. Mahurin, H. Liu, M. P. Paranthaman and S. Dai, *J. Mater. Chem. A. Mater.*, 2015, **3**, 22989–22995.

76 N. S. Bobbitt, M. L. Mendonca, A. J. Howarth, T. Islamoglu, J. T. Hupp, O. K. Farha and R. Q. Snurr, *Chem. Soc. Rev.*, 2017, **46**, 3357–3385.

77 Y. Liu, A. J. Howarth, N. A. Vermeulen, S. Y. Moon, J. T. Hupp and O. K. Farha, *Coord. Chem. Rev.*, 2017, 101–111.

78 Z. Chen, K. Ma, J. J. Mahle, H. Wang, Z. H. Syed, A. Atilgan, Y. Chen, J. H. Xin, T. Islamoglu, G. W. Peterson and O. K. Farha, *J. Am. Chem. Soc.*, 2019, **141**, 20016–20021.

79 E. Leung, U. Müller, J. K. W. Sandler, G. Skupin, M. Yamamoto and A. van der Net, *US Patent, 13,257,787*, 2019.

80 Y. Inokuma, T. Arai and M. Fujita, *Nat. Chem.*, 2010, **2**, 780–783.

81 K. Biradha and M. Fujita, *Angew. Chem. – Int. Ed.*, 2002, **41**, 3392–3395.

82 O. Ohmori, M. Kawano and M. Fujita, *J. Am. Chem. Soc.*, 2004, **126**, 16292–16293.

83 O. Ohmori, M. Kawano and M. Fujita, *Angew. Chem. – Int. Ed.*, 2005, **44**, 1962–1964.

84 Y. Inokuma, S. Yoshioka, J. Ariyoshi, T. Arai and M. Fujita, *Nat. Protoc.*, 2014, **9**, 246–252.

85 M. Hoshino, A. Khutia, H. Xing, Y. Inokuma and M. Fujita, *IUCrJ*, 2016, **3**, 139–151.

86 T. R. Ramadhar, S. L. Zheng, Y. S. Chen and J. Clardy, *Acta Crystallogr., Sect. A*: *Found. Crystallogr.*, 2015, **71**, 46–58.

87 T. R. Ramadhar, S.-L. Zheng, Y.-S. Chen and J. Clardy, *Chem. Commun.*, 2015, **51**, 11252–11255.

88 G. W. Waldhart, N. P. Mankad and B. D. Santarsiero, *Org. Lett.*, 2016, **18**, 6112–6115.

89 Q. Du, J. Peng, P. Wu and H. He, *Trends Anal. Chem.*, 2018, **102**, 290–310.

90 N. Zigon, T. Kikuchi, J. Ariyoshi, Y. Inokuma and M. Fujita, *Chem. Asian J.*, 2017, **12**, 1057–1061.

91 T. Mitsuhashi, T. Kikuchi, S. Hoshino, M. Ozeki, T. Awakawa, S.-P. Shi, M. Fujita and I. Abe, *Org. Lett.*, 2018, **20**, 5606–5609.

92 R. D. Kersten, S. Lee, D. Fujita, T. Pluskal, S. Kram, J. E. Smith, T. Iwai, J. P. Noel, M. Fujita and J. K. Weng, *J. Am. Chem. Soc.*, 2017, **139**, 16838−16844.

93 K. Kai, M. Sogame, F. Sakurai, N. Nasu and M. Fujita, *Org. Lett.*, 2018, **20**, 3536–3540.

94 S. Hoshino, T. Mitsuhashi, T. Kikuchi, C. P. Wong, H. Morita, T. Awakawa, M. Fujita and I. Abe, *Org. Lett.*, 2019, **21**, 6519–6522.

95 Y. Hayashi, K. Ohara, R. Taki, T. Saeki and K. Yamaguchi, *Analyst*, 2018, **143**, 1475–1481.

96 K. Ohara, A. Nakai and K. Yamaguchi, *Eur. J. Mass Spectrom.*, 2015, **21**, 413–421.

97 Y. Hayashi, K. Ohara, R. Taki, T. Saeki and K. Yamaguchi, *Anal. Chim. Acta*, 2019, **1064**, 80–86.

98 L. Rosenberger, C. von Essen, A. Khutia, C. Kühn, K. Georgi, A. K. H. Hirsch, R. W. Hartmann and L. Badolo, *Eur. J. Pharm. Sci.*, 2021, **164**, 105884.

99 S. Takizawa, K. Kishi, Y. Yoshida, S. Mader, F. A. Arteaga, S. Lee, M. Hoshino, M. Rueping, M. Fujita and H. Sasai, *Angew. Chem. – Int. Ed.*, 2015, **54**, 15511–15515.

100 S. S. Goh, P. A. Champagne, S. Guduguntla, T. Kikuchi, M. Fujita, K. N. Houk and B. L. Feringa, *J. Am. Chem. Soc.*, 2018, **140**, 4986–4990.

101 T. Mitsuhashi, L. Barra, Z. Powers, V. Kojasoy, A. Cheng, F. Yang, Y. Taniguchi, T. Kikuchi, M. Fujita, D. J. Tantillo, J. A. Porco and I. Abe, *Angew. Chem. – Int. Ed.*, 2020, **59**, 23772–23781.

102 E. V. Vinogradova, P. Müller and S. L. Buchwald, *Angew. Chem. – Int. Ed.*, 2014, **53**, 3125–3128.

103 A. G. O-Brien, A. Maruyama, Y. Inokuma, M. Fujita, P. S. Baran and D. G. Blackmond, *Angew. Chem. – Int. Ed.*, 2014, **53**, 11868–11871.

104 J. V. Knichal, H. J. Shepherd, C. C. Wilson, P. R. Raithby, W. J. Gee and A. D. Burrows, *Angew. Chem. – Int. Ed.*,2016, **55**, 5943–5946.

105 V. Duplan, M. Hoshino, W. Li, T. Honda and M. Fujita, *Angew. Chem. – Int. Ed.*, 2016, **55**, 4919–4923.

106 S. Yoshioka, Y. Inokuma, V. Duplan, R. Dubey and M. Fujita, *J. Am. Chem. Soc.*, 2016, **138**, 10140–10142.

107 N. Zigon, M. Hoshino, S. Yoshioka, Y. Inokuma and M. Fujita, *Angew. Chem. – Int. Ed.*, 2015, **54**, 9033–9037.

108 I. Morita, T. Mori, T. Mitsuhashi, S. Hoshino, Y. Taniguchi, T. Kikuchi, K. Nagae, N. Nasu, M. Fujita, T. Ohwada and I. Abe, *Angew. Chem. – Int. Ed.*, 2020, **59**, 3988–3993.

109 J. M. Bijovet, A. F. Peerdeman and A. J. van Bommel, *Nature*, 1951, **168**, 271–272.

110 K. Yamaguchi, J. Yamaguchi, A. Studer and K. Itami, *Chem. Sci*, 2012, **3**, 2165–2169.

111 S. Yoshioka, Y. Inokuma, M. Hoshino, T. Sato and M. Fujita, *Chem. Sci.*, 2015, **6**, 3765–3768.

112 S. Lee, M. Hoshino, M. Fujita and S. Urban, *Chem. Sci.*, 2017, **8**, 1547–1550.

113 W. De Poel, P. T. Tinnemans, A. L. L. Duchateau, M. Honing, F. P. J. T. Rutjes, E. Vlieg and R. De Gelder, *Crys. Growth Des.*, 2018, **18**, 126–132.

114 R. Dubey, K. Yan, T. Kikuchi, S. Sairenji, A. Rossen, S. S. Goh, B. L. Feringa and M. Fujita, *Angew. Chem. – Int. Ed.*, 2021, **60**, 1–6.

115 F. Habib, D. A. Tocher and C. J. Carmalt, *Mater. Today Proc.*, 2022, **56**, 3766–3773.

116 N. Zigon, V. Duplan, N. Wada and M. Fujita, *Angew. Chem. – Int. Ed.*, 2021, **60**, 2–21.

117 E. Sanna, E. C. Escudero-Adán, C. López, P. Ballester, C. Rotger and A. Costa, *J. Org. Chem.*, 2016, **81**, 5173–5180.

118 E. Sanna, A. Bauzá, E. C. Escudero-Adán, C. Rotger, A. Frontera and A. Costa, *Crys. Growth Des.*, 2017, **17**, 3611–3615.

119 C. Chen, Z. Di, H. Li, J. Liu, M. Wu and M. Hong, *CCS Chemistry*, 2021, **3**, 1352–1362.

120 S. Lee, E. A. Kapustin and O. M. Yaghi, *Science*, 2016, **353**, 808–811.

121 X. Pei, H. B. Bürgi, E. A. Kapustin, Y. Liu and O. M. Yaghi, *J. Am. Chem. Soc.*, 2019, **141**, 18862–18869.

122 L. Wang, C. E. Moore and S. M. Cohen, *Crys. Growth Des.*, 2017, **17**, 6174–6177.

123 D. Balestri, D. Capucci, N. Demitri, A. Bacchi and P. Pelagatti, *Materials*, 2017, **10**, 1–12.

124 F. Sakurai, A. Khutia, T. Kikuchi and M. Fujita, *Chem. – Eur. J.*, 2017, **23**, 15035–15040.

125 G.-H. Ning, K. Matsumura, Y. Inokuma and M. Fujita, *Chem. Commun.*, 2016, **52**, 7013–7015.

126 W. de Poel, P. Tinnemans, A. L. L. Duchateau, M. Honing, F. P. J. T. Rutjes, E. Vlieg and R. de Gelder, *Chem. – Eur. J.*, 2019, **25**, 14999–15003.

127 R. D. J. Lunn, D. A. Tocher, P. J. Sidebottom, M. G. Montgomery, A. C. Keates and C. J. Carmalt, *Crys. Growth Des.*, 2020, **20**, 7238–7245.

128 Y. Inokuma, S. Yoshioka, J. Ariyoshi, T. Arai, Y. Hitora, K. Takada, S. Matsunaga, K. Rissanen and M. Fujita, *Nature*, 2013, **501**, 262.

129 S. Y. Zhang, L. Wojtas and M. J. Zaworotko, *J. Am. Chem. Soc.*, 2015, **137**, 12045–12049.

130 S. Y. Zhang, C. X. Yang, W. Shi, X. P. Yan, P. Cheng, L. Wojtas and M. J. Zaworotko, *Chem*, 2017, **3**, 281–289.

131 S. Y. Zhang, D. Fairen-Jimenez and M. J. Zaworotko, *Angew. Chem. – Int. Ed.*, 2020, **59**, 17600–17606.

132 A. Saito, T. Sawada and M. Fujita, *Angew. Chem. – Int. Ed.*, 2020, **59**, 20367–20370.

133 M. Mon, R. Bruno, J. Ferrando-Soria, L. Bartella, L. Di Donna, M. Talia, R. Lappano, M. Maggiolini, D. Armentano and E. Pardo, *Mater Horiz*, 2018, **5**, 683–690.

134 S. Yuan, C. Lollar, X.-Y. Yang, A. Alsalme, H.-C. Zhou and J.-S. Qin, *Mater. Chem. Front.*, 2017, **1**, 1764–1767.

135 Q. F. Qiu, C. X. Chen, Z. W. Wei, C. C. Cao, N. X. Zhu, H. P. Wang, D. Wang, J. J. Jiang and C. Y. Su, *Inorg. Chem.*, 2019, **58**, 61–64.

136 S. Turega, W. Cullen, M. Whitehead, C. A. Hunter and M. D. Ward, *J. Am. Chem. Soc.*, 2014, **136**, 8475–8483.

137 W. Cullen, S. Turega, C. A. Hunter and M. D. Ward, *Chem. Sci*, 2015, **6**, 625–631.

138 C. G. P. Taylor, J. R. Piper and M. D. Ward, *Chem. Commun.*, 2016, **52**, 6225–6228.

139 C. G. P. Taylor, S. P. Argent, M. D. Ludden, J. R. Piper, C. Mozaceanu, S. A. Barnett and M. D. Ward, *Chem. – Eur. J.*, 2020, **26**, 3054–3064.

140 C. Taylor, J. Train and M. Ward, *Chemistry*, 2020, **2**, 510–524.

141 T. Matsumoto, R. Nakashima, A. Yamano and K. Nishino, *Biochem. Biophys. Res. Commun.*, 2019, **518**, 402–408.

142 T. R. Huber, E. C. McPherson, C. E. Keating and C. D. Snow, *Bioconjug. Chem.*, 2018, **29**, 17–22.

143 L. M. Hayes, N. J. Press, D. A. Tocher and C. J. Carmalt, *Crys. Growth Des.*, 2017, **17**, 858–863.

144 L. M. Hayes, C. E. Knapp, K. Y. Nathoo, N. J. Press, D. A. Tocher and C. J. Carmalt, *Crys. Growth Des.*, 2016, **16**, 3465–3472.

145 S. Carnesecchi, K. Langley, F. Exinger, F. Gosse and F. Raul, *J. Pharmacol. Exp. Ther.*, 2002, **301**, 625–630.

146 S. M. Ibrahim, E. S. El-Denshary and D. M. Abdallah, *PLoS One*, 2015, **10**, 1–17.

147 A. Rioja, A. R. Pizzey, C. M. Marson and N. S. B. Thomas, *FEBS Lett*, 2000, **467**, 291–295.

148 A. G. Staines, P. Sindelar, M. W. H. Coughtrie and B. Burchell, *Biochem. J.*, 2004, **384**, 637–645.

149 F. Habib, D. A. Tocher, N. J. Press and C. J. Carmalt, *Microporous Mesoporous Mater.*, 2020, **308**, 110548.

150 K. Yan, R. Dubey, T. Arai, Y. Inokuma and M. Fujita, *J. Am. Chem. Soc.*, 2017, **139**, 11341–11344.

151 Y. Inokuma, S. Yoshioka, J. Ariyoshi, T. Arai, Y. Hitora, K. Takada, S. Matsunaga, K. Rissanen and M. Fujita, *Nature*, 2013, **495**, 461–466.

152 CrystalisPro: Yarton, England, 2015.

153 G. M. Sheldrick, *Acta Crystallogr., Sect A*: *Found. Crystallogr.*, 2008, **64**, 112–122.

154 O. V. Dolomanov, L. J. Bourhis, R. J. Gildea, J. A. K. Howard and H. Puschmann, *J. Appl. Crystallogr.*, 2009, **42**, 339–341.

155 E. Sanna, E. C. Escudero-Adán, A. Bauzá, P. Ballester, A. Frontera, C. Rotger and A. Costa, *Chem. Sci.*, 2015, **6**, 5466–5472.

156 Y. Inokuma, K. Matsumura, S. Yoshioka and M. Fujita, *Chem. Asian J.*, 2017, **12**, 208–211.

157 Y. Zou, C. Yu, Y. Li and M. S. Lah, *CrystEngComm*, 2012, **14**, 7174–7177.

158 Y. Zhang, Q. Wang, Y. J. Xiao, J. Han and X. L. Zhao, *Polyhedron*, 2012, **33**, 127–136.

159 N. Wada, K. Kageyama, Y. Jung, T. Mitsuhashi and M. Fujita, *Org. Lett*, 2021, **23**, 9288–9291.

160 X. Song, Y. Zou, X. Liu, M. Oh and M. S. Lah, *New J. Chem.*, 2010, **34**, 2396–2399.

161 C. Singh, S, Mukhopadhyay and I. Hod, *Nano Converge*., 2021, **8**, 1–10.